

Sustainable and Resilient Transport Infrastructure

Lead Guest Editor: Sara Moridpour

Guest Editors: Xiaobo Qu, Nirajan Shiwakoti, and Samiul Hasan





Sustainable and Resilient Transport Infrastructure

Journal of Advanced Transportation

Sustainable and Resilient Transport Infrastructure

Lead Guest Editor: Sara Moridpour

Guest Editors: Xiaobo Qu, Nirajan Shiwakoti, and
Samiul Hasan



Copyright © 2021 Hindawi Limited. All rights reserved.

This is a special issue published in "Journal of Advanced Transportation." All articles are open access articles distributed under the Creative Commons Attribution License, which permits unrestricted use, distribution, and reproduction in any medium, provided the original work is properly cited.

Chief Editor

Gonçalo Homem de Almeida Correia, The Netherlands

Editorial Board

Kun An, China
José M. Armingol, Spain
Vittorio Astarita, Italy
Socrates Basbas, Greece
Francesco Bella, Italy
Abdelaziz Bensrhair, France
María Calderon, Spain
Juan-Carlos Cano, Spain
Giulio E. Cantarella, Italy
Maria Castro, Spain
Mei Chen, USA
Nicolas Chiabaut, France
Steven I. Chien, USA
Maria Vittoria Corazza, Italy
Luca D'Acierno, Italy
Andrea D'Ariano, Italy
Alexandre De Barros, Canada
Stefano de Luca, Italy
Rocío de Oña, Spain
Luigi Dell'Olio, Spain
Cédric Demonceaux, France
Lelitha Devi, India
Sunder Lall Dhingra, India
Roberta Di Pace, Italy
Dilum Dissanayake, United Kingdom
Jing Dong, USA
Yuchuan Du, China
Juan-Antonio Escareno, France
Saber Fallah, United Kingdom
Zhixiang Fang, China
Haneen Farah, The Netherlands
Francesco Galante, Italy
Yuan Gao, China
Indrajit Ghosh, India
Ricardo Giesen, Chile
Ren-Yong Guo, China
Yanyong Guo, China
Md. Mazharul Haque, Australia
Jérôme Ha#rri, France
Evelien van der Hurk, Denmark
Hocine Imine, France
Erik Jenelius, Sweden
Rui Jiang, China



Peter J. Jin, USA
Sheng Jin, China
Mehmet Karaköse, Turkey
Lina Kattan, Canada
Mehdi Keyvan-Ekbatani, New Zealand
Victor L. Knoop, The Netherlands
Alexandra Kondyli, USA
Alain Lambert, France
Michela Le Pira, Italy
Ludovic Leclercq, France
Seungjae Lee, Republic of Korea
Jaeyoung Lee, USA
Zhi-Chun Li, China
Ruimin Li, China
Keping Li, China
Christian Liebchen, Germany
Dung-Ying Lin, Taiwan
Yue Liu, USA
Chung-Cheng Lu, Taiwan
Tom Hao Luan, China
Filomena Mauriello, Italy
Luis Miranda-Moreno, Canada
Rakesh Mishra, United Kingdom
Tomio Miwa, Japan
Andrea Monteriù, Italy
Sara Moridpour, Australia
Giuseppe Musolino, Italy
Jose E. Naranjo, Spain
Aboelmagd Noureldin, Canada
Mehdi Nourinejad, Canada
Eneko Osaba, Spain
Eleonora Papadimitriou, The Netherlands
Dongjoo Park, Republic of Korea
Paola Pellegrini, France
Luca Pugi, Italy
Hesham Rakha, USA
David Rey, Australia
Meaad Saberi, Australia
Nirajan Shiwakoti, Australia
Ziqi Song, USA
Amanda Stathopoulos, USA
Lijun Sun, Canada
Jinjun Tang, China




Richard S. Tay, Australia
Daxin Tian, China
Alejandro Tirachini, Chile
Long Truong, Australia
Avinash Unnikrishnan, USA
Pascal Vasseur, France
Antonino Vitetta, Italy
Francesco Viti, Luxembourg
S. Travis Waller, Australia
Jianjun Wu, China
Hongtai Yang, China
Shamsunnahar Yasmin, Australia
Vincent F. Yu, Taiwan
Jacek Zak, Poland
Guohui Zhang, USA
Jing Zhao, China
Zuduo Zheng, Australia
Ming Zhong, China
Yajie Zou, China

Contents

Sustainable and Resilient Transport Infrastructure

Sara Moridpour , Xiaobo Qu , Nirajan Shiwakoti, and Samiul Hasan
Editorial (2 pages), Article ID 1576315, Volume 2021 (2021)

A New Method Based on Field Strength for Road Infrastructure Risk Assessment

Yi Li  and Yuren Chen
Research Article (13 pages), Article ID 6379146, Volume 2018 (2018)

A State-of-the-Art Review on Empirical Data Collection for External Governed Pedestrians Complex Movement

Xiaomeng Shi , Zhirui Ye , Nirajan Shiwakoti, and Offer Grembek
Review Article (42 pages), Article ID 1063043, Volume 2018 (2018)



Causation Analysis of Hazardous Material Road Transportation Accidents by Bayesian Network Using Genie

Xiaoli Ma , Yingying Xing , and Jian Lu 
Research Article (12 pages), Article ID 6248105, Volume 2018 (2018)




Impact of a Lower Conservation Budget on Road Safety Indices

M. Rojo , H. Gonzalo-Orden , A. Linares , and L. dell'Olio 
Research Article (9 pages), Article ID 9570465, Volume 2018 (2018)





Reliability-Based Estimation of Traffic Interruption Probability due to Road Waterlogging

Manuel Contreras-Jara, Tomás Echaveguren , José Vargas Baecheler, Alondra Chamorro Giné , and Hernán de Solminihac Tampier
Research Article (12 pages), Article ID 2850546, Volume 2018 (2018)

Innovative Bike-Sharing in China: Solving Faulty Bike-Sharing Recycling Problem

Shan Chang , Rui Song , Shiwei He , and Guo Qiu
Research Article (10 pages), Article ID 4941029, Volume 2018 (2018)

Hierarchical Matching of Traffic Information Services Using Semantic Similarity

Zongtao Duan , Lei Tang , Zhiliang Kou , and Yishui Zhu 
Research Article (12 pages), Article ID 2041503, Volume 2018 (2018)

Flexible Emergency Vehicle Network Design considering Stochastic Demands and Inverse-Direction Lanes

Hua Wang , Ling Xiao, and Zhang Chen 
Research Article (14 pages), Article ID 2524838, Volume 2018 (2018)

Editorial

Sustainable and Resilient Transport Infrastructure

Sara Moridpour ¹, Xiaobo Qu ², Nirajan Shiwakoti,³ and Samiul Hasan⁴

¹*Civil and Infrastructure Engineering Discipline, School of Engineering, RMIT University, GPO Box 2476, Melbourne 3001, Australia*

²*Department of Architecture and Civil Engineering, Chalmers University of Technology, Gothenburg, Sweden*

³*Manufacturing, Materials and Mechatronics Discipline, School of Engineering, RMIT University, GPO Box 2476, Melbourne 3001, Australia*

⁴*Department of Civil, Environmental, and Construction Engineering, University of Central Florida, Orlando, FL, USA*

Correspondence should be addressed to Sara Moridpour; sara.moridpour@rmit.edu.au

Received 3 December 2018; Accepted 2 March 2021; Published 16 March 2021

Copyright © 2021 Sara Moridpour et al. This is an open access article distributed under the Creative Commons Attribution License, which permits unrestricted use, distribution, and reproduction in any medium, provided the original work is properly cited.

Transport infrastructure is the lifeline of modern economy and significantly contributes to economic growth and our well-being. Transport infrastructure is not just about moving people and goods, but it is also an essential part of the continued economic growth and social development of countries. Our transport infrastructure is also increasingly complex and subject to a range of hazards or failures. A sustainable and resilient transport infrastructure provides access to jobs and other services with minimum environmental impacts and is able to withstand disruption and absorb disturbance by adapting to changing conditions, including climate change. This special issue aims at identifying and discussing a range of challenges that are faced in delivering safe, sustainable, and smart transport infrastructure as well as introducing innovative approaches to resolve these problems and challenges. We hope that this special issue would attract a major attention of the peers. 25 papers were submitted to this special issue, 8 of which were accepted for publication. As the guest editors of this special issue, we would like to summarize the 8 accepted papers as follows.

A paper authored by Y. Li and Y. Chen [1] focuses on evaluating the impact of road infrastructure on driving safety. This paper proposes two models to quantify the impact of road infrastructure on drivers. The models comprise four parameters including mass of vehicles, mass of infrastructure, warning level, and kinetic energy of road infrastructure. The models also consider the impact of drivers' subjective visual perception of road infrastructure.

A review paper by X. Shi et al. [2] focuses on examining the challenges and opportunities for empirical studies on the pedestrian's complex movements. This paper presents a systematic review on the empirical data collection for multidirectional crowd complex movements.

A paper authored by X. Ma et al. [3] explores the risk factors that influence road accidents involving hazardous materials. For this purpose, the paper presents a Bayesian network structure using Dempster–Shafer evidence theory. The Bayesian network model is capable of exploring the most probable factor or combination leading to accident, and it can predict the occurrence of the accident by setting the influence degree of a specific factor.

A paper authored by M. Rojo et al. [4] presents an economic analysis and evaluates the impact of budget reductions on increased accident rates. This paper focuses on the road safety indexes in Spain as a case study. The risk of accident, accident severity, and fatalities are considered in evaluating the road safety index. Linear regression technique is used in this paper to identify the relation between lower budget and higher road safety indices.

Authored by M. Contreras-Jara et al., [5] one paper proposes a procedure to estimate the traffic interruption probability caused by floods (still water regime) in roads. The procedure uses the first-order reliability method to estimate traffic interruption probabilities, based on the difference between the probability density functions of still water depth and vehicle wading height. The vehicle wading height based

on the geometric characteristics of light and heavy vehicles was developed.

S. Chang et al. [6] present a framework to minimise the faulty bike-sharing recycling. The framework minimizes the total recycling costs by taking the route optimization and loading capacity ratio as constraints. In this paper, an area in Beijing, China, has been used as a case study to validate the accuracy and performance of the proposed framework.

Z. Duan et al. [7] propose a multilevel matching method for traffic information services based on semantic technology. The similarity at the function level between services is computed by grouping the connections between the services into inheritance and noninheritance relationships. The paper also presents a three-layer framework with a semantic similarity measure that requires less time and space cost than the existing methods since the scale of candidate services is significantly smaller than the whole transportation network.

H. Wang et al. [8] present a bilevel optimization model to design the transport network with stochastic demands and emergency vehicle lanes. Two groups of users including passenger car users and emergency vehicle travellers have been considered in this paper. The bilevel optimization model has been formulated, where the upper level model aims to determine the optimal design of emergency vehicle lanes and the lower level model uses the user equilibrium principle to forecast the route choice of road users. A simulation-based genetic algorithm is proposed to solve the model.

Conflicts of Interest

The editors declare that there are no conflicts of interest regarding the publication of this editorial.

Acknowledgments

The guest editors would like to express their appreciation to all authors, reviewers, editorial team, *Journal of Advanced Transportation* team, and Hindawi for great support to make this special issue possible.

Sara Moridpour
Xiaobo Qu
Nirajan Shiwakoti
Samiul Hasan

References

[1] Y. Li and Y. Chen, "A new method based on field strength for road infrastructure risk assessment," *Journal of Advanced Transportation*, vol. 2018, Article ID 6379146, 13 pages, 2018.

[2] X. Shi, Z. Ye, N. Shiwakoti, and O. Grembek, "A state-of-the-art review on empirical data collection for external governed pedestrians complex movement," *Journal of Advanced Transportation*, vol. 2018, Article ID 1063043, 42 pages, 2018.

[3] X. Ma, Y. Xing, and J. Lu, "Causation analysis of hazardous material road transportation accidents by Bayesian network using genie," *Journal of Advanced Transportation*, vol. 2018, Article ID 6248105, 12 pages, 2018.

[4] M. Rojo, H. Gonzalo-Orden, A. Linares, and L. dell'Olio, "Impact of a lower conservation budget on road safety indices," *Journal of Advanced Transportation*, vol. 2018, Article ID 9570465, 9 pages, 2018.

[5] M. Contreras-Jara, T. Echaveguren, J. Vargas Baechele, A. Chamorro Giné, and H. Solminihac Tampier, "Reliability-based estimation of traffic interruption probability due to road waterlogging," *Journal of Advanced Transportation*, vol. 2018, Article ID 2850546, 12 pages, 2018.

[6] S. Chang, R. Song, S. He, and G. Qiu, "Innovative bike-sharing in China: solving faulty bike-sharing recycling problem," *Journal of Advanced Transportation*, vol. 2018, Article ID 4941029, 10 pages, 2018.

[7] Z. Duan, L. Tang, Z. Kou, and Y. Zhu, "Hierarchical matching of traffic information services using semantic similarity," *Journal of Advanced Transportation*, vol. 2018, Article ID 2041503, 12 pages, 2018.

[8] H. Wang, L. Xiao, and Z. Chen, "Flexible emergency vehicle network design considering stochastic demands and inverse-direction lanes," *Journal of Advanced Transportation*, vol. 2018, Article ID 2524838, 14 pages, 2018.

Research Article

A New Method Based on Field Strength for Road Infrastructure Risk Assessment

Yi Li  and Yuren Chen

The Key Laboratory of Road and Traffic Engineering, Ministry of Education, College of Transportation Engineering, Tongji University, No. 4800 Caoan Hwy., Shanghai 201804, China

Correspondence should be addressed to Yi Li; smilesusanly@163.com

Received 23 April 2018; Revised 3 July 2018; Accepted 6 September 2018; Published 25 September 2018

Guest Editor: Xiaobo Qu

Copyright © 2018 Yi Li and Yuren Chen. This is an open access article distributed under the Creative Commons Attribution License, which permits unrestricted use, distribution, and reproduction in any medium, provided the original work is properly cited.

Because road infrastructures have significant impact on driving safety, their risk levels need to be evaluated dynamically according to drivers' perception. To achieve this, this paper proposes two field strength models to quantify the impact of road infrastructures on drivers. First, road infrastructures are classified into two types (continuous and discrete). Then, two field strength models for these types are proposed. Continuous field strength model describes the impact of long-belt-shape infrastructure by differential and integral methods. Discrete field strength model describes the static and dynamic characteristics of infrastructures. This model includes four parameters: mass of vehicles, mass of infrastructures, warning level, and kinetic energy of road infrastructures. The field strength is a relative concept, which changes with vehicle state. At the end of this paper, risk assessment principles are listed to clarify the nature of road infrastructure risk evaluation. A workflow of risk assessment and a case study are presented to illustrate the application of this novel method. The result of this study shows that ① the field strength is positively related to its risk level; ② the distribution of road infrastructure risks explains driver behaviour correctly; ③ drivers tend to keep driving in low-risk area. These findings help to explain the impact mechanism of road infrastructures on drivers, which can be applied in AI-based driving assistance system in the future.

1. Introduction

Road infrastructures are basic components of traffic environment. China has built more than 40,000km highway in the last five years. In such circumstance, a large number of roadside facilities need to be assessed. They are not only the structure of road alignment, but also the guidance for drivers. Past studies have proposed a lot of models and systems for road infrastructure assessment.

(1) *Studies on the Relationship between Road Infrastructure and Driver's Visual Perception.* Drivers do not capture infrastructure information through direct contact. More than 80% of such information is obtained from visual perception [1, 2]. Plenty of experiments have been done to verify it. It showed that different traffic environment would result in different driving intention and behaviour [3]. Road line ratio from driver's view was collected through field tests by Victor [4]. The results showed that it would decrease with the climb of driver's vision pressure. Wang et al. (2006) regarded the

road infrastructure information as a series of stimulation. If the stimulation density from the infrastructure was in a proper range, then driver behaviour would be safe. On the other hand, some eye movement criteria (spot distribution, spot strength, etc.) were used to evaluate the visual burden caused by small radius and small angle of road alignment [5]. The results indicated that sharp radius would result in large visual burden for drivers. Different sweeping duration on road condition also showed some certain impact on lane keeping behaviour [6].

Other researchers focused on identifying such influence at intersections where the infrastructures were more various. Corresponding models were built to describe the relationship between real-world experimental data and driver's inner pressure [7]. Werneke and Vollrath [8] did field and simulated tests at intersections, and they concluded that poor planning of infrastructures near intersections would lead to severe vehicle collisions. Similar tests were conducted on mountain highway. The cross analysis between driver's vision pressure and psychological tension confirmed the importance of

proper road shoulder width and access management [9–11]. Besides, drivers' speed adaption behaviour was proved to vary with different road infrastructures and traffic complexity conditions. Complex infrastructure information would significantly result in frequent speed adaption behaviour [12].

Based on such tests and analysis, it can be seen that scientific infrastructure arrangement and proper infrastructure information are important for driving safety [13, 14].

(1) *Studies on Driver's Vision Pressure Field.* As a part of "Human-Vehicle-Road" circle, road infrastructures will influence the whole driving environment. Therefore, the risk of road infrastructure should be assessed dynamically from the view of its user-driver. The risk assessment is only valid when the interaction between infrastructure and driver does exist. Based on such understanding, driver's vision pressure field theory is proposed as the extension of artificial potential field theory [15]. In his theory, there was a potential field in which objects would attract and exclude the moving objects, and this was the source of movement. This theory assumed that objects were pushed under virtual force. It has been widely applied in solving robot path planning problem. Similarly, the moving vehicles can be regarded as a kind of movement in a potential field composed of road infrastructures. Then, many pressure field models were built according to this theory: ① discrete pressure field model [16] explained driver's decision pattern; ② vehicle path planning model combined pressure field theory and elastic band theory to predict vehicle's path (Thomas and Thorsten 2008); ③ driver's workload theory helped to estimate the impact of other traffic on drivers [17]. With the development of road scanning technology, more infrastructure information and indexes are available for precise analysis [18]. Moreover, the pressure field was simulated to visualize its impact on vehicle movement [19]. These studies helped to quantify the impact of road infrastructures on drivers, and such impact was also known as driving safety field proposed by Wang et al. [20, 21]. In driving safety field, road infrastructures were the sources of static potential field that had an important role in collision warning algorithm. Based on this, a dynamic 3D virtual hazard potential field model was built to calculate the field energy of infrastructures for driving decision assistance [22, 23]. It can be seen that the whole road environment is a physical field, and the road infrastructures build the framework of it (Ni 2013).

Past studies mainly focus on four aspects: ① the relationship between pressure field and real road environment; ② what is the physical rule of this pressure field; ③ how to explain such field phenomenon from drivers' view; ④ how to apply this theory in road risk assessment. Therefore, driver's vision pressure field still needs a deep study on the interaction between road infrastructures and drivers. This paper will focus on its application on risk assessment of road infrastructure.

(3) *Studies on Road Infrastructure Risk Assessment Methods.* Road infrastructure assessment is a major topic in traffic safety. In India, planning and building safe road infrastructure have been proposed as a high priority [24].

To reduce the negative influence of road infrastructures, the project MARVin in Austria built a database which included accident data and road parameters (radius, gradient, etc.). The risk of road infrastructure was assessed through comparison between tested road and nonaccident road. Two roads shared similar parameters, but they had different speed limits or weather conditions. Then high-crash-risk road sections or infrastructures can be spotted [25]. A similar method was used in risk model proposed by Appleton [26]. By comparison with benchmark road in New Zealand, the researcher got personal risk and collective risk scores. The score was the product of risk level and feature extent. Zhang and Hu [27] built a modified Bayesian network model to assess the facility risks on freeways, in which traffic data or field survey data were applied to calibrate parameters of the model. The results showed that smaller model result resulted in higher facility risk, and the threshold was 0.5. Bayesian network was also applied in multirisk assessment of road infrastructure system, and fully probabilistic approach was adopted to integrate multirisk interactions at both hazard and fragility levels [28].

Road infrastructure assessment is also a part of macroscopic road management, which focuses on road-user risk caused by road infrastructure. CEDR-project developed a risk assessment framework to obtain the risk of pavement, structure, and drainage in network level for most of the European road administrations [29]. Specifically, systematic risk model described the relationship among road infrastructure, vehicle, and driver. Multidimensional probability distribution quantified cause-and-effect chain of the risk impact of infrastructure on vehicle [30]. Other studies took the concept of infrastructure risk as collision risk. No collision means no risk [31]. Besides, improper facility was also a main reason for unsafe behaviour, such as speeding [32], distraction [33], and run-off-road crashes [34, 35].

Recently, intelligent vehicles which can collect vehicle movement and roadside information have been widely developed. With such technology, a series of experiments were conducted in northern Virginia. The results indicated that wide shoulder had significant impact on driver behaviour change [36]. Severe accidents would increase with improper slopes, bends, or pavement surface conditions for HGV (Heavy Goods Vehicles) [37].

It can be seen that past studies on risk assessment of road infrastructure mainly focused on performance comparison and systematic assessment. They presented general comments, but they ignored the interaction between infrastructures and users (e.g., drivers) [38]. Recently, Scott-Parker et al. [39] have tested drivers stress in response to different infrastructures, but they did not explain its impact mechanism. To overcome this weakness, this paper regards drivers as assessors of road infrastructures. Their subjective visual pressure is the key to evaluate the risk levels of nearby facilities. Corresponding field strength models and risk assessment methods are discussed in detail in this paper. This helps to quantify the relationship between driver behaviour and road infrastructures, and it also presents a better understanding on the nature of road infrastructure risk assessment. The concept

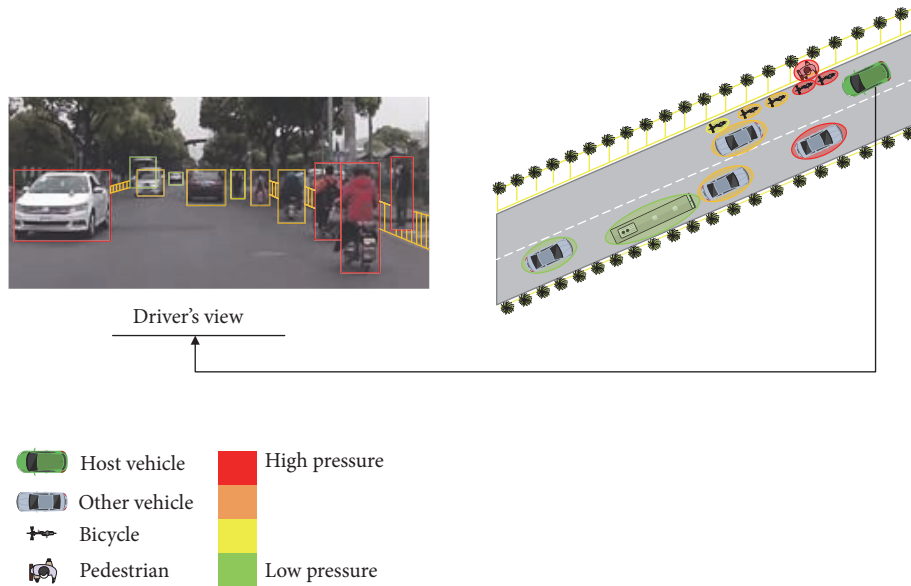


FIGURE 1: Conceptual image of pressure field from driver's view.

of pressure sources and field strength models may become the foundation of risk assessment system.

This paper is organized as follows. Section 1 introduces the achievements and weaknesses of past studies on driver's vision pressure field and road infrastructure risk assessment methods. Section 2 classifies some common road infrastructures based on pressure sources. Section 3 describes the field strength model of two road infrastructure types. Section 4 presents some assessment principles and a case study. Section 5 concludes the achievements and limits of this paper.

2. Classification of Road Infrastructure Based on Pressure Sources

In a complex traffic system, road infrastructure is a critical part. It does not have direct contact with vehicles, but it has influence on driver behaviour. In this paper, we define this mechanism as pressure field, which is not visible but measurable. Figure 1 shows a conceptual image of pressure field from driver's view.

The chance of direct collision between vehicle and road infrastructure is small; however driver behaviour continuously changes under the restrictions of nearby road infrastructures (including road geometry, road facilities, and other road users). This means that the pressure field is similar to gravity field, electric field, and magnetic field, which can force the vehicles to accelerate, decelerate, or change lane. If the risk level of road infrastructure is too high, it will form a stressful road environment for drivers, which may lead to unsafe driver behaviour. Therefore, a scientific risk assessment method for road infrastructure is necessary to understand and quantify such impact.

As the basis of road infrastructure assessment, we first need to classify some common road infrastructures. The classification is based on physical features of road infrastructures.

Although other factors like weather, visibility, time of day, etc. may also have some impact on driver behaviour [40, 41], we eliminate these factors by experiments only on sunny days during 8:00 to 15:00 with good visibility in this research.

There are various shapes of infrastructures on road, but most of them are continuous type and discrete type. Continuous road infrastructures have continuous impact on the vehicles during the driving process. They are mostly long-belt-shape facilities standing or attaching to the road surface. Discrete road infrastructures are arranged separately on road. Although there are many kinds of discrete infrastructures, they can be mainly divided into two types: independent and centralized. Typical independent discrete infrastructures are traffic signs or signals. Centralized discrete infrastructures consist of a number of independent discrete infrastructures, such as disperse barriers. Tables 1 and 2 show some typical continuous and discrete road infrastructures, respectively.

The road infrastructures have two kinds of effect on vehicles: exclusion and attraction. The exclusion effect forces the vehicles to keep a certain distance from pressure sources. The attraction effect, however, leads the vehicles to move towards the pressure sources. Table 3 shows the pressure effect of some typical pressure sources.

Some elements in Table 3 are listed in both exclusion and attraction columns because they show different impacts on different vehicle types. For example, bus lane has attraction effect on buses in rush hour. However, it shows exclusive effect on other cars. Besides, in off-peak hours it becomes an ordinary lane, and it has no restriction at all. Meanwhile, some elements only have attraction effect on some vehicles in some specific circumstances. For example, emergency parking lane has no effect on normal vehicles, but it has great attraction effect on out-of-control vehicles.

Based on the above classification and the discussion, we will build two models to quantify the impact of these two road infrastructure types on drivers.

TABLE I: Typical continuous road infrastructure.



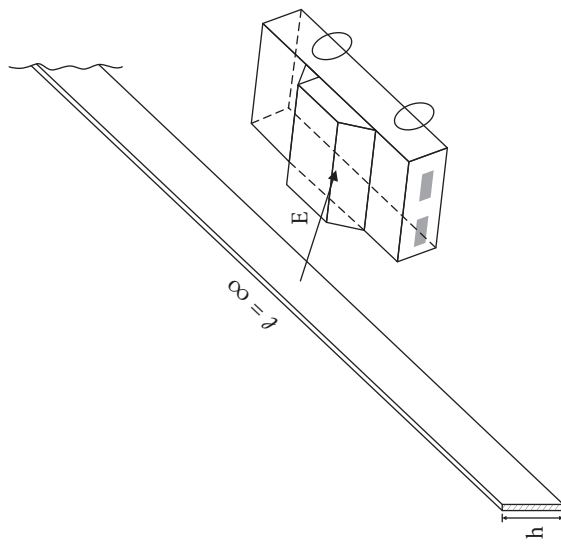


| Name | Figure | Name | Figure | Illustration |
|-------------------------|--|---------------------|---|--|
| Central Separation Belt |  | Double amber lines |  |  |
| Continuous barrier |  | Single lane marking |  | |

TABLE 2: Typical discrete road infrastructure.

| Name | Figure | Name | Figure | Illustration |
|-----------------------------------|--|------------------|---|---|
| Disperse barrier |  | Prohibitory sign |  |  |
| Accommodation lane sign |  | Warning sign |  | |
| Traffic signal |  | Directional sign |  | |
| Nearby vehicle/bicycle/pedestrian |  | | | |

TABLE 3: The pressure effect of typical pressure sources.

| Pressure sources | Pressure effect | |
|------------------|--------------------------------------|--|
| | Exclusion | Attraction |
| Lane marking | Prohibitory marking | Amber dash marking ^b |
| | Warning marking | Lane dash marking ^b |
| Road sign | Prohibitory sign | Directional sign |
| | Warning sign | Intersection waiting area ^b |
| | Accommodation lane sign ^a | Accommodation lane sign ^a |
| | Intersection guide line ^a | Intersection guide line ^a |
| | Traffic signal (red/yellow) | Traffic signal (green) |
| Barrier | Guardrail | Escape lane ^b |
| | Crash barrier | Emergency parking lane ^b |
| | Working zone | |

Note. a. The element shows different pressure effect under different circumstances; b. the element only is shown as a certain kind of pressure effect in some circumstances.

3. Field Strength Model of Different Road Infrastructure Types

3.1. *Continuous Road Infrastructure Field Strength Model.* To simplify the calculation, the host vehicles is represented by a rectangle object ($a \times b \times c$). The origin of the coordinate system is the geometrical center. The positive Y-axis points to the direction of vehicle movement. Figure 2 shows the simplified vehicle model and coordinate system.

Because a continuous road infrastructure always has a relative long dimension compared to other dimensions (see Figure 2), the differential analysis can be used to select the microsource unit of such item (ds : microunit, width= dz , length= ∞). Figure 3 shows the impact of field strength of microsource unit on vehicle in z plane.

Then, the corresponding field strength of this microsource unit can be calculated as follows.

$$dE = \frac{\vartheta}{\alpha \cdot l} dz = \frac{\tau}{\alpha \cdot \pi \cdot \|\vec{x} + \vec{y} + \vec{z}\|_2} dz \quad (1)$$

where dE is the field strength of microsource unit ds ; dz is the width of microsource unit ds ; α is the reliability parameter of continuous field source, which consists of four levels: 1-rigid, 2-semirigid, 3-flexible, and 4-traversable.

l is the boundary length of field range. When the infrastructure is in the center of road, the field range is centrosymmetric distributed around pressure sources. When it locates at roadside, the range covers a 1/4 circle area around pressure sources.

τ is the characteristic parameter of continuous field source, which shows the protection intensity of field source. The value of this parameter depends on the "Specification for Design of Highway Safety Facilities" (JTG D81-2017) in China. To cover different levels of guardrail and lane marking, τ is divided into eight levels, shown in Table 4.

According to Figures 3 and 4, the microfield source is infinitely small along z -axis, so the vehicle is parallel to the microfield source along y -axis. If the infrastructure locates

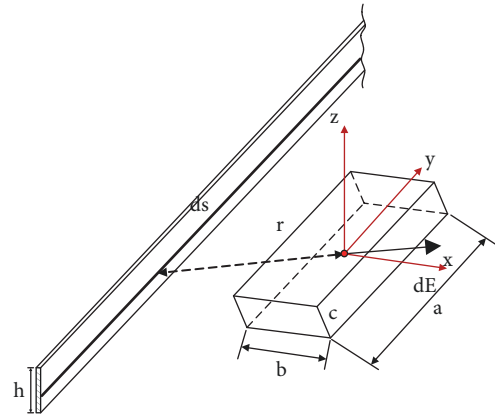
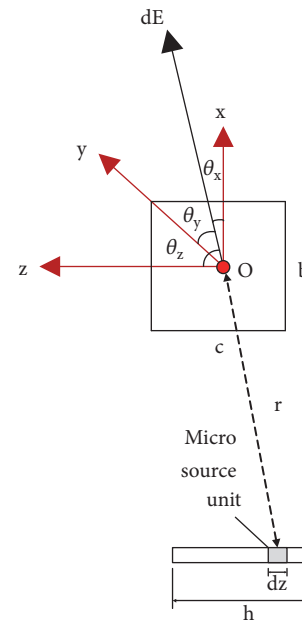


FIGURE 2: Simplified vehicle and coordinate system.



dE : the field strength of micro source unit ds

FIGURE 3: Field strength of microsource unit.

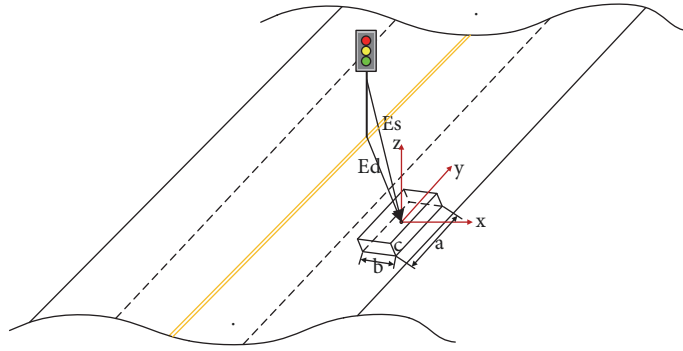
FIGURE 4: Static field strength (E_s) and dynamic field strength (E_d) of independent pressure source.

TABLE 4: The level of characteristic parameter of continuous field source.

| Protection intensity | τ | Protection intensity | τ |
|----------------------|--------|------------------------------|--------|
| Dash lane marking | 1 | A/ A_m -class protection | 5 |
| White lane marking | 2 | SB/ SB_m -class protection | 6 |
| Amber lane marking | 3 | SA/ SA_m -class protection | 7 |
| B-class protection | 4 | SS-class protection | 8 |

in the center of road, the field strength along x -axis can be calculated as follows.

$$\begin{aligned}
 dE_x &= \frac{\tau \cdot dz}{\alpha \cdot l} \cdot \cos \theta_x \\
 &= \frac{\tau \cdot x / \sqrt{x^2 + z^2}}{\alpha \cdot \pi \cdot \sqrt{(|x| - b/2)^2 + (|z| - b/2 \cdot z/x)^2}} dz \\
 &= \frac{\tau}{\alpha \pi} \cdot \frac{|x| - b/2}{(|x| - b/2)^2 + (|z| - b/2 \cdot z/x)^2} dz
 \end{aligned} \quad (2)$$

Then the whole field strength function can be obtained as follows.

$$E_x = \int_{-c/2}^{h-c/2} \frac{\tau}{\alpha \pi} \cdot \frac{|x| - b/2}{(|x| - b/2)^2 + (|z| - b/2 \cdot z/x)^2} dz \quad (3)$$

This function shows that the field strength along x -axis will change with the distance between the vehicle and infrastructure.

3.2. Discrete Road Infrastructure Field Strength Model. Compared with continuous infrastructures, discrete infrastructures not only appear occasionally but also have instruction and guidance information. The field strength of a discrete infrastructure consists of two parts: static field strength and dynamic field strength (see Figures 4 and 5).

The overall field strength can be obtained as follows.

$$\vec{E}_{dis} = \vec{E}_s + \vec{E}_d \quad (4)$$

where \vec{E}_{dis} is the overall field strength of a discrete infrastructure pressure source; \vec{E}_s is the static field strength of a

discrete infrastructure pressure source; \vec{E}_d is the dynamic field strength of a discrete infrastructure pressure source.

The concept of static field strength is similar to the field strength of continuous sources. It reflects the inherent characteristics of an independent pressure source. The distribution of its field intensity is within the circle (in the middle of road) or semicircle (on the side of road) around the pressure sources. Figure 6 shows the decomposition of static field strength.

In Figure 6, the mass center is the original point of field strength. Its coordinate is as follows.

$$\begin{aligned}
 \bar{x} &= \frac{\iiint xu(x, y, z) dv}{m} = \frac{\iiint x dv}{V} \\
 \bar{y} &= \frac{\iiint yu(x, y, z) dv}{m} = \frac{\iiint y dv}{V} \\
 \bar{z} &= \frac{\iiint zu(x, y, z) dv}{m} = \frac{\iiint z dv}{V}
 \end{aligned} \quad (5)$$

where $(\bar{x}, \bar{y}, \bar{z})$ is the coordinate of mass center; V is the volume of field source; m is the mass of field source.

The distance (r_1) between the field source and vehicle is as follows.

$$r_1 = \sqrt{\left(\sqrt{\bar{x}^2 + \bar{y}^2} + \frac{b}{2 \cos \theta_x}\right)^2 + \left(|\bar{z}| + \frac{b \cot \theta_z}{2 \cos \theta_x}\right)^2} \quad (6)$$

Then the static field strength can be obtained:

$$E_s = \begin{cases} \frac{\beta \cdot m_{source}}{r_1^2}, & \text{independent pressure source} \\ \sum_{i=1}^n \frac{\beta_i \cdot m_i}{r_1^2}, & \text{centralized pressure source,} \end{cases} \quad (7)$$

where m_{source} is the inertial characteristics of field source, which can be quantified by mass; β is the warning level of field source, which is divided into three levels; see Table 5.

Compared with static field strength, dynamic field strength shows guidance effect on traffic flow, so it covers only a specific direction of traffic flow. In reference to point-charge field theory in physics, discrete pressure source and

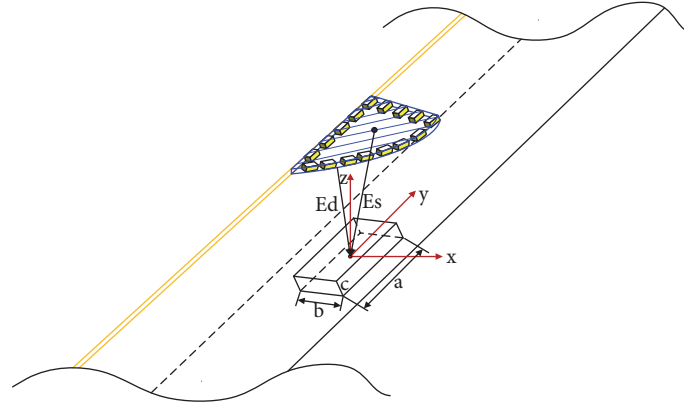


FIGURE 5: Static field strength (E_s) and dynamic field strength (E_d) of centralized pressure source.

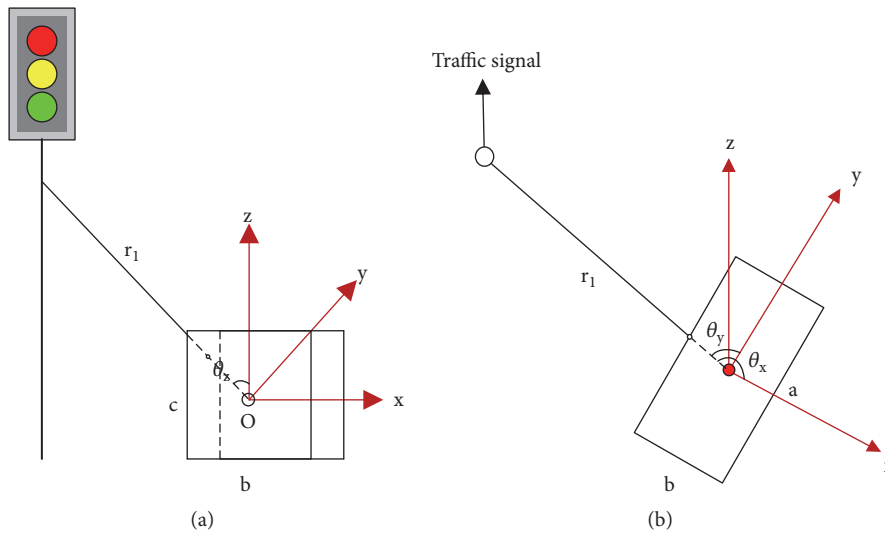


FIGURE 6: Static field strength decomposition. ((a) longitudinal, (b) overlook).

TABLE 5: Warning level of field source.

| Level | Infrastructure |
|-------|---|
| 1 | Warning sign/Accommodation lane sign/Directional sign |
| 2 | Prohibitory sign/Traffic signal |
| 3 | Disperse barrier |

vehicle can be regarded as a couple of energetic bodies, so the dynamic field strength is as follows.

$$E_d = \begin{cases} \frac{\beta \cdot \zeta}{r_2^2}, & \text{independent pressure source} \\ \frac{\beta_{cen} \cdot \zeta}{r_2^2}, & \text{centralized pressure source} \end{cases} \quad (8)$$

where r_2 is the vertical distance from vehicle to infrastructure, $r_2 = \sqrt{x^2 + y^2}$; β_{cen} is the warning level of the group field

source; ζ is the warning kinetic energy of field source, which is the required kinetic energy for host vehicle. For example, in car-following situation $\zeta = (1/2)m_{front\ car}v_{front\ car}^2$; in speed limit situation $\zeta = (1/2)m_{host}v_{limit}^2$.

4. Risk Assessment Principles and Case Study

In this section, the above models are utilized to assess the risk of road infrastructures with a case study.

First, some risk assessment principles need to be declared. (In this paper, risk source is equal to pressure source.)

(1) *Variability of Risk Source Type under Different Scenes.* In Section 2, we classify the road infrastructures into two types. In the case of multisource combination, the types of some field sources change with their directional text and time limit. This leads to an opposite risk assessment result (see the example of bus lane in Section 2). Therefore, before assessing the road infrastructure risk, we should check the pressure source type and state first.

TABLE 6: Indexes of pressure sources.

| No | Infrastructure | Pressure effect | Indexes | Illustration |
|----|--------------------|-----------------|--|--------------|
| 1 | Continuous barrier | Exclusion | $\tau=5$ $\alpha=2$ $h=2.5\text{m}$ | |
| 2 | Lane marking | Attraction | Dash line | |
| 3 | Discrete barrier | Exclusion | $m_{\text{source}}=225\text{kg}$ $h=0.7\text{m}$ | |
| 4 | Host vehicle | / | $m_{\text{host}}=1500\text{kg}$ $b=1.8\text{m}$ $c=2\text{m}$ $v_{\text{host}}=40\text{km/h}$ | |
| * | Lane width | / | 3.5m | |

(2) *Traffic-Rule-Based Pressure Source Priority.* Traffic rules and guidance clarify the right-of-way and drivers' behaviour standard. Similarly, we divide the pressure source priority into four levels. Among these priority levels, driver's safety and vehicle collision prevention are the most important. The specific priority levels are described as follows.

Priority 1: Fixed road infrastructure in driver's view.

Priority 2: Prohibitory sign/line or signal.

Priority 3: Warning sign/line or signal.

Priority 4: Traversable line, directional sign/line or signal.

In the process of pressure combination, the priority of each pressure source needs to be evaluated. First, combine the field strength of Priority 1. Then, add the combination results of lower priorities on the previous result. This forms a priority-based level system, which is easy for intelligent detection and analysis in the future.

(3) *The Relativity of Road Infrastructure Risk.* There are various risk sources (pressure sources) in road environment and different drivers would perceive different risk levels in multisource field. Generally, such characteristic can be explained in two aspects.

① When facing with the same pressure source, drivers will perceive different priority according to their vehicle types. For example, some road infrastructures only restrict the passage of truck, so they have high priority for truck drivers and low priority for vehicle drivers.

② When the same driver drives the same vehicle along the road several times, the risk level and combination of road infrastructures vary with vehicle position and vehicle state.

Therefore, the road infrastructure risk is a changeable and relative factor. It needs to be analyzed and calculated specifically in each scenario.

Next, according to the principles discussed above, we put forward an example (a section on Cao'an Hwy., Shanghai, China) with continuous and discrete road infrastructures to show the workflow of risk assessment based on the models proposed above. The indexes of pressure sources are listed in Table 6.

To explain the risk assessment clearly, we draw the assessment workflow with the example data in Figure 7. Each view and vehicle state of current moment during driving process is a series of data input for the assessment.

- (i) Firstly, each infrastructure in driver's view is classified according to its physical features (continuous or discrete), and its pressure indexes are also collected with vehicle state data. (In this paper, we assume that all indexes of road infrastructures are digitalized and stored in a database, which can be collected intelligently on road.)
- (ii) Secondly, based on the vehicle and pressure source data, we can grade the priority level (e.g., P1 and P4) of each infrastructure.
- (iii) Thirdly, the field strength of each priority is obtained based on the above results of classification and individual field strength calculation (P1: 11.32~175.68, P4: -14.14~-4.46). Moreover, the overall field strength of the whole road infrastructure environment in driver's view can be obtained (E: -2.15~171.22).
- (iv) Then, the risk of each infrastructure needs to be assessed according to a risk level guide which can be customized to meet road authorities' needs. In this particular example, four risk levels are provided in Table 7. If the risk level of infrastructure is below the minimum threshold, then the infrastructure is regarded as a safe one. If the field strength is within the other three intervals, corresponding risk level can be calibrated.
- (v) Finally, we can get the risk assessment result of current view of road infrastructure.

In this example, the discrete barrier on roadside shows high risk for drivers on the nearest lane. Continuous barriers are safe for driving, and the dash lane markings have attractive effect on vehicle movement.

To show the impact of risk assessment results on driver behaviour, corresponding vehicle trajectories (pink dots and white arrow) are drawn on the field strength diagram. Figure 8 shows the test data of 20 drivers and average vehicle trajectory in this situation. It can be seen that all drivers chose to change lane in order to keep away from the high field strength area. They always kept their trajectories in low/no risk area. However, these trajectories were not the same because each driver had his/her own vision perception and risk assessment result. If some drivers got high pressure

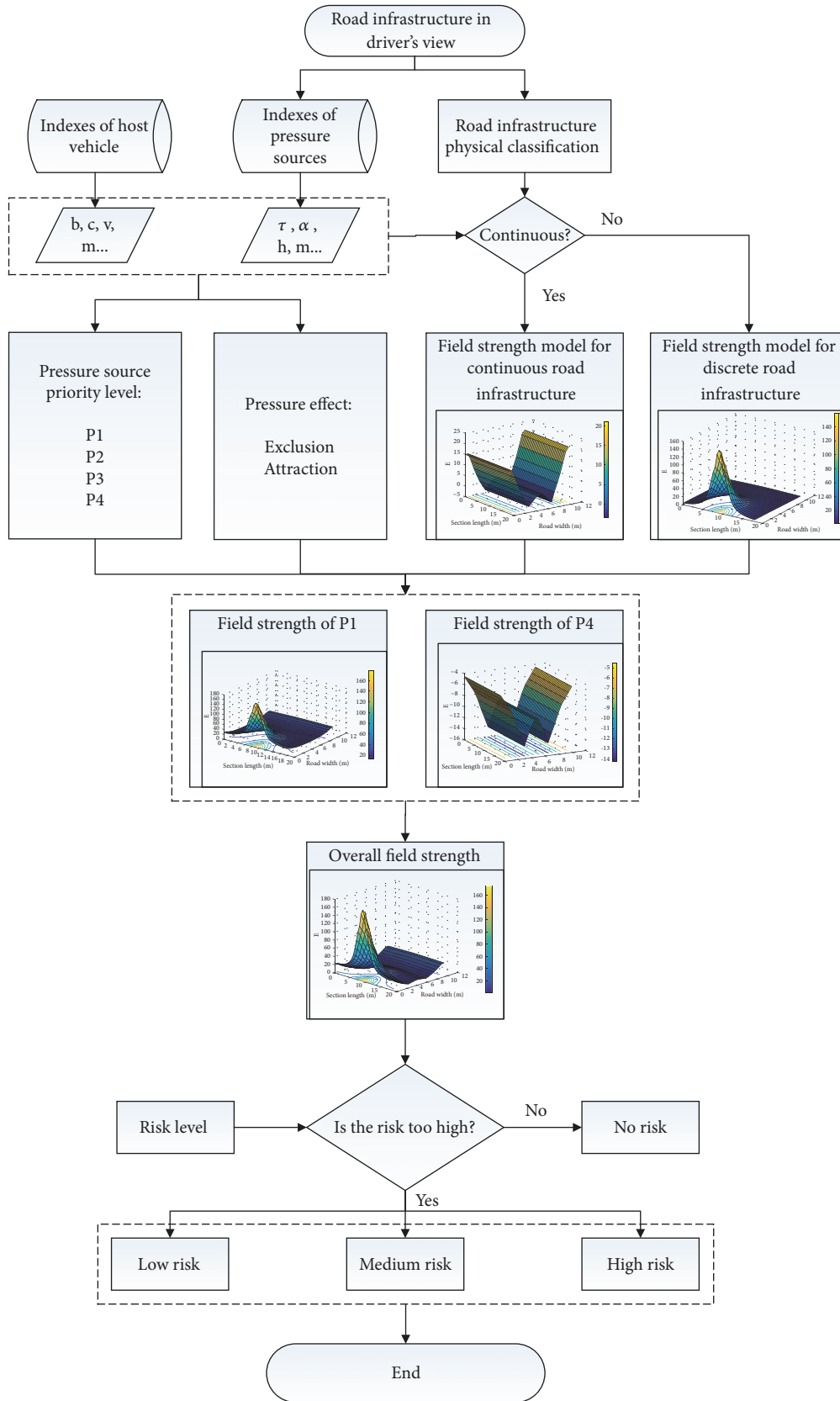


FIGURE 7: Workflow of road infrastructure risk assessment with test data.

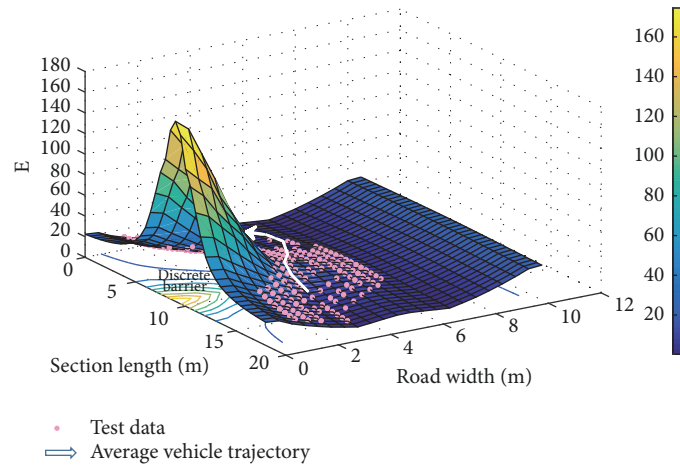


FIGURE 8: Vehicle trajectories in 3D field strength diagram.

TABLE 7: Risk levels of road infrastructure (case study).

| Risk level | Field strength | Explanation |
|-------------|--------------------|--|
| No risk | $E < 60$ | The infrastructure is good enough for safe driving. |
| Low risk | $60 \leq E < 100$ | The infrastructure is safe for most drivers, but it is risky for a small part of drivers in harsh weather. |
| Medium risk | $100 \leq E < 140$ | The infrastructure is quite safe under normal condition, but it is risky for a large part of drivers in harsh weather. |
| High risk | $E \geq 140$ | The infrastructure is risky for most drivers, and it may lead to severe traffic problem. |

earlier than others, then their psychology index (such as heart rate) would force them to react more quickly [42]. Although drivers' reactions are different, the average behaviour shows that ① the field strength model can quantify the road infrastructure risk correctly; ② driver behaviour will change with the risk levels of nearby road infrastructures, so it verifies the necessary of this assessment study and the importance of road infrastructure planning.

5. Conclusion

This paper presents a new method and novel field strength models for road infrastructure risk assessment. Past risk assessment methods are mainly based on the physical indexes of road infrastructures. Driver's perception and its impact mechanism are neglected in such methods, so they are static and inflexible. The risk assessment method we present here takes driver's subjective visual perception of road infrastructures as an important factor. This driver-vision-based method helps to quantify such process, which overcomes the weakness of traditional methods. In other words, our method provides a dynamic and specific way to measure the risk impact of road infrastructures on driver behaviour. The main contributions of this research are as follows. The classification method of typical road infrastructures is provided. All infrastructures are components of road environment, which can be quantified by field strength. Because different kinds of road infrastructures have different pressure impact on

drivers, we build two field strength models. Continuous field strength model describes the persistent impact on driving behaviour. Discrete field strength model shows the static and dynamic impact of the infrastructures on drivers. Based on the above models and analysis, three risk assessment principles show the nature of risk source evaluation. Finally, the workflow of risk assessment is presented with a case study, and corresponding risk levels are listed and explained.

However, there are still some limits in this research. Firstly, we assume that all characteristics of road infrastructures have been intelligently collected. This may be possible for some advanced autopilot vehicles or connected vehicles, but it is hard for traditional vehicles or platforms. Secondly, as each frame of recorded videos from drivers' view needs to be analyzed, the amount of calculation is huge. Therefore, high-speed calculation, transmission, and distributed procession will be thresholds for online analysis. Thirdly, we only discuss the overall risk level of road infrastructures for all drivers. Nevertheless, this risk assessment method is based on the field strength captured from driver's view, so different drivers may have different driving preference and decisions during the trip, which may lead to some deviation among drivers. Fourthly, we mainly divide common road infrastructures into continuous type and discrete type, but there are still various infrastructures and features to be analyzed for precise assessment in the future. Besides, the influence of bad weather and poor visibility is not considered in the pressure calculation in this research, which needs to be analyzed with more

test data under various weather conditions. In the following studies, a more elaborate and dynamic risk evaluation system is necessary for personalized service.

Data Availability

The data used to support the findings of this study are included within the article.

Conflicts of Interest

The authors declare that they have no conflicts of interest regarding the publication of this paper.

Acknowledgments

This work was supported by Zhejiang Provincial Communication Department [Grant no. 2015]07].

References

- [1] S. Sivaraman and M. M. Trivedi, "Looking at vehicles on the road: a survey of vision-based vehicle detection, tracking, and behavior analysis," *IEEE Transactions on Intelligent Transportation Systems*, vol. 14, no. 4, pp. 1773–1795, 2013.
- [2] B. Yu and Y. Chen, "Driving Comfort Evaluation of Urban Road from Driver's Visual Perception," in *Proceedings of the 15th COTA International Conference of Transportation Professionals*, pp. 2570–2579, Beijing, China.
- [3] T. Deng, K. Yang, Y. Li, and H. Yan, "Where Does the Driver Look? Top-Down-Based Saliency Detection in a Traffic Driving Environment," *IEEE Transactions on Intelligent Transportation Systems*, vol. 17, no. 7, pp. 2051–2062, 2016.
- [4] T. W. Victor, J. L. Harbluk, and J. A. Engström, "Sensitivity of eye-movement measures to in-vehicle task difficulty," *Transportation Research Part F: Traffic Psychology and Behaviour*, vol. 8, no. 2, pp. 167–190, 2005.
- [5] X. Pan, Q. Fang, and H. Jiang, "Driving Visual Demand-based Safety Evaluation of Mountainous Highway Horizontal Curve," *Journal of Tongji University. Natural Science*, vol. 38, no. 12, pp. 1763–1766, 2010.
- [6] W. J. Horrey and C. D. Wickens, "Focal and Ambient Visual Contributions and Driver Visual Scanning in Lane Keeping and Hazard Detection," *Proceedings of the Human Factors and Ergonomics Society Annual Meeting*, vol. 48, no. 19, pp. 2325–2329, 2016.
- [7] Z. H. Khattak, M. D. Fontaine, and R. A. Boateng, "Evaluating the impact of adaptive signal control technology on driver stress and behavior using real-world experimental data," *Transportation Research Part F: Traffic Psychology and Behaviour*, vol. 58, pp. 133–144, 2018.
- [8] J. Werneke and M. Vollrath, "What does the driver look at? the influence of intersection characteristics on attention allocation and driving behavior," *Accident Analysis & Prevention*, vol. 45, pp. 610–619, 2012.
- [9] Y. Yun-xing, C. Fang, and Z. Yong-fu, "Research on Visual Behavior Characteristics of Drivers in Downhill Sections of the Mountainous Expressway," *Highway*, vol. 1, pp. 132–137, 2018.
- [10] L. Zhong, X. Zhao, H. Ding et al., "Experimental Research on Safety Impact of Inside Shoulder Width on Drivers without Speed Limitation," *Journal of Highway & Transportation Research Development*, 2015.
- [11] K. Dixon and L. Brown, "Assessing how drivers of through vehicles react to driveway activity," *Transportation Research Record*, no. 2404, pp. 77–84, 2014.
- [12] O. Oviedo-Trespalacios, M. M. Haque, M. King, and S. Washington, "Effects of road infrastructure and traffic complexity in speed adaptation behaviour of distracted drivers," *Accident Analysis & Prevention*, vol. 101, pp. 67–77, 2017.
- [13] M. S. Young, J. M. Mahfoud, N. A. Stanton, P. M. Salmon, D. P. Jenkins, and G. H. Walker, "Conflicts of interest: the implications of roadside advertising for driver attention," *Transportation Research Part F: Traffic Psychology and Behaviour*, vol. 12, no. 5, pp. 381–388, 2009.
- [14] S. Bendak and K. Al-Saleh, "The role of roadside advertising signs in distracting drivers," *International Journal of Industrial Ergonomics*, vol. 40, no. 3, pp. 233–236, 2010.
- [15] O. Khatib, J. Warren, V. De Sapio, and L. Sentis, "Human-Like Motion from Physiologically-Based Potential Field," in *Building the Information Society*, vol. 156 of *IFIP International Federation for Information Processing*, pp. 747–748, Springer US, Boston, MA, 2004.
- [16] Y. Sha and Q. Shi, "Pedestrian Simulation Model based on Discrete Potential Field," *Highway Engineering*, vol. 34, no. 2, pp. 153–156, 2009.
- [17] E. Teh, S. Jamson, and O. Carsten, "Mind the gap: Drivers underestimate the impact of the behaviour of other traffic on their workload," *Applied Ergonomics*, vol. 67, pp. 125–132, 2018.
- [18] T. Sattel, T. Hesse, and C. Sondermann-Wölke, "Experimental study of evasion maneuvers with a potential field-based assistance function for collision avoidance," *VDI-Berichte*, no. 2009, pp. 475–493, 2008.
- [19] H. Wang and T. Wu, "New vector field microcosmic model for traffic flow," *China Journal of Highway and Transport*, vol. 16, pp. 99–102, 2003 (Chinese).
- [20] J. Wang, J. Wu, X. Zheng, D. Ni, and K. Li, "Driving safety field theory modeling and its application in pre-collision warning system," *Transportation Research Part C: Emerging Technologies*, vol. 72, pp. 306–324, 2016.
- [21] J. Wang, J. Wu, and Y. Li, "Concept, Principle and Modeling of Driving Risk Field Based on Driver-vehicle-road Interaction," *China Journal of Highway and Transport*, vol. 29, pp. 105–114, 2016.
- [22] J. Ji, H. Peng, W. Chi et al., "Decision Making for Vehiel Collision Avoidance Based on Dangerous Potential Field," *SAE-China Congress & Exhibition*, vol. 2, 2015.
- [23] J. Ji, P. Ji, and H. Peng, "Design of 3D Virtual Dangerous Potential Field for Vehicle Active Collision Avoidance," *Automotive Engineering Magazine*, vol. 38, no. 9, pp. 1065–1071, 2016.
- [24] R. V. Ponnaluri and Y. D. Santhi, "Road crash history and risk groups in India: Need for new initiatives and safety policies," *Transportation Research Record*, no. 2114, pp. 64–71, 2009.
- [25] S. Peter, P. Maurer, and R. Stütz, *MARVIN-Model for Assessing Risks of Road Infrastructure*, Arsenal Research, Vienna, Austria, 2007.
- [26] I. Appleton, "Road Infrastructure Safety Assessment," in *Proceedings of the 4th IRTAD Conference*, Seoul, Korea, 2009.
- [27] D. Zhang and X. Hu, "Risk Assessment of Traffic Facility on Freeway Based on a Modified Bayesian Network Model,"

- Journal of Transport Information and Safety*, vol. 34, no. 5, pp. 102–107, 2016.
- [28] P. Gehl, *Bayesian Networks for The Multi-Risk Assessment of Road Infrastructure*, UCL (University College London), 2017.
- [29] A. Weninger-Vycudil, B. Brozek, R. Spielhofer, C. Britton, and M. Oldfield, “Integration of cross asset risk assessment into road infrastructure asset management,” in *Proceedings of the IABSE Conference, Geneva 2015: Structural Engineering: Providing Solutions to Global Challenges*, pp. 1010–1016, Switzerland, September 2015.
- [30] J. Bald, K. Stumpf, and T. Wallrabenstein, “Systematic risk analysis for safety assessments of road systems,” *Journal of the Acoustical Society of America*, vol. 123, no. 5, pp. 3466–3466, 2008.
- [31] S. SUGIURA, Y. KANAMORI, A. TAKAGI, F. KURAUCHI, and H. MORIMOTO, “Development of integrated asset management technique of road infrastructure based on risk evaluation,” *Journal of Japan Society of Civil Engineers, Ser. F4 (Construction and Management)*, vol. 67, no. 4, pp. I.103–I.112, 2011.
- [32] M. S. Nemmag, R. Rahman, M. M. Rohani et al., “Analysis of Speeding Behaviour During Approaching the U-Turn Facility Road Segment Based On Driving Simulation Test,” *Matec Web of Conferences*, vol. 103, p. 08008, 2017.
- [33] G. K. Kountouriotis and N. Merat, “Leading to distraction: Driver distraction, lead car, and road environment,” *Accident Analysis & Prevention*, vol. 89, pp. 22–30, 2016.
- [34] S. Matena, A. Hegewald, W. Louwse et al., “Reduction of head-on collisions and run-off-the-road-accident. Report D 3.2 of the RiPCORD-iSEREST project (Road Infrastructure Safety Protection - Core-Research and Development for Road Safety in Europe; Increasing safety and reliability of secondary road),” 2009.
- [35] M. Tziotis, V. Pyta, N. Mabbott et al., “Road safety engineering risk assessment part 10: rural run-off-road crashes,” *Ran Off Road Crashes*, 2010.
- [36] J. Schorr, S. H. Hamdar, and C. Silverstein, “Measuring the safety impact of road infrastructure systems on driver behavior: Vehicle instrumentation and real world driving experiment,” *Journal of Intelligent Transportation Systems: Technology, Planning, and Operations*, vol. 21, no. 5, pp. 364–374, 2017.
- [37] M. Gothié, V. Cerezo, and F. Conche, “Relationship between road infrastructure characteristics and HGV accidents,” in *Proceedings of the International Conference on Heavy Vehicles, HVTT10: 10th International Symposium on Heavy Vehicle Transportation Technologies*, pp. 319–331, 2008.
- [38] R. Jobanputra and M. Vanderschuren, “Micro-simulation modelling of the impact of infrastructure provision and vehicle and pedestrian behaviour on road crash risk,” in *Proceedings of the 3rd International Conference on Road Safety and Simulation*, 2011.
- [39] B. Scott-Parker, C. Jones, and J. Tucker, “Driver stress in response to infrastructure and other road users: simulator research informing an innovative approach to improving road safety,” in *Proceedings of the Australasian Road Safety Conference 2016*, Canberra, ACT, Australia, 2016.
- [40] S. H. Hamdar, L. Qin, and A. Talebpour, “Weather and road geometry impact on longitudinal driving behavior: Exploratory analysis using an empirically supported acceleration modeling framework,” *Transportation Research Part C: Emerging Technologies*, vol. 67, pp. 193–213, 2016.
- [41] K. McCann and M. D. Fontaine, “Assessing driver speed choice in fog with the use of visibility data from road weather information systems,” *Transportation Research Record*, vol. 2551, pp. 90–99, 2016.
- [42] Yi Li, Yuren Chen, and Fan Wang, “The Impact of Traffic Environmental Vision Pressure on Driver Behaviour,” *Journal of Advanced Transportation*, vol. 2018, Article ID 4941605, 12 pages, 2018.

Review Article

A State-of-the-Art Review on Empirical Data Collection for External Governed Pedestrians Complex Movement

Xiaomeng Shi ^{1,2,3} Zhirui Ye ^{1,2,3} Nirajan Shiwakoti,⁴ and Offer Grembek⁵

¹Jiangsu Key Laboratory of Urban ITS, Southeast University, China

²Jiangsu Province Collaborative Innovation Center of Modern Urban Traffic Technologies, China

³School of Transportation, Southeast University, 2 Dongnandaxue Rd, Nanjing, Jiangsu 211189, China

⁴School of Engineering, RMIT University, Carlton, Melbourne, VIC 3053, Australia

⁵Safe Transportation Research & Education Center, Institute of Transportation Studies, UC Berkeley, 2614 Dwight Way, Berkeley, CA 94720-7374, USA

Correspondence should be addressed to Zhirui Ye; yezhirui@seu.edu.cn

Received 24 April 2018; Revised 3 August 2018; Accepted 14 August 2018; Published 2 September 2018

Academic Editor: Shamsunnahar Yasmin

Copyright © 2018 Xiaomeng Shi et al. This is an open access article distributed under the Creative Commons Attribution License, which permits unrestricted use, distribution, and reproduction in any medium, provided the original work is properly cited.

Complex movement patterns of pedestrian traffic, ranging from unidirectional to multidirectional flows, are frequently observed in major public infrastructure such as transport hubs. These multidirectional movements can result in increased number of conflicts, thereby influencing the mobility and safety of pedestrian facilities. Therefore, empirical data collection on pedestrians' complex movement has been on the rise in the past two decades. Although there are several reviews of mathematical simulation models for pedestrian traffic in the existing literature, a detailed review examining the challenges and opportunities on empirical studies on the pedestrians complex movements is limited in the literature. The overall aim of this study is to present a systematic review on the empirical data collection for uni- and multidirectional crowd complex movements. We first categorized the complex movements of pedestrian crowd into two general categories, namely, external governed movements and internal driven movements based on the interactions with the infrastructure and among pedestrians, respectively. Further, considering the hierarchy of movement complexity, we decomposed the externally governed movements of pedestrian traffic into several unique movement patterns including straight line, turning, egress and ingress, opposing, weaving, merging, diverging, and random flows. Analysis of the literature showed that empirical data were highly rich in straight line and egress flow while medium rich in turning, merging, weaving, and opposing flows, but poor in ingress, diverging, and random flows. We put emphasis on the need for the future global collaborative efforts on data sharing for the complex crowd movements.

1. Introduction

Pedestrian traffic is an essential mode in a multimode and multilevel transportation system. In contrast with vehicular traffic, pedestrians tend to change their speed and direction more frequently resulting in complex interactions with other pedestrians, transport modes, and the traffic infrastructures. These interactions can be generally categorized into four types: Pedestrian to Infrastructure (P2I), Pedestrian to Pedestrian (P2P), Pedestrian to Motor Vehicle (P2V), and Pedestrian to Nonmotorized Transportation (P2N) [1]. In transport hubs (e.g., inside train station) or mass gathering (e.g., a concert), the interaction types for pedestrian traffic are

typically limited to P2I and P2P. The simple maneuver could be pedestrians walking relatively straight in one direction at uniform speed (unidirection movement) to their destination. However, as the direction of movements and speed changes (e.g., multidirection movements), this can lead to complex interactions and competitiveness among pedestrians [2]. The movements of pedestrians to a large extent are governed by external factors such as infrastructure constraints (e.g., people at bottlenecks are forced to slow down as a result of space competitions) and maintaining proximity from other moving objects (e.g., a pedestrian has to change his/her walking direction for collision avoidance purpose). As a result, we observe pedestrian crowd movement ranging from

unidirectional to multidirectional movement at major public infrastructure such as train stations, sports stadiums, and other outdoor or indoor public gatherings. These multidirectional movements can result in increased number of conflicts resulting in delays and congestion [3]. In addition, the additional delays due to conflicts can increase egress time during emergency evacuation thereby impacting the efficiency of the evacuation process [4]. Further, the additional delays can cause impatience among escapee resulting in pushing behavior which can lead to trampling and stampede [5]. Recent studies have discovered that the small architectural modifications in an escape area can have large potential effects in terms of outflow and safety of individuals [3, 6–11]. Therefore, pedestrian crowd movements and interactions with the escape area or infrastructure is a subject of greater research interests among researchers working in the field of transport engineering, infrastructure engineering, and architecture. As such, these complex multidirectional movements have been studied extensively in the past [2, 3, 9, 12, 13]. Both microscopic and macroscopic approaches have been proposed to understand the mechanism of the pedestrian complex movements [3].

Recent advancements in computer processing power have prompted the researchers to collect and analyze the empirical data to a finer grain for model calibration and validation. Therefore, empirical data collections through controlled laboratory experiments have been on the rise in the past decade [2]. Although there are several reviews of mathematical simulation models for pedestrians' traffic in the existing literature, only few studies have reviewed the state of the art of empirical data for pedestrian traffic [2, 14]. Even those limited studies have examined the empirical data collection for pedestrian traffic from broader perspective rather than exploring the detailed debates, challenges, and opportunities for multidirectional complex movements. To the authors' knowledge, there is no detailed and systematic review on empirical data collection for pedestrians' complex traffic movement in the literature.

Therefore, the overall aim of this paper is to present a systematic review on the empirical data collection for uni- and multidirectional complex movements. Considering the length and scope of this paper, we restrict the review to only uni- and multidirectional movements governed by external factor by considering only P2I and P2P interactions. Please note that pedestrian traffic can also be governed by internal interactions among pedestrians which can lead to some self-motivated movement behaviors such as overtaking [15], self-slowness [16], queuing [17], and grouping [18], as well as crowds' self-organization phenomena such as 'faster-is-slower' effect [5], "lane formation" [9, 19], "zipper effects" [20, 21], "herding" [22], and 'freezing-by-heating' [23]. These emergent behaviors are driven by the individual's self-consciousness or the internal interactions within the crowd. These movement types have been identified as the underlying mechanisms of several crowd disasters [24–33]. For example, under severely congested situation, the individual body's movements are largely restricted by the surrounding pedestrians and any secondary increase of flow could result

in the forward and backward compression waves leading to stampede accidents [24, 27].

The exclusive review of this internally governed behavior is not within the scope of this review. However, we have occasionally mentioned these phenomena when examining externally governed movement patterns at instances where the internally governed movements also played an important role in the efficiency of pedestrians walking operations. Also, this review is not intended to review the mathematical models for pedestrian traffic or the results obtained from simulation models on complex movements. Interested readers on simulation models for pedestrian traffic can look into the review work by Duives et al. (2013) [34]. This is necessary to balance the breadth and the depth of the review article.

Our paper is structured as follows. Section 2 describes the methodology of this literature review paper. Section 3 gives the classification methods of the complex movement pattern. Section 4 presents the discussion based on the reviews. Finally in Section 5, the summary of this review article is presented.

2. Methodology

We used Boolean searches of databases to obtain literatures from electronic database including ISI Web of Science, Scopus, and Google Scholar. Other online social platforms such as Researchgate and Mendeley as well as well-known conference proceedings in this field such as the Pedestrian and Evacuation Dynamics (PED), Traffic and Granular Flows (TGF), and Transportation Research Board (TRB) were also used as the search database. We first checked the literature review papers related to pedestrian traffic topic, especially multidirectional movements, published in recent years. The literature search was then further supplemented by relevant publications in the reference lists of those recent publications.

The time period for the review is based on the past two decades (from 1998 to 2018) as it is the time-frame where we witnessed a significant advancement made to the data collection and modeling of pedestrian traffic. Only papers published in English are considered in this review as they are widely accessible to the researchers. We only reviewed the articles published in journal, conference, and book or book chapters. Therefore data from the government reports, industry related journals, or other sources are not considered. If the reviewed conference papers were extended and published in journals afterwards, we considered only the journal paper as the primary source and vice versa.

Reference management software, Mendeley Desktop, was adopted for the collection of literature, organization of the document, and generation of the cited list. This tool significantly improved the efficiency of writing the review paper.

3. Complex Movements of Pedestrian Flow

Complex movements are the aggregates of individual and crowd collective motions. To decompose the collective movement into critical movement behaviors, many researchers have studied the crowd motion behaviors both from pedestrian traffic system and other biological systems [35, 36].

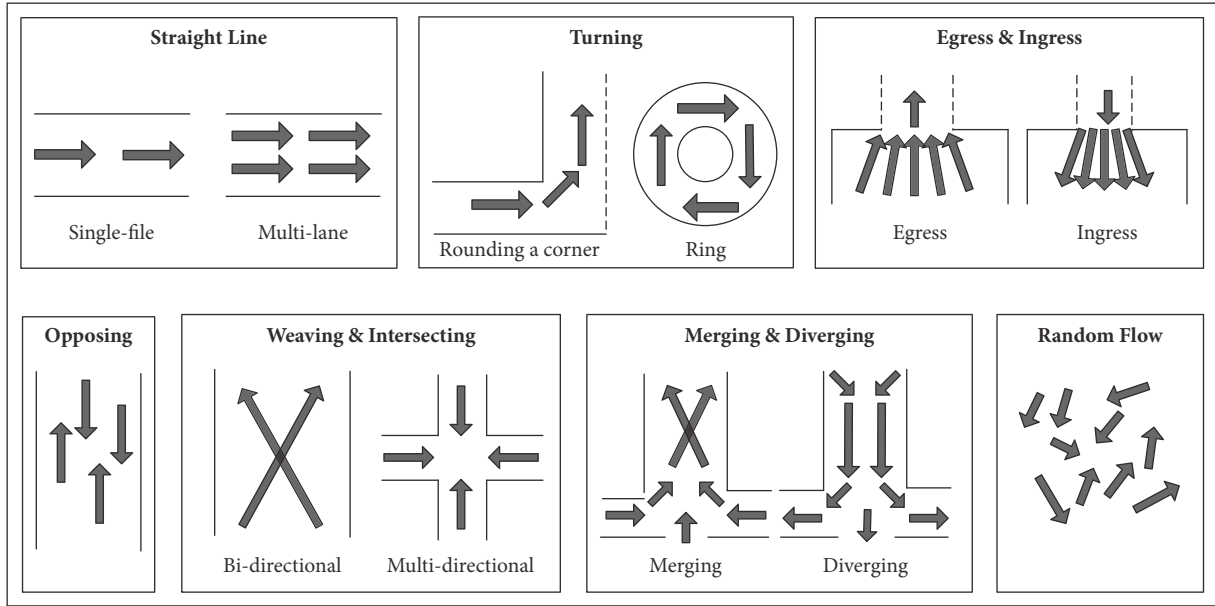


FIGURE 1: Conceptual diagrams of external governed complex movements.

However, a generic classification of pedestrian crowd behaviors is still missing from the literature [34, 35]. To the authors' knowledge, a review on the hierarchy of the crowd motion behaviors with regard to the movement complexity is missing in the literature.

Duives et al. (2013) proposed a classification of crowd motion cases based on the flow patterns [34]. They decomposed the crowd movements into eight motion based cases belonging to two categories: unidirectional flow (straight flow, rounding a corner, entering, and exiting) and multi-directional flow (bidirectional flow, 2-strips crossing flows, >2-strips crossing flows, and random crossing flows without focal point). They stated that the mix of these cases could be able to cover the entire range of complex movements. In addition, they also summarized six types of self-organization phenomena from the literature: lane formation, 'stop-and-go' waves, turbulent flows, herding, the zipper effect, and the 'faster-is-slower' effect. However, the focus of that paper is the assessment of crowd simulation models, rather than the empirical evidences under each crowd motion phenomenon.

Based on the classification of interrupted and uninterrupted flows in vehicular traffic [37] and considering the predominant driving forces of complex interactions, we classify complex movements into two categories:

- (i) *Externally Governed Movement*. Movements are strongly restricted/affected by external factors such as infrastructure constraints (e.g., merging pedestrian crowd flow at T-intersection [38]). Pedestrians have to change their desired walking manner due to the competition of space and time. Therefore, under this category, movements are aggregated into patterns which have strong relationships with the geometrics of architectural configurations. In addition, the interpersonal interactions are also predominately

affected by the external environments but not the internal factors.

- (ii) *Internally Driven Movement*. Movements are spontaneously organized within the crowd in an observable manner under appropriate situations. Under this category, the formulations of crowd movement patterns are less influenced by external factors. And the interpersonal interactions are usually driven by pedestrian's willingness to behave his/her own manner or follow others' behaviors (e.g., lane formation within a pedestrian crowd [19]).

In this paper, we build our review based on the eight classifications as stated by Duives et al. (2013) and discussed earlier. Additionally, we have extended and considered other complex movements that have been investigated theoretically or empirically in the literature such as turning, weaving, merging, and diverging movements as shown in Figure 1.

Figure 2 shows the classification of complex movements that shows the category of pedestrians' movements under external governed and internal driven movements. The external governed movements include unidirectional and multi-directional flows while internal driven movements include individual and crowd motion behaviors and self-organized phenomena. A dotted line representing the interface between internal driven and external governed movements is also drawn demonstrating that there could be overlap between these two types of movements (e.g., a merging flow may display 'faster-is-slower effect' or "lane formation"). As stated earlier in the introduction section, the scope of this paper is to review the externally governed pedestrian crowd movement. Figure 2 displays the conceptual diagram of these flow patterns as shown in the Figure 1 with a stepwise hierarchy. Starting with a simple straight unidirection movement, the pedestrian crowd movement can get complex as we move

3.1. Straight Line. Straight line walking, as the basic form of walking, refers to the kind of unidirectional movement (i.e., without any direction change). It has been used as a benchmark for pedestrian dynamics studies. Datasets for straight line walking can be seen in several well-recognized handbooks in transportation and fire engineering fields as well as many early studies on pedestrian traffic [49–55]. Some early year's empirical data were not well documented as of missing details due to the limitation of the traditional data collection techniques. In addition, large discrepancy existed in these studies for the insufficient influence factor consideration and uncontrollability. In this section, we highlight the recent empirical data collected through more advanced techniques [48, 56–59].

As shown in Figure 1, straight line walking can be segmented into single-file and multilanes movements. In single-file movement, pedestrian has no lateral interaction with other pedestrians; i.e., the interactions are purely longitudinal. Meanwhile, multilanes straight line movement requires the consideration of the horizontal oscillations from the other walking streamlines.

Single-file movement experiments were carried out with participants from different cultural background. It is worth mentioning that despite that many experiment setups in straight line walking are loop corridors/passageways, most of them have not considered the turning movements at corners and restricted the measuring areas to the straight parts. Such oval-shaped loop corridors are also different from the settings of ring-shaped corridors where pedestrian kept turning during their movements [57, 60].

Seyfried et al. (2005) set up experiments in a loop corridor with up to 34 German participants [57]. Through manual video analysis, velocity-density relationships for single-file movement were determined and compared with the movement on 2D plane. They found little difference between single-file movement and 2D plane movement in terms of density range and concluded that the internal friction and other lateral interventions had little influence on density-speed relations. Later, Liu et al. (2009) replicated Seyfried et al. (2005)'s setup and performed a similar single-file movement experiment involving Chinese participants [61]. Through the trajectories derived from automatic image processing, velocity, density, amplitude, and frequency of lateral oscillation, time headway values and distributions were calculated. They also observed that the lateral oscillations change with velocity or density. As density increased, time headway amplified while spacing reduced. After comparing the results with Seyfried et al. (2005), they found that their results exhibited higher speed under same density.

In the same year, Chattaraj et al. (2009) also carried out the same experiments in India to compare the fundamental diagrams of straight line movement with those from Seyfried et al. (2005) in Germany [62]. They found significant cultural difference between the two groups. For example, German group tend to have more minimum personal space than Indian group while German group was more sensitive to the increase in density than Indian group. In addition, they also discovered that the length of corridor have no influence on the fundamental diagram. Apart from the effect of corridor

length, boundary condition effects on fundamental diagrams were also empirically examined. Zhang et al. (2015) set up the similar corridors with Seyfried et al. (2015) with closed and open boundaries [63]. The influence boundary conditions on flow properties including the fundamental diagrams and density transition over time were investigated. They found that boundary condition has an effect on the flow properties and the effect was exceedingly high at jamming state. Under same density level, the velocities were lower under closed boundary condition. Cao et al. (2016) also set up the similar single-file experiments with 80 young students and 47 aged people in China [64]. It was discovered that jams tend to occur in mixed group due to the variation of maneuverability and self-adaptive abilities.

Recently, Seyfried's team further continued their researches on single-file movement by considering the stepping behaviors of pedestrian locomotion. Adopting the similar setups, Wang et al. (2018) organized 196 participants to walk in the oval passageway at different densities [65]. Step length, step frequency, swaying amplitude, and step synchronization were measured from trajectories. They found that power functions had better goodness-of-fit than linear function in terms of describing the relations between step length and frequency and speed. In addition, the relations between swaying amplitude and speed could be segmented into two regimes. Likewise, Cao et al. (2018) further analyzed the experiment data in Cao et al. (2016) with the similar analysis of stepping behavior with Wang et al. (2018) [66]. They discovered additional findings on age effects on stepping behavior, e.g., young people tend to control the lateral movement better than the old people. They also fitted the relations between step frequency and speed and found a quadratic fit in three groups of experiments which were different than those observed with Wang et al. (2018). Moreover, they observed no significant effect of height and gender on the fundamental diagram.

In terms of multilanes movements, Daamen and Hoogendoorn (2003) performed a series of controlled experiments with 60–80 human participants [56]. Their experiments included straight line walking scenarios with different desired speed and density levels (Experiment 1-3). Flow characteristics such as density and speed distribution, travel time, and fundamental diagrams were calculated from the extracted video trajectories. Likewise, Helbing et al. (2005) organized about 100 college students to walk through a straight passageway bounded with desks and chairs [9]. Bottleneck was created by moving the desk to narrow the passageway along the walking line. Mean flow and time headways were counted from videos. Results were compared between the corridor setups with and without bottleneck and they found significant capacity drop in bottleneck situation under unidirectional cases.

Similarly, Asano et al. (2007) conducted crowd experiments in a campus with 94 students [12]. Flow demand (30, 94) and controllability (with/without instruct to walk) were considered in straight line scenario. Multilanes walking features with different desired speed level in each stream were also investigated. Trajectories were extracted from video and headway-speed relationship for straight flow was calculated

for different cases. Likewise, Zhang et al. (2011) performed a series of large-scale experiments in well-designed corridors with up to 350 people [58]. Controlling the number of pedestrians, width of corridor, width of entrance, and exits, 28 runs of straight line experiments were performed. From the individual trajectories extracted using a software called PeTrack [67], the influences of density measurement methods and corridor width on fundamental diagrams were analyzed. It was found that, for density less than 3.5 m^{-2} , measurements method had minor influence and the specific flow was independent of corridor width as the density level was not highly congested.

More recently, Seyfried's team reported their new large-scale experiments results in Cao et al. (2017) [13]. About 2000 participants were involved in this series of experiments, including multilanes straight line movements in a corridor with a width of 5 m. Fundamental diagrams for different density measurements were presented and the estimated specific flow for unidirectional flow was 1.4 Ped/m/s at density level of 1.5 Ped/m^2 . Likewise, Sharifi et al. (2017) conducted a series of laboratory experiments in a circuit corridor that contained straight line passageway [68, 69]. Heterogeneity of crowd dynamics was investigated through the involvement of 189 normal people and 42 disabled people [70]. Trajectories of participants were extracted through automatic video processing and the macroscopic and microscopic crowd motion parameters were calculated. Capacities and level-of-service for straight line facilities with disabled people were further analyzed through the modeling of time headway [71].

Several field studies of straight line movement on different types of walking facilities were carried out [72–74]. To calibrate and validate Legion's simulation model, Berrou et al. (2007) collected 4762 valid samples of pedestrians' walking speeds from 18 hours of video recorded by 23 cameras in New York City Transit Station. The researchers compared their results (mean speed 1.50 m/s with standard deviation of 0.21 m/s) with several published free speed statistics. Similarly, to derive pedestrian's walking speed distribution on a long stairway, Kretz et al. (2008) carried out a field observation at a stadium in Germany [72]. 485 pedestrians were observed and divided into three categories according to the degree of influence by surrounding people. Results showed that the maximum horizontal walking speeds distribution exhibited $0.4 \text{ m} - 0.5 \text{ m/s}$ depending on density level. They also compared the speed distribution with a short stairway case and found the speed in a long stairway could be the half of that on a short stairway. They also discovered the gap of lack of a universal scaling factor for the speed on stairs relying on the length of stairway. Regarding high density situation in multilanes straight flow, Zhang et al. (2013) collected a field data of dense crowd during a mass gathering event through the combined use of camera and active infrared counter [73]. Flow rate and velocity of the crowd were measured and the fundamental diagrams were painted and compared with previous studies. Three additional flow operational indices including flow rate/velocity transition, velocity field, and speed map were calculated. Results suggested that the capacity for the street was estimated between 1.73 and 1.98 /m/s under normal situation and the density should be controlled under 5 /m^2 .

Apart from human subjects, several researchers also investigated the straight line movement through animal experiments and examined their relevancy to pedestrian crowd movement. John et al. (2009) reported the collective dynamics of straight line movements of ants on trails creating a nature-like experiments [75]. They observed no overtaking maneuvers in ants traffic trails but noticed the ants platoons that could be forecasted by simple models. It was observed that the flow increased monotonically with the density and no jam branch could be observed. Sharp contrast was found in ants traffic as compared with vehicular traffic and other transport modes where overtaking and congestion are frequently observed. John et al. (2009)'s findings were observed under nonstressed situations. To examine the straight line movement of stressed ants, Wang and Song (2016) made a passageway (1cm wide and 20 cm long) to measure the stressed ants' movements with different body size [76]. Fundamental diagrams were presented for both small and large ants. They found no evidence of jamming in stressed ants trails which was in line with John et al. (2009)'s findings. Also, they observed that speed seemed to be constant with density. Likewise, they also noted the differences of ants traffic behavior comparing to vehicular and pedestrian traffic in terms of fundamental diagrams.

3.2. Turning. Turning movement can be regarded as the response to the requirement of changing walking direction. It is usually associated with walking maneuver around corners or at exits, angled corridors, or ring corridor scenarios [77]. For single turning movement, the number of walking streamlines does not change before and after turning process and turning flow does not interact with flows in other direction. Therefore, turning movement can be also categorized into unidirectional flow.

It is worth mentioning that turning movement in this review has different meaning than those gait-level of works such as body-turning behavior as the turning movement should show direction change in the general walking streamlines [78].

Literatures documented several simulation studies on turning movements [79–82]. In addition, empirical evidences could be found with both human subjects and biological entities [81, 83–85].

Regarding turning movements around the corners and exits, Yanagisawa et al. (2009) organized 18 participants to perform an experiment with a special attention on the turning locomotion at bottlenecks [83]. They found the theoretical relations of turning angle on the parameters of floor field model under different cases. They compared the theoretical results with empirical data and found the complete agreements. In addition, obstacle effects were also examined by placing a column with 20 cm diameter in front of the exit and the increment of outflow from the obstacle was observed. Apart from the straight line experiments, Zhang et al. (2012) also carried out turning experiments at the cornered corridor with 2.4m width [84]. Fundamental diagram of turning flows at a corner was observed. With regard to turning movements around stair corners, Burghardt et al. (2013) organized experiments to observe the turning movements on

stairways [86]. They presented the fundamental diagrams and conducted profiles analysis of density, velocity, and specific flow at stairways corner and compared their results with four planning handbooks. They found that the turning bends could be the potential constraints for safety issue so that stairs without bend should be preferred by designers.

In terms of turning movements at angled-corridor, Dias et al. (2014) performed controlled experiments to obtain the microscopic characteristics of 16 individuals walkers in angle-changing corridors (0° , 45° , 60° , 90° , 135° , and 180°) under three different desired speed levels (normal walking, faster walking, and slow running) [77, 87]. They found the speed drop at a fixed turning region and the dimensions of such region was independent with turning angle but was dependent with desired speed levels. It was observed that the speed around the corner dropped with the increment of turning angle. Later, Dias et al. (2015) extended their previous turning experiments with up to 55 participants [88]. It was found that the longitudinal spacing between pedestrians tends to increase with the increased speed. The collected data were further utilized to develop an optimal trajectories algorithm and to calibrate a cellular automation model [79, 89]. Similarly, Sharifi et al. (2014) and Sharifi et al. (2017)'s experiments also included two angled corridors (right and oblique angle) as well as a spiral stairs with right corners [68, 90]. Walking speed distributions and time-space diagrams for both homogenous and heterogeneous flows were analyzed from the calculation of extracted trajectories. Their results exhibited a correspondence with Dias et al. (2014) as the speed reduction increased with the rise of turning angle [87]. Recently, Seyfried's team reported the results of two sets of experiments in Sieben et al. (2017) [91]. One experiment set a right-angle corridor with two narrow entrances and more than 270 people were asked to enter the corridor. Density bursts and fluctuations were observed at turning sections. Apart from turning angle, the curve radius of turning region was also considered in a recent experiment in China. Sun et al. (2017) studied the combined effects of turning angle and bend radius on the operational characteristics of pedestrians [92]. Results indicated that, under different flow volumes, the cumulative density and average speed of pedestrian flow were affected by both angle and radius effect. Angle's effect was more significant than radius, and the influence was maximized in right-angle case.

In terms of ring-shaped corridor scenarios, Jelić et al. (2012) performed single-file walking experiments with up to 28 pedestrians in a ring corridor with inner radius of 2 m and outer radius of 4.5m [93]. They derived their fundamental diagrams and instantaneous velocity and distance headway from both global and local measurements and compared the density-velocity relations with Seyfried et al. (2005) [57]. Their results showed that three linear regimes could be discovered from the velocity-spatial-headway relations which could be useful for further modeling. Likewise, Moussaïd et al. (2012) organized 119 people in France and adopted the same ring corridor as Jelić et al. (2012) with an advanced thinking of bidirectional flow design and allowance of overtaking maneuver [93, 94]. They found the transitions between organized traffic state and disorganized stated and

the unstable dynamics arose from the speed variations. Later in China, Kuang et al. (2015) performed a simplified single-file experiments with up to 26 students walking in a circular path with open boundary [95]. From video observation, they discovered the velocity variation, step fluctuation, and the delay from 'stop-and-go' waves.

To investigate the flow states under hypercongested situation, Jin et al. (2017) organized up to 278 college students to walk in a ring corridor with an inner width of 2 m and outer width of 4 m [60]. As a combined consideration of Jelić et al. (2012) and Moussaïd et al. (2012), both unidirectional and bidirectional flows were considered and the state transitions were described before and after lane formation process [93, 94]. Also, the fundamental diagrams for both flows were calculated and compared with previous works. Recently, Rahman et al. (2017) established similar experiments with Dias et al. (2014) considering the impact of different turning angles (60° , 90° , and 135°) on walking velocity [87, 96]. Results showed that instead of a linear decrement of speed with angle as discovered in Dias et al. (2014), 90° corridor exhibited the lowest mean speed of the participants. They also found that pedestrians preferred walking at the inner side of the corridor due to the shorter path.

Animal-based turning experiment and its relevancy to pedestrian crowd under panic conditions started from Shiwakoti et al. (2011) [7, 80]. The experiments described the egress of panicking ants from a squared and a circular rooms with an attention on the turning movement effects on egress dynamics. Results showed that turning movements could have negative effects on ants' outflows. The findings were also compared with a real-life in-store stampede where turning movement occurred at the door and the results showed a consistency between humans and ants in terms of the negative effects of turning movements. They also found that the placement of an obstacle at the exits could increase the flow. Later, Dias et al. (2012) set up a similar experiment with panicking ants egressing from a squared chamber [81]. They also found the flow reduction arose from turning movement that the flow was 20% lower than straight movement. Dias et al. (2013) further set up a more complex environments with turning, merging, and weaving configurations [97]. Escape rates under four angles of turning corridors (30° , 45° , 60° , and 90°) were compared with straight corridor and the flow reduction percentages were -8%, -20%, -16%, and -27%, respectively.

3.3. Egress and Ingress. Egress refers to the movement process of or exiting/outflow of a space while ingress means the opposite action, i.e., entering/inflow of a space. This two processes are also named as "entering and exiting", "inflow and outflow", or "inlet and outlet" by some other studies. As shown in Figure 2, egress and ingress process can be interpreted as the combination of straight line and turning movements. Since there is no direction change during egress and ingress process, the two types of movements also belong to the unidirectional flows. Egress and ingress movements often occur at fixed bottleneck sites such as exit and entrance. Space competition resulting from bottleneck geometric restriction is the main cause for the flow reduction.

Given the imperative role of egress process for both daily activities and emergency evacuations, during the past two decades, crowd egress has been one of the most popular topics among all the complex movements. Literatures are quite rich in egress experiments using both humans and animals under normal and emergency situations. Based on the past studies in this topic, the geometric of bottlenecks can be divided into two general categories, i.e., channel or corridor bottleneck and door bottleneck.

In addition to the measurements of the macroscopic and microscopic flow characteristics, the top two research topics for egress and ingress movements are the influence of bottleneck width on capacity, and the performance of obstacles near the exits. Specific flow rate of exit segment is often considered as the benchmark for comparison analysis among different measuring results.

Regarding channel/corridor bottleneck, Daamen and Hoogendoorn (2003)'s experiments series included the egress of crowd into a channel bottleneck with a width of 1 m and 2 m, respectively [56]. They further presented the detailed analysis results in Hoogendoorn and Daamen (2005) [20]. The microscopic flow characteristics for the two bottlenecks were analyzed and compared to the straight corridor without bottleneck. Based on the analysis, the researchers found the self-organized phenomena including the "lane formation" and the "zipper" effect.

With respect to door bottleneck, Helbing et al. (2005) conducted egress experiments under both regular and panic-like escape situations [9]. They examined the effect of placing an obstacle near the exit on the outflow and found the obstacle placement could avoid the clogging effect and increase the flow under both competitive intensities. Likewise, in Japan, Nagai et al. (2006) examined the effect of different movement maneuvers (walking and crawling) on the egress flow through a door [98]. They found the increase in the mean escape time with the number of walker as well as crawlers. It was observed that the mean flow increased with density and saturated at the capacity of the door. Later in China, Zhang et al. (2008) organized 60 students to egress a classroom with fixed exit width of 1.1 m [99]. Based on video observation, they calculated the distribution of pre-movement times, velocity variations, continuous outflow at exit, dislocable queue, and monopolizing exit. They discovered that evacuation times displayed a normal distribution and arrival time and escape order showed linear dependence with similar slope. It was also noticed that coordination among escapers is beneficial to the outflow.

To examine the quantitative relations between the width of bottleneck and the specific flow, Kretz et al. (2006) organized 94 participants (40, 80 persons cases) to walk through a door of varying widths ranging from 40 cm to 120 cm with a stepwise increment of 20 cm [100]. Time headway and specific flow were analyzed for different scenarios. Results showed that the specific flow declined with the increase of width when the door only allowed one person to pass and remained a constant value at larger width. They also compared the flow results with other studies. Similarly, Seyfried et al. (2009) performed controlled experiments controlling the channel width from 0.8 m to 1.2 m with a stepwise increment

of 0.1 m [21]. They measured the specific flow under different density levels (20, 40, and 60 pedestrians). Individual velocities, local densities, and time gaps for different width of the corridors were analyzed from the trajectories. They discovered that bottleneck capacity increased almost linearly with width and congestion might occur below maximum capacity.

Likewise, to develop an automatic trajectory extraction software for pedestrians, Boltes et al. (2010) organized 250 pedestrians to walk in two types of bottleneck corridors [67]. Microscopic characteristics such as the spatial and temporal variations at bottlenecks were analyzed later by Liddle et al. (2010) and Liddle et al. (2011) [101, 102]. They stated the reasons behind the flow fluctuations at bottlenecks as a physical effect, i.e., a new stepping function manner that could be only performed at bottleneck.

Later in China, Song et al. (2011) and Tian et al. (2012) carried out similar experiments with Seyfried et al. (2009) considering exit corridor width from 0.5 m to 1.4 m with a stepwise length of 0.1 m [103, 104]. Flow features such as average speeds, group speeds, density-speed-flow relations, and time headway distributions were analyzed. They also compared their specific flow results with Kretz et al. (2006) and found an agreement before 0.7 m and large disagreement after 0.7 m. In contrast with the previous focus on narrow bottlenecks, Liao et al. (2014) adopted a wide door with up to 5 m width to study the egress flow characteristics [105]. Density-velocity relationships inside the bottleneck were found to be independent with door width. In addition, a linear dependency was discovered between the flow and the bottleneck width.

The optimal design of exit areas also attracted empirical researchers. Sun et al. (2017) conducted controlled experiments in a subway station environment to examine the funnel shape bottleneck design on pedestrian flow operation [106]. Testing different angles of funnel shape, the optimal funnel angle was found between 46° and 65° under all flow conditions. This result was in agreement with the previous empirical evidences on turning angle effects, as the funnel shaped exit design could reduce turning angle and conflicts at exit regions [10].

Thereafter, more influence variables were considered to study the egress capacity at bottleneck especially with regard to the heterogeneity flow. Daamen and Hoogendoorn (2010 and 2012) conducted a series of experiments to examine the door capacities considering different door width (from 50 cm to 275 cm), population composition, stress level, and the presence of door [107, 108]. After a series of statistical tests, except for stress level, all the other parameters passed the significance tests. Later, Garcimartín et al. (2014) and Garcimartín et al. (2016) conducted a series of egress experiments considering door width (0.69 m, 0.75 m) and competitiveness (low, moderate, and high) [109, 110]. They discovered that the time headways displayed a heavy-tailed distributions while the burst sizes decayed exponential distribution.

Bode et al. (2015) involved 12 pedestrians to egress from a room with 6 exits considering the social group effects on egress time [111]. Their results suggested that the presence of social groups increased egress times. Further,

no clear time variation was found between individual and group movements. Similarly, von Krüchten et al. (2016) and von Krüchten and Schadschneider (2017) arranged 32–46 participants (dividing into social groups with 4, 6, and 8 people) to egress a narrow door with widths of 0.8m and 1.2m [112, 113]. Macroscopic and microscopic features of the egress flows were analyzed. They discovered that coordinated social grouping, e.g., queuing at exit and moving in a compact manner, could be beneficial to the outflow by reducing the conflicts. This finding also indicated that cooperative compact movements had different effects on the flow operation than the bursts release after clogging. Similarly, Nicolas et al. (2016 and 2017) examined the effects of individual's selfish and selfishness behaviors on the global flow characteristics by organizing 80 people to egress through a narrow doorway with a 72 cm width [114, 115]. They found that flow increased monotonically with density and the selfish fraction. It was an interesting finding that “selfishness does not mean coordination” because evading behavior could also lag the flow. A tradeoff between the number of evading and overtaking behaviors at the bottleneck that could maximize the flow should be further studied.

Concerning the ingress movement from the outside area into a confined space, only a few of empirical studies could be found. Ezaki et al. (2016) conducted controlled experiments employing a single-file stream of pedestrians successively ingress into a confined room with closed boundary [116]. Collective features, e.g., location and density distribution and individual characteristics such as the choice of location, were analyzed from video recordings. The revealed pattern such as people preferred to select location near corner indicated the significance of psychological and anticipative factors around an individual. The same year in China, Liu et al. (2016) drafted 40 students to reproduce the ingress and egress process in a rectangular room with a 1 m entrance and 1.5m exit [117]. It was discovered that the ingress order had a significant influence on pedestrian's location distribution in the steady state and the egress order. They also found that inactive pedestrians had a negative effect on the movement as they impeded the flow. Another experiment in Sieben et al. (2017) aimed at reproducing the entrance process of music events [91]. More than 270 people rounding a semicircle room were asked to enter into two narrow exits. It was found that there was a sharp increase of density from 3.8 to 8 Ped/m² within 10s.

Regarding field data, Cepolina and Tyler (2005) observed the ingress and egress process of metro passengers flowing into the entrance of escalator in London underground station. They discovered the temporal transition of inflow and outflow from the video. In addition, they established the inflow and outflow relationships at a bottleneck with a width of 80 cm. Apart from the individual walking speed in straight movement, Berrou et al. (2007) also observed the ingress process of passengers entering a train station from a high view [74]. Simulation parameters required by crowd simulation software Legion [118], such as the estimate arrival rate and preferred speed, exit flow, and densities, were extracted from the videos and adopted to set up simulation scenarios. Results showed that the simulated flows and densities were in line with empirical data.

Apart from the empirical investigation of human subjects, animals experiment approaches in studying egress movements are also found in the literature.

Most of the animal experiments were carried out using ants. The experiment setups for ants egress experiments were developed to replicate the similar set up for human experiments, i.e., circular chamber [8, 119, 120], squared chamber [121–123], and squared chamber with oblique corner near exits [124–126]. The common parameter measured is the escape flow at exits. Animal models have been the popular choice to study stressful condition like panic behavior as ethical considerations prevent creating a panic-like situation in pedestrian crowd situation [7].

Altshuler et al. (2005) established a circular chamber with two symmetrically located exits to examine the symmetry breaking phenomena in panicking ants [119]. It was discovered that under panic state, the use of two exits were asymmetrical while the use of exits displayed symmetric under normal situation. Later, Shiwakoti et al. (2009), Shiwakoti et al. (2010), and Shiwakoti et al. (2011) conducted ants experiments to study the effect of exit location and obstacle placement on outflow of panicking ants [7, 120, 127]. It was found that corner exits tend to have higher flow compared to middle exits in squared chambers. Also, the placement of obstacle could in general increase the flow as compared with column free situation. Burd et al. (2010) followed Shiwakoti et al. (2009)'s experiments to study ants' nested behaviors in normal state [8]. They also found the obstacle could increase the egress flow of normal ants. Soria et al. (2012) found the ‘faster-is-slower’ effect in ants traffic under various stress levels [124]. Their results also exhibited no selfish traffic behavior among ants. Likewise, Boari et al. (2013) observed the consistence finding in terms of the lack of selfish behavior [125]. However, ‘faster-is-slower’ effect was not found in their result. Later, Parisi et al. (2015) further analyzed Soria et al. (2012)'s data and carried out a discussion with human traffic rules [128].

Recently in China, Wang et al. (2015) used a single-exit chamber with different exit widths to perform ants egress experiments under stressed situations [121]. They found that the average flow was independent linearly on the exit width which was in contrast with human behaviors. Wang et al. (2016) further built a two-exit chamber to study ants egress through exits with the change of exit location and spacing [122]. It was found that the most efficient exit layout was the longest spacing of the two exits and this finding was correspondent with Shiwakoti et al. (2013) [123]. Symmetric breaking was also observed among stressed ants along with Altshuler et al. (2005). They also discovered the different performance of Social Force Model with respect to describing humans and ants movement in positions analysis, density map, velocity direction, and trajectories.

Another insect that has been used to study crowd collective movement is woodlice. Sobhani et al. (2014) and Sobhani et al. (2015) placed 120 panicking woodlice in a squared chamber with a 1 cm-width middle exit [129, 130]. Densities in near exit region and the flow of the exits were measured based on video analysis and then the relationship between jam density and exit capacity and the fundamental diagrams

for near exit region were discovered. They found that the fundamental diagrams for animals in panic status had some variations with the normal situation. And as the rise of stress level among woodlice, the number of blockage near the exit increased.

Apart from ants and woodlice experiments, several researchers used mice to study the egress movement under stressed conditions. Saloma et al. (2003) carried out an experiment with 60 mice egressing from a water pool onto a dry land through door bottleneck with different widths and separations [131]. It was observed that mice behavior was to some extent similar to the simulated results from pedestrian models. Self-organized queuing could be observed at the width that could only allow one mice to pass at the same time. As the door width increased, the self-organized pattern was broken due to the space competition. Saloma et al. (2015) further analyzed their experiments data from the aspects of individual training and crowded degree [132]. They found that prior training of individual mouse could increase the escape efficiency compared with the untrained situation. The training effects were more significant under more crowded situation.

Later in China, Lin et al. (2016) purchased a group of 95 female mice with a uniform body size to perform experiments in a dry rectangular ground with 2 cm width middle exit [133]. Different number of Joss-sticks was burned into smoke to stimulate the mice escape at various level of panic or stress. It was observed that egress time and the number of clogs increased with the levels of stress. It was concluded that the selfish competitive behavior displayed by mice was the main cause for the increase of egress time. Lin et al. (2017) further improved their experiment setting with a consideration of obstacle placement distance and the partition of near exit regions [134]. It was observed that the placement of obstacle could increase the flow by a maximum of 36% and 26% for regular exit region and partitioned exit region, respectively. The same group of researchers further analyzed the effects of exit width and position on mice egress movements. Chen et al. (2017) found that enough exit width enabling two mice pass the exit side by side could avoid 'faster-is-slower' effect [135]. Further, Chen et al. (2018) found that 'faster-is-slower' effect was less likely to occur at corner exits than middle exits [136]. In another mice egress experiments, Oh and Park (2017) examined the influence of the exit angle on egress dynamics with a group of 50 mice [137]. They found that, in general, mean velocity and total egress time decreased with angle.

Regarding larger animals, Zuriguel et al. (2014) studied the egress dynamics by observing the feeding process of sheep flock passing through a narrow fence with in a farm [138]. They found that the time headway of sheep flock exhibited a power-law distribution and the burst sizes obeyed an exponential decay. To further investigate the door width and obstacle effects, Garcimartín et al. (2015) compared the effect of 77 cm and 94 cm doors in with and without obstacle situations [139]. By examining the mean egress time per animal for the four scenarios, it could be found that the most efficient setup was the 94 cm door with obstacle and the least case was the 77 cm door without obstacle. Zuriguel et

al. (2016) further studied the effect of obstacle position on the egress flow [140]. They found obstacle position had an influence on the sheep flow and 80 cm was the best distance for the 77 cm door.

3.4. Opposing. Multidirectional movements are more complex compared with unidirectional movements due to the increase possibilities of interactions. The simplest case of multidirectional flows is usually called 'bidirectional' flow where movements are only operated in two directions.

Opposing movement refers to the situation when two streams of people coming from two opposed directions confront at a confined region. It can be also named as counterflow adopted by many studies [141–145]. Because there can only be two direction of flows in opposing movements, in this case, opposing can be regarded as a special scenario of bidirectional flows (or head-on weaving) where the two streamlines interact with an angle of 180° .

Opposing movements can be frequently observed in the daily life such as the boarding and alighting process in a crowded metro station, the movements on bridge during special events [146, 147]. In addition, opposing movements have been identified as the cause of several crowd disasters around the global occurring from the early 1980s to the late 2010s [3, 32].

Given its imperative role in practice, due amount of research efforts has been put into the study of opposing movement which include many empirical evidences.

Several Japanese researchers conducted opposing experiments with an initial purpose to validate the lattice gas model proposed by Tajima and Nagatani (2001) [148]. Isobe et al. (2004) organized up to 70 people to walk from two opposed sides of a rectangular corridor [141]. They presented the evolutions of arrival time and mean velocity as the increase of density. They found that, as the rise of density, the arrival time increased but the mean velocity decreased. Nagai et al. (2005) performed similar experiments with both walkers and crawlers in the opposing case [142]. The arrival time of crawler was dependent on the initial location and the mean arrival time increased with density. In addition to the straight line scenario, Asano et al. (2007) also included an opposing scenario. They illustrated the headway-speed relationships of opposing flows and found that mean speed tend to decrease in shorter headways.

In Europe, controlled experiments of opposing movements were first conducted by Daamen and Hoogendoorn (2003) [56]. Their experiment series also included the case of opposing movements. They applied the similar configuration of their previous straight line and egress scenarios including the desired speed and density levels. However, they only provided the qualitative analysis results for the bottleneck scenarios. Likewise, Helbing et al. (2005)'s experiments sets also contained the opposing movements in a corridor with a short and a long bottlenecks [9]. They presented the flow values and time gaps distributions for the two opposing cases and results showed that long bottleneck was worse than short bottleneck in terms of the effects on opposing movements. Later, Kretz et al. (2006) carried out an opposing experiment with 67 participants in a 2 m width corridor [143]. They

calculated the passing times, speeds, and flows and found that the sum of flow in opposing flow was larger than the straight line flow. They also investigated the lane formation and symmetric breaking in opposing flows and presented the frequency of number of lanes in the corridor.

Moussaïd et al. (2009) performed laboratory experiments (40 participants) and field observations (2670 samples) including opposing movement [149]. In their findings, individual's side preference in the evading maneuvers occurring in opposing movement was interpreted as a behavioral coordination behavior as a result of cultural differences. In Dutch, Versluis (2010) conducted a series of laboratory experiments considering age, body size, gender, free speed, travel purpose, maneuverability, pedestrian number, and predicted postencroachment time [150]. They investigated the lateral and longitudinal evasion of pedestrians with a mean value of 0.26m and 0.11m/s for opposing case. Back to Germany, Seyfried's team also collected datasets for opposing movement. Zhang et al. (2012) separated the opposing flows into stable separated lanes and dynamical multilanes flows with balanced and unbalanced flow ratio based on different ordering levels. They painted the fundamental diagrams for each flow types with different corridor width and compared the results with their previous straight line movement data [151]. Results indicated that ordering levels and density measurement methods did not significantly affect the fundamental diagrams. They also compared the maximum flow values of bidirectional data (1.5 Ped/m/s) with their previous unidirectional data (2.0 Ped/m/s). In addition to unidirectional flow, Cao et al. (2017) also reported the experiment results of opposing movements in a corridor with a width of 4 m [13]. Under the density level of 1.5Ped/m², the estimated specific flow value for opposing movements was 1.1Ped/m/s. This value was observed to be significantly lower than the unidirectional movement.

To investigate the impact of social group and flow ratio on opposing movement, Gorrini et al. (2016) organized controlled walking experiments in Japan [42]. Their results suggested that the rise of flow ratio had negative impact on the speed of pedestrians. Walking in groups could slow the speed because of the difficulty in moving coordination among group members. In contrast, coordination effects were also found to be positive in opposing movement. To explore the experimental evidence in the "gridlock" effect existing in CA models when simulating the opposing movement, Xue et al. (2017) conducted comparative experiments in both discrete and continuous space [152]. Through the time step analysis of pedestrians' position as well as the global density and specific flow, gridlock was not observed even under high density opposing flow. This result demonstrated the remarkable collaboration behaviors of pedestrian group movement especially at congested situation.

Recently, opposing movements were also investigated in animal systems. Wang et al. (2018) observed the bidirectional movement characteristics for nested ants with loaded and unloaded status through a less competitive experiment [153]. They measured the speed for unloaded and loaded ants, distance headway distribution over speed, and the spatial-temporal analysis of encounter behaviors through trajectories. Results showed that ants appeared to be equally sensitive

to distance headway in both uni- and bidirectional flows. Head-on encounter behaviors with the following ants could reduce movement efficiency. Unloaded ants tend to spend more time in communicating with encountering ants than the loaded ones. However, quantitative comparison with vehicular and pedestrian traffic was not conducted.

3.5. Weaving and Intersecting. In opposing flows, the interacting angle of the two streamlines remains a constant value of 180°. Past studies have highlighted that oblique interacting angle of different streamlines can also have a significant impact on the crowd movements [12, 87, 150].

In this study, weaving movement refers to the situation when two streams of pedestrian flows arrive at a fixed region (such as an intersection) at the same time and they can only keep their walking direction by cross over the other steam (please refer Figure 1). It is a commonly observed type of multidirectional movement as more than two numbers of streams may involve in the interactions. Weaving has several alternative forms such as intersecting and crossing, and if the number of involving streams is only 2, it can be also categorized into bidirectional movement.

The first empirical study on weaving movement for pedestrians was found in Daamen and Hoogendoorn (2003) [56]. However, no empirical analysis results for opposing flows were presented in the study. Later, Helbing et al. (2005)'s experiment sets also contained a right-angle weaving scenario with two stripes of flows [9]. Compared to their straight line data, they found the stripe formation phenomenon as there was a significant irregularity and clusters in the passing time. Asano et al. (2007) further analyzed the speed-density relationships ($\text{Speed} = A + B * \text{Density}$) under the impact of interacting angle [12]. They found that parameter A was significantly influenced by several angles (0°, 45°, and 90°) while parameter B was not influenced by the angles except for the right-angle case. Apart from the opposing movement reviewed in the above section, Versluis (2010) also considered oblique interacting angle including 45°, 90°, and 135°. It was found that the angle exhibited a positive effect on mean interaction point and showed a negative effect on mean longitudinal evasion. Similarly, Plaue and Chen (2011) organized two groups of people (54:46) to participant a right-angle weaving experiment [154]. They applied a crowd density estimation method to analyze the trajectories extracted from video. It was found that the nearest-neighbor kernel density method could provide a reasonable estimate of the density of human crowds. Back to Seyfried's new experiments, Cao et al. (2017) also reported the results of weaving scenarios including the right-angle bidirectional and four-directional weaving flows [13]. Similarly, at the density level of 1.5Ped/m², the estimated specific flow for bidirectional and four-directional weaving flows was 1.2m/s and 1.1m/s.

In Hong Kong, Wong et al. (2010) performed controlled experiments considering five intersecting angles (0°, 45°, 90°, 135°, and 180°) [155]. The aggregate empirical data were used to calibrate a model and the results showed highly significance. Adopting the calibrated model, they compared the mean speed transitions with reference stream under different density ratio and total densities. The researchers

found that as the rise of angle, the speed for reference stream decreased. Later, Wu and Lu (2013) conducted weaving experiments considering the dimension of passageway and flow ratio [156]. They defined a pedestrian weaving zone (PWZ) and discovered the flow characteristics within PWZ. They found that the flow values and flow ratios were more concerned with PWZ instead of the entire walking region. They also established a utility function to assess the PWZ operations based on three novel indices, i.e., weaving intensity, trajectory offset ratio, and density distribution factor of weaving points. Likewise, Sun et al. (2014) performed controlled experiments with 50 students to understand the mechanism of weaving movement at congested situations. Along with the flow characteristics of weaving movements, they also found that weaving tend to occur within an area which was in line with Wu and Lu (2013). Later, Lian et al. (2015) performed a four-directional intersecting experiments with 364 young Chinese students [157]. They examined the effects of side preference on lane formation and the placement of obstacle on the flow stability. It was discovered that lane formation process could be faster when students selected right-hand lane in the corridor. In addition, the placement of obstacle in the middle of the intersection could stabilize the intersecting flows. Sun et al. (2017) and Sun et al. (2018) further investigated the impact of intersecting angles and obstacle effects on intersecting movements [149, 158]. It was found that the effects of angles on flow speed vary at different flow conditions. But the effects of the size of the circular obstacle were monotonous with the speed increment and acceleration dispersion.

Animal-based interesting studies could be only found in the ants experiments conducted by Dias et al. (2013) [97]. In addition to the turning configuration, they also set up a junction corridor with right angle that enabled the bidirectional weaving movements. They discovered the transitions between the two weaving streams; i.e., one moving stream could block the other stream.

3.6. Merging and Diverging. Merging movement can be regarded as the combination of turning and weaving movement. It can be frequently observed at angled corridors/passageways such as T-junction or the stair-floor interface of a high-rise building. Moreover, merging configurations have also been identified as the causes for several stampede accidents including the famous Love Parade disaster [3, 32]. Due to the multiplication of the interactions among turning and weaving movements, merging movements are more complex.

Empirical evidences on merging movements were not sufficient before the year of 2014 [4, 58, 159, 160]. There was a burst of empirical studies on merging behaviors in the most recent four years [3, 161–168].

Boyce et al. (2012) examined the merging behaviors at stair-floor interfaces by performing evacuation drills with 581 participants in three buildings. They noted that the location of stair-floor connection points and the population composition could have a potential influence on merging flow patterns. The same year, Ma et al. (2012) conducted a similar evacuation drills in ultra-high-rise building [169].

They also observed that the merging behaviors at stair-floor interface could impede the flow of evacuees. To replicate the emptying process of mass gathering events in a stadium, Burghardt et al. (2013) performed controlled experiments in the exit of a football stadium where pedestrians moved from spectator seats upon receiving the signal and successively formed three stable streamlines merging into the outlet doors [86]. They only presented the fundamental diagrams of the downstream stairs; details on the merging characteristics were not analyzed. More recently, Huo et al. (2016) performed evacuation drills with 73 participants in a 9-floor high-rise building [161]. They discovered the negative effect of merging behavior on total evacuation time and speed through quantitatively comparison.

With respect to the merging flows on ground surface, Zhang et al. (2011 and 2012) performed merging experiments at T-junctions and compared the fundamental diagrams of merging with straight walking [58, 84]. After deriving the fundamental diagrams of merging flows, they found an increase in speed within after merging areas compared to before merging regions. Shiwakoti et al. (2015) studied the impact of merging angle and desired speed on the microscopic characteristics of merging flows in before and after merging areas. They found that, as the rise of merging angle, the reduction in speed increased. Similarly, Aghabayk et al. (2014 and 2015) also investigated the crowd merging behaviors considering merging angles and desired speed with asymmetric design of corridor [162, 163]. They found that the arrival and departure flow increased with speed and time headways decreased with speed. It was observed that merging angle was also influential to flow and time headways which was in consistent with the findings from Shiwakoti et al. (2015).

Later, Shahhoseini et al. (2016) conducted ants experiments to further understand the merging angle effects (60°, 90°, and 120°) [164]. They found the negative effects of merging angle in ant trials in panic situation. Further, Shahhoseini et al. (2017) combined the factors of merging angle and symmetrical configuration and designed 5 types of merging corridors to perform laboratory experiments with human subjects [170]. It was discovered that the merging behaviors of ants and humans displayed similarly effects arising from differences in architectural configurations.

Same year in China, Lian et al. (2017) established a merging configuration of branched flow merged into main flow with a further consideration of changing the width of branched corridor (0.8m, 1.6m, and 2.4m) [165]. It was observed that the merging ratios had a significant influence on the operations of upstream and downstream of merging areas for pedestrians flow. In the same year, Cuesta et al. (2017) performed merging experiments in a mock-up tunnel with 77 participants to reproduce the merging process of passengers exiting from the train and pedestrians walking on the platform [171]. They used the distribution of instantaneous specific flow to represent the flow dynamics. It was found that merging section had negative effects on the outflow of people at rail tunnel in terms of specific flow.

As illustrated in Figure 2, diverging movement can be defined as a reverse process of merging movement, where a

united stream of pedestrians separated into multiple streams with different destinations. Different from the fluctuating flows near a bottleneck, the flow states are stable in both before and after diverging.

A few empirical studies on exit choice behaviors could be categorized into diverging movements. Haghani et al. (2016) and Haghani and Sarvi (2017) performed exit choice experiments considering various exit number (2, 3, and 4) and exit position and exit width (50cm, 100 cm) [172, 173]. Instead of movement characteristics, their focuses were in the decision-making aspects. In another exit choice experiments, Wagoum et al. (2017) reported the flow features, e.g., flow, density relationships of the participants at exits. It was found that under normal situation individual's choice of exit only was dependent on the shortest distance while under higher density situation the load balancing for two exits could be observed.

3.7. Random Flow. Researchers have tried to reproduce the random flow situations by conducting experiments with multiple crossing flows. Dyer et al. (2008) set up a circle with sixteen equally angle-divided directions on the edge [174]. People were asked to stand inside at the center of the circle and individuals would be informed with a direction to walk outside the circle. They tested the role of prior information of walking direction and the conflicting directional information on the group directional decision-making. However, the flow characteristics of the experiments were not analyzed as the researchers were more interested on the psychological aspects of the participants. However, it is to be noted that there is a greater need of empirical data to predict the walking directions and potential conflicts due to random flow.

Researchers from computer vision field have also contributed to the empirical understanding of random flow. Zhou et al. (2012) analyzed the collective behaviors a crowd of pedestrians in a train station walking in random flow directions [175]. Using a mixture model of dynamic pedestrian agents, the future trajectories of pedestrians were predicted based on the observed past trajectories. Also, they classified the random walkers into various collective motion patterns and visualized them in different clusters.

3.8. Summary. Table 1 shows the summary of key findings and recommendations from the literature that conducted empirical studies on the externally governed complex multidirectional pedestrian traffic movements. The table shows the source of the literature, the movement type, the type of infrastructure considered (walking facility, bottleneck, and obstacle), subjects considered (pedestrians, animals), controllability of the variables (controlled laboratory experiments, field observation), and competitiveness among pedestrians (normal, emergency/evacuation drills, and panic). Further, the table provides a summary of the key findings, limitations, and recommendations for future studies and further use of the data generated from a particular literature in other studies. The filled dot in the table shows what approach has been followed in a particular literature while empty cell shows missing approach in a particular literature.

From the table, it is clear that initial studies have focused mainly on the empirical studies of unidirectional pedestrian flow, mostly at the corridor or at the bottleneck like door. Recent empirical studies have focused more on the complex multidirectional movements like weaving, crossing, and merging/diverging. Further, most of the studies are conducted under normal walking conditions. There have been increasing interests on the pedestrians' multidirectional movements under emergency or panicked conditions in recent time. As such, there has been rise in the study of animal models, particularly their relevancy to pedestrian traffic under emergency conditions.

In the next section, we present a discussion on the implications of these findings and directions for future research.

4. Discussions

Empirical data of complex pedestrian crowd movements are playing increasing imperative role in the verification and validation of crowd simulation models, design and planning of pedestrian walking facilities, scheme and evaluation of evacuation plans, development of image processing and visualization tools, coding of game engines, and trajectory planning for robots as well as the understanding of the nature of collective traffic phenomena in biology systems. Therefore, as observed from the literature review, there has been surge on empirical data collection and analysis over the past two decades. From the synthesis of the findings from these literatures, we have identified some opportunities and challenges as described in the following sections.

4.1. Anticipation of Future Empirical Data Requirements. To evaluate the current work and identify the research gaps based on the reviewed empirical studies, we utilize the data in Table 1 based on the number of studies and their belonging to each category. The summary of the statistics is presented in Figure 3.

Figure 3(a) summarizes the number of studies conducted over three time periods (2003-2007, 2008-2012, and 2013-2018) under each movement type. From the general trend of column height showing in Figure 3(a), we can notice that egress and straight line movements are the most popular topics among empirical studies while diverging and random flows are less studied through empirical approach. Also, from the distribution of studies, we can observe that earlier studies (2003-2007) in unidirectional flow have large proportion of straight line and egress experiments while multidirectional flow contains study mostly on the opposing and weaving movements. Meanwhile in the recent decade (2008-2018), researchers not only continue to explore the empirical evidences in straight line and egress movements, but also started to collect empirical data on turning, merging, and ingress movements. The emergence of increased studies on these movement patterns may arise as a result of several recent crowd disasters that involved turning and merging movements [32]. It can be further noticed that the dynamic features of diverging and random flows still require further research attentions.

TABLE 1: Summary of empirical results on externally governed complex pedestrian traffic movements.

| Ref. | Source | Movement Type | Infrastructure | | Subject | | Controllability | | | Competitiveness | | | Summaries | | Further Data Usage |
|-------|-------------------------------|---|---------------------------------------|------------|----------|--------|-----------------|------------|-------|-----------------|-----------|-------|--|--|--------------------|
| | | | Facility Type | Bottleneck | Obstacle | Animal | Pedestrian | Laboratory | Field | Normal | Emergency | Panic | Key Findings | Limitations & Future Recommendations | |
| [56] | Daamen and Hoogendoorn (2003) | Straight line; Egress; Opposing; Intersecting | Narrow corridor; Large hallway ground | • | • | • | • | • | • | • | • | • | <p>(i) Demonstrate a detailed process for designing controlled experiments</p> <p>(ii) Define and calculate the microscopic and macroscopic characteristics from trajectories for straight, opposing and intersecting flows</p> <p>(iii) Find different pedestrian walking features with and without bottleneck</p> <p>(i) Only present the analysis of bottleneck experiments data were further analyzed [20, 176, 177]</p> <p>(ii) Data analysis methods are not comprehensive</p> | (i) Bottleneck experiments data were further analyzed [20, 176, 177] | |
| [131] | Saloma et al. (2003) | Egress (Mice) | Water pool | • | • | • | • | • | • | • | • | • | <p>(i) Burst sizes of mice egress through the exit exhibit exponential or power-law distribution depending on exit size</p> <p>(ii) Self-organized queuing behavior can be observed when the door width only enables one mice to pass</p> <p>(iii) The queue will be broken with the increase of door width</p> <p>(i) Whether the findings from the mice can be applicable of humans should be further studies by comparing with empirical data</p> | (i) Further analysis of the experiments data considering the effect of prior individual training [132] | |
| [141] | Isobe et al. (2004) | Opposing | Narrow channel | • | • | • | • | • | • | • | • | • | <p>(i) Experiment data can help improve the lattice gas model by considering the front watching effect and back step</p> <p>(ii) Jamming transition is not found in experiment</p> | (i) The experiment data have not been used for the analysis of microscopic flow features | |
| [142] | Nagai et al. (2005) | Opposing | Narrow corridor | • | • | • | • | • | • | • | • | • | <p>(i) The arrival time of crawler depends highly on the initial location</p> <p>(ii) Mean arrival time increases with density</p> | (i) It is interesting to know how the vision condition among crawlers affect the opposing movement | |

TABLE I: Continued.

| Ref. | Source | Movement Type | Infrastructure | | Subject | | Controllability | | | Competitiveness | | | Panic | Key Findings | Summaries Limitations & Future Recommendations | Further Data Usage |
|-------|-------------------------|--|-------------------|------------|----------|--------|-----------------|------------|-------|-----------------|-----------|--|-------|--|---|--|
| | | | Facility Type | Bottleneck | Obstacle | Animal | Pedestrian | Laboratory | Field | Normal | Emergency | | | | | |
| [57] | Seyfried et al. (2005) | Straight line | Narrow passageway | | | | • | • | • | | | | | (i) Determine the fundamental diagram for single-file movements (ii) Single-file and 2D movements have agreements on velocity-density relations (iii) Required length and velocities indicated a linear relation | (i) Lack of automatic trajectories extraction (ii) Participants did not behave like real life walking in experiments | (i) Across cultural comparison of fundamental diagrams [6], [62] |
| [178] | Cepolina & Tyler (2005) | Ingress; Egress | Narrow corridor | • | | | • | • | • | | | | | (i) Capacity drop at bottleneck arises from a geometric issue and a time effect (ii) Discover the relationships between average inflow and outflow | (i) The data comparison is not reasonable due to different setups | (i) – |
| [9] | Helbing et al. (2005) | Straight line; Opposing; Intersecting; Egress; Counteracting | Narrow passageway | • | • | • | • | • | • | • | | | | (i) Boundary conditions influence capacity of facilitates and the headway distribution of pedestrians (ii) The proper use of obstacle can stabilize flow patterns and increase flow fluidity (iii) For opposing flows, long bottleneck is less efficient than short bottleneck (iv) For intersecting flows, lane formation is the result of a significant irregularity and clusters in the passing time (v) Several design solutions are proposed based on simulations | (i) Additional empirical data are needed to verify the proposed design solutions (ii) More psychological factors of pedestrians should be considered | (i) – |

TABLE I: Continued.

| Ref. | Source | Movement Type | Infrastructure | | Subject | | Controllability | | | Competitiveness | | | Key Findings | Summaries Limitations & Future Recommendations | Further Data Usage |
|-------|------------------------|---------------|---------------------|------------|----------|--------|-----------------|------------|-------|-----------------|-----------|-------|--|---|--|
| | | | Facility Type | Bottleneck | Obstacle | Animal | Pedestrian | Laboratory | Field | Normal | Emergency | Panic | | | |
| [119] | Alshuler et al. (2005) | Egress (Ants) | Chamber | ● | ● | ● | ● | ● | ● | ● | ● | ● | (i) Symmetric breaking can be found in panicking ants | (i) The ants' data can be used for comparison with the symmetric breaking phenomena in humans | (i) - |
| [100] | Kretz et al. (2006) | Egress | Width-changing door | ● | ● | ● | ● | ● | ● | ● | ● | ● | (i) Specific flow decrease with the increase of width when the width is under 100cm and keeps a constant when the width exceeds 100cm | (i) Further experiments should consider the heterogeneous group | (i) Data have been used to compare with ants experiments [7] |
| [143] | Kretz et al. (2006) | Opposing | Corridor | ● | ● | ● | ● | ● | ● | ● | ● | ● | (i) Total flow is always larger in opposing movement than straight line movement (ii) The number of lanes in opposing flow can be as much as 4 | (i) Repeated experiments should be carried out considering elderly people, different corridor width and shape, side preference etc. | (i) - |
| [98] | Nagai et al. (2006) | Egress | Room | ● | ● | ● | ● | ● | ● | ● | ● | ● | (i) Channel capacity is different for walkers and crawlers (75 vs. 35) (ii) Mean escape time increases with the number of walkers and crawlers (iii) Mean flow increases with density till reaching the capacity or clog occurs (iv) Lattice gas model can reproduce the egress of walker and crawlers well in a correspondence with empirical data | (i) Detailed gait characteristics of walker and crawlers should be analyzed by introducing more advanced computer vision techniques | (i) - |

TABLE I: Continued.

| Ref. | Source | Movement Type | | Infrastructure | | Subject | | Controllability | | Competitiveness | | Panic | Key Findings | Summaries | Further Data Usage |
|-------|-------------------------|---------------------------------------|-----------------------|----------------|--------|------------|------------|-----------------|--------|-----------------|--|-------|---|---|--------------------|
| | | Facility Type | Bottleneck | Obstacle | Animal | Pedestrian | Laboratory | Field | Normal | Emergency | | | | | |
| [12] | Asano et al. (2007) | Straight line; Opposing; Intersecting | Restricted passageway | | | | | | | | | | (i) Crossing angle may affect speed-density parameters (ii) Distance headway affects mean speed | (i) Require considering heterogeneity in crowds (i) Development of a combined micro-meso-model [179] | |
| [74] | Berrou et al. (2007) | Straight line; Ingress; Opposing | Passageway; door | | | | | | | | | | (i) Strong context-dependencies require to be considered into the modeling of crowd motion pattern (i) Flow characteristics for the different directional flows are not analyzed | (i) - | |
| [174] | Dyer et al. (2008) | Random flow | Circle room | | | | | | | | | | (i) Small directionally informed pedestrian can guide the group to targeted directions without verbal communication (i) 485 individuals' walking speed on a long stairway (ii) Mean upward walking speed on a long stairway can be half of that on a short stairway | (i) Further analysis on three new questions [180] | |
| [72] | Kretz et al. (2008) | Straight line | Stairs | | | | | | | | | | (i) No universal scaling factor for speed on stairways in dependence of the stairway length | (i) - | |
| [99] | Zhang et al. (2008) | Egress | Room | | | | | | | | | | (i) Evacuation times display a normal distribution (ii) Arrival time and escape order shows linear dependence with similar slope (iii) Coordination among escapers is beneficial to the outflow | (i) Assumptions cannot be tested under panic situations (i) - | |
| [62] | Chattaraj et al. (2009) | Straight line | Narrow passageway | | | | | | | | | | (i) Free flow speed keeps the same between Indian and German participants (ii) German tend to have more minimum personal space than Indian (iii) German are more sensitive to the increase in density than Indian (iv) The length of corridor does not have influence on the fundamental diagram | (i) Lack of a method that can measure the dependence of fundamental diagram on security distance (i) - | |

TABLE I: Continued.

| Ref. | Source | Movement Type | Infrastructure | | Subject | | Controllability | | | Competitiveness | | | Panic | Key Findings | Summaries Limitations & Future Recommendations | Further Data Usage |
|-------|-------------------------|-------------------------|-------------------|------------|----------|--------|-----------------|------------|-------|-----------------|-----------|---|--|---|---|-----------------------|
| | | | Facility Type | Bottleneck | Obstacle | Animal | Pedestrian | Laboratory | Field | Normal | Emergency | | | | | |
| [75] | John et al. (2009) | Straight line (Ants) | Nature path | | | ● | | ● | | | | ● | (i) No overtaking behavior in straight movement ants trails (ii) No jammed branch for ant traffic in straight movement (iii) No hysteresis and synchronized flow in ant traffic | (i) Lack of the exploration of analogy between ants traffic system and other traffic systems such as vehicular flow and pedestrian flow | (i) – | |
| [61] | Liu et al. (2009) | Straight line | Narrow passageway | | ● | | ● | | | | | ● | (i) Lateral oscillation remains 5.5 cm at free flow (ii) With the increase of density, the velocity drops, the lateral oscillation rises and the time headway surges | (i) No clear explanation on the differences with Seyfried et al. (2015)'s results | (i) – | |
| [181] | Moussaïd et al. (2009) | Straight line; Opposing | Narrow corridor | ● | ● | | ● | | | | | ● | (i) Individual evading behaviors for straight and opposing situations are different (ii) Side preference can be interpreted as a coordination behavior or a cultural bias | (i) Successive interaction with other people should be investigated | (i) – | |
| [21] | Seyfried et al. (2009) | Egress | Narrow corridor | ● | ● | | ● | | | | | ● | (i) Bottleneck capacity rises with the widen of width (ii) Jam can occur at below max. capacity situation (iii) Zipper effect starts to be observed at the bottleneck width of 0.7m (iv) Absolute values and figures from a lab experiment cannot simply be adopted for design usage. | (i) Panic and emergency situation have not been considered | (i) – | |
| [120] | Shiwakoti et al. (2009) | Egress (Ants) | Chamber | ● | ● | | ● | | | | | ● | (i) Placement of obstacle near the exit can increase the flow in general cases (ii) Corner exits tend to have higher flow comparing to middle exits in squared chambers | (i) Lack of human empirical data on obstacle performance and exit location effect | (i) Development of an animal-based microscopic model [7, 127]. (ii) Study the effect of obstacle on egress dynamics [123]. | |

TABLE I: Continued.

| Ref. | Source | Movement Type | | Infrastructure | | Subject | | Controllability | | | Competitiveness | | | Summaries | | Further Data Usage |
|-------|-------------------------------|---------------------------------------|--------------------------|----------------|--------|------------|------------|-----------------|--------|-----------|--|---|--|-----------|--|--------------------|
| | | Facility Type | Bottleneck | Obstacle | Animal | Pedestrian | Laboratory | Field | Normal | Emergency | Panic | Key Findings | Limitations & Future Recommendations | | | |
| [83] | Yanagisawa et al. (2009) | Turnings Egress | Wide-changing bottleneck | ● | ● | ● | ● | ● | ● | ● | <p>(i) The introduction of turning and conflicts functions to floor field model agree well with empirical data</p> <p>(ii) Outflow depends on the position of obstacle near the exits</p> <p>(iii) About four pedestrians are trying to exit at the same time when the exit width is 50cm</p> | <p>(i) The floor field model is not intelligent enough to capture the lane formation process as empirical data indicate</p> | (i) – | | | |
| [67] | Boltes et al. (2010) | Egress | Bottleneck corridor | ● | ● | ● | ● | ● | ● | ● | <p>(i) Automatic trajectories extraction can be realized in PeTrack with high accuracy in space and time based on markers</p> | <p>(i) The recognition approach needs to be replaced for marker-less tracking</p> | (i) Analysis of the bottleneck flow patterns [101, 102]. | | | |
| [8] | Burd et al. (2010) | Egress (Ants) | Chamber | ● | ● | ● | ● | ● | ● | ● | <p>(i) Obstacle can increase the ants' egress flow under normal nested situations</p> <p>(i) Capacity increases with the rise of stress level at 220cm width and the finding reverses at 110cm width</p> | <p>(i) Comparison of non-panic data with panic data is required</p> | (i) – | | | |
| [107] | Daamen and Hoogendoorn (2010) | Egress | Narrow door | ● | ● | ● | ● | ● | ● | ● | <p>(ii) Population with more children has the highest capacity (mean value of 3.31P/m/s)</p> <p>(iii) Population with 5% disabled people has the lowest capacity (mean value of 2.02P/m/s)</p> <p>(iv) The open door leads to more interactions between participants resulting in reduce in speed and outflow</p> | <p>(i) Latent factors on pedestrian dynamics should be analyzed</p> | (i) Data were used to calibrate several pedestrian simulation models [182] | | | |
| [150] | Versluis (2010) | Straight line; Intersecting; Opposing | Passageway in a hall | ● | ● | ● | ● | ● | ● | ● | <p>(i) 88% movements are related lateral and longitudinal interaction</p> <p>(ii) Approach side has no effect on the overtaking side</p> <p>(iii) Pedestrians prefer larger lateral evasion in opposing condition and larger longitudinal evasion in intersecting condition</p> <p>(iv) As the rise of interacting angle, mean interaction point increases and mean longitudinal evasion decreases</p> | <p>(i) Variable selections, measurement and experimental setups should be improved</p> | (i) Collision avoidance behavior was analyzed [183] | | | |

TABLE I: Continued.

| Ref. | Source | Movement Type | | Infrastructure | | Obstacle | | Subject | | Controllability | | | Competitiveness | | | Panic | Key Findings | Summaries Limitations & Future Recommendations | Further Data Usage |
|-------|-------------------------|------------------------------------|------------------------------------|-----------------------------|------------|----------|--------|------------|------------|-----------------|--------|-----------|-----------------|-----------|--|---|--|---|-----------------------|
| | | Facility Type | Intersection | Facility Type | Bottleneck | Obstacle | Animal | Pedestrian | Laboratory | Field | Normal | Emergency | Normal | Emergency | | | | | |
| [155] | Wong et al. (2010) | Intersecting | Intersecting | Passageway in a stadium | | | | | | | | | | | | (i) Conflict-induced interactions increase with the angle (ii) People are less willing to follow the front pedestrian to reduce conflicts (iii) The capacity for intersecting flow grows with the increasingly imbalance of pedestrian density ratio | (i) Cultural factors should be considered in pedestrian models (ii) Field observation data should be collected for intersecting flows | (i) Further analysis on the look-ahead behavior of pedestrians [184] (ii) Using a Bayesian inference method to improve the current model [185] | |
| [154] | Plane et al. (2011) | Intersecting | Intersecting | Entrance area of a building | | | | | | | | | | | | (i) Nearest-neighbour kernel density method is suitable for the density estimation of human crowds (ii) Turning movements create push and delay in egress | (i) The flow characteristics have not been analyzed enough | (i) - | |
| [80] | Shiwakoti et al. (2011) | Turning; Egressing (Humans & Ants) | Turning; Egressing (Humans & Ants) | Circular chamber; Doorway | | | | | | | | | | | | (i) Column at the exit can increase the flow of panicking ants (iii) Observation of the in-store stampede shows consistency with ants experiments | (i) Need a scaling model to find the analogism between animals and humans quantitatively | (i) Develop an animal-based model to simulate unidirectional crowd movement [7] | |
| [103] | Song et al. (2011) | Egress | Egress | Wide-changing corridor | | | | | | | | | | | | (i) Compare with Kretz et al. (2006), densities outside the bottleneck region is the same, densities are higher and velocities are smaller inside the bottleneck (i) Use four density measurements methods and automatic video processing (ii) Specific flow is independent of corridor width under less congested situation without bottleneck (iii) Fundamental diagrams for different shapes of facilities are not comparable | (i) The explanation for the difference between the compared researches are not fully explained | (i) Further analyze of experiments data [104] | |
| [58] | Zhang et al. (2011) | Straight line; Merging | Straight line; Merging | Wide-changing corridor | | | | | | | | | | | | (i) Influence of crowd heterogeneity on the shape of fundamental diagrams has not been discussed | (i) - | | |

TABLE I: Continued.

| Ref. | Source | Movement Type | Infrastructure | | Subject | | Controllability | | | Competitiveness | | | Panic | Key Findings | Summaries | Limitations & Future Recommendations | Further Data Usage |
|-------|------------------------|-------------------------------|--------------------------|------------|----------|--------|-----------------|------------|-------|-----------------|-----------|--|-------|---|---|---|--------------------|
| | | | Facility Type | Bottleneck | Obstacle | Animal | Pedestrian | Laboratory | Field | Normal | Emergency | | | | | | |
| [159] | Boyce et al. (2012) | Merging | Stair-floor interface | | | | | | | | | | | (i) Location of stair-floor connections have influences on merging flows (ii) Population composition affects the merging patterns | (i) Lack of real panic data on merging flows | (i) - | |
| [81] | Dias et al. (2012) | Straight line; Turning (Ants) | Chamber | | | | | | | | | | | (i) Right angled path are 20% less efficient than straight path | (i) Design solutions are not proposed based on the results | (i) - | |
| [93] | Jelić et al. (2012) | Turning | Ring corridor | | | | | | | | | | | (i) Provide a measurement method for instantaneous fundamental diagrams (ii) Velocity-distance headway relations can be used to segment three linear regimes | (i) The overall cross-cultural comparison is weak | (i) - | |
| [169] | Ma et al. (2012) | Merging | Ultra high-rise building | | | | | | | | | | | (i) Merging behavior can affect the flow of evacuees (ii) Overtaking behavior can be frequently observed on the refugee floor | (i) It should be a more significant contribution if the individuals' entire evacuation process can be tracked | (i) - | |
| [94] | Moussaïd et al. (2012) | Turning; Opposing | Ring corridor | | | | | | | | | | | (i) Find the transition between organized and disorganized states in pedestrian traffic (ii) Unstable dynamics is the result of speed variations among pedestrians | (i) The underlying reason for the speed variations has not been explored | (i) - | |
| [124] | Soria et al. (2012) | Egress (Ants) | Chamber | | | | | | | | | | | (i) Selfish behavior does not exist in ants traffic (ii) Discover the faster-is-slower effect in escaping ants under different stress levels | (i) Lack of discussion and comparison with human empirical data | (i) Faster-is-slower effects of ants are revisited and compared with human crowds [128] | |

TABLE I: Continued.

| Ref. | Source | Movement Type | Infrastructure | | Subject | | Controllability | | | Competitiveness | | | Summaries | | Further Data Usage | |
|-------|-------------------------|---------------------------------------|-----------------|------------|----------|--------|-----------------|------------|-------|-----------------|-----------|-------|--------------|---|--|--|
| | | | Facility Type | Bottleneck | Obstacle | Animal | Pedestrian | Laboratory | Field | Normal | Emergency | Panic | Key Findings | Limitations & Future Recommendations | | |
| [151] | Zhang et al. (2012) | Opposing; Intersecting | Corridor | | | | ● | | | | | | | (i) Bi-directional flow is classified into stable separated lanes (SSL), dynamical multi-lanes (DML) flows with balanced and unbalanced flow ratio (BFR, UFR) (ii) Density measurement methods do not affect fundamental diagrams significantly (iii) Different ordering flows do not affect fundamental diagrams significantly | (i) Experiments under hyper-congested situation should be further conducted | (i) – |
| [84] | Zhang et al. (2012) | Turnings Merging | Corridor | | | | ● | | | | | | | (i) Present Voronoi diagrams for speed and density distribution over space for turning and merging flows (i) Pedestrians tend to accelerate their speed after merging | (i) No further analysis on turning movements considering locomotion characteristics | (i) Same data were used for developing PeTrack [186] |
| [125] | Boari et al. (2013) | Egress (Ants) | Chamber | | | | ● | | | | | | | (i) Ants' egress efficiency is independent of hurry degree (ii) Selfish egress behavior is not found in ants traffic (iii) Faster-is-slower effect is not observed | (i) The further underlying reasons for the results difference are not discussed well | (i) – |
| [86] | Burghardt et al. (2013) | Turning | Stairs | | | | ● | | | | | | | (i) Maximum specific flow values are up to 1.25m/s for upward movement and 1.22m/s for downward movement (ii) Stairs without bends are preferred | (i) Stairs evacuation data on turning bend section should be compared | (i) – |
| [97] | Dias et al. (2013) | Turning; Merging; Intersecting (Ants) | Complex chamber | | | | ● | | | | | | | (i) Turning angle affects escape flow significantly (ii) Clogging transitions can be found in intersecting flows | (i) Effects of intersecting and merging should be further investigated | (i) – |

TABLE I: Continued.

| Ref. | Source | Movement Type | Infrastructure | | Subject | Controllability | | | Competitiveness | | | Key Findings | Summaries Limitations & Future Recommendations | Further Data Usage | |
|-------|------------------------|---------------|----------------|------------|---------|-----------------|--------|------------|-----------------|-------|--------|--------------|--|---|--|
| | | | Facility Type | Bottleneck | | Obstacle | Animal | Pedestrian | Laboratory | Field | Normal | | | | Emergency |
| [156] | Wu and Lu (2013) | Weaving | Corridor | | | | | | | | | | (i) The effects of weaving are more significant within a region (ii) Flow values and flow ratios are significant with the operation of weaving area | (i) Safety indices for pedestrian weaving zones can be further established | (i) Level-of-service for pedestrian weaving zone were analyzed [187] |
| [73] | Zhang et al. (2013) | Straight line | Long street | | | | | | | | | | (i) Combine use of camera and active infrared counter (ii) A complete dataset of flow rate and velocity for high density straight flow (iii) Find the boundary effect of uni-directional dense laminar flow (iv) Multi-directional flow data cannot be directly applied to uni-directional flow | (i) Measurements cannot reach individual trajectory level (ii) Personal and crowd collective factors are not investigated (iii) Data availability and usability are unknown | (i) - |
| [163] | Aghabayk et al. (2014) | Merging | Corridor | | | | | | | | | | (i) Crowd arrival and departure flow increase with the rise of desired speed (ii) Time headways decrease with speed (iii) Merging angle affects flow and headways | (i) Lack of detailed analysis within the merging regions | (i) More detailed analysis in a journal paper [162] |
| [77] | Dias et al. (2014) | Turning | Corridor | | | | | | | | | | (i) Speed tends to reduce at a fixed region around turning point (ii) The speed reduction increases with the rise of merging angle | (i) Sample size is not enough (ii) High density situation should be investigated | (i) Develop the optimal trajectories method for turning manoeuvres [89] |
| [105] | Liao et al. (2014) | Egressing | Wide door | | | | | | | | | | (i) The density and speed inside the bottleneck are independent on the width of door (ii) A linear dependency is observed between flow and bottleneck width | (i) The flow and density are calculated using the trajectories under both stable and unstable state | Trajectories were further utilized to test a method that can measure the steady flow state [188] |

TABLE I: Continued.

| Ref. | Source | Movement Type | | Infrastructure | | Subject | | Controllability | | | Competitiveness | | | Summaries | | Further Data Usage |
|-------|---------------------------|----------------------|----------------------|----------------|--------|------------|------------|-----------------|--------|-----------|-----------------|--------------|--------------------------------------|---|--|--|
| | | Facility Type | Bottleneck | Obstacle | Animal | Pedestrian | Laboratory | Field | Normal | Emergency | Panic | Key Findings | Limitations & Future Recommendations | | | |
| [129] | Sobhani et al. (2014) | Egressing (woodlice) | Chamber | ● | ● | ● | ● | ● | ● | ● | ● | ● | ● | (i) Fundamental diagrams near exit regions for animal flow have differences in normal and panic situations. (ii) Stress level of woodlice has positive relation with the number of blockages near the exit | (i) Quantitative comparison between animals and humans should be conducted to test their hypothesis | (i) More detailed analysis with the same datasets [130] |
| [189] | Sun et al. (2014) | Opposing; Weaving | Corridor | ● | ● | ● | ● | ● | ● | ● | ● | ● | ● | (i) Weaving conflicts tends to be centralized within a stable region (ii) Lane changing behaviors are modelled in weaving movements | (i) The asymmetric of weaving area location may arise from the organization of experiments | (i) Data were further analyzed to reproduce subway corridor flow [190] |
| [109] | Garcimartin et al. (2014) | Egress | Room | ● | ● | ● | ● | ● | ● | ● | ● | ● | ● | (i) Time headways display a heavy-tailed distribution (ii) Burst sizes fit an exponential function | (i) Steady state flows should be measured to fit the model | (i) Extended analysis were conducted [110] |
| [138] | Zurigueta et al. (2014) | Egress (Sheep) | Width-changing fence | ● | ● | ● | ● | ● | ● | ● | ● | ● | ● | (i) Time headways for sheep passing the bottleneck displays a power-law distribution (ii) The burst sizes for sheep flock obey an exponential decay (iii) Universal laws that can describe the flow and clogs of different particle systems are established | (i) Require more real life empirical data on human egress considering the effect of obstacle size and position | (i) Use the sheep data to study the effect of door width and obstacle placement on sheep flow [139] (ii) Effect of obstacle position on flow and clogging patterns were further studied [140] |
| [111] | Bode et al. (2015) | Egress | Room | ● | ● | ● | ● | ● | ● | ● | ● | ● | ● | (i) Social grouping behavior has negative effects on egress efficiency (ii) No clear time differences can be found between individual and group movements in front of the exits | (i) Samples might not be enough | (i) - |

TABLE I: Continued.

| Ref. | Source | Movement Type | Infrastructure | | Subject | | Controllability | | | Competitiveness | | | Summaries | | Further Data Usage | |
|-------|-------------------------|---------------|-------------------------|------------|----------|--------|-----------------|------------|-------|-----------------|-----------|-------|--------------|--|--|--|
| | | | Facility Type | Bottleneck | Obstacle | Animal | Pedestrian | Laboratory | Field | Normal | Emergency | Panic | Key Findings | Limitations & Future Recommendations | | |
| [88] | Dias et al. (2015) | Turning | Angle-changing corridor | | | ● | ● | ● | ● | ● | | | | (i) Longitudinal spacing between pedestrians tends to rise as speed increases (ii) Speed levels affect flow-density and speed-spacing relationships (i) Among Chinese students, walking in the right-hand side can accelerate the lane formation process (ii) Obstacle can help to stable intersecting flows | (i) Require further investigation on the combined effects under complex environments (i) The effect of smoothing the corners of the intersection can be a future work | (i) Data were utilized to calibrate a cellular automation model [79] |
| [157] | Lian et al. (2015) | Intersecting | Corridor | ● | ● | ● | ● | ● | ● | ● | | | | (i) Find the speed variation, step fluctuation and delay from Stop-and-Go waves in single-file ring movement (i) Pedestrian tends to reduce velocity in merging zone (ii) The speed reduction is significantly with merging angle and desired speed (iii) The speed reduction can impede the flow of out stream corridor (i) Experiments with more participants should be conducted (ii) Effect of blocked vision should be studied | (i) Insides of flow characteristics are not presented | (i) – |
| [95] | Kuang et al. (2015) | Turning | Ring path | | ● | ● | ● | ● | ● | ● | | | | | (i) – | |
| [166] | Shiwakoti et al. (2015) | Merging | Corridor | | ● | ● | ● | ● | ● | ● | | | | | (i) – | |
| [121] | Wang et al. (2015) | Egress (Ants) | Chamber | ● | ● | ● | ● | ● | ● | ● | | | | (i) Accuracy of data extraction should be improved (ii) Mean flow is independent linearly on the exit width (iii) Exit width affects the time headway (iv) Ant's group size affects the flow at certain exit width | (i) Accuracy of data extraction should be improved | (i) – |

TABLE I: Continued.

| Ref. | Source | Movement Type | Infrastructure | | Subject | | Controllability | | | Competitiveness | | | Key Findings | Summaries Limitations & Future Recommendations | Further Data Usage |
|-------|-----------------------|---------------|-----------------------|------------|----------|--------|-----------------|------------|-------|-----------------|-----------|-------|---|--|-----------------------|
| | | | Facility Type | Bottleneck | Obstacle | Animal | Pedestrian | Laboratory | Field | Normal | Emergency | Panic | | | |
| [63] | Zhang et al. (2015) | Straight line | Narrow corridor | | | | | ● | ● | ● | | | (i) Boundary has an effect on fundamental diagram (ii) Higher maximal specific flow can be detected under open boundary condition (iii) Stop-and-go waves can be observed under closed boundary condition | (i) Lack of empirical data of high density situations for this setup (i) - | |
| [116] | Ezaki et al. (2016) | Ingress | Room | ● | | | | ● | ● | ● | | | (i) Individual prefers to select location near corner and wall (ii) Flow avoidance, boundary preference, distance cost and angle cost are modelled | (i) Design and guidance solutions for ingress can be further presented (i) - | |
| [42] | Gorrini et al. (2016) | Opposing | Corridor | | | | | ● | ● | ● | | | (i) Higher flow ratio has negative influence on speed (ii) Walking in group is less efficient than individual walker | (i) The impact of coordination movement should be further investigated (i) - | |
| [161] | Huo et al. (2016) | Merging | Stair-floor interface | | | | | ● | ● | ● | | | (i) Merging movement at stair landings decrease the speed and increase the total evacuation time | (i) More detailed analysis on the interaction mechanisms on the stair-floor interfaces are required (i) - | |
| [133] | Lin et al. (2016) | Egress (Mice) | Room | ● | ● | ● | ● | ● | ● | ● | | | (i) Burning joss-sticks can be used to stimulate mice to different stress levels (ii) Egress time and the number of clogs increase with levels of stimulus (iii) Faster-is-slower effect is observed | (i) The quantitative relationships between the stress levels of the mice and the burning of joss-sticks should be presented (ii) The effect of obstacle was further analyzed [134] (iii) The effect of exit position was further analyzed [136] (iii) The effect of bottleneck width was further analyzed [135] | |

TABLE I: Continued.

| Ref. | Source | Movement Type | Infrastructure | | Subject | | Controllability | | | Competitiveness | | | Panic | Key Findings | Summaries Limitations & Future Recommendations | Further Data Usage |
|-------|-----------------------|--------------------|----------------|------------|----------|--------|-----------------|------------|-------|-----------------|-----------|---|---|--|--|-----------------------|
| | | | Facility Type | Bottleneck | Obstacle | Animal | Pedestrian | Laboratory | Field | Normal | Emergency | | | | | |
| [191] | Liu et al. (2016) | Ingress; Egress | Room | ● | ● | ● | ● | ● | ● | ● | ● | ● | (i) Ingress order has significant influence on the location of people in steady state and the egress order (ii) Crowd distribution in steady state is not uniform (iii) Inactive person may affect inflow and outflow process | (i) The method to detect steady state is questionable (i) – | | |
| [117] | Liu et al. (2016) | Ingress | Room | ● | ● | ● | ● | ● | ● | ● | ● | ● | (i) Ingress order is significant with individual's location distribution in the steady state and the egress order. (ii) Inactive pedestrians contribute a negative effect on the movement | (i) The effects of inhomogeneous composition are not necessarily negative (i) – | | |
| [114] | Nicolas et al. (2016) | Egress | Room | ● | ● | ● | ● | ● | ● | ● | ● | ● | (i) Flow increases monotonically with density (ii) Selfishness behavior may impede the egress flow at bottleneck (iii) A generalized zipper effect is observed (iv) Faster-is-slower effect is not observed | (i) Latent parameter effects should be further analyzed (i) A more comprehensive journal paper [115] | | |
| [3] | Shi et al. (2016) | Merging | Corridor | | | | | | | | | | (i) Merging angle and flow direction affect flow characteristics such as flow and time headway (ii) Blocked vision effects can be found at merging section (iii) Branched merging flow is less safe than opposed merging flow | (i) Safety indices for merging section should be established (ii) Level-of-service for merging region should be evaluated (i) Further analysis of merging case [38] (ii) Further analysis of vision condition [192] | | |

TABLE I: Continued.

| Ref. | Source | Movement Type | Infrastructure | | Subject | | Controllability | | | Competitiveness | | | Key Findings | Summaries Limitations & Future Recommendations | Further Data Usage |
|-------|--|------------------------------|-------------------------|------------|----------|--------|-----------------|------------|-------|-----------------|-----------|-------|---|--|--|
| | | | Facility Type | Bottleneck | Obstacle | Animal | Pedestrian | Laboratory | Field | Normal | Emergency | Panic | | | |
| [164] | Shahhoseini et al. (2016) | Merging (Ants) | Angle-changing chamber | ● | ● | ● | ● | ● | ● | ● | ● | ● | (i) Merging layouts can create stop-and-go waves (ii) Merging angle affects traffic flow characteristics | (i) Comparison analysis with human data are needed | (i) Compare ants data with human experiments with similar setups [193] |
| [92] | Sun et al. (2016) | Turning | Angle-changing corridor | ● | ● | ● | ● | ● | ● | ● | ● | ● | (i) Smoothed turning curve point design based on the Beijing subway corridor angle (ii) Flow characteristics are significant with different angles and radii (iii) Right angle corridor has large impact on the cumulative density and mean speed | (i) The boundary materials of the corridor are not solid | (i) – |
| [113] | von Krüchten and Schadschneider (2016) | Egress | Square room | ● | ● | ● | ● | ● | ● | ● | ● | ● | (i) Queuing at the exit can shorten egress time comparing with board distribution (ii) Moving as a compact crowd can increase the egress flow | (i) Differences between ordered compactly movement and the bursts after dogs are not discussed | (i) More detailed analysis were published in a journal [112] |
| [76] | Wang and Song (2016) | Straight line; Egress (Ants) | Restricted passageway | ● | ● | ● | ● | ● | ● | ● | ● | ● | (i) No jam among stressed ants trails (ii) Speed seems to be constant with density | (i) Effect of stressfulness is not quantified | (i) – |
| [122] | Wang et al. (2016) | Egress (Ants) | Chamber | ● | ● | ● | ● | ● | ● | ● | ● | ● | (i) Stressed ants exhibit symmetry breaking (ii) Escape flow reaches the peak when the spacing of two exits is largest (iii) Social force model has different performance in terms of describing the traffic rules of ants and humans | (i) Comparison with human empirical data is encouraged | (i) – |

TABLE 1: Continued.

| Ref. | Source | Movement Type | Infrastructure | | Subject | | Controllability | | | Competitiveness | | | Panic | Key Findings | Summaries Limitations & Future Recommendations | Further Data Usage |
|-------|----------------------|---|----------------|------------|----------|--------|-----------------|------------|-------|-----------------|-----------|--|-------|--|--|-----------------------|
| | | | Facility Type | Bottleneck | Obstacle | Animal | Pedestrian | Laboratory | Field | Normal | Emergency | | | | | |
| [13] | Cao et al. (2017) | Straight line; Opposing; Intersecting | Corridor | | | | | • | | | | | | (i) The difference in the effects of measurements of fundamental diagrams gradually appears as the increase of density level (ii) No difference is found between bi-directional and four-directional flows in fundamental diagrams under same density level (i) Merging impedes the evacuation efficiency in tunnel (ii) Merging decreases the rail car flow and the walkway flow (iii) As the increase of height difference between rail car exit and walkway, the more walkway flow dominates the flow (iv) No gender effects can be found in deference behavior | (i) Microscopic properties should be further analyzed for uni-, bi-, four-directional flows | (i) - |
| [17] | Cuesta et al. (2017) | Merging | Tunnel | • | • | • | • | • | | | | | | (i) Experiments should be conducted in real tunnel for more realism | (i) - | |
| [165] | Lian et al. (2017) | Merging | Corridor | • | • | • | • | • | | | | | | (i) Lane formation can be found in main flow (ii) Main and branched flow can be mutual bottleneck when the flow saturated at the 2.4m width branched corridor (iii) Speed in main channel decreases as the approaching of merging areas in 1.6m and 2.4m corridors (i) Uni-directional flow experiment exhibits four traffic states: free flow, congested, over-congested and hyper congested state (ii) Transition from stopped state and moving state can be observed under hyper-congested situation (iii) Flow rates in over-capacity situation are almost constant (iv) Three types of lane formations could be found in bi-directional flows | (i) More statistical approaches should be applied to verify the effects of different variables | (i) - |
| [60] | Jin et al. (2017) | Turning | Ring corridor | | • | • | • | • | | | | | | (i) The segmentation of steady flow states is done by manual observation | (i) - | |

TABLE I: Continued.

| Ref. | Source | Movement Type | Infrastructure | | Subject | | | Controllability | | | Competitiveness | | | Panic | Key Findings | Summaries Limitations & Future Recommendations | Further Data Usage |
|-------|---------------------------|------------------------|-----------------------------------|------------|----------|--------|------------|-----------------|-------|--------|-----------------|---|---|---|---|--|-----------------------|
| | | | Facility Type | Bottleneck | Obstacle | Animal | Pedestrian | Laboratory | Field | Normal | Emergency | | | | | | |
| [137] | Oh and Park (2017) | Egress (Mice) | Angle-changing chamber | ● | ● | ● | ● | ● | ● | ● | ● | ● | ● | (i) Mice do not often follow the ideal route (ii) Total mean velocity, total egress time decrease with the exit angle | (i) Empirical validation with human crowd data should be considered | (i) – | |
| [96] | Rahman et al. (2017) | Turning | Angle-changing corridor | ● | ● | ● | ● | ● | ● | ● | ● | ● | ● | (i) L-shaped corridor has the lowest average speed compared with 60° and 135° (ii) Participant prefers to walk in the inner side of the corridor due to the shorter walking distance | (i) More advanced statistical methods should be applied to examine the mixed variable effects | (i) – | |
| [170] | Shahhoseini et al. (2017) | Merging | Corridor | ● | ● | ● | ● | ● | ● | ● | ● | ● | ● | (i) Asymmetric setups can create more delays compared to symmetric setups (ii) Asymmetric setups also can create more imbalance between merging streams | (i) Further analysis within the merging sections should be conducted | (i) Find the faster-is-slower effects in merging sections [167] (ii) Compare the data with ants experiments [193] | |
| [68] | Sharifi et al. (2017) | Straight line; Turning | Loop corridor | ● | ● | ● | ● | ● | ● | ● | ● | ● | ● | (i) Homogenous flow experience a 75% capacity drop at bottleneck (ii) Disable people need more space to keep their desired speed (iii) Larger spacing is kept within the groups with wheelchair users | (i) Gait-level features of disabled people and normal people should be a further research direction | (i) Analysis of the data with a focus on speed distribution [90] and time headway [71] | |
| [91] | Sieben et al. (2017) | Ingress; Turning | Semicircle & right-angle corridor | ● | ● | ● | ● | ● | ● | ● | ● | ● | ● | (i) Spatial structures have influence on entrance dynamics in terms of density, waiting time and speed transition (ii) Constriction effects are found in both structures | (i) Experiments with single exit and dual exits can be further conducted | (i) – | |

TABLE I: Continued.

| Ref. | Source | Movement Type | Infrastructure | | Subject | | Controllability | | | Competitiveness | | Panic | Key Findings | Summaries Limitations & Future Recommendations | Further Data Usage |
|-------|----------------------|--------------------|------------------|------------|----------|--------|-----------------|------------|-------|-----------------|-----------|-------|---|--|---|
| | | | Facility Type | Bottleneck | Obstacle | Animal | Pedestrian | Laboratory | Field | Normal | Emergency | | | | |
| [152] | Xue et al. (2017) | Opposing | Ground with grid | | | | | | | | | | (i) Comparative experiments to examine the gridlock effect in CA model (ii) Gridlock is not spotted even under high density opposing flow | (i) Different competitiveness levels should be considered | (i) - |
| [17] | Wagoum et al. (2017) | Diverging/ Turning | Corridor | | | | | | | | | | (i) Under normal situation people choice exit only concerned with shortest path (ii) Under high density situation, the load balancing for two exits can be detected (i) Young people tend to control the lateral movement better than the aged people (ii) Step length increases as the rise of velocity and they exhibit a quadratic relation for three groups (iii) Gender and height effects on fundamental diagrams are not found | (i) Experiment data under emergency situations should be used for comparison [194] | (i) Further development of a route choice model [194] |
| [66] | Cao et al. (2018) | Straight line | Narrow corridor | | | | | | | | | | (i) More statistical analysis should be applied to test the significance among the relations (i) The width and length of corridor are fixed (ii) Extra obstacle effects are not considered | (i) Study the heterogeneous crowd considering age composition [64] | (i) - |
| [158] | Sun et al. (2017) | Egress | Narrow corridor | | | | | | | | | | (i) Use of funnel shape exit design with different angles (ii) The optimal funnel angle is between 46° to 65° | (i) The width and length of corridor are fixed (ii) Extra obstacle effects are not considered | (i) - |

TABLE I: Continued.

| Ref. | Source | Movement Type | Infrastructure | | Subject | | Controllability | | | Competitiveness | | | Key Findings | Summaries Limitations & Future Recommendations | Further Data Usage |
|-------|--------------------|-------------------------|-----------------------|------------|----------|--------|-----------------|------------|-------|-----------------|-----------|-------|--|--|---|
| | | | Facility Type | Bottleneck | Obstacle | Animal | Pedestrian | Laboratory | Field | Normal | Emergency | Panic | | | |
| [158] | Sun et al. (2017) | Intersecting | Ground | ● | ● | ● | ● | ● | ● | ● | ● | ● | (i) Effects of 5 types of intersecting angle and obstacle implement under three flow conditions are investigated (ii) The influences of angles on flow operation speed vary at different flow conditions | (i) The effects of obstacle shapes and positions are not considered | (i) Obstacle effects in intersecting roundabout region is further studied [149] |
| [65] | Wang et al. (2018) | Straight line | Narrow passageway | | ● | ● | ● | ● | ● | ● | ● | ● | (i) Effects of height on step length and duration change with density (ii) Step length & frequency-speed relations can be better described by power function (iii) Swaying amplitude-speed relations can be segmented into two regimes | (i) Unintended factors affecting the stepping characteristics should be eliminated | (i) – |
| [153] | Wang et al. (2018) | Straight line; Opposing | Restricted passageway | ● | ● | ● | ● | ● | ● | ● | ● | ● | (i) Ants show unified sensitivity to distance headway in both uni- and bi-directional flow (ii) Head-on encounter and evading behaviors can be frequently observed (iii) Ants spend more time for encounter communication than humans (iv) Following behavior of ants can improve the flow of opposing movement | (i) Quantitative comparison with empirical data in bi-directional vehicular traffic and pedestrian traffic is encouraged | (i) – |

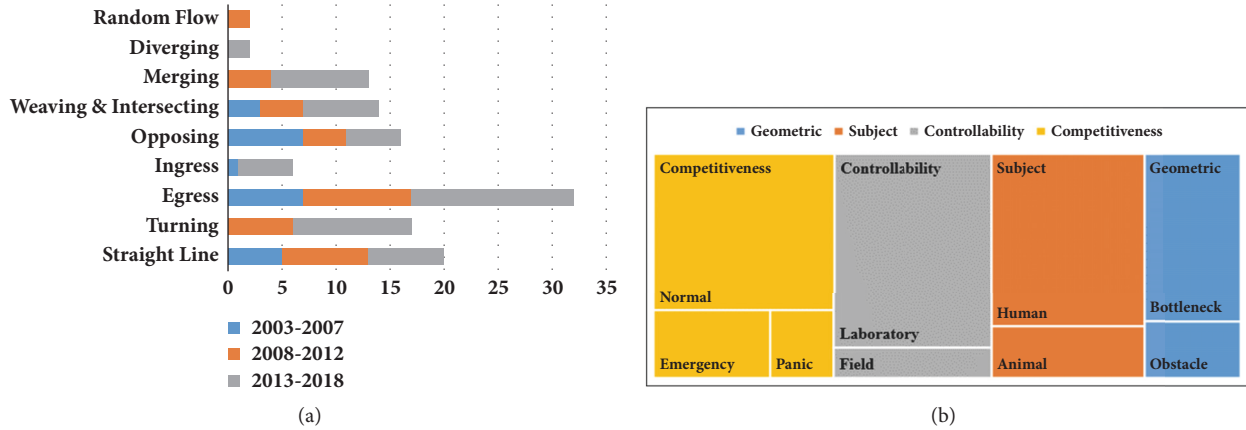


FIGURE 3: Summary statistics from Table 1. (a) Histogram diagram illustrating the distributions of the quantity and proportion of empirical studies on different multidirectional movements over different time periods. (b) Tree map to compare the proportion of the empirical study that focused on competitiveness, controllability, subjects, and geometric conditions.

In addition to the flow-based summary, we also present the comparison of contextual-based statistics of the reviewed studies in a set of nested rectangles as shown in Figure 3(b). The hierarchy of data generated from Table 1 in terms of the geometric (bottleneck or obstacle), investigating subject (human or animal), controllability (laboratory experiment or field observation), and competitiveness (normal or emergency or panic status) is presented in Figure 3(b).

Overall, laboratory experiments occupy the predominant proportion compared with field observations. In addition, the majority of empirical evidences are in human subjects while it is minor in biological entities. Regarding the study on competitive behavior, studies are mostly conducted under normal status but less in emergency and panic situations. Therefore, in future, empirical studies that can improve our understanding on mechanisms of multidirectional movements under emergency situations need to be investigated.

4.2. SWOT Analysis for Empirical Data Collection Approaches.

During the review process, we find that the data collection methods can have substantial influences on the obtained results. To help researchers select the suitable approach to satisfy their data requirements, assessments of different data collection approaches in terms of their underlying internal advantages and disadvantages as well as the potential external factors that can exploit or obstruct the advantages are needed.

Therefore, we perform comparative SWOT (Strengths, Weaknesses, Opportunities, and Threats) analysis for different data collection methods to identify the positive and negative prospects and classifying them into internal (Strengths and Weaknesses) and external (Opportunities and Threats) factors [195].

We conducted a first set of SWOT analysis to examine the variations of controllability of experiments between laboratory experiments versus field observations.

The utmost advantage for laboratory experiments is the strong controllability towards investigating targets that satisfied the straightforward requirements. Researchers can set up the predesigned walking environment, select the satisfying

participants, choose the intended data measurement techniques, or even define the manners of movements by giving instructions or pressing forces to the participants. Through such purpose-oriented approach, the specific influencing factors of the crowd movements can be examined one by one in a flexible manner and in detail. Therefore, empirical data from laboratory experiments should be the suitable materials for the development of microscopic models. However, the benefits of the well controllability for laboratory experiments may have to tradeoff with the risk of not completely representing the real-life situation. For instance, differences between the pedestrian movements during emergency escape and laboratory experiments have been quantitatively compared in Shiwakoti (2016) [196]. It is suggested that the physiological aspects of pedestrian should be further examined such as the effect of peoples' consciousness of their involvement in an experiment on their performed behaviors [197]. Moreover, not all the factors are controllable especially in animal experiments. This is perhaps the right reason for the absence of opposing experiments using biological entities. Further, due to the simplifications of the experiment setups, the effects of latent uncontrolled variables can also affect the global results and such effects might be amplified due to the control of certain variables. Therefore, in the future, in-depth statistical analysis should be conducted to examine the interactions of manifest and latent variables of pedestrian dynamics by using more comprehensive empirical datasets. Nevertheless, the advancements made on data collection and analysis techniques as well as optimal experimental design methods may help increase the size of the database, improve the data accuracy of experiments, and reduce the time and labour costs of the researchers.

With regard to field observation, the major pros for this approach are the authenticity of data quality and the relative lower baseline requirement to carry out the field observation. Field data can represent the real-life circumstance giving no other effects such as the subjects' awareness of being monitored. In addition, it can be easily implemented, e.g., placing a camera at a fixed location or even using the

TABLE 2: SWOT analysis for laboratory experiments versus field observations.

| Laboratory Experiments | |
|---|---|
| Strengths | Weaknesses |
| (i) Specific dependent and independent variables can be controlled and examined one by one flexibly (ii) Repeated measures can be realized easily (iii) Save a lot of time comparing with field observation to capture the intended samples | (i) Discrepancy exists between real life situation (ii) Uncontrolled latent variables may have effects on the global dynamics (iii) Contextual limitations on the experiments targets and purposes |
| Opportunities | Threats |
| (i) The application of emerging data collection and processing methods can attract more researchers to perform experiments (ii) Optimal experiments design can help lower the cost and save the time (iii) A comprehensive empirical database can add on the values of current experimental data (iv) Advanced statistical approaches might improve the performance of empirical data in verification and validation processes | (i) Organization and performance of experiments require a lot of money and labour (ii) Data integration is hard due to the barriers among disciplines |
| Field Observations | |
| Strengths | Weaknesses |
| (i) Ground truth data (ii) Labour cost effective and easy to carry out (iii) Large quantity of existing datasets | (i) Take long time to obtain adequate samples (ii) Not easy to capture specific behavior compared with laboratory experiments (iii) Restrictions of access into certain areas or contexts |
| Opportunities | Threats |
| (i) Smart city can provide vast data source for collecting pedestrian movement behaviors (ii) Big data solutions might be able to reduce the need of data quality (iii) Advancement in image processing industry offer the chance to collect large scale field data | (i) Complex patterns and behaviors are difficult to recognize and capture from field data (ii) Privacy & security issues should be highlighted as the potential large scale in data volume (iii) Minimize the effects of the placement of cameras or UAVs on the investigating subjects |

exiting videos shot by surveillance devices. However, there are limitations of field observation as well. First of all, not all the areas or contexts are permitted to conduct field observation research because of privacy and security reasons. This point is particularly suitable to the unmanned aircraft vehicle (UAV) as many countries have banned UAVs and drones in their restricted airspaces. Second, it usually takes a long time period or requires switching various sites to capture the intended contexts and obtain the adequate samples. Fortunately, the emerging of smart cities and big data analytics provide opportunities for large field data collection from multiple sources. Recent technological advances in the imaging-sensing industry and the machine learning research community have made previously inaccessible data largely available. The imaging industry enables high-resolution (1080p) CCTV cameras to perform crowd monitoring. Therefore, real time field data collection and short term analysis of pedestrian crowd have been implemented in many cities [198]. Meanwhile, the ubiquity of smartphones has also offered various opportunities for collecting pedestrian traffic data in the real-life fields [199]. Consequently, the relating issues on personal privacy and public information security should also be the threats for this approach.

The highlights of the SWOT analysis for laboratory experiments and field observations are summarized in Table 2.

We further conducted a second set of SWOT analysis between animal-based approach versus human-based approach.

The foremost strength for animal-based approach is identified as the possibility of conducting real panic experiments using biological entities. Further, animal behaviors can be more easily captured through laboratory experiments or field observations with lower cost than human approaches. Although there exists obvious discrepancy between animal movement and human motion, the empirical data in panicking animals are also more 'life-like' than many mathematical models [36, 196]. There is opportunity to use the animal models to further improve our understanding of collective motion. For example, the communication and coordination mechanisms of ants can be further examined to develop the methods for controlling human crowd [127].

In terms of human-based approach, apart from the most apparent advantage of ground truth data, we also highlight the advantage of providing instructions to pedestrians as the secondary pro in conducting experiments with human subjects. However, human data show large contextual

TABLE 3: SWOT analysis for animal-based approaches versus human-based approaches.

| Animal-Based Approaches | |
|---|---|
| Strengths | Weaknesses |
| <ul style="list-style-type: none"> (i) Real panic experiments can be performed (ii) Relative lower cost than human experiments (iii) Can be more life-like than mathematical models | <ul style="list-style-type: none"> (i) Taxonomic differences in animals with humans (ii) Less convincing to some crowd researchers in terms of contextual realism |
| Opportunities | Threats |
| <ul style="list-style-type: none"> (i) Biological intelligence can be beneficial to mankind e.g. ants show more coordination in panic escape than humans (ii) Animal behaviors can be used as the education materials for children to augment their safety awareness in terms of evacuation (iii) Resolving optimal design issue in panic escape | <ul style="list-style-type: none"> (i) The universal law for the scaling of different species of biological entities with various body sizes (ii) Further analysis of the behavioural similarities and dissimilarities between animals and humans (iii) The selection of organisms for different experimental design (iv) Conduct experiments using panicking animals may arise debates from bestiarian |
| Human-Based Approaches | |
| Strengths | Weaknesses |
| <ul style="list-style-type: none"> (i) Ground truth data of real pedestrians (ii) Participants are more instructive than animals | <ul style="list-style-type: none"> (i) Panic experiments cannot be performed due to ethical and safety reasons (ii) Contextual dependency |
| Opportunities | Threats |
| <ul style="list-style-type: none"> (i) Emerging virtual interactive techniques such as AR and VR can help examine human behaviors in more extreme scenarios | <ul style="list-style-type: none"> (i) Risk free/immigration experimental design methods (ii) Physiological aspects of humans during collective movements should be further exploited |

dependency arising from both internal and external factors such as heterogeneity and behavioral uncertainty. Therefore, future empirical databases should be enriched with more psychological aspects [196]. In addition, one major con for human approach is the prohibition of performing dangerous panic experiments due to the ethical and safety reasons. However, the emerge of virtual interactive techniques such as augmented reality (AR) and virtual reality (VR) can help examine human behaviors in more extreme scenarios including the panic escape [200]. Also, researchers should also explore risk free or risk immigration experimental design methods to extend the research scopes to extreme behaviors.

The summaries of the SWOT analysis for animal-based approaches versus human-based approaches are presented in Table 3.

4.3. Future Global Collaborative Efforts on Empirical Data Collection. In the future, in order to accelerate the path of crowd dynamics research, a comprehensive open-source empirical database on root of the different external complex movement patterns and internal influence variables should be established. To realize this goal, interdiscipline collaborations should be encouraged. Some of the researchers from various disciplines have made their datasets available to the public such as open videos and trajectories datasets of controlled laboratory experiments [201], pedestrian crossing behaviors on street [202], field datasets of pedestrian's walking behaviors in train station, school forum or gallery [203–205], and collective motion databases for computer vision analysis [206]. All the above datasets contain pedestrian trajectories

and some of the researchers have also uploaded the original videos.

Therefore, mutual assistance and cooperation should be encouraged between research groups across disciplines and across regions around the world. A data-sharing platform should be established so that all researchers working in this field can contribute their datasets.

During our review study, we noticed that many empirical data are not well recorded and have little possibilities for further usage due to the limitations of experiments setups or measuring methods. Therefore, a common standard guidance on performing controlled experiments and field observations should be developed. Further, automatic image processing tools that can restore the trajectories from the published papers can be developed in future to make full use of the existing empirical studies.

Further, researchers working in this field should come together to establish a series of quantitative standardization methods to normalize the empirical data [207]. Also, a comprehensive guideline and standard for performing controlled laboratory experiments are required.

5. Conclusions

Collective motion of pedestrian traffic is sophisticated under complex environments. To better understand the underlying mechanism of collective crowd movements, a lot of empirical studies were carried out through controlled laboratory experiments and field observations with humans subjects and non-human biological entities under various scenarios. However, a comprehensive review of the detailed classification of these

empirical works from the aspects of complex movements was absent in the literature.

To this end, in this review article, we first categorized the complex movements of pedestrian crowd into two general categories, i.e., external governed movements and internal driven movements based on the governing factors of the motion pattern. Further, considering the hierarchy of movement complexity, we decomposed the external governed movements of pedestrian traffic into several motion based patterns including straight line, turning, egress and ingress, opposing, weaving, merging, diverging, and random flows. Then, we reviewed the related literatures under each motion based pattern with a focus on the complex movement characteristics. Further, a series of evaluations were performed towards each reviewed empirical study in terms of the geometrics setups (whether contained bottleneck or obstacle), investigating subjects (humans or animals), controllability (laboratory experiments or field observations), and competitiveness (under normal, emergency, or panic situations). Moreover, the key findings, limitations, or future recommendations and the further usage of the empirical data in other studies were summarized in a table.

Summary statistics from the aggregated table showed that empirical data were highly rich in straight line, egress flow, and medium rich in turning, merging, weaving, and opposing, but poor in ingress, diverging, and random flows. Researchers were more concerned with human subjects than animal subjects and laboratory experiments were more preferred than field observations. Empirical data were mostly collected under normal situations but less in emergency and panic conditions. Likewise, the studies on bottleneck effects were more popular than the obstacle effects.

We further presented the comparative SWOT analysis for different data collection approaches that included two comparisons: laboratory experiments versus field observation and animal-based approaches versus human-based approaches. At last, we put emphasis on the need for the future global collaborative efforts on data sharing and developing guideline for performing controlled laboratory experiments for the pedestrians complex movements.

Conflicts of Interest

The authors declare that they have no conflicts of interest.

Acknowledgments

This research is sponsored by National Science Foundation of China (no. 71701108) and National Science Foundation of Zhejiang Province (no. LQ17E080007). The third coauthor would like to acknowledge the funding received from ARC Linkage Project LP120200361 for his contribution in this paper.

References

- [1] X. Shi, *Empirical Investigation on Pedestrian Complex Movement Characteristics and Interaction Behaviors [Ph.D. thesis]*, Southeast University, 2018.
- [2] X. Shi, Z. Ye, N. Shiwakoti, and Z. Li, "A Review of Experimental Studies on Complex Pedestrian Movement Behaviors," in *Proceedings of the 15th COTA International Conference of Transportation Professionals, CICTP 2015*, pp. 1081–1096, American Society of Civil Engineers, Reston, VA, USA, 2015.
- [3] X. Shi, Z. Ye, N. Shiwakoti, D. Tang, C. Wang, and W. Wang, "Empirical investigation on safety constraints of merging pedestrian crowd through macroscopic and microscopic analysis," *Accident Analysis & Prevention*, vol. 95, pp. 405–416, 2016.
- [4] E. R. Galea, G. Sharp, and P. J. Lawrence, "Investigating the representation of merging behavior at the floor—stairs interface in computer simulations of multi-floor building evacuations," *Journal of Fire Protection Engineering*, vol. 18, no. 8, pp. 291–316, 2008.
- [5] D. Helbing, I. Farkas, and T. Vicsek, "Simulating dynamical features of escape panic," *Nature*, vol. 407, no. 6803, pp. 487–490, 2000.
- [6] R. Escobar and A. De La Rosa, "Architectural design for the survival optimization of panicking fleeing victims," in *Advances in Artificial Life*, pp. 97–106, 2003.
- [7] N. Shiwakoti, M. Sarvi, G. Rose, and M. Burd, "Animal dynamics based approach for modeling pedestrian crowd egress under panic conditions," *Procedia - Social and Behavioral Sciences*, vol. 17, pp. 438–461, 2011.
- [8] M. Burd, N. Shiwakoti, M. Sarvi, and G. Rose, "Nest architecture and traffic flow: large potential effects from small structural features," *Ecological Entomology*, pp. no–no, 2010.
- [9] D. Helbing, L. Buzna, A. Johansson, and T. Werner, "Self-organized pedestrian crowd dynamics: experiments, simulations, and design solutions," *Transportation Science*, vol. 39, no. 1, pp. 1–24, 2005.
- [10] N. Shiwakoti, M. Sarvi, and M. Burd, "Using non-human biological entities to understand pedestrian crowd behaviour under emergency conditions," *Safety Science*, vol. 66, pp. 1–8, 2014.
- [11] N. Shiwakoti, X. Shi, Z. Ye, Y. Liu, and J. Lin, "A comparative study of pedestrian crowd flow at middle and corner exits," in *Proceedings of the Australasian Transport Research Forum 2016*, 2016, http://atrf.info/papers/2016/files/ATRF2016_Full_papers_resubmission_147.pdf.
- [12] M. Asano, M. Kuwahara, and S. Tanaka, "Multi-directional pedestrian flow model based on empirical data," in *Proceedings of the 11th World Conference on Transport Research*, 2007, <http://trid.trb.org/view.aspx?id=877133>.
- [13] S. Cao, A. Seyfried, J. Zhang, S. Holl, and W. Song, "Fundamental diagrams for multidirectional pedestrian flows," *Journal of Statistical Mechanics: Theory and Experiment*, vol. 2017, no. 3, p. 033404, 2017.
- [14] M. Haghani and M. Sarvi, "Crowd behaviour and motion: Empirical methods," *Transportation Research Part B: Methodological*, vol. 107, pp. 253–294, 2018.
- [15] J. K. K. Yuen and E. W. M. Lee, "The effect of overtaking behavior on unidirectional pedestrian flow," *Safety Science*, vol. 50, no. 8, pp. 1704–1714, 2012.
- [16] Y. Zhao, T. Lu, M. Li, and L. Tian, "The self-slowng behavioral mechanism of pedestrians under normal and emergency conditions," *Physics Letters A*, vol. 381, no. 37, pp. 3149–3160, 2017.
- [17] A. U. Kemloh Wagoum, A. Tordeux, and W. Liao, "Understanding human queuing behaviour at exits: an empirical study," *Royal Society Open Science*, vol. 4, 2017.

- [18] M. Moussaïd, N. Perozo, S. Garnier, D. Helbing, and G. Theraulaz, "The walking behaviour of pedestrian social groups and its impact on crowd dynamics," *PLoS ONE*, vol. 5, no. 4, Article ID e10047, 2010.
- [19] S. P. Hoogendoorn and W. Daamen, "Self-organization in walker experiments," in *Traffic Granul. Flow '03*, p. 11, 2004.
- [20] S. P. Hoogendoorn and W. Daamen, "Pedestrian behavior at bottlenecks," *Transportation Science*, vol. 39, no. 2, pp. 147–159, 2005.
- [21] A. Seyfried, O. Passon, B. Steffen, M. Boltes, T. Rupperecht, and W. Klingsch, "New insights into pedestrian flow through bottlenecks," *Transportation Science*, vol. 43, no. 3, pp. 395–406, 2009.
- [22] D. J. Low, "Following the crowd," *Nature*, vol. 407, no. 6803, pp. 465–466, 2000.
- [23] D. Helbing, I. J. Farkas, and T. Vicsek, "Freezing by heating in a driven mesoscopic system," *Physical Review Letters*, vol. 84, no. 6, pp. 1240–1243, 2000.
- [24] D. Helbing, A. Johansson, and H. Z. Al-Abideen, "Crowd turbulence: the physics of crowd disasters," 2007, <https://arxiv.org/abs/0708.3339>.
- [25] X. Yang, Z. Wu, and Y. Li, "Difference between real-life escape panic and mimic exercises in simulated situation with implications to the statistical physics models of emergency evacuation: The 2008 Wenchuan earthquake," *Physica A: Statistical Mechanics and its Applications*, vol. 390, no. 12, pp. 2375–2380, 2011.
- [26] B. Krausz and C. Bauckhage, "Loveparade 2010: Automatic video analysis of a crowd disaster," *Computer Vision and Image Understanding*, vol. 116, no. 3, pp. 307–319, 2012.
- [27] D. Helbing and P. Mukerji, "Crowd disasters as systemic failures: analysis of the Love Parade disaster," *EPJ Data Science*, vol. 1, no. 1, 2012.
- [28] M. D'Orazio, L. Spalazzi, E. Quagliarini, and G. Bernardini, "Agent-based model for earthquake pedestrians' evacuation in urban outdoor scenarios: Behavioural patterns definition and evacuation paths choice," *Safety Science*, vol. 62, pp. 450–465, 2014.
- [29] Z. Gu, Z. Liu, N. Shiwakoti, and M. Yang, "Video-based analysis of school students' emergency evacuation behavior in earthquakes," *International Journal of Disaster Risk Reduction*, vol. 18, pp. 1–11, 2016.
- [30] G. Bernardini, E. Quagliarini, and M. D'Orazio, "Towards creating a combined database for earthquake pedestrians' evacuation models," *Safety Science*, vol. 82, pp. 77–94, 2016.
- [31] H. Gayathri, P. M. Aparna, and A. Verma, "A review of studies on understanding crowd dynamics in the context of crowd safety in mass religious gatherings," *International Journal of Disaster Risk Reduction*, vol. 25, pp. 82–91, 2017.
- [32] G. K. Still, "Crowd Disasters, Crowd Saf. Risk Anal," 2018, <http://www.gkstill.com/CV/ExpertWitness/CrowdDisasters.html>.
- [33] J. J. Fruin, "The causes and prevention of crowd disasters," in *Engineering for Crowd Safety*, pp. 1–10, 1993.
- [34] D. C. Duives, W. Daamen, and S. P. Hoogendoorn, "State-of-the-art crowd motion simulation models," *Transportation Research Part C: Emerging Technologies*, vol. 37, pp. 193–209, 2013.
- [35] V. J. Kok, M. K. Lim, and C. S. Chan, "Crowd behavior analysis: A review where physics meets biology," *Neurocomputing*, vol. 177, pp. 342–362, 2016.
- [36] T. Vicsek and A. Zafeiris, "Collective motion," *Physics Reports*, vol. 517, no. 3, pp. 71–140, 2012.
- [37] R. P. Roess, E. S. Prassas, and W. R. Mcshane, *Traffic Engineering*, Pearson/Prentice Hall, 2011.
- [38] N. Shiwakoti, X. Shi, Z. Ye, and W. Wang, "Empirical study on pedestrian crowd behaviour in right angled junction," in *Proceedings of the Australasian Transport Research Forum*, p. 12p, 2015.
- [39] X. Chen, M. Treiber, V. Kanagaraj, and H. Li, "Social force models for pedestrian traffic – state of the art," *Transport Reviews*, vol. 38, no. 5, pp. 625–653, 2018.
- [40] X. Jia, H. Yue, X. Tian, and H. Yin, "Simulation of pedestrian flow with evading and surpassing behavior in a walking passageway," *Simulation*, vol. 93, no. 12, pp. 1013–1035, 2017.
- [41] M. Haghani and M. Sarvi, "Following the crowd or avoiding it? Empirical investigation of imitative behaviour in emergency escape of human crowds," *Animal Behaviour*, vol. 124, pp. 47–56, 2017.
- [42] L. Crociani, A. Gorrini, K. Nishinari, and S. Bandini, "Social Groups and Pedestrian Crowds: Experiment on Dyads in a Counter Flow Scenario," in *Proceedings of the Proceedings of the 8th International Conference on Pedestrian and Evacuation Dynamics (PED2016)*, Hefei, China, 2016.
- [43] M. Kremer and L. G. Debo, "Herding in a Queue: A Laboratory Experiment," *SSRN Electronic Journal*, pp. 12–28, 2013.
- [44] G. K. Still, *Crowd Dynamics*, University of Warwick, 2000.
- [45] S. Hoogendoorn and W. Daamen, "Self-organization in pedestrian flow," in *Traffic Granul. Flow '03*, pp. 373–382.
- [46] D. Helbing, P. Molnár, I. J. Farkas, and K. Bolay, "Self-organizing pedestrian movement," *Environment and Planning B: Planning and Design*, vol. 28, no. 3, pp. 361–383, 2001.
- [47] D. Helbing, "Traffic and related self-driven many-particle systems," *Reviews of Modern Physics*, vol. 73, no. 4, pp. 1067–1141, 2001.
- [48] D. Helbing, A. Johansson, and H. Z. Al-Abideen, "Dynamics of crowd disasters: An Empirical Study," *Physical Review E: Statistical, Nonlinear, and Soft Matter Physics*, vol. 75, no. 4, Article ID 046109, 2007.
- [49] J. J. Fruin, *Pedestrian Planning and Design*, vol. 77, Elevator World, Inc, 1971.
- [50] *Transportation Research Board, Highway Capacity Manual*, National Research Council, Washington, DC, USA, 2010.
- [51] A. Gupta and N. Pundir, "Pedestrian flow characteristics studies: a review," *Transport Reviews*, vol. 35, no. 4, pp. 445–465, 2015.
- [52] U. Weidmann, *Transporttechnik der Fussgänger, Transporttechnische Eigenschaften des Fussgängerverkehrs (Literaturauswertung)*, 1993.
- [53] V. M. Predtechenskii and A. I. Milinskii, *Planning for Foot Traffic in Buildings (translated from the Russian)*, 1969.
- [54] R. A. Klein, *SFPE Handbook of Fire Protection Engineering*, 5th edition, 2016.
- [55] W. H. K. Lam, J. F. Morrall, and H. Ho, "Pedestrian flow characteristics in Hong Kong," *Transportation Research Record Journal of the Transportation Research Board*, vol. 1995, pp. 56–62, 1995.
- [56] W. Daamen and S. Hoogendoorn, "Controlled experiments to derive walking behaviour," *European Journal of Transport and Infrastructure Research*, vol. 3, pp. 39–59, 2003.
- [57] A. Seyfried, B. Steffen, W. Klingsch, and M. Boltes, "The fundamental diagram of pedestrian movement revisited," *Journal of Statistical Mechanics: Theory and Experiment*, no. 10, Article ID P10002, pp. 41–53, 2005.

- [58] J. Zhang, W. Klingsch, A. Schadschneider, and A. Seyfried, "Transitions in pedestrian fundamental diagrams of straight corridors and T-junctions," *Journal of Statistical Mechanics: Theory and Experiment*, vol. 2011, no. 6, Article ID P06004, 2011.
- [59] J. Zhang and A. Seyfried, "Empirical Characteristics of Different Types of Pedestrian Streams," *Procedia Engineering*, vol. 62, pp. 655–662, 2013.
- [60] C.-J. Jin, R. Jiang, S. C. Wong et al., "Large-scale pedestrian flow experiments under high-density conditions," 2017, <https://arxiv.org/abs/1710.10263>.
- [61] X. Liu, W. Song, and J. Zhang, "Extraction and quantitative analysis of microscopic evacuation characteristics based on digital image processing," *Physica A: Statistical Mechanics and its Applications*, vol. 388, no. 13, pp. 2717–2726, 2009.
- [62] U. Chattaraj, A. Seyfried, and P. Chakroborty, "Comparison of pedestrian fundamental diagram across cultures," *Advances in Complex Systems (ACS)*, vol. 12, no. 3, pp. 393–405, 2009.
- [63] J. Zhang, A. Tordeux, and A. Seyfried, "Effects of boundary conditions on single-file pedestrian flow," in *Proceedings of the 9th International Conference on Cellular Automata, ACRI 2014*, J. Wąs, G. C. Sirakoulis, and S. Bandini, Eds., pp. 462–469, Springer International Publishing, Cham, Switzerland, 2015.
- [64] S. Cao, J. Zhang, D. Salden, J. Ma, C. Shi, and R. Zhang, "Pedestrian dynamics in single-file movement of crowd with different age compositions," *Physical Review E: Statistical, Nonlinear, and Soft Matter Physics*, vol. 94, no. 1, 2016.
- [65] J. Wang, M. Boltes, A. Seyfried, J. Zhang, V. Ziemer, and W. Weng, "Linking pedestrian flow characteristics with stepping locomotion," *Physica A: Statistical Mechanics and its Applications*, vol. 500, pp. 106–120, 2018.
- [66] S. Cao, J. Zhang, W. Song, C. Shi, and R. Zhang, "The stepping behavior analysis of pedestrians from different age groups via a single-file experiment," *Journal of Statistical Mechanics: Theory and Experiment*, vol. 2018, no. 3, p. 033402, 2018.
- [67] M. Boltes, A. Seyfried, B. Steffen, and A. Schadschneider, "Automatic Extraction of Pedestrian Trajectories from Video Recordings," in *Pedestrian and Evacuation Dynamics*, W. W. F. Klingsch, C. Rogsch, A. Schadschneider, and M. Schreckenberg, Eds., pp. 43–54, Springer, Berlin, Germany, 2010.
- [68] M. S. Sharifi, K. Christensen, A. Chen, D. Stuart, Y. S. Kim, and Y. Chen, "A large-scale controlled experiment on pedestrian walking behavior involving individuals with disabilities," *Travel Behaviour and Society*, vol. 8, pp. 14–25, 2017.
- [69] M. S. Sharifi, *Analysis and modeling of pedestrian walking behaviors involving individuals with disabilities*, Utah State University, 2016, <https://digitalcommons.usu.edu/etd/4959>.
- [70] M. S. Sharifi, D. Stuart, K. Christensen, and A. Chen, "Traffic Flow Characteristics of Heterogeneous Pedestrian Stream Involving Individuals with Disabilities," *Transportation Research Record*, vol. 2537, pp. 111–125, 2015.
- [71] M. S. Sharifi, D. Stuart, K. Christensen, and A. Chen, "Time Headway Modeling and Capacity Analysis of Pedestrian Facilities Involving Individuals with Disabilities," *Transportation Research Record*, vol. 2553, pp. 41–51, 2016.
- [72] T. Kretz, A. Grünebohm, A. Kessel, H. Klüpfel, T. Meyer-König, and M. Schreckenberg, "Upstairs walking speed distributions on a long stairway," *Safety Science*, vol. 46, no. 1, pp. 72–78, 2008.
- [73] X. L. Zhang, W. G. Weng, H. Y. Yuan, and J. G. Chen, "Empirical study of a unidirectional dense crowd during a real mass event," *Physica A: Statistical Mechanics and its Applications*, vol. 392, no. 12, pp. 2781–2791, 2013.
- [74] J. L. Berrou, J. Beecham, P. Quaglia, M. A. Kagarlis, and A. Gerodimos, "Calibration and validation of the Legion simulation model using empirical data," in *Pedestrian and Evacuation Dynamics*, pp. 167–181, 2007.
- [75] A. John, A. Schadschneider, D. Chowdhury, and K. Nishinari, "Trafficlike collective movement of ants on trails: absence of a jammed phase," *Physical Review Letters*, vol. 102, no. 10, pp. 1–4, 2009.
- [76] S. Wang and W. Song, "Experimental Study of Ant Movement in a Straight Passageway under Stress Conditions," *Journal of Insect Behavior*, vol. 29, no. 6, pp. 735–743, 2016.
- [77] C. Dias, O. Ejtemai, M. Sarvi, and M. Burd, "Exploring Pedestrian Walking through Angled Corridors," *Transportation Research Procedia*, vol. 2, pp. 19–25, 2014.
- [78] C. Jin, R. Jiang, J. Yin, L. Dong, and D. Li, "Simulating bi-directional pedestrian flow in a cellular automaton model considering the body-turning behavior," *Physica A: Statistical Mechanics and its Applications*, vol. 482, pp. 666–681, 2017.
- [79] C. Dias and R. Lovreglio, "Calibrating cellular automaton models for pedestrians walking through corners," *Physics Letters A*, vol. 382, no. 19, pp. 1255–1261, 2018.
- [80] N. Shiwakoti, M. Sarvi, G. Rose, and M. Burd, "Consequence of Turning Movements in Pedestrian Crowds during Emergency Egress," *Transportation Research Record*, vol. 2234, no. 1, pp. 97–104, 2011.
- [81] C. Dias, M. Sarvi, N. Shiwakoti, and M. Burd, "Turning Angle Effect on Emergency Egress: Experimental Evidence and Pedestrian Crowd Simulation," *Transportation Research Record*, vol. 2312, no. 1, pp. 120–127, 2012.
- [82] A. Matsui, T. Mashiko, and T. Nagatani, "Traffic flow of mobile objects through obstacles: Turning and translational objects," *Physica A: Statistical Mechanics and its Applications*, vol. 388, no. 2–3, pp. 157–173, 2009.
- [83] D. Yanagisawa, A. Kimura, A. Tomoeda et al., "Introduction of frictional and turning function for pedestrian outflow with an obstacle," *Physical Review E: Statistical, Nonlinear, and Soft Matter Physics*, vol. 80, no. 3, Article ID 036110, 2009.
- [84] J. Zhang, W. Klingsch, T. Rupperecht, A. Schadschneider, and A. Seyfried, *Empirical Study of Turning And Merging of Pedestrian Streams in T-Junction*, 2011.
- [85] N. Shiwakoti, M. Sarvi, C. Dias, and M. Burd, "Understanding crowd panic at turning and intersection through model organisms," in *Pedestrian and Evacuation Dynamics*, pp. 1175–1183, Springer International Publishing, Cham, Switzerland, 2014.
- [86] S. Burghardt, A. Seyfried, and W. Klingsch, "Performance of stairs—fundamental diagram and topographical measurements," *Transportation Research Part C: Emerging Technologies*, vol. 37, pp. 268–278, 2013.
- [87] C. Dias, O. Ejtemai, M. Sarvi, and N. Shiwakoti, "Pedestrian Walking Characteristics through Angled Corridors," *Transportation Research Record*, vol. 2421, no. 1, pp. 41–50, 2014.
- [88] C. Dias, M. Sarvi, O. Ejtemai, and M. Burd, "Elevated Desired Speed and Change in Desired Direction," *Transportation Research Record*, vol. 2490, pp. 65–75, 2015.
- [89] C. Dias, M. Sarvi, and M. Asano, "Optimal trajectories for constrained pedestrian turning manoeuvres," in *Proceedings of the 8th International Conference on Pedestrian and Evacuation Dynamics*, pp. 1–9, Hefei, China, 2016.
- [90] M. S. Sharifi, D. Stuart, K. Christensen, A. Chen, Y. S. Kim, and Y. Chen, "Analysis of walking speeds involving individuals with disabilities in different indoor walking environments," *Journal of Urban Planning and Development*, vol. 142, no. 1, 2014.

- [91] A. Sieben, J. Schumann, A. Seyfried, and D. R. Chialvo, "Collective phenomena in crowds—Where pedestrian dynamics need social psychology," *PLoS ONE*, vol. 12, no. 6, p. e0177328, 2017.
- [92] L. Sun, L. Cui, S. Qiu, L. Yao, and J. Rong, "Impact on pedestrian flow of bends in passenger access tunnels," *Proceedings of the Institution of Civil Engineers - Transport*, pp. 1–10, 2017.
- [93] A. Jelić, C. Appert-Rolland, S. Lemerrier, and J. Pettré, "Properties of pedestrians walking in line: Fundamental diagrams," *Physical Review E: Statistical, Nonlinear, and Soft Matter Physics*, vol. 85, no. 3, 2012.
- [94] M. Moussaïd, E. G. Guilloit, M. Moreau et al., "Traffic instabilities in self-organized pedestrian crowds," *PLoS Computational Biology*, vol. 8, no. 3, Article ID e1002442, 2012.
- [95] H. Kuang, M.-J. Cai, X.-L. Li, and T. Song, "Asymmetric effect on single-file dense pedestrian flow," *International Journal of Modern Physics C*, vol. 26, no. 6, 1550064, 13 pages, 2015.
- [96] N. A. Rahman, N. A. Alias, and S. H. M. Adenan, "Empirical investigation of trajectories and desired walking velocity of pedestrian walking through angled-corridor," in *AIP Conference Proceedings*, AIP Publishing LLC, 2017.
- [97] C. Dias, M. Sarvi, N. Shiwakoti, O. Ejemai, and M. Burd, "Investigating collective escape behaviours in complex situations," *Safety Science*, vol. 60, pp. 87–94, 2013.
- [98] R. Nagai, M. Fukamachi, and T. Nagatani, "Evacuation of crawlers and walkers from corridor through an exit," *Physica A: Statistical Mechanics and its Applications*, vol. 367, pp. 449–460, 2006.
- [99] J. Zhang, W. Song, and X. Xu, "Experiment and multi-grid modeling of evacuation from a classroom," *Physica A: Statistical Mechanics and its Applications*, vol. 387, no. 23, pp. 5901–5909, 2008.
- [100] T. Kretz, A. Grünebohm, and M. Schreckenberg, "Experimental study of pedestrian flow through a bottleneck," *Journal of Statistical Mechanics: Theory and Experiment*, vol. 2006, no. 10, pp. P10014–P10014, 2006.
- [101] J. Liddle, A. Seyfried, B. Steffen et al., "Microscopic insights into pedestrian motion through a bottleneck, resolving spatial and temporal variations," 2011, <https://arxiv.org/abs/1105.1532>.
- [102] J. Liddle, A. Seyfried, and B. Steffen, "Analysis of bottleneck motion using Voronoi diagrams," in *Pedestrian and Evacuation Dynamics*, pp. 833–836, 2010.
- [103] W. Song, J. Zhang, and A. Seyfried, "Experimental Study of Pedestrian Flow in the Channel through Bottleneck," in *Pedestrian and Evacuation Dynamics*, R. D. Peacock, E. D. Kuligowski, and J. D. Averill, Eds., pp. 875–879, Springer, Boston, MA, USA, 2011.
- [104] W. Tian, W. Song, J. Ma, Z. Fang, A. Seyfried, and J. Liddle, "Experimental study of pedestrian behaviors in a corridor based on digital image processing," *Fire Safety Journal*, vol. 47, pp. 8–15, 2012.
- [105] W. Liao, A. Seyfried, J. Zhang, M. Boltes, X. Zheng, and Y. Zhao, "Experimental Study on Pedestrian Flow through Wide Bottleneck," *Transportation Research Procedia*, vol. 2, pp. 26–33, 2014.
- [106] L. Sun, W. Luo, L. Yao, S. Qiu, and J. Rong, "A comparative study of funnel shape bottlenecks in subway stations," *Transportation Research Part A Policy & Practice*, vol. 98, pp. 14–27, 2017.
- [107] W. Daamen and S. Hoogendoorn, "Capacity of doors during evacuation conditions," *Procedia Engineering*, vol. 3, pp. 53–66, 2010.
- [108] W. Daamen and S. P. Hoogendoorn, "Emergency Door Capacity: Influence of Door Width, Population Composition and Stress Level," *Fire Technology*, vol. 48, no. 1, pp. 55–71, 2012.
- [109] A. Garcimartín, I. Zuriguel, J. Pastor, C. Martín-Gómez, and D. Parisi, "Experimental Evidence of the 'Faster Is Slower' Effect," *Transportation Research Procedia*, vol. 2, pp. 760–767, 2014.
- [110] A. Garcimartín, D. R. Parisi, J. M. Pastor, C. Martín-Gómez, and I. Zuriguel, "Flow of pedestrians through narrow doors with different competitiveness," *Journal of Statistical Mechanics: Theory and Experiment*, no. 4, pp. 1–16, 2016.
- [111] N. W. Bode, S. Holl, W. Mehner, A. Seyfried, and G. Xiao, "Disentangling the Impact of Social Groups on Response Times and Movement Dynamics in Evacuations," *PLoS ONE*, vol. 10, no. 3, p. e0121227, 2015.
- [112] C. von Krüchten and A. Schadschneider, "Empirical study on social groups in pedestrian evacuation dynamics," *Physica A: Statistical Mechanics and its Applications*, vol. 475, pp. 129–141, 2017.
- [113] C. von Krüchten, F. Müller, A. Svachiy, O. Wohak, and A. Schadschneider, "Empirical study of the influence of social groups in evacuation scenarios," in *Traffic and Granular Flow '15*, pp. 65–72, Springer International Publishing, Cham, Switzerland.
- [114] A. Nicolas, S. Bouzat, and M. Kuperman, "Influence of selfish and polite behaviours on a pedestrian evacuation through a narrow exit: A quantitative characterisation," in *Proceedings of the 8th International Conference on Pedestrian and Evacuation Dynamics*, Hefei, China, 2016.
- [115] A. Nicolas, S. Bouzat, and M. N. Kuperman, "Pedestrian flows through a narrow doorway: Effect of individual behaviours on the global flow and microscopic dynamics," *Transportation Research Part B: Methodological*, vol. 99, pp. 30–43, 2017.
- [116] T. Ezaki, K. Ohtsuka, M. Chraïbi et al., "Inflow Process of Pedestrians to a Confined Space," *Collective Dynamics*, vol. 1, 2016.
- [117] X. Liu, W. Song, L. Fu, and Z. Fang, "Experimental study of pedestrian inflow in a room with a separate entrance and exit," *Physica A: Statistical Mechanics and its Applications*, vol. 442, pp. 224–238, 2016.
- [118] Legion Software — Science in Motion, Legion Software, 2018, <http://www.legion.com/legion-software>.
- [119] E. Altshuler, O. Ramos, Y. Núñez, J. Fernández, A. J. Batista-Leyva, and C. Noda, "Symmetry breaking in escaping ants," *The American Naturalist*, vol. 166, no. 6, pp. 643–649, 2005.
- [120] N. Shiwakoti, M. Sarvi, G. Rose, and M. Burd, "Enhancing the Safety of Pedestrians during Emergency Egress," *Transportation Research Record*, vol. 2137, no. 1, pp. 31–37, 2009.
- [121] S. Wang, W. Lv, W. Song, and D. R. Chialvo, "Behavior of Ants Escaping from a Single-Exit Room," *PLoS ONE*, vol. 10, no. 6, p. e0131784, 2015.
- [122] S. Wang, S. Cao, Q. Wang, L. Lian, and W. Song, "Effect of exit locations on ants escaping a two-exit room stressed with repellent," *Physica A: Statistical Mechanics and its Applications*, vol. 457, pp. 239–254, 2016.
- [123] N. Shiwakoti and M. Sarvi, "Enhancing the panic escape of crowd through architectural design," *Transportation Research Part C: Emerging Technologies*, vol. 37, pp. 260–267, 2013.
- [124] S. Soria, R. Josens, and D. Parisi, "Experimental evidence of the 'Faster is Slower' effect in the evacuation of ants," *Safety Science*, vol. 50, no. 7, pp. 1584–1588, 2012.
- [125] S. Boari, R. Josens, D. R. Parisi, and J. A. Marshall, "Efficient Egress of Escaping Ants Stressed with Temperature," *PLoS ONE*, vol. 8, no. 11, p. e81082, 2013.

- [126] J. M. Pastor, A. Garcimartín, P. A. Gago et al., “Experimental proof of faster-is-slower in systems of frictional particles flowing through constrictions,” *Physical Review E: Statistical, Nonlinear, and Soft Matter Physics*, vol. 92, no. 6, 2015.
- [127] N. Shiwakoti, M. Sarvi, G. Rose, and M. Burd, “Biologically Inspired Modeling Approach for Collective Pedestrian Dynamics under Emergency Conditions,” *Transportation Research Record*, vol. 2196, no. 1, pp. 176–184, 2010.
- [128] D. R. Parisi, S. A. Soria, and R. Josens, “Faster-is-slower effect in escaping ants revisited: Ants do not behave like humans,” *Safety Science*, vol. 72, pp. 274–282, 2015.
- [129] A. Sobhani, M. Sarvi, D. Duives, O. Ejtemai, K. Aghabayk, and S. Hoogendoorn, “Exploring the relationship of exit flow and jam density in panic scenarios using animal dynamics,” *Transportation Research Procedia*, pp. 745–751, 2014.
- [130] A. Sobhani, M. Sarvi, D. Duives, O. Ejtemai, K. Aghabayk, and S. Hoogendoorn, “Exploring the Relationship of Exit Flow and Jam Density in Panic Scenarios Using Animal Dynamics,” *Transportation Research Procedia*, vol. 2, pp. 745–751, 2015.
- [131] C. Saloma, G. J. Perez, G. Tapang, M. Lim, and C. Palmes-Saloma, “Self-organized queuing and scale-free behavior in real escape panic,” *Proceedings of the National Academy of Sciences of the United States of America*, vol. 100, no. 21, pp. 11947–11952, 2003.
- [132] C. Saloma, G. J. Perez, C. A. Gavile, J. J. Ick-Joson, and C. Palmes-Saloma, “Prior individual training and self-organized queuing during group emergency escape of mice from water pool,” *PLoS ONE*, vol. 10, no. 2, 2015.
- [133] P. Lin, J. Ma, T. Liu, T. Ran, Y. Si, and T. Li, “An experimental study of the “faster-is-slower” effect using mice under panic,” *Physica A: Statistical Mechanics and its Applications*, vol. 452, pp. 157–166, 2016.
- [134] P. Lin, J. Ma, T. Y. Liu et al., “An experimental study of the impact of an obstacle on the escape efficiency by using mice under high competition,” *Physica A: Statistical Mechanics and its Applications*, vol. 482, pp. 228–242, 2017.
- [135] Y. Zhang, J. Ma, Y. Si et al., “Required width of exit to avoid the faster-is-slower effect in highly competitive evacuation,” *Chinese Physics B*, vol. 26, no. 8, p. 084504, 2017.
- [136] J. M. Chen, P. Lin, F. Y. Wu, D. L. Gao, and G. Y. Wang, “Revisit the faster-is-slower effect for an exit at a corner,” *Journal of Statistical Mechanics: Theory and Experiment*, vol. 2018, no. 2, p. 023404, 2018.
- [137] H. Oh and J. Park, “Main factor causing “faster-is-slower” phenomenon during evacuation: rodent experiment and simulation,” *Scientific Reports*, vol. 7, no. 1, 2017.
- [138] I. Zuriguel, D. R. Parisi, R. C. Hidalgo et al., “Clogging transition of many-particle systems flowing through bottlenecks,” *Scientific Reports*, vol. 4, no. 1, 2014.
- [139] A. Garcimartín, J. M. Pastor, L. M. Ferrer, J. J. Ramos, C. Martín-Gómez, and I. Zuriguel, “Flow and clogging of a sheep herd passing through a bottleneck,” *Physical Review E: Statistical, Nonlinear, and Soft Matter Physics*, vol. 91, no. 2, 2015.
- [140] I. Zuriguel, J. Olivares, J. M. Pastor et al., “Effect of obstacle position in the flow of sheep through a narrow door,” *Physical Review E: Statistical, Nonlinear, and Soft Matter Physics*, vol. 94, no. 3, 2016.
- [141] M. Isobe, T. Adachi, and T. Nagatani, “Experiment and simulation of pedestrian counter flow,” *Physica A: Statistical Mechanics and its Applications*, vol. 336, no. 3-4, pp. 638–650, 2004.
- [142] R. Nagai, M. Fukamachi, and T. Nagatani, “Experiment and simulation for counterflow of people going on all fours,” *Physica A: Statistical Mechanics and its Applications*, vol. 358, no. 2-4, pp. 516–528, 2005.
- [143] T. Kretz, A. Grünebohm, M. Kaufman, F. Mazur, and M. Schreckenberg, “Experimental study of pedestrian counterflow in a corridor,” *Journal of Statistical Mechanics: Theory and Experiment*, no. 10, Article ID P10001, 2006.
- [144] Z. Yang, Y. Zhang, and O. Grembek, “Combining traffic efficiency and traffic safety in countermeasure selection to improve pedestrian safety at two-way stop controlled intersections,” *Transportation Research Part A: Policy and Practice*, vol. 91, pp. 286–301, 2016.
- [145] M. Muramatsu, T. Irie, and T. Nagatani, “Jamming transition in pedestrian counter flow,” *Physica A: Statistical Mechanics and its Applications*, vol. 267, no. 3-4, pp. 487–498, 1999.
- [146] Q. Zhang, B. Han, and D. Li, “Modeling and simulation of passenger alighting and boarding movement in Beijing metro stations,” *Transportation Research Part C: Emerging Technologies*, vol. 16, no. 5, pp. 635–649, 2008.
- [147] S. Seriani and R. Fernandez, “Pedestrian traffic management of boarding and alighting in metro stations,” *Transportation Research Part C: Emerging Technologies*, vol. 53, pp. 76–92, 2015.
- [148] Y. Tajima and T. Nagatani, “Scaling behavior of crowd flow outside a hall,” *Physica A: Statistical Mechanics and its Applications*, vol. 292, no. 1-4, pp. 545–554, 2001.
- [149] L. Sun, S. Hao, Q. Gong, S. Qiu, and Y. Chen, “Pedestrian roundabout improvement strategy in subway stations,” in *Proceedings of the Institution of Civil Engineers - Transport*, vol. 171, pp. 20–29, 2017.
- [150] D. Versluis, *Microscopic Interaction Behavior between Individual Pedestrians*, 2010.
- [151] J. Zhang, W. Klingsch, A. Schadschneider, and A. Seyfried, “Ordering in bidirectional pedestrian flows and its influence on the fundamental diagram,” *Journal of Statistical Mechanics: Theory and Experiment*, vol. 2012, Article ID P02002, 2012.
- [152] S. Xue, R. Jiang, B. Jia, Z. Wang, and X. Zhang, “Pedestrian counter flow in discrete space and time: experiment and its implication for CA modelling,” *Transportmetrica B: Transport Dynamics*, pp. 1–16, 2017.
- [153] Q. Wang, W. Song, J. Zhang, and S. Lo, “Bi-directional movement characteristics of *Camponotus japonicus* ants during nest relocation,” *Journal of Experimental Biology*, 2018.
- [154] M. Plaue, M. Chen, G. Bärwolff, and H. Schwandt, “Trajectory Extraction and Density Analysis of Intersecting Pedestrian Flows from Video Recordings,” in *Photogrammetric Image Analysis*, vol. 6952 of *Lecture Notes in Computer Science*, pp. 285–296, Springer, Berlin, Germany, 2011.
- [155] S. C. Wong, W. L. Leung, S. H. Chan et al., “Bidirectional pedestrian stream model with oblique intersecting angle,” *Journal of Transportation Engineering*, vol. 136, no. 3, pp. 234–242, 2010.
- [156] J. Wu and S. Lu, “Feature Analysis and Operation Evaluation of Pedestrian Weaving Zone,” *Transportation Research Record*, vol. 2393, no. 1, pp. 66–74, 2013.
- [157] L. Lian, X. Mai, W. Song, Y. K. Kit Richard, X. Wei, and J. Ma, “An experimental study on four-directional intersecting pedestrian flows,” *Journal of Statistical Mechanics: Theory and Experiment*, vol. 2015, Article ID P08024, 2015.
- [158] L. Sun, Q. Gong, S. Hao, C. Wang, and Y. Chen, “Experimental Study of Oblique Pedestrian Streams,” *PROMET - Traffic Transportation*, vol. 30, pp. 151–10, 2018.

- [159] K. E. Boyce, D. A. Purser, and T. J. Shields, "Experimental studies to investigate merging behaviour in a staircase," *Fire and Materials*, vol. 36, no. 5-6, pp. 383-398, 2012.
- [160] X. Shi and W. Wang, *Characteristics of Merging Pedestrian Flows at Congested Situation*, 2015.
- [161] F. Huo, W. Song, L. Chen, C. Liu, and K. M. Liew, "Experimental study on characteristics of pedestrian evacuation on stairs in a high-rise building," *Safety Science*, vol. 86, pp. 165-173, 2016.
- [162] K. Aghabayk, M. Sarvi, O. Ejtemai, and A. Sobhani, "Impacts of Different Angles and Speeds on Behavior of Pedestrian Crowd Merging," *Transportation Research Record*, vol. 2490, pp. 76-83, 2015.
- [163] K. Aghabayk, O. Ejtemai, M. Sarvi, and A. Sobhani, "Understanding Pedestrian Crowd Merging Behavior," *Transportation Research Procedia*, vol. 2, pp. 768-773, 2014.
- [164] Z. Shahhoseini, M. Sarvi, and M. Saberi, "Insights toward characteristics of merging streams of pedestrian crowds based on experiments with panicked ants," *Transportation Research Record*, vol. 2561, pp. 81-88, 2016.
- [165] L. Lian, X. Mai, W. Song, Y. K. K. Richard, Y. Rui, and S. Jin, "Pedestrian merging behavior analysis: An experimental study," *Fire Safety Journal*, vol. 91, pp. 918-925, 2017.
- [166] N. Shiwakoti, Y. Gong, X. Shi, and Z. Ye, "Examining influence of merging architectural features on pedestrian crowd movement," *Safety Science*, vol. 75, pp. 15-22, 2015.
- [167] Z. Shahhoseini, M. Sarvi, and M. Saberi, "Pedestrian crowd dynamics in merging sections: Revisiting the "faster-is-slower" phenomenon," *Physica A: Statistical Mechanics and its Applications*, vol. 491, pp. 101-111, 2018.
- [168] M. Chen, J. Wang, Y. Zhi, and L. Gao, "Effect of the Ratio of the Branch Inflow to the Total Inflow on Evacuation Efficiency of Pedestrians Merging at T-junctions," *Procedia Engineering*, vol. 211, pp. 70-77, 2018.
- [169] J. Ma, W. Song, W. Tian, S. Lo, and G. Liao, "Experimental study on an ultra high-rise building evacuation in China," *Safety Science*, vol. 50, no. 8, pp. 1665-1674, 2012.
- [170] Z. Shahhoseini, M. Sarvi, M. Saberi, and M. Haghani, "Pedestrian Crowd Dynamics Observed at Merging Sections," *Transportation Research Record*, vol. 2622, pp. 48-57, 2017.
- [171] A. Cuesta, O. Abreu, A. Balboa, and D. Alvear, "An experimental data-set on merging flows in rail tunnel evacuation," *Tunnelling and Underground Space Technology*, vol. 70, pp. 155-165, 2017.
- [172] M. Haghani, M. Sarvi, Z. Shahhoseini, M. Boltes, and J. Jing, "How Simple Hypothetical-Choice Experiments Can Be Utilized to Learn Humans' Navigational Escape Decisions in Emergencies," *PLoS ONE*, vol. 11, no. 11, p. e0166908, 2016.
- [173] M. Haghani and M. Sarvi, "Stated and revealed exit choices of pedestrian crowd evacuees," *Transportation Research Part B: Methodological*, vol. 95, pp. 238-259, 2017.
- [174] J. R. G. Dyer, C. C. Ioannou, L. J. Morrell et al., "Consensus decision making in human crowds," *Animal Behaviour*, vol. 75, no. 2, pp. 461-470, 2008.
- [175] B. Zhou, X. Wang, and X. Tang, "Understanding collective crowd behaviors: Learning a Mixture model of Dynamic pedestrian-Agents," in *Proceedings of the 2012 IEEE Conference on Computer Vision and Pattern Recognition (CVPR)*, pp. 2871-2878, Providence, RI, USA, June 2012.
- [176] M. Campanella, S. Hoogendoorn, and W. Daamen, "Improving the Nomad microscopic walker model," *IFAC Proceedings Volumes*, vol. 42, no. 15, pp. 12-18, 2009.
- [177] T. Robin, G. Antonini, M. Bierlaire, and J. Cruz, "Specification, estimation and validation of a pedestrian walking behavior model," *Transportation Research Part B: Methodological*, vol. 43, no. 1, pp. 36-56, 2009.
- [178] E. Cepolina and N. Tyler, "Understanding Capacity Drop for designing pedestrian environments, Walk 21 Everyday Walk. Cult," (2005), http://discovery.ucl.ac.uk/1412/1/Cepolina_Tyler_paper_Walk21.pdf.
- [179] M. Asano, T. Iryo, and M. Kuwahara, "Microscopic pedestrian simulation model combined with a tactical model for route choice behaviour," *Transportation Research Part C: Emerging Technologies*, vol. 18, no. 6, pp. 842-855, 2010.
- [180] J. R. G. Dyer, A. Johansson, D. Helbing, I. D. Couzin, and J. Krause, "Leadership, consensus decision making and collective behaviour in humans," *Philosophical Transactions of the Royal Society B: Biological Sciences*, vol. 364, no. 1518, pp. 781-789, 2009.
- [181] M. Moussaïd, D. Helbing, S. Garnier, A. Johansson, M. Combe, and G. Theraulaz, "Experimental study of the behavioural mechanisms underlying self-organization in human crowds," *Proceedings of the Royal Society B Biological Science*, vol. 276, no. 1668, pp. 2755-2762, 2009.
- [182] W. Daamen and S. Hoogendoorn, "Calibration of pedestrian simulation model for emergency doors by pedestrian type," *Transportation Research Record*, vol. 2316, pp. 69-75, 2012.
- [183] D. R. Parisi, P. A. Negri, and L. Bruno, "Experimental characterization of collision avoidance in pedestrian dynamics," *Physical Review E: Statistical, Nonlinear, and Soft Matter Physics*, vol. 94, no. 2, 2016.
- [184] R. Guo, S. C. Wong, Y. Xia, H. Huang, W. H. Lam, and K. Choi, "Empirical Evidence for the Look-Ahead Behavior of Pedestrians in Bi-directional Flows," *Chinese Physics Letters*, vol. 29, no. 6, p. 068901, 2012.
- [185] S. Xie, S. C. Wong, W. H. K. Lam, and A. Chen, "Development of a bidirectional pedestrian stream model with an oblique intersecting angle," *Journal of Transportation Engineering*, vol. 139, no. 7, pp. 678-685, 2013.
- [186] M. Boltes, J. Zhang, A. Seyfried, and B. Steffen, "T-junction: Experiments, trajectory collection, and analysis," in *Proceedings of the IEEE International Conference on Computer Vision Workshops (ICCV '11)*, pp. 158-165, Barcelona, Spain, November 2011.
- [187] J. Wu, S. Lu, Y. Wang, and X. Liu, "Level of Service Evaluation Method of Pedestrian Weaving Area," in *Proceedings of the 96th Annual Meeting on Transportation Research Board*, pp. 1-16, Washington, DC, USA, 2017.
- [188] W. Liao, A. Tordeux, A. Seyfried et al., "Measuring the steady state of pedestrian flow in bottleneck experiments," in *Physica A: Statistical Mechanics and its Applications*, pp. 1-13, 2016.
- [189] L. Sun, Z. Yang, J. Rong, and X. Liu, "Study on the Weaving Behavior of High Density Bidirectional Pedestrian Flow," *Mathematical Problems in Engineering*, vol. 2014, Article ID 765659, 9 pages, 2014.
- [190] J. Qiao, L. Sun, X. Liu, and J. Rong, "Reducing the impact of speed dispersion on subway corridor flow," *Applied Ergonomics*, vol. 65, pp. 362-368, 2017.
- [191] Y. Liu, X. Shi, Z. Ye, N. Shiwakoti, and J. Lin, "Controlled experiments to examine different exit designs on crowd evacuation dynamics," in *CICTP 2016: Green and Multimodal Transportation and Logistics*, pp. 779-790, American Society of Civil Engineers, Reston, VA, USA, 2016.
- [192] N. Shiwakoti, X. Shi, Z. Ye, Y. Gong, and W. Wang, "Empirical Investigation on merging crowd behaviour with and without

- blocked vision,” in *Proceedings of the World Conference on Transport Research*, Shanghai, China, 2016.
- [193] Z. Shahhoseini, M. Sarvi, and E. Ito, “Collective movements of pedestrians: How we can learn from simple experiments with non-human (ant) crowds,” *PLoS ONE*, vol. 12, no. 8, p. e0182913, 2017.
- [194] W. Liao, A. U. Kemloh Wagoum, and N. W. Bode, “Route choice in pedestrians: determinants for initial choices and revising decisions,” *Journal of the Royal Society Interface*, vol. 14, no. 127, p. 20160684, 2017.
- [195] G. Warnaby, *Marketing Strategy*, JMark Management LLC, 1999, <http://ezproxy.library.capella.edu/login?url=http://search.ebsco-host.com/login.aspx?direct=true&db=bth&AN=5659377&site=ehost-live&scope=site>.
- [196] N. Shiwakoti, “Understanding differences in emergency escape and experimental pedestrian crowd egress through quantitative comparison,” *International Journal of Disaster Risk Reduction*, vol. 20, pp. 129–137, 2016.
- [197] S. Gwynne, E. Kuligowski, K. Boyce et al., “Enhancing egress drills: Preparation and assessment of evacuee performance,” *Fire and Materials*.
- [198] A. Leeson, P. Alvarez, and S. Ghosh, “Understanding How Big Data and Crowd Movements will Shape the Cities of Tomorrow,” in *Proceedings of the European Transport Conference*, Frankfurt, Germany, 2014, <http://abstracts.aetransport.org/paper/index/id/4296/confid/19>.
- [199] X. Shi, X. Zhao, Z. Ye, N. Shiwakoti, and J. Lu, “Estimating pedestrian walking characteristics by use of smartphone sensing: an experimental study,” in *Proceedings of the 17th COTA conference International Conference of Transportation Professionals (CICTP2017)*, American Society of Civil Engineers, 2017.
- [200] R. Lovreglio, V. Gonzalez, and Z. Feng, “Prototyping virtual reality serious games for building earthquake preparedness: the auckland city hospital case study,” 2018, <https://arxiv.org/abs/1802.09119>.
- [201] Civil-Security-and-Traffic, Jülich-Supercomputing-Center, and Forschungszentrum-Jülich, *Data Archive of Experimental Data from Studies about Pedestrian Dynamics*, 2018, <http://ped.fz-juelich.de/db/>.
- [202] Pablo Augusto Negri, GSdataset-PANKit - Traffic Intersection Video Sequence DataSet, 2017, <http://pablonegri.free.fr/Downloads/GSdataset-PANKit.htm>.
- [203] CSAI, Vittorio Emanuele II Gallery Dataset, An Annot. Video about Pedestr. Gr. Dyn. Proxemic Behav, 2013.
- [204] B. Zhou, *Grand Central Station Dataset, Train Stn. Dataset*, 2012, <http://www.ee.cuhk.edu.hk/~xgwang/grandcentral.html>.
- [205] B. Majecka, *Edinburgh Informatics Forum Pedestrian Database*, 2010, <http://homepages.inf.ed.ac.uk/rbf/FORUMTRACKING/>.
- [206] B. Zhou, *Collective Motion Database*, 2013, <http://mmlab.ie.cuhk.edu.hk/projects/collectiveness/dataset.htm>.
- [207] W. Song and L. Fu, “Verification and validation methods,” in *Evacuation Model*, pp. 81–102, 2016.

Research Article

Causation Analysis of Hazardous Material Road Transportation Accidents by Bayesian Network Using Genie

Xiaoli Ma , Yingying Xing , and Jian Lu 

The Key Laboratory of Road and Traffic Engineering, Ministry of Education, Tongji University, 4800 Cao'an Road, Shanghai 201804, China

Correspondence should be addressed to Jian Lu; jianjohnlu@tongji.edu.cn

Received 1 April 2018; Accepted 28 May 2018; Published 5 August 2018

Academic Editor: Xiaobo Qu

Copyright © 2018 Xiaoli Ma et al. This is an open access article distributed under the Creative Commons Attribution License, which permits unrestricted use, distribution, and reproduction in any medium, provided the original work is properly cited.

With the increase of hazardous materials (Hazmat) demand and transportation, frequent Hazmat road transportation accidents had arisen the widespread concern in the community. Thus, it is necessary to analyze the risk factors' implications, which would make the safety of Hazmat transportation evolve from "passive type" to "active type". In order to explore the influence of risk factors resulting in accidents and predict the occurrence of accidents under the combination of risk factors, 839 accidents that have occurred for the period 2015–2016 were collected and examined. The Bayesian network structure was established by experts' knowledge using Dempster-Shafer evidence theory. Parameter learning was conducted by the Expectation-Maximization (EM) algorithm in Genie 2.0. The two main results could be likely to obtain the following. (1) The Bayesian network model can explore the most probable factor or combination leading to the accident, which calculated the posterior probability of each risk factor. For example, the importance of three or more vehicles in an accident leading to the severe accident is higher than less vehicles, and in the absence of other evidences, the most probable reasons for "explosion accident" are vehicles carrying flammable liquids, larger quantity Hazmat, vehicle failure, and transporting in autumn. (2) The model can predict the occurrence of accident by setting the influence degrees of specific factor. Such that the probability of rear-end accidents caused by "speeding" is 0.42, and the probability could reach up to 0.97 when the driver is speeding at the low-class roads. Moreover, the complex logical relationship in Hazmat road transportation accidents could be obtained, and the uncertain relation among various risk factors could be expressed. These findings could provide theoretical support for transportation corporations and government department on taking effective measures to reduce the risk of Hazmat road transportation.

1. Introduction

In recent years, the demand for hazardous materials (Hazmat) has increased, resulting in increasing transportation requirement. More than 95% Hazmat require off-site transportation in China, and 63% are transported by road in Brazil, as well as 90% in the United States [1, 2]. However, Hazmat could provide the great convenience for people's life, but also significant risks to environment and human health exist. For instance, a total of 3744 heavy trucks were involved in severe accidents in the United States, of which 3% were carrying Hazmat [3]. On January 11, 2015, a tanker truck carrying gasoline collided with a bus in Pakistan, causing 57 deaths. And a tanker truck carrying liquid ammonia collided with a van, resulting in a large-scale spill of liquid ammonia, leading to 28 deaths and the number of poisons was up to 350 on

March 29, 2005, which arose on negative social impacts in China [4].

Hazmat transportation accidents would be able to produce catastrophic influence on human health, public safety, environment, and property due to the special characteristic of Hazmat, attracting more attention from general public and government on the management of Hazmat road transportation. Thus, how to improve the transportation condition and reduce the risk of transportation have become important and urgent problems for the industrial development. A growing amount studies about Hazmat transportation and production have been conducted [5–7]. Therefore, the need for investigating risk factors that contribute to Hazmat accident and the relationship of risk factors are highlighted to reduce the risk of Hazmat transportation. To that end, the effective method to describe and evaluate the accident process is causation

analysis, which could be used to determine government priorities related to the implementation of prevention measures [8]. And causation analysis also could provide the theoretical support for actionable information of controlling over the risk factors for the transportation corporations. In addition, exploring the most probable factor or combination leading to accidents and predicting accidents are the important research topics in the field of Hazmat safety, reducing the frequency and severity of accidents.

2. Literature Review

The purpose of this study is to explore risk factors to reduce the risk of Hazmat road transportation. Many studies have been conducted by using statistical methods. Haastrup and Brockhoff [9] statistically analyzed the cases of Hazmat accidents in Western Europe, and 39% of accidents occurred during transportation; in 682 accidents the consequence included fatality. A study about Hazmat transportation accidents divided risk factors into human, vehicle, packing, transportation facilities, road conditions, and environmental conditions [5]. Shen [10] studied 708 accidents with Hazmat in China from 2004 to 2011 and found that accidents easily occurred at expressways, and the higher probability of spill accident is associated with accident type. Fang et al. [11] concluded that speeding was the main reason for Hazmat transportation accidents through the analysis of accident data between 1999 and 2013.

Although statistical methods could analyze the relationships between accidents and the risk factors, they cannot account for the interplay among different factors and fail to reflect the fact that an accident is not usually the result of a single factor [12]. The use of causation analysis theory for accidents could extract the accident mechanism and accident models from a large number of typical accidents. For instance, Jason et al. [13] conducted the study about the influence of vehicle, occupant, driver, and environmental characteristics on accident injuries involved with heavy-duty trucks, and the conclusion was obtained by using the heteroskedastic ordered probit models, which showed that the likelihood of severe accident is estimated to rise with the more vehicles involved in accident. Uddin and Huynh [14] used an ordered probit model to explore the relationship among drivers, vehicles, roadways, environment, temporal characteristics, and the severity of accident. There was a study by using logit model to study the driver's behaviors effect on accidents, and the results indicated that the more significant risk factors were speeding, not using seatbelt, drivers' age, and drivers with no valid license [15]. In addition, the Bayesian network and tree-based methods were considered to explore deeper accident mechanisms, which is increasingly utilized in traffic accidents analysis. For instance, Oña et al. [16] classified traffic accidents based on the severity of injuries by using the Bayesian networks; the factors associated with fatal or severe accidents were identified by inference, such as accident type, the driver's age, and lighting. In order to simplify the model, Mujalli et al. [17] used Bayesian networks to reduce the number of variables in the study of analyzing the accidents severity on rural roads, and the result showed that the number

of variables could reduce up to 60% (the variables considered are accident type, age, atmospheric factors, gender, lighting, number of injured, and occupants involved), maintaining the good performance of models. Zhao et al. [18] pointed that the three most significant factors influencing Hazmat transportation by applying Bayesian networks were human factors, the transport vehicles and facilities, and the packaging and loading of Hazmat. Chen et al. [19] analyzed the between-accident variance and within-accident correlations by using Bayesian network and explored the risk factors influencing accidents and their heterogeneous impacts on accident severity in rural roads. And in order to improve the efficiency of emergency rescue of Hazmat transportation road accidents, a study was conducted to evaluate the time of accidents dealing based on the Bayesian network [20]. In addition, the Bayesian network model could also be used to describe the probability and risk of accidents [21–24].

However, despite many studies on the traffic accidents and Hazmat accidents, most of them are studied based on the analysis of specific, isolated, and single factor [25, 26]. Moreover, the characteristic of Hazmat was not taken into consideration during the analysis of accidents, limiting the studies of risk factors in Hazmat road transportation. In addition, the statistical methods could reveal the inherent rules on the occurrence of accidents, but the relationship of risk factors was not observed, which cannot reflect the accident mechanism. The application of causal analysis model (such as Bayesian network) can explain the correlation between risk factors and further explain the accident mechanism, but the Bayesian network structure may exist subjectivity due to the experts' knowledge, leading to incorrect description of relationships between nodes in the Bayesian network structure. Therefore, Hazmat road transportation accidents in China from 2015 to 2016 are considered as the research object to explore the potential risk factors of accidents based on experts' knowledge. The Bayesian network is used to explore the most probable factor or combination leading to accident and determine the correlation between the risk factors, providing the decision-making basis for Hazmat transportation corporations and government departments to reduce the risk of Hazmat transportation.

3. Database

The Hazmat transportation accident data was obtained from State Work Accident Briefing System, and Chemical Accidents Information Network for two years (2015–2016) in China, and the weather data was obtained from the China Meteorological Administration. The regional distribution of Hazmat transportation accidents is shown in Figure 1. The database considered in the study contains 839 records, and each record contains detailed information including the date, time, location, type of accidents, type and number of vehicles involved in accident, driver characteristic, the quantity and categories of Hazmat, accident consequence, causes of accident, and a detailed description of the accident. Sixteen variables extracted from the database were considered as the significant factors, which are shown in Table 1.

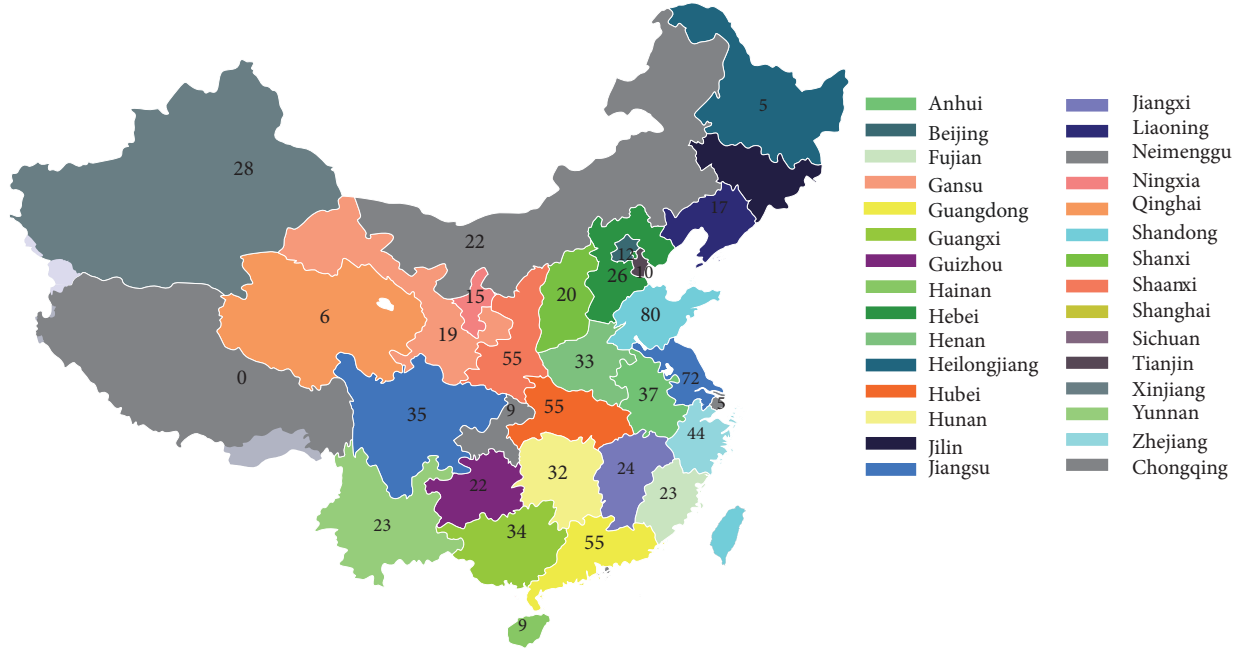


FIGURE 1: Regional distribution of accidents.

Accident information is accident type (rear-end, side-swipe, rollover, collision, and vehicle failure) and accident consequence (explosion, fire, spill, and nonspill). Previous studies [14, 27] divided injury severity into five categories; the accident severity in the paper is considered as no injury, severe injury, and fatality. Simplified classification of accident severity could ease the issue of potential relationship of related consequences of an accident and ensure the sufficient sample size for the Bayesian network model [28, 29]. In the paper, the simplified classification of accident severity would obtain the better results.

Hazmat information is Hazmat categories and quantity of Hazmat transportation.

Driver information is characteristics of the driver, such as age and behavior.

Location information is road surface condition and accident location (such as Group one, Group two, Group three, and Group four); the special road section including intersection, freeway service areas, toll stations, and gas stations are considered in the study.

Vehicle information is type and number of vehicles involved in accident.

Environment information is time distribution of accident (hour, day, and month), visibility (dawn: 5:00 to 6:59 am, day: 7:00 am to 4:59 pm, dusk: 5:00 to 6:59 pm, and dark: 7:00 pm to 4:59 am), and weather conditions (sunny, cloudy, rainy and snowy, and fog and haze) [18].

4. Methodology

4.1. Definition of Bayesian Network. Bayesian network is considered as the effective method to describe the causality between the risk factors and the output in the system, also referred to as the belief network. The Bayesian network is

a Directed Acyclic Graph (DAG) and nodes represent variable status, while the directed edges represent dependencies between variables. The relationship or confidence coefficient between variables could be described by using Conditional Probability Table (CPT). The Bayesian formula is considered as the basis for the Bayesian network model, which could be expressed as

$$P(X | Y) = \frac{P(Y | X) \times P(X)}{P(Y)} \quad (1)$$

where $P(X | Y)$ is the probability of X under the condition of a known event Y . $P(Y | X)$ is the conditional probability of Y at the occurrence of X . And the joint distribution of two random variables X and Y can be expressed as

$$P(X, Y) = P(X) P(Y | X) \quad (2)$$

where $P(X)$ is called the prior probability and $P(Y | X)$ is the posterior probability. Combined with the chain rules, reducing the complexity of the probability model, the joint distribution of n variables is

$$P(X_1, X_2, \dots, X_n) = P(X_1) P(X_2 | X_1) \dots P(X_n | X_1, X_2, \dots, X_{n-1}) \quad (3)$$

and the joint distribution also could be expressed as

$$P(X_1, X_2, \dots, X_n) = \prod_{i=1}^n P(X_i | \text{Parent}(X_i)) \quad (4)$$

where $X = \{X_1, X_2, \dots, X_n\}$, setting S is a network structure, P is a set of local probability distributions associated with each variable, X_i denotes the variable node, and $\text{Parent}(X_i)$ denotes the father node of X_i in S .

TABLE 1: Variables of Hazmat road transportation accidents.

| Factors | Variables | Variables description | Discretization | Frequency | Percentage | |
|------------------------|-----------------------|------------------------------------|----------------|-----------|------------|--------|
| Hazmat factors | Hazmat categories | Explosives | 1 | 27 | 3.20% | |
| | | Toxic gases | 2 | 158 | 18.90% | |
| | | Flammable liquids | 3 | 429 | 51.10% | |
| | | Corrosives | 4 | 121 | 14.40% | |
| | | others | 5 | 104 | 12.40% | |
| Driver factors | Quantity of Hazmat | <10 | 1 | 127 | 15.10% | |
| | | 10-24 | 2 | 284 | 33.80% | |
| | | 25-39 | 3 | 358 | 42.70% | |
| | | ≥40 | 4 | 70 | 8.40% | |
| | | Age | 24-35 | 1 | 144 | 17.20% |
| 36-45 | 2 | | 644 | 76.70% | | |
| 46-60 | 3 | | 51 | 6.10% | | |
| Behaviors | Inappropriate driving | | 1 | 13 | 1.50% | |
| | Speeding | | 2 | 36 | 4.30% | |
| | Fatigue driving | 3 | 20 | 2.40% | | |
| | Normal driving | 4 | 770 | 91.80% | | |
| | Accident location | Group one | 1 | 360 | 42.90% | |
| Group two | | 2 | 336 | 40.00% | | |
| Group three | | 3 | 59 | 7.00% | | |
| Group four | | 4 | 84 | 10.10% | | |
| Location factors | | Special section | Intersection | 1 | 18 | 2.10% |
| | Freeway service areas | | 2 | 50 | 6.00% | |
| | Toll stations | | 3 | 78 | 9.30% | |
| | Gas stations | | 4 | 23 | 2.70% | |
| | Road surface | | Normal | 5 | 670 | 79.90% |
| Dry | | 1 | 794 | 94.60% | | |
| Wet | | 2 | 45 | 5.40% | | |
| Season | | Spring | 1 | 227 | 27.10% | |
| | | Summer | 2 | 258 | 30.70% | |
| | Autumn | 3 | 186 | 22.20% | | |
| | Winter | 4 | 168 | 20.00% | | |
| | Weekly distribution | Weekends | 1 | 198 | 23.60% | |
| Weekdays | | 2 | 641 | 76.40% | | |
| Environment factors | | Weather | Sunny | 1 | 202 | 24.10% |
| | | | Cloudy | 2 | 347 | 41.40% |
| | | | Rainy & snow | 3 | 268 | 31.90% |
| | Fog & haze | | 4 | 22 | 2.60% | |
| | Visibility | | dawn | 1 | 94 | 11.20% |
| day | | 2 | 409 | 48.70% | | |
| dusk | | 3 | 60 | 7.20% | | |
| dark | | 4 | 276 | 32.90% | | |
| Vehicle factors | | Total vehicle involved in accident | 1 | 1 | 503 | 59.90% |
| | 2 | | 2 | 276 | 32.90% | |
| | 3 | | 3 | 31 | 3.70% | |
| | ≥4 | | 4 | 29 | 3.50% | |
| | Type of vehicle | | Bus & Truck | 1 | 13 | 1.55% |
| Private cars & Truck | | 2 | 42 | 5.01% | | |
| Non-motor & Truck | | 3 | 11 | 1.31% | | |
| Bus&Private cars&Truck | | 4 | 10 | 1.19% | | |
| Trucks | | 5 | 763 | 90.94% | | |

TABLE I: Continued.

| Factors | Variables | Variables description | Discretization | Frequency | Percentage |
|-------------------|----------------------|-----------------------|----------------|-----------|------------|
| Accidents factors | Accident type | Rear-end | 1 | 189 | 22.50% |
| | | Sideswipe | 2 | 20 | 2.40% |
| | | Rollover | 3 | 340 | 40.50% |
| | | Collision | 4 | 145 | 17.30% |
| | | Vehicle failure | 5 | 145 | 17.30% |
| | Accident consequence | Explosion | 1 | 25 | 3.00% |
| | | Fire | 2 | 96 | 11.40% |
| | | Spill | 3 | 682 | 81.30% |
| | | Non-spill | 4 | 36 | 4.30% |
| | | No injury | 1 | 656 | 78.19% |
| | Severity of accident | Severe injury | 2 | 139 | 16.57% |
| | | Fatality | 3 | 44 | 5.24% |

The construction of the Bayesian network model consists of following steps:

(1) Parameter determination: analyze the risk factors of Hazmat road transportation, and determine the variables needed for modeling (nodes of the Bayesian network), which could be shown in Table 1.

(2) Structure learning: determine the dependencies or independencies relationships between variables (nodes), so that a directed acyclic network structure was constructed.

(3) Parameter learning: based on the given Bayesian network structure, determine the CPT for each node, and the dependence relationship between random variables could be described quantitatively.

4.2. Structure Learning. The scientific network structure needs continuous iterations. At present, there are three methods to construct a Bayesian network structure [30]. (1) Construct the network structure subjectively through experts' knowledge. (2) Determine the network structure objectively via the analysis of data. (3) Construct the network structure based on experts' knowledge and data analysis. The method used in the paper for accident causation analysis is that establishing a preliminary Bayesian network structure based on the model assumption and then the network structure is adjusted with experts' knowledge and data analysis, avoiding the disadvantage of strong subjectivity and enormous amount of data computing. The Bayesian network structure is constructed as shown in Figure 2.

Steps for Building a Bayesian Network Structure

(1) Establish a preliminary Bayesian network structure based on the assumptions of model.

(2) Use Delphi method to determine the relationship between risk factors. In general, there are four possible relationships between variables:

(A) F_i directly lead to F_j , which could be represented as $F_i \rightarrow F_j$.

(B) F_j directly lead to F_i , which could be represented as $F_i \leftarrow F_j$.

(C) The relationship between variables cannot be determined, which could be represented as $F_i \longleftrightarrow F_j$.

(D) There is no relationship between variables, which could be represented as $F_i \perp F_j$.

(3) Synthesize results from multiple experts. D-S evidence theory is used to reduce the subjectivity of experts' knowledge, and the correlation between variables could be determined. The Dempster synthesis rule formula could be expressed as

$$M(A) = K \cdot \sum_{A_1 \cap A_2 \cap \dots \cap A_n} m_1(A_1) m_2(A_2) \dots m_n(A_n)$$

$$\forall A \subseteq \Theta, A \neq \emptyset, A_1, A_2, \dots, A_n \subset \Theta,$$

$$K = \left(\sum_{A_1 \cap A_2 \cap \dots \cap A_n \neq \emptyset} m_1(A_1) m_2(A_2) \dots m_n(A_n) \right)^{-1}$$

$$= \left(1 - \sum_{A_1 \cap A_2 \cap \dots \cap A_n = \emptyset} m_1(A_1) m_2(A_2) \dots m_n(A_n) \right)^{-1}$$
(5)

where A represents the possible relationship between variables, m_i represents the mass function, equaling to the expert opinions, and n represents the number of experts.

(4) As the relationship of variables cannot be obtained by Delphi and D-S evidence theory, the mutual information value of variables should be calculated. And the entropy can be expressed as

$$H(F_i) = \sum_{F_i} P(F_i) \log \frac{1}{P(F_i)} = - \sum_{F_i} P(F_i) \log P(F_i) \quad (6)$$

Conditional entropy is a measure of the uncertainty of a random variable F_i under the condition of giving F_j , which can be expressed as

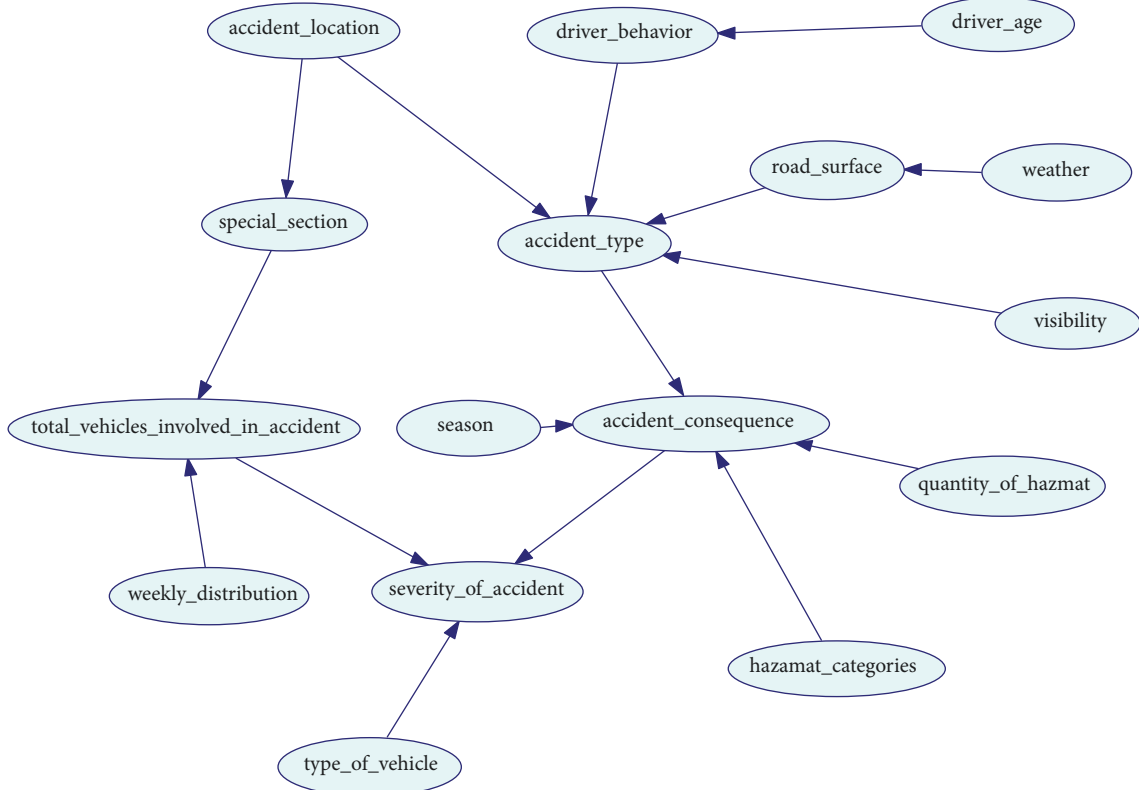


FIGURE 2: The Bayesian network structure for Hazmat transportation accidents.

$$\begin{aligned}
 H(F_i | F_j) &= \sum_{F_i} P(F_i | F_j) \log \frac{1}{P(F_i | F_j)} \\
 &= - \sum_{F_i} P(F_i | F_j) \log P(F_i | F_j)
 \end{aligned} \quad (7)$$

Before obtaining F_j , the uncertainty of F_i is $H(F_i)$, and after obtaining F_j , the uncertainty of F_i is $H(F_i | F_j)$, so that the difference of $H(F_i)$ and $H(F_i | F_j)$ is considered as the mutual information, which is expressed as

$$\begin{aligned}
 I(F_i, F_j) &= H(F_i) - H(F_i | F_j) \\
 &= \sum_{F_i} \sum_{F_j} P(F_i, F_j) \cdot \log_2 \frac{P(F_i, F_j)}{P(F_i)P(F_j)}
 \end{aligned} \quad (8)$$

4.3. Parameter Learning. There are missing data on Hazmat road transportation accidents; the Expectation- Maximization (EM) algorithm is considered as the effective method to perform the maximum likelihood estimation for a set of parameters θ from the incomplete dataset [31–33]. The EM algorithm starts with randomly assigning a configuration θ^0 for θ by the system. Suppose that θ^t is the outcome after t iterations. The calculation process mainly involved two steps: Expectation Step (E-Step) and Maximization Step (M-Step).

Consider that D_m is missing sample, and X_m is the set of all variables with missing value in the sample D_m . Set $X_m = x_m$, and the complete dataset would be obtained by adding

x_m to D_m . All of the possible result would be considered by EM algorithm due to that X_m may have more possibility, so the weight w_{x_m} is assigned for each possible result by EM algorithm, and the weighted sample could be given by

$$(D_m, X_m = x_m) [w_{x_m}] \quad (9)$$

where $w_{x_m} = P(X_m = x_m | D_m, \theta^t)$, and the weight ranges from 0 to 1.

E-Step: suppose the log-likelihood function of θ based on D^t .

$$\begin{aligned}
 m(\theta | D^t) &= \sum_{t=1}^m \sum_{x_m \in X_m} P(X_m = x_m | D_m, \theta^t) \\
 &\quad \cdot \log P(D_m, X_m = x_m | \theta)
 \end{aligned} \quad (10)$$

where $D = (D_1, D_2, \dots, D_m)$, and $m(\theta | D, \theta^t) = m(\theta | D^t)$ is referred to as the expected log-likelihood function. In the iteration, due to the characteristic of D , which is invariant, the formula could be expressed as

$$\begin{aligned}
 M(\theta | \theta^t) &= m(\theta | D, \theta^t) \\
 &= \sum_{t=1}^m \sum_{x_m \in X_m} P(X_m = x_m | D_m, \theta^t) \\
 &\quad \cdot \log P(D_m, X_m = x_m | \theta)
 \end{aligned} \quad (11)$$

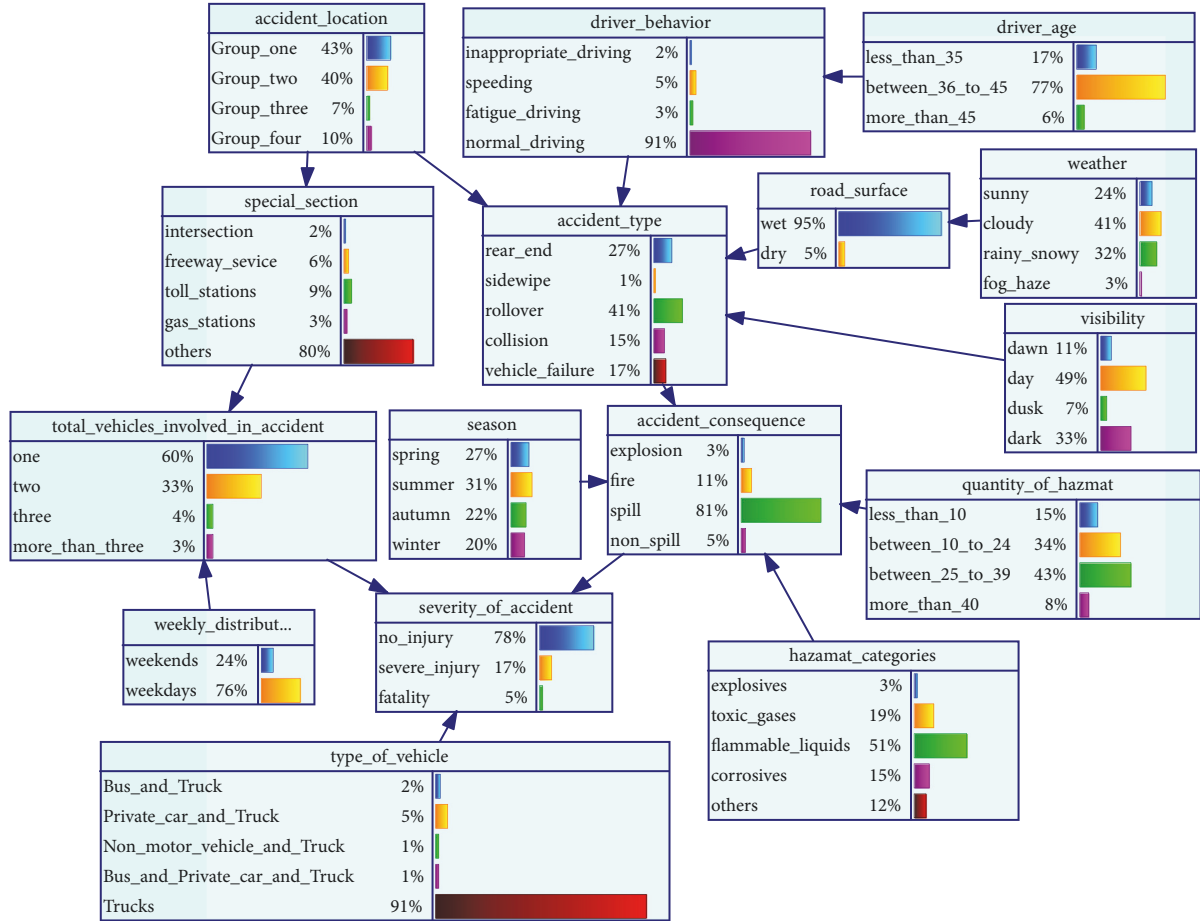


FIGURE 3: The Bayesian network model after parameter learning in Genie 2.0.

M-Step: calculate the value of θ when $M(\theta | \theta^t)$ have reached the maximum:

$$\theta_{ijk}^{t+1} = \begin{cases} \frac{m_{ijk}^t}{\sum_{k=1}^{r_i} m_{ijk}^t} & \sum_{k=1}^{r_i} m_{ijk}^t > 0 \\ \frac{1}{r_i} & \sum_{k=1}^{r_i} m_{ijk}^t \leq 0 \end{cases} \quad (12)$$

where m_{ijk}^t is the sum of sample weights in the dataset D^t .

5. Results

The guidance for the variable selection and classification were followed by the analysis of accident data and previous studies [6, 34–36]. In the paper, sixteen variables are considered as the significant risk factors, as shown in Table 1. There are numerous types of software to establish the Bayesian network efficiently, such as Netica, Genie, Bayes Net Toolbox, and Analytica. In the paper, Genie2.0 (developed by the Decision Systems Laboratory, the University of Pittsburgh) was considered as the effective tool to finish the Bayesian network parameter learning by using EM algorithm, which would make the construction, analysis, and visualization of Bayesian network be performed efficiently, simplifying

the calculation. And the network parameters are repeatedly iterated by using the accident data; the conditions for the termination of calculation are as follows: (1) the variation of the posterior probability for single risk factor is less than 1%; (2) the cumulative variation of posterior probability for the entire network is less than 15%. The results were shown in Figure 3.

5.1. Causal Inference. The Bayesian network could be used to calculate the posterior probability of risk factors under conditions of an accident and obtain the most likely factors or combinations that caused accidents. Set the “explosion” in “accident consequence” as the example to explore the causal inference, and the evidence variable is “explosion”. As shown in Figure 4, the probabilities of risk factors are obtained through the update function of the Genie. And the probability of “autumn” in “season” increases from 22% to 35%; “vehicle failure” (referred as the tire blowout, spontaneous combustion, tanker damage) in “accident type” increases from 17% to 37%; the quantity of Hazmat increases from 8% to 20% for the category of more than 40 tons; “flammable liquids” in “Hazmat categories” increase from 51% to 65%; and the explosives increase from 3% to 8%. These findings mean that, in the absence of other evidences, the most probable reasons for “explosion” are vehicles carrying

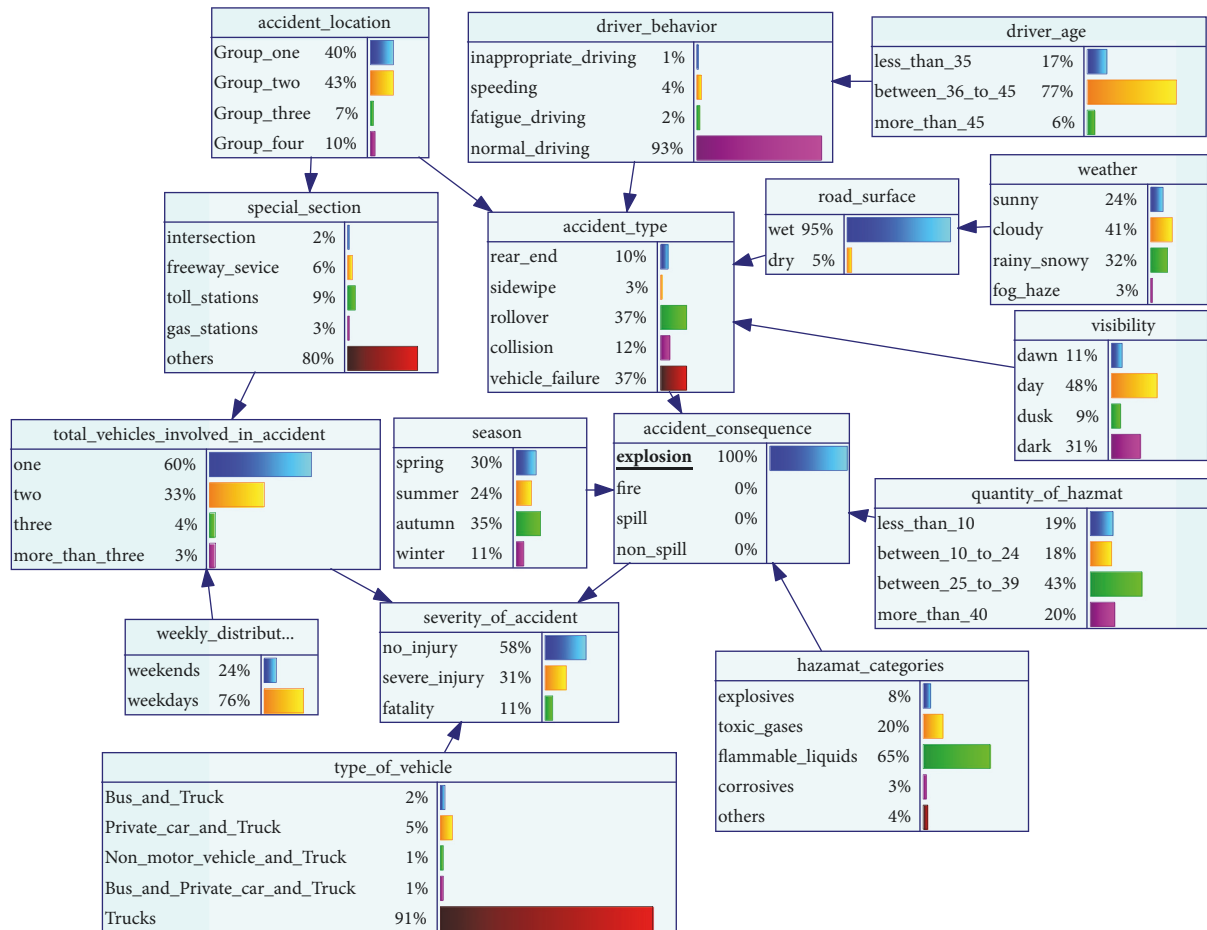


FIGURE 4: Posterior probability when the variable is “explosion”.

flammable liquids, larger quantity of Hazmat, vehicle failure, and transporting in autumn.

In addition, if the “fatality” in the “severity of accident” is considered as the evidence variable, the probability change of “total vehicle involved accident” could be obtained. The probability of “three” increases from 4% to 11%, and “more than three” is increasing from 3% to 9%. This may be explained by the fact that the importance of 3 or more vehicles in an accident leads to the severe accident being higher than less vehicles. Moreover, as for the accident consequence, the probability of “spill” decreases; meanwhile the “explosion” (3% to 6%) and fire (11% to 18%) have increased. Due to the special characteristic of Hazmat, explosion and fire would cause a larger area affected and can easily result in casualties, especially in the urban road and higher population densities [26].

5.2. Accident Prediction. Based on the bidirectional reasoning, not only could the Bayesian network model obtain the risk factors or the combination caused accidents, but also the probability of accidents could be calculated under the risk factors or combination, for example, in Genie, setting the “speeding” in “driver behavior” as an evidence variable, meaning that the status of evidence variable is considered as 100%. As can be seen from Figure 5, the probability of

“rear-end” in “accident type” is found to increase from 27% to 42%, indicating that the drivers’ speeding could be more prone to lead to rear-end accidents. This is because the vehicle is difficult to control under the condition of speeding, and the braking time is longer. And previous studies have shown that driving behavior could significantly affect the severity of traffic accidents [37–39].

As shown in Figure 6, in addition to “speeding”, it is assumed that the transportation route is on low-class roads; that is, “Group four” in the “accident location” is considered as the evidence variable, and the probability of the entire network is automatically updated. It can be found that the probability of “rollover” in “accident type” further increases from 42% to 97%. This finding shows that “driver behavior” and “accident location” would affect the probability of “rollover” accident on different degrees. Therefore, when the driver is speeding on low-class roads, the more attention should be paid on the rollover accident.

6. Discussion and Conclusions

6.1. Hazmat Factors. Flammable liquids have the highest posterior probability (0.51) and would easily result in explosion. This could be explained by that increasing demand for the flammable liquid and decreasing reliability of transporting

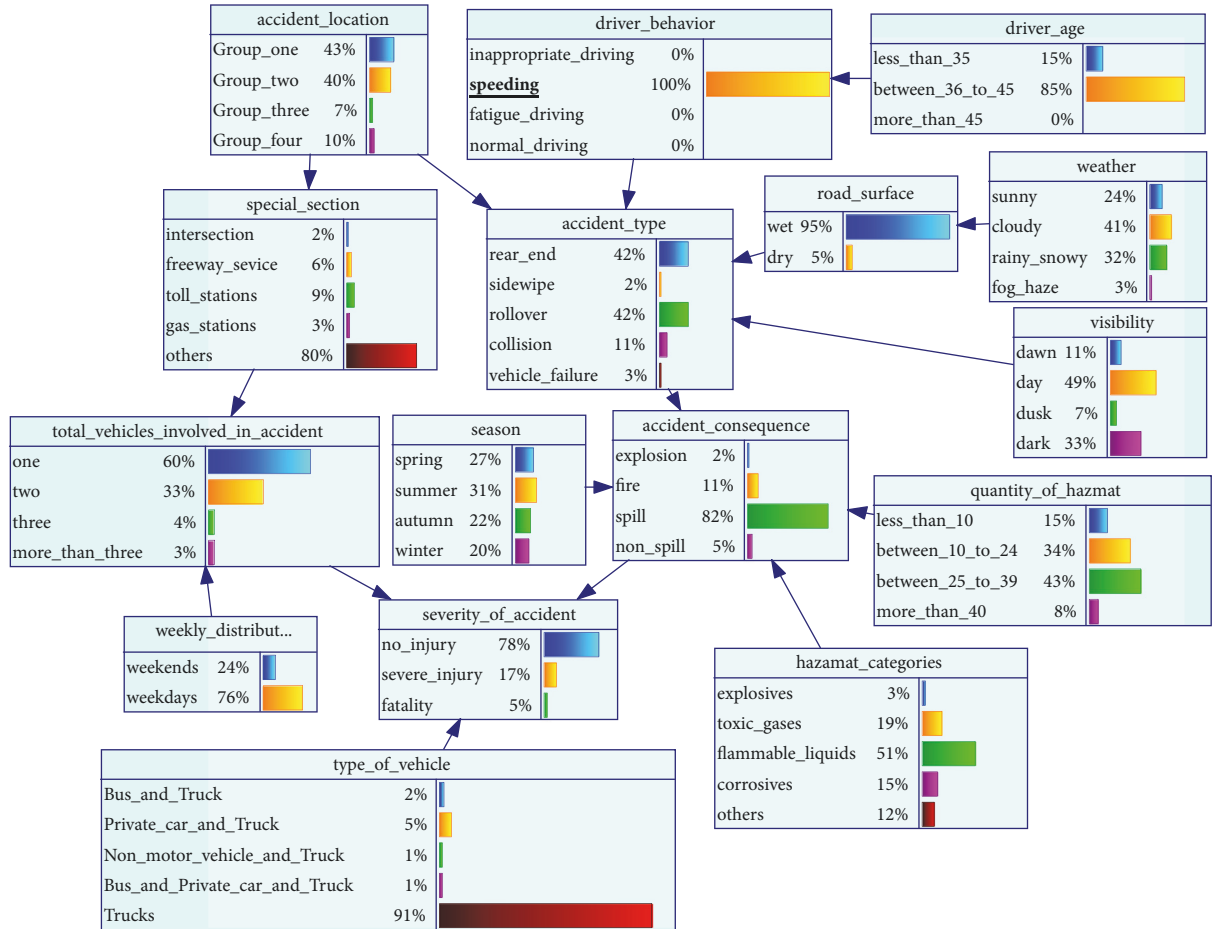


FIGURE 5: Accident prediction when the evidence variable is “speeding”.

flammable liquids due to the single-mode packaging. The quantity of Hazmat transported would significantly affect the severity of accident. The larger the quantity of Hazmat transportation, the larger the inertia of the transportation vehicles, making it not easy to control the emergency [40]. Moreover, the larger quantity of Hazmat transportation is prone to the serious consequences, such as explosion and spill, threatening people’s health and environment [10].

6.2. *Driver Factors.* Previous studies have shown the relationship between driver’s age and the severity of accidents [27, 41, 42]. According to the model results, the younger driver (less than 35) would be more prone to inappropriate driving behavior, which indicates the need for carrying out education programs and training for younger drivers. Tavris et al. [43] also found that younger drivers were much more likely to be involved in severe and fatal accidents. As for the driving behavior, speeding is more likely to lead to rollover accident, especially on the low-class road. This could ascribe the small amount of lanes and the road condition defects on low-class roads, and the speeding would make Hazmat slosh or move around inside the tank, which can constantly shift the vehicle weight, leading to vehicle to rollover due to the off balance [44, 45].

6.3. *Location Factors.* The model results show that “Group one” (the posterior probability is 0.43) and “Group two” (the posterior probability is 0.40) in “accident location” are likely to be associated with severe accidents, which could be attributed by the combination of higher average speed and larger speed dispersion. More importantly, “Group one” and “Group two” roads are considered as the major transport corridors for Hazmat [10, 46]. In addition, some special sections would also considered as the significant risk factors; this could be explained by the fact that there are more interference factors (such as line of sight, pedestrians, and signal lights) at intersections and the greater potential explosion risk around the gas stations [47].

6.4. *Environment Factors.* Hazmat road transportation accidents would easily occur at summer (the posterior probability is 0.31), which is attributed to the characteristic of Hazmat, such as flammable and explosive. And the posterior probability of accidents occurring at weekdays is 0.76, which could be explained by that freeway could be toll-free on important holidays, resulting in significant increase of traffic volume, which could decrease the speed of vehicles. Moreover, Hazmat transportation vehicles were not allowed to drive on freeway (Pan, 2013). Weather is a significant factor for the Hazmat transportation, with cloudy having the

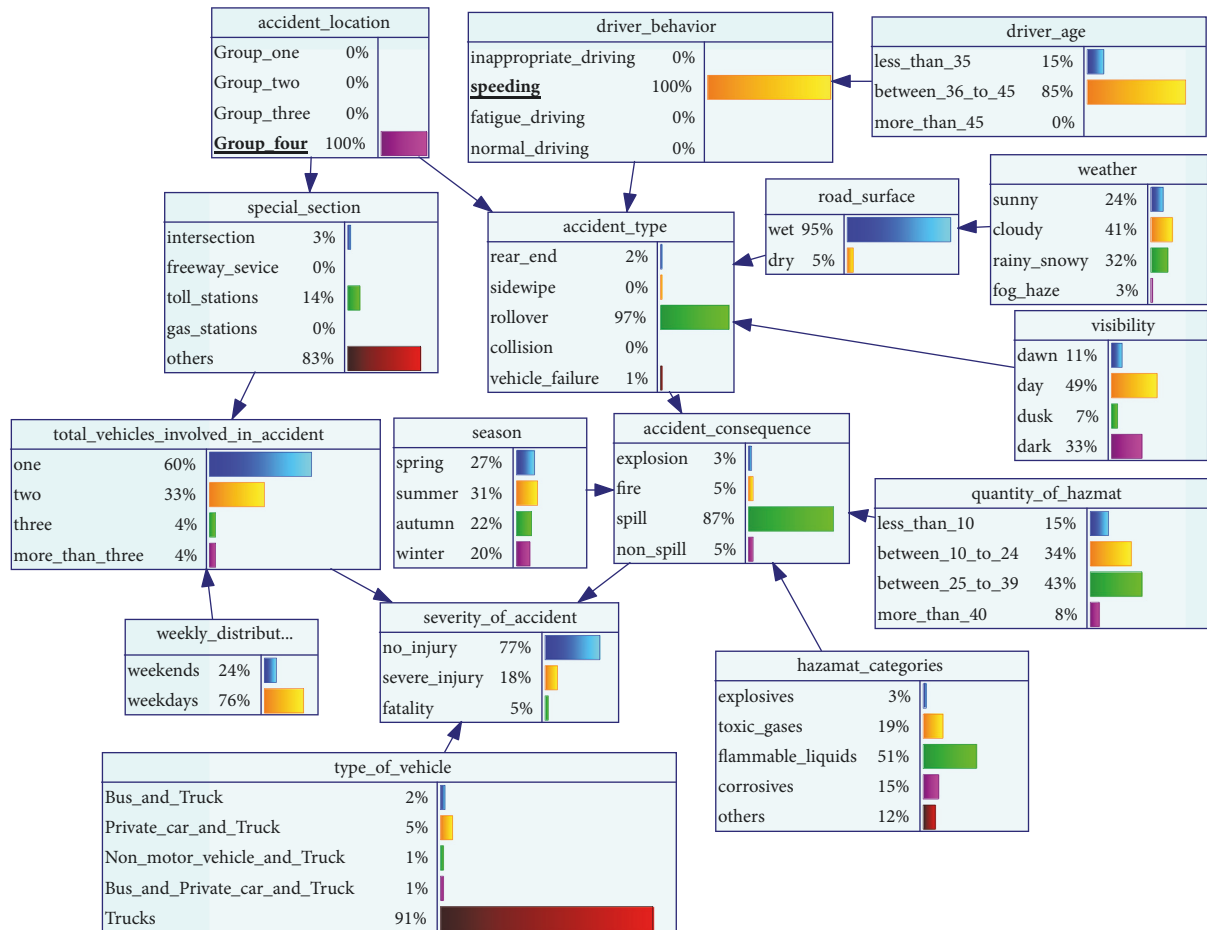


FIGURE 6: Accident prediction when the evidence variable are “speeding” and “Group four”.

highest posterior probability (0.41) followed by rainy (0.32). This could be ascribed that the driver’s mood and visual would be decreased in cloudy and rainy, and the rainy would lower the friction coefficient of roads due to the thin film of water existing between the road surface and tires, which could make the road slippery, increasing the braking distance effectively [48, 49]. Regarding visibility, daytime has the highest posterior probability (0.49), and the dark is 0.33. This is because most transportation corporations are more likely to transport Hazmat at daytime in China [50]. In addition, poor visibility at night would make drivers tired, resulting in driver fatigue, especially from 11:00 pm to 3:00 am [51]. In the sample of accident data, drivers are more prone to fatigue status accounting for 62% of total accidents from 7:00 pm to 4:59 am.

6.5. Vehicle Factors. As for the total vehicles involved in accident, “more than three” would easily result in higher severity of accidents. And the private car involved in accident would cause the severe accident. Two reasons could explain these findings: one is that more vehicles would cause more people involved in accidents, resulting in more people injured; another one is the disparity in mass and speed of trucks compared to other vehicles. In case of an accident,

lighter vehicles (such as private cars) usually absorb the greatest part of the kinetic energy and suffer from more severe injury.

6.6. Accident Factors. Many studies have shown the significant relationship of accidents type and severity, indicating that the rollover accident is associated with the higher severity of accident [16, 44]. The Bayesian network results show that rollover accident has the highest posterior probability (0.41). The reason could be that Hazmat sloshing or moving around inside the tank can constantly shift the vehicle weight, making the vehicle off balance, causing the transportation vehicle to roll over, especially during abrupt evasive maneuvers or turning the vehicle [10]. In addition, as for the consequence of accident, the posterior probability of spill could reach up to 0.81, threatening human health and environment. The result could be explained by that Hazmat releasing could immediately result in poisoning and suffocation, which is difficult for people on-site to escape quickly, resulting in severe and fatality accident [50].

In summary, the occurrence of Hazmat road transportation accidents is unexpected, random, dangerous, and potential. Frequent accidents imply that it is necessary to explore risk factors by using accident mechanism. Bayesian network

is the effective method to deal with uncertainties, which exhibit the potential hierarchical relation by the Directed Acyclic Graph. In the paper, the Bayesian network was developed based on experts' knowledge and modified based on the Hazmat road transportation accident data (N=839) in China. The Bayesian network structure was established by using Genie 2.0, and the results of network structure model reveal the influence of risk factors resulting in accidents and the relationship among risk factors. The study shows that the posterior probability of the Bayesian network could provide effective method for finding the important factors and the factors combination of accidents. These findings could provide theoretical guidance, which could help transportation corporations and government departments take necessary measures to reduce the frequency of Hazmat accidents. More importantly, it must be noted that the aforementioned results were obtained by analyzing the data sample collected from State Work Accident Briefing System and Hazardous Chemical Accidents Communications, which could be existing limitations. As for the further studies, the conclusions should be more generalizable if the dataset had larger size of sample and accidents from multiple states.

Data Availability

The data used to support the findings of this study are available from the corresponding author upon request.

Conflicts of Interest

The authors declare that they have no conflicts of interest.

Acknowledgments

This study has been supported by projects of the National Natural Science Foundation of China (no. 71671127).

References

- [1] K. G. Zografos and K. N. Androustopoulos, "A decision support system for integrated hazardous materials routing and emergency response decisions," *Transportation Research Part C: Emerging Technologies*, vol. 16, no. 6, pp. 684–703, 2008.
- [2] F. G. Cordeiro, B. S. Bezerra, A. S. P. Peixoto, and R. A. R. Ramos, "Methodological aspects for modeling the environmental risk of transporting hazardous materials by road," *Transportation Research Part D: Transport and Environment*, vol. 44, pp. 105–121, 2016.
- [3] Federal Motor Carrier Safety Administration (FMCSA), "Large Truck and Bus Crash Facts 2014," <https://www.fmcsa.dot.gov/sites/fmcsa.dot.gov/files/docs/Large-Truck-and-Bus-Crash-Facts-2014%28April%202016%29.pdf>, 2016.
- [4] J. Zhao L, "Risk Analysis of Dangerous Chemicals Transportation," *Systems Engineering-Theory Practice*, vol. 27, no. 12, pp. 117–122, 2007.
- [5] W. Y. Hua and A. Tong P, "Risk Analysis on Road Transport System of Dangerous Chemicals," *China Safety Science Journal*, vol. 15, no. 2, pp. 8–12, 2005.
- [6] L. Zhao J, P. Wu, and K. Xu, "Statistic analysis and countermeasures on dangerous chemical accidents in China," *China Safety Science Journal*, 2009.
- [7] J. Yang, F. Li, J. Zhou, L. Zhang, L. Huang, and J. Bi, "A survey on hazardous materials accidents during road transport in China from 2000 to 2008," *Journal of Hazardous Materials*, vol. 184, no. 1-3, pp. 647–653, 2010.
- [8] T. Kauppinen and J. Rantanen, "Work and Health Country Profiles and National Surveillance Indicators in Occupational Health and Safety," *Applied Occupational & Environmental Hygiene*, vol. 17, no. 9, p. 603, 2002.
- [9] P. Haastrup and L. Brockhoff, "Severity of accidents with hazardous materials. A comparison between transportation and fixed installations," *Journal of Loss Prevention in the Process Industries*, vol. 3, no. 4, pp. 395–405, 1990.
- [10] X. Shen, Y. Yan, X. Li, C. Xie, and L. Wang, "Analysis on Tank Truck Accidents Involved in Road Hazardous Materials Transportation in China," *Traffic Injury Prevention*, vol. 15, no. 7, pp. 762–768, 2014.
- [11] K. Fang, G. Y. Ke, and M. Verma, "A routing and scheduling approach to rail transportation of hazardous materials with demand due dates," *European Journal of Operational Research*, vol. 261, no. 1, pp. 154–168, 2017.
- [12] F. Bird and G. Germain, *Practical Loss Control Leadership*, International Loss Control Institute, Duluth, GA, USA, Revised edition, 1990.
- [13] J. D. Lemp, K. M. Kockelman, and A. Unnikrishnan, "Analysis of large truck crash severity using heteroskedastic ordered probit models," *Accident Analysis & Prevention*, vol. 43, no. 1, pp. 370–380, 2011.
- [14] M. Uddin and N. Huynh, "Factors influencing injury severity of crashes involving HAZMAT trucks," *International Journal of Transportation Science and Technology*, vol. 7, no. 1, pp. 1–9, 2018.
- [15] E. K. Adanu and S. Jones, "Effects of Human-Centered Factors on Crash Injury Severities," *Journal of Advanced Transportation*, vol. 2017, no. 1528, pp. 1–11, 2017.
- [16] J. De Oña, R. O. Mujalli, and F. J. Calvo, "Analysis of traffic accident injury severity on Spanish rural highways using Bayesian networks," *Accident Analysis & Prevention*, vol. 43, no. 1, pp. 402–411, 2011.
- [17] R. O. Mujalli and J. De Oña, "A method for simplifying the analysis of traffic accidents injury severity on two-lane highways using Bayesian networks," *Journal of Safety Research*, vol. 42, no. 5, pp. 317–326, 2011.
- [18] L. J. Zhao, X. L. Wang, and Y. Qian, "Analysis of factors that influence hazardous material transportation accidents based on Bayesian networks: a case study in China," *Safety Science*, vol. 50, no. 4, pp. 1049–1055, 2012.
- [19] C. Chen, G. Zhang, X. C. Liu et al., "Driver injury severity outcome analysis in rural interstate highway crashes: a two-level Bayesian logistic regression interpretation," *Accident Analysis & Prevention*, vol. 97, pp. 69–78, 2016.
- [20] J. Chen, M. Zhang, S. Yu, and J. Wang, "A Bayesian Network for the Transportation Accidents of Hazardous Materials Handling Time Assessment," *Procedia Engineering*, vol. 211, pp. 63–69, 2018.
- [21] M. Deublein, M. Schubert, B. T. Adey, J. Köhler, and M. H. Faber, "Prediction of road accidents: a Bayesian hierarchical approach," *Accident Analysis & Prevention*, vol. 51, pp. 274–291, 2013.

- [22] C. Xu, W. Wang, P. Liu, and Z. Li, "Calibration of crash risk models on freeways with limited real-time traffic data using Bayesian meta-analysis and Bayesian inference approach," *Accident Analysis & Prevention*, vol. 85, pp. 207–218, 2015.
- [23] C. Tang, Y. Yi, Z. Yang, and J. Sun, "Risk analysis of emergent water pollution accidents based on a Bayesian Network," *Journal of Environmental Management*, vol. 165, pp. 199–205, 2016.
- [24] X. Zou and W. L. Yue, "A Bayesian Network Approach to Causation Analysis of Road Accidents Using Netica," *Journal of Advanced Transportation*, 2017.
- [25] R. Bubbico, S. Di Cave, B. Mazzarotta, and B. Silveti, "Preliminary study on the transport of hazardous materials through tunnels," *Accident Analysis & Prevention*, vol. 41, no. 6, pp. 1199–1205, 2009.
- [26] R. A. Garrido and A. C. Bronfman, "Equity and social acceptability in multiple hazardous materials routing through urban areas," *Transportation Research Part A: Policy and Practice*, vol. 102, pp. 244–260, 2016.
- [27] T. Usman, L. Fu, and L. F. Miranda-Moreno, "Analysis of factors affecting winter collision severity," in *Meeting of the Transportation Research Board*, Washington, DC, USA, 2013.
- [28] F. Chen and S. Chen, "Injury severities of truck drivers in single- and multi-vehicle accidents on rural highways," *Accident Analysis & Prevention*, vol. 43, no. 5, pp. 1677–1688, 2011.
- [29] S. Islam, S. L. Jones, and D. Dye, "Comprehensive analysis of single- and multi-vehicle large truck at-fault crashes on rural and urban roadways in Alabama," *Accident Analysis & Prevention*, vol. 67, pp. 148–158, 2014.
- [30] Q. Xiaohu, L. Li, and Z. Ying, "A traffic accident prediction method based on Bayesian network model," *Computer Simulation*, vol. 22, no. 11, pp. 230–232, 2005.
- [31] S. L. Lauritzen, "The EM algorithm for graphical association models with missing data," *Computational Statistics & Data Analysis*, vol. 19, no. 2, pp. 191–201, 1995.
- [32] F. V. Jensen and T. D. Nielsen, "Bayesian Networks and Decision Graphs," *Technometrics*, vol. 50, no. 1, p. 362, 2012.
- [33] J. Zhou, W. Xu, X. Guo, and J. Ding, "A method for modeling and analysis of directed weighted accident causation network (DWACN)," *Physica A: Statistical Mechanics and its Applications*, vol. 437, pp. 263–277, 2015.
- [34] J. Abellán, G. López, and J. de Oña, "Analysis of traffic accident severity using decision rules via decision trees," *Expert Systems with Applications*, vol. 40, no. 15, pp. 6047–6054, 2013.
- [35] R. O. Mujalli, G. López, and L. Garach, "Bayes classifiers for imbalanced traffic accidents datasets," *Accident Analysis & Prevention*, vol. 88, pp. 37–51, 2016.
- [36] A. Iranitalab and A. Khattak, "Comparison of four statistical and machine learning methods for crash severity prediction," *Accident Analysis & Prevention*, vol. 108, pp. 27–36, 2017.
- [37] L. Fridström and S. Ingebrigtsen, "An aggregate accident model based on pooled, regional time-series data*," *Accident Analysis & Prevention*, vol. 23, no. 5, pp. 363–378, 1991.
- [38] G. F. Ulfarsson, S. Kim, and E. T. Lentz, "Factors affecting common vehicle-to-vehicle collision types: Road safety priorities in an aging society," *Transportation Research Board*, vol. 1980, no. 1, pp. 70–78, 2006.
- [39] G. Zhang, K. K. W. Yau, X. Zhang, and Y. Li, "Traffic accidents involving fatigue driving and their extent of casualties," *Accident Analysis & Prevention*, vol. 87, pp. 34–42, 2016.
- [40] A. Vorster, "Transporting dangerous goods worldwide: materials handling logistics," *South African Pharmaceutical Cosmetic Review*, 2015.
- [41] A. P. Jones and S. H. Jørgensen, "The use of multilevel models for the prediction of road accident outcomes," *Accident Analysis & Prevention*, vol. 35, no. 1, pp. 59–69, 2003.
- [42] S. Kaplan and C. G. Prato, "Risk factors associated with bus accident severity in the United States: a generalized ordered logit model," *Journal of Safety Research*, vol. 43, no. 3, pp. 171–180, 2012.
- [43] D. R. Tavis, E. M. Kuhn, and P. M. Layde, "Age and gender patterns in motor vehicle crash injuries: Importance of type of crash and occupant role," *Accident Analysis & Prevention*, vol. 33, no. 2, pp. 167–172, 2001.
- [44] C. S. Duncan, A. J. Khattak, and F. M. Council, "Applying the ordered probit model to injury severity in truck-passenger car rear-end collisions," *Transportation Research Record*, no. 1635, pp. 63–71, 1998.
- [45] A. Montella, L. Imbriani, and F. Mauriello, "Factors Contributing to Run-off-the-Road Severe Crashes," in *Proceedings of the Transportation Research Board 94th Annual Meeting*, Washington, DC, USA, 2015.
- [46] A. Oggero, R. M. Darbra, M. Muñoz, E. Planas, and J. Casal, "A survey of accidents occurring during the transport of hazardous substances by road and rail," *Journal of Hazardous Materials*, vol. 133, no. 1–3, pp. 1–7, 2006.
- [47] R. Tay and S. M. Rifaat, "Factors contributing to the severity of intersection crashes," *Journal of Advanced Transportation*, vol. 41, no. 3, pp. 245–265, 2010.
- [48] Q. Lin and W. A. Nixon, "Effects of Adverse Weather on Traffic Crashes: Systematic Review and Meta-Analysis," *Transportation Research Record Journal of the Transportation Research Board*, vol. 2055, no. 2055, pp. 139–146, 2008.
- [49] P. Konstantopoulos, P. Chapman, and D. Crundall, "Driver's visual attention as a function of driving experience and visibility. Using a driving simulator to explore drivers' eye movements in day, night and rain driving," *Accident Analysis & Prevention*, vol. 42, no. 3, pp. 827–834, 2010.
- [50] H.-D. Zhang and X.-P. Zheng, "Characteristics of hazardous chemical accidents in China: A statistical investigation," *Journal of Loss Prevention in the Process Industries*, vol. 25, no. 4, pp. 686–693, 2012.
- [51] J. Pahukula, S. Hernandez, and A. Unnikrishnan, "A time of day analysis of crashes involving large trucks in urban areas," *Accident Analysis & Prevention*, vol. 75, pp. 155–163, 2015.

Research Article

Impact of a Lower Conservation Budget on Road Safety Indices

M. Rojo ¹, H. Gonzalo-Orden ¹, A. Linares ¹ and L. dell'Olio ²

¹Department of Civil Engineering, University of Burgos, Burgos 09001, Spain

²Department of Transports, University of Cantabria, Santander 39005, Spain

Correspondence should be addressed to M. Rojo; mrarce@ubu.es

Received 26 April 2018; Revised 11 July 2018; Accepted 22 July 2018; Published 30 July 2018

Academic Editor: Sara Moridpour

Copyright © 2018 M. Rojo et al. This is an open access article distributed under the Creative Commons Attribution License, which permits unrestricted use, distribution, and reproduction in any medium, provided the original work is properly cited.

Over the past few years, several countries, including Spain, have been experiencing a period of economic recession. As a result, these governments have reduced their budgets for transport infrastructures (both construction and maintenance operations). The main objective of this study is to analyze whether these budget reductions have an effect on increased accident rates and to perform an assessment of their real economic benefit. Thus, we analyze whether significant changes over recent years are perceptible in the road safety indexes in Spain, in terms of risk, accident fatality, and accident severity. The relation between lower budgets and higher road safety indices is analyzed through linear regression techniques. The results show a strong relation between the Risk Index and the maintenance budget, measured as an average of the last years. In addition, a final economic assessment demonstrates that this reduction in investment had no real economic benefits, especially as the costs of the accidents exceeded the savings in the conservation plans.

1. Introduction

The consequences of the current economic crisis have affected many countries over the past few years, which have meant that government road construction and maintenance budgets have been reduced. Another consequence of the economic recession is the high reduction in the number and length of journeys by road.

Thus, if we take into account the fact that the number of accidents has remained constant over the past few years, even though traffic volumes are lower, we can conclude that the risk of an accident per kilometre of road has in fact increased. In this paper, a possible relationship between lower construction and conservation budgets and the ratio of accidents is assessed.

To do so, we need to locate the key parameter to analyze this relationship. If we look at the bibliography, we can see different points of view. Hakim et al. [1] presented a critical review of state-of-the-art macro models for road accidents, to identify which variables are more effective, in order to improve levels of road safety: vehicles-kilometre, vehicle fleet, income (in its various forms), percentage of young drivers, intervention policies such as speed limits, periodic vehicle inspection, and minimum alcohol-drinking age. Zou and Yue

[2] studied the causes of road accidents by using a Bayesian Network approach. Rifaat and Chin [3] analyzed the severity of accidents using ordered probit models, giving broad consideration to driver characteristics, roadway features, vehicle types, pedestrian characteristics, and crash characteristics.

Chin and Tan [4] adapted the techniques usually employed for road safety audits in Singapore, in order to develop a Road Safety Performance Rating for the quantitative evaluation of safety deficiencies. The application of road safety audits began there in 1998, though they are named “safety reviews”, as they are not a compulsory checklist to approve a project. Even more, since the review process is usually qualitative in nature, there are some doubts about their significance and their utility. Hence, the authors developed a quantitative approach to obtain a Road Safety Performance Index (RSPI), a related Road Safety Performance Chart (RSPC), and a Road Safety Performance Rating (RSPR) that can serve as a benchmark for comparisons between various road projects.

In addition, de Leur and Sayed [5] analyzed the objectives that a Road Safety Risk Index must achieve and how to develop it correctly. Hermans et al. [6] focused on an essential step in the construction process of a composite road safety performance indicator: the assignment of weights to the

TABLE 1: Evolution of investment in roads [21].

| Year | Overall road budget (M€) | Road construction budget (M€) | Road maintenance and safety budget (M€) |
|------|--------------------------|-------------------------------|---|
| 2008 | 4,778 | 2,822 | 1,219 |
| 2009 | 5,414 | 2,886 | 1,324 |
| 2010 | 5,114 | 3,478 | 1,257 |
| 2011 | 3,011 | 1,445 | 1,085 |
| 2012 | 3,160 | 1,268 | 873 |
| 2013 | 2,963 | 1,084 | 818 |
| 2014 | 2,153 | 1,148 | 818 |
| 2015 | 2,194 | 1,154 | 935 |
| 2016 | 2,383 | 1,174 | 1,058 |
| 2017 | 2,121 | 955 | 958 |

individual indicators. Holló et al. [7] highlighted the limitations of road safety performance indicators, based on examples of certain countries from Central Europe, to conclude that exposure and the socioeconomic climate appear to have a high impact on road safety. Finally, Mannering et al. [8] and Kumar et al. [9] noted the heterogeneity of road-accident data and their specific analyzes which took that issue into account. A similar analysis was conducted by Imprialou and Quddus [10], who studied how to improve the data collection of accidents, in order to achieve a more usable database.

Various studies have analyzed the effects of socioeconomic variables on road safety [11–15]. However, it now appears to be of interest to study them once more, since the characteristics of both roads and economy have changed considerably. Law et al. [16] analyzed the effects of the recent economic crisis and the Motorcycle Safety Programme (MSP) on motorcycle-related accidents, casualties, and fatalities in Malaysia. Although their analysis found a reduction in the number of motorcycle-related accidents and fatalities, the authors concluded that the MSP was the main cause for this reduction, with no signs of separate effects due to the economic crisis. On the contrary, Yannis et al. [17] analyzed the effect of annual changes in Gross Domestic Product (GDP) on annual changes in mortality rates, by employing some mixed linear models for 27 European countries over the period between 1975 and 2011. They concluded that a GDP increase is associated with an increase in mortality rates. Yanqun et al. [18] and Goniewicz et al. [19] analyzed traffic safety at a global level and proposed some possible actions and programs for its improvement. Finally, Loo et al. [20] developed an exhaustive review of road safety strategies in Hong Kong, concluding that significant improvements would require the restructuring of road safety activities.

Following this introduction to the problem, Section 2 will show the evolution of the road safety parameters over the years that are under study. Comparisons between risk levels and budgets will be presented Section 3, and the relations between them will be analyzed with linear regression techniques and discussed. Likewise, an economic assessment of the effects of lower budgets will be set out. Finally, the last

section will offer some concluding remarks and a summary of the main findings of the study.

2. Data Analysis

In this section, the data during the recession period (2009–2014) will be analyzed, both economically and from the point of view of road safety. Thus, it is important to establish the extent of the budget reductions for road construction and maintenance, in order to relate it to possible increases in the risk indexes.

The data reflect economic issues, especially the budget allocations for road works, dividing them into the construction of new roadways and conservation and maintenance operations for the network. In addition, the vehicle fleet and the total volume of registered traffic flows (measured in vehicles per km) are also studied. Finally, with regard to the data on safety, both the accident injury rates and the amount of fatalities (within a period of 30 days from the accident) are analyzed. The period of analysis is between 2008 and 2016, allowing us to visualize the evolution of all these parameters during the economic crisis. These data were mainly gathered from various websites of the Spanish Government, as specified in the following sections.

2.1. Economic Analysis. Firstly, it is necessary to establish the annual budget for road construction and maintenance works. The country under analysis is Spain, so the data were gathered from statistical sources available from the Ministry of Public Works Spanish Government [21].

The last deep recession in Spain lasted from 2009 to 2014, although data were obtained from 2008 to 2017, in order to gain a complete overview of the evolution of the budgets. In addition, we have classified them by construction and maintenance budgets, because of their different characteristics and their impact on road safety. The figures for this period are shown in Table 1.

Firstly, we can note that both the road construction and the maintenance budgets decreased significantly between 2009/2010 and 2013. Specifically, the reduction amounted to 69% for the road construction budget between 2009 and 2013

TABLE 2: Evolution of accidents [23–26].

| Year | Injury Accidents | | Fatalities (30 days) | |
|------|------------------|-----------------|----------------------|-----------------|
| | Value | Δ previous year | Value | Δ previous year |
| 2008 | 43,831 | -- | 2,466 | -- |
| 2009 | 40,789 | -7% | 2,130 | -14% |
| 2010 | 39,174 | -4% | 1,928 | -9% |
| 2011 | 35,878 | -8% | 1,603 | -17% |
| 2012 | 35,425 | -1% | 1,442 | -10% |
| 2013 | 37,297 | 5% | 1,230 | -15% |
| 2014 | 35,147 | -6% | 1,247 | 1% |
| 2015 | 34,558 | -2% | 1,248 | 0% |
| 2016 | 36,721 | 6% | 1,291 | 3% |

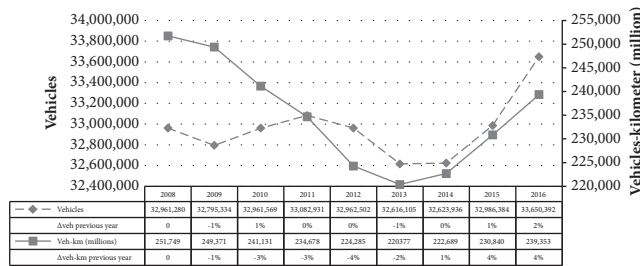


FIGURE 1: Evolution of vehicle fleet and registered traffic [22, 23].

and a 38% for maintenance and safety operation from 2010 to 2013. Once this period was over, the budgets began to rise again in 2015, achieving similar values of 2011/2012 by the end of 2016, very much lower compared with the previous ones. Moreover, in 2017, they were decreased again in a very high proportion. It is important to note that the division of these budgets has been slightly different since 2015, so the data are not completely comparable.

On the other hand, it is interesting to compare these values with the traffic volumes supported by the road in these years. Figure 1 shows how both the vehicle fleet volume and the recorded traffic flows on interurban tracks evolved during the period under consideration.

We can note that although the size of the vehicle fleet increased in 2011, there were two “troughs” for the vehicle fleet: in 2009 and 2013. Following that year, it underwent slight increases in 2014, compared with the previous year. On the other hand, if we analyze the traffic volumes (measured in vehicle-kilometres travelled), we can see a continuous descendent trend from 2008 to 2013, after which its minimum value increased, coinciding with the severest years of the economic crisis, although that trend changed in 2014, with a slight growth that continued until 2016.

Finally, if we analyze the distribution of the vehicle fleet, we can see that, in 2016 (the most recent year with published statistics), 71% of vehicles were cars, 15% were trucks and vans, 10% were motorcycles and mopeds, and the remaining 4% were buses, tractors, and other vehicles types. More interesting is the fact that, in 2016, the average age was 11.5 years for light vehicles and 13.5 years for trucks and vans [23],

demonstrating how the vehicle fleet in Spain was affected by suffered the economic crisis, as were other sectors.

2.2. Road Safety Analysis. In this section, we analyze the accident statistics corresponding to the same period. Table 2 shows the number of accidents and the number of fatalities (within 30 days) on Spanish roads. There, we can see that, in general terms, both data are descending during the period of the economic crisis, while the number of accidents experienced only slight growth between 2012 and 2013, reaching its historical minimum value in 2015. On the contrary, the number of fatal victims was higher than the minimum in 2013, and since that year it increased slightly.

It is obvious that increasingly effective passive safety systems in modern vehicles would probably have influenced the fatality and severity indices, since personal injuries are fortunately reduced by a high percentage. However, the fact that there was no increase in accidents after a certain date (even when the traffic volumes increased) appears to point to a relationship with the budget reductions for roads and, therefore, for road maintenance.

To verify this hypothesis, the standard road safety indices were calculated: risk, fatality, and severity indexes. The probability of traffic accidents occurring for each driven kilometre is shown by the Risk Index. In the case of the Fatality Index, the likelihood of death in a traffic accident is a quantifiable value. Finally, the Severity Index indicates the probability of dying once an accident has been occurred. Equations (1) to (3) show the expressions to obtain these indices [27]:

$$\begin{aligned}
 \text{Risk Index} &= RI \\
 &= \frac{\text{Number of accidentes involving victims}}{10^8 \text{ vehicles} - \text{kilometre}} \quad (1)
 \end{aligned}$$

$$\begin{aligned}
 \text{Fatality Index} &= FI \\
 &= \frac{\text{Number of fatalities (within 30 days)}}{10^8 \text{ vehicles} - \text{kilometre}} \quad (2)
 \end{aligned}$$

$$\begin{aligned}
 \text{Severity Index} &= SI \\
 &= \frac{\text{Number of fatalities (within 30 days)}}{100 \text{ accidentes involving victims}} \quad (3)
 \end{aligned}$$

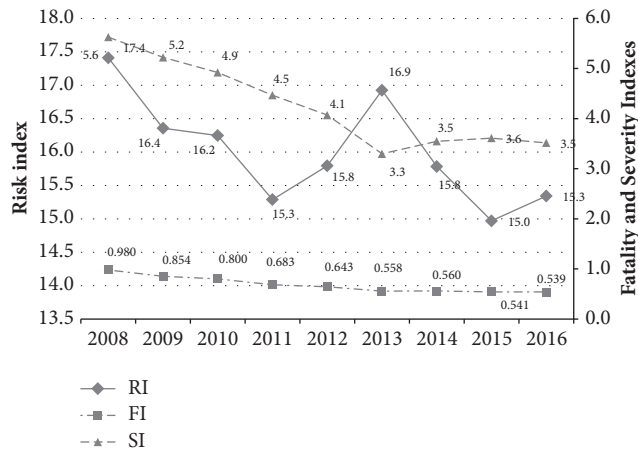


FIGURE 2: Evolution of the Road Safety Indices.

These indexes can be employed to analyze and, in some cases, even to forecast the accidents rate and their consequences, as proposed by Commandeur et al. [28].

Employing the data presented in Figure 1 and Table 2, we can calculate each one of these indices. The results are shown in Figure 2, where we can see that both the Fatality and the Severity Indexes show a decreasing trend, except in 2014, with a slight increase in the FI compared with previous years. Nevertheless, the trend of the Risk Index is clearly opposed, with an initial minimum in 2011, but followed by a high increase until 2013, coinciding with the last few years of the economic recession, and then another low value in 2015.

As previously noted, the passive safety systems of automobiles, increasingly more sophisticated and efficient, are one of the main causes of the decrease in both the Fatality and the Severity Indexes. But the Risk Index is related more to the state of the road (and to the active safety systems of vehicles, as well), so we can analyze whether the reduction in conservation and maintenance budgets might have had some influence on its dramatic growth between 2011 and 2013.

This hypothesis agrees with Hakkert et al. [29], who discussed the problems associated with the use of exposure and risk and gave examples of various safety studies. Their conclusion was that these terms should in practice be defined within the context of the issue under study. For each application, the correct exposure measure should be used: in the case of transport, the most widely used measure of exposure was the number of kilometres travelled for each travel mode (vehicles-kilometre travelled). In addition, Chan, Huang, and Yan [30] studied the effect of asphalt pavement conditions on traffic accidents, by using negative binomial regression models.

3. Comparison between Economic and Accidents Data

In this section, the economic and the road safety data presented in the previous chapters will be compared, in order to analyze the influence of one on the other. Initially,

the possible existence of a relationship between the annual road budgets (overall or only for conservation purposes) and safety indexes will be discussed. Afterwards, a brief economic assessment of this relationship will be done, by comparing the savings in maintenance with the eventual higher costs due to accidents.

3.1. Relationship between Annual Budgets and Safety Indexes. The possible relationship between the data gathered on annual budgets and the rate of endangerment will be analyzed. The reasons for selecting this ratio are due to the lower influence of passive safety systems, increasingly sophisticated and widespread in the vehicle fleet, on the Risk Index, rather than the calculated ones.

Thus, we employed regression techniques to determine the possible correlation between the different budgets and the Risk Index. Even though the results of various types of regression tests were quite similar, we finally chose the linear models. As previously mentioned, the budget data between 2009 and 2014 were included in the analysis, as the rest of the data were not directly comparable, due to the change in their structures.

In Figure 3, the relations between the road budgets and the Risk Index of the following year are shown, as the impact of a low conservation budget was not immediately detected, except for a certain period. Figure 4 shows the same effect two years later. We can observe that the trends in these figures show an increase in both the slope of the regression line and the R2 index over time. However, the R2 indexes were not strong enough in some cases.

Finally, rather than with the budgets of the preceding year, the analysis of the relation of the Risk Index, with the average of the previous years, is even more illustrative. Figures 5 and 6 show the results of this relationship. There we can see that not only that the gradient of the regression line grows (in an absolute value), but also that the coefficients of determination R2 started to reach significant values: higher than 95% with the budgets over the 3 preceding years.

Therefore, we can conclude this section by pointing out that there is a relationship between the budgets for roads and their endangerment. This relationship is much more clear and intense when we specifically analyze budgets for maintenance operations. We can also see that a decrease in the maintenance budget has an effect on the Risk Index for the following years, because the deterioration of roadways has a higher impact on road safety over subsequent years rather than in the year that corresponds to the budget allocations. If instead of considering the annual value of budgets, we take the average of the previous years (much more realistic), the coefficient of determination reaches levels that are higher than 95%, which are considerably significant for our purposes.

3.2. Economic Assessment. Finally, in this section, we will analyze whether these reductions in road budgets are economically profitable or whether the costs associated with the new accidents outweigh the savings. For this purpose, we shall employ the regression line obtained in Figure 6, which shows the relationship between the Risk Index (RI) and the

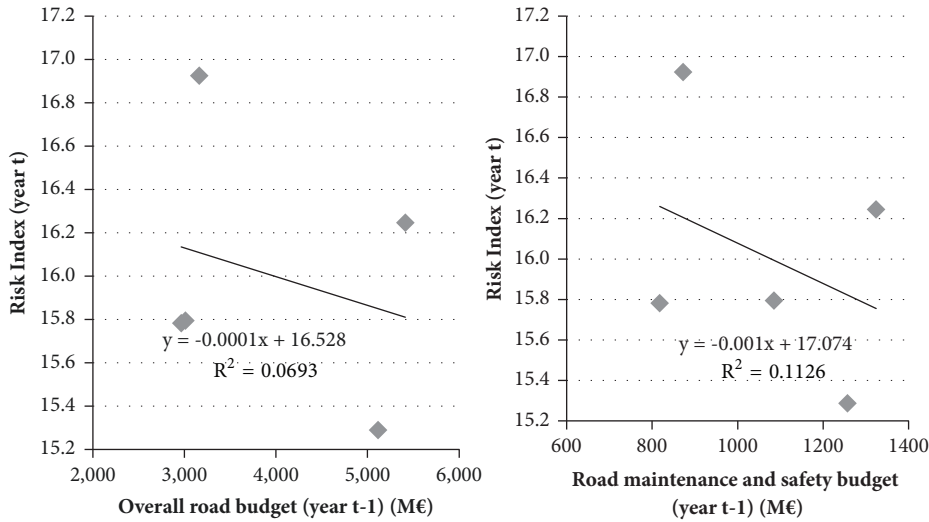


FIGURE 3: Relationship between Risk Index (year t) and Road Budgets (year t-1).

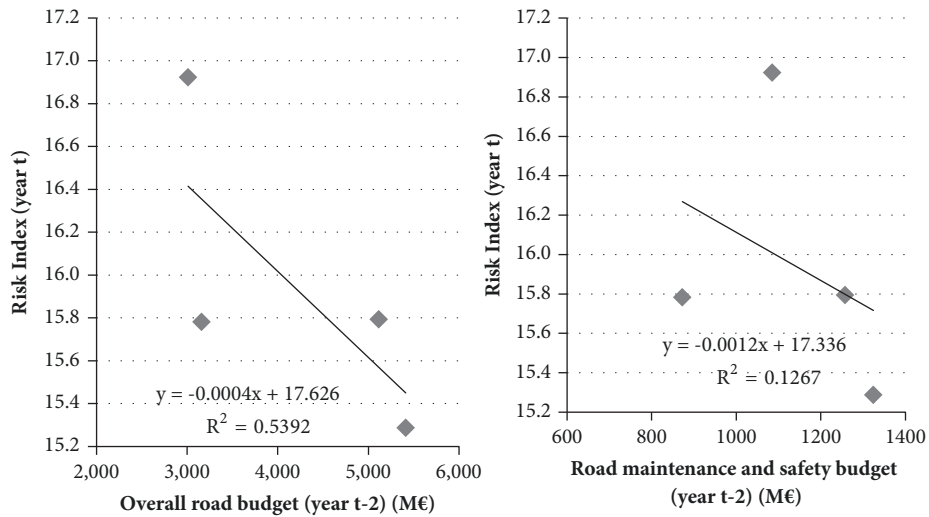


FIGURE 4: Relationship between Risk Index (year t) and Road Budgets (year t-2).

average road maintenance budget over the previous 3 years, in millions of Euros (MB_3). This equation is presented in the following:

$$RI = 25.695 - 0.0082 \cdot MB_3 \tag{4}$$

Combining this equation with (1), we can directly relate the maintenance budget to the number of accidents involving victims (AV) and the traffic volume measured in vehicles-kilometre travelled (VKT), as shown in the following:

$$RI = \frac{AV}{VKT (10^8)} = 10^8 \cdot \frac{AV}{VKT} \rightarrow \tag{5}$$

$$AV = \frac{VKT}{10^8} \cdot (25.695 - 0.0082 \cdot MB_3)$$

Thus, once we have established the real number of VKT over the last few years of the recession, we can estimate how many

accidents could have been produced, if the budgets had been maintained at the same levels before the economic crisis. As we can see in Table 1, the MB_3 has varied during the period of study, in a range from 1267 M€ in 2011 (average from 2008 to 2010) to 925 M€ in 2014 (average from 2011 to 2013).

Therefore, we propose, in view of the real value of VKT in each year, three different scenarios: Scenario 1 with the highest budget values at all times; Scenario 2 with the average of these margins; and Scenario 3 with the real values. These scenarios and their corresponding estimated number of accidents are shown in Table 3.

Comparing these values with those presented in Table 2, we can see that more than 3,900 accidents involving victims could have been avoided, had the road maintenance budgets remained constant at the same levels as 2011 (scenario 1). Even in the intermediate hypothesis (scenario 2), roughly 1,300 accidents could have been prevented between 2012 and 2013.

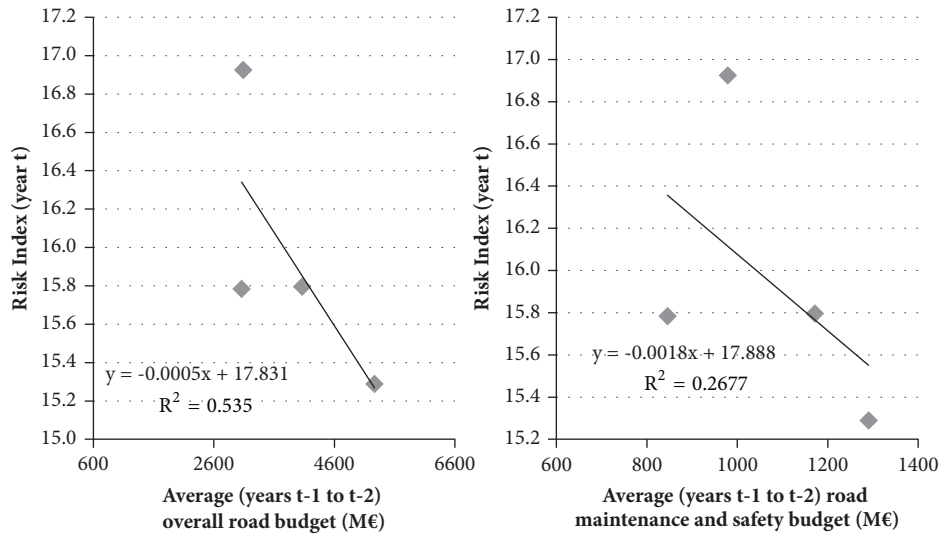


FIGURE 5: Relationship between Risk Index and Average Values of Road Budgets (2 previous years).

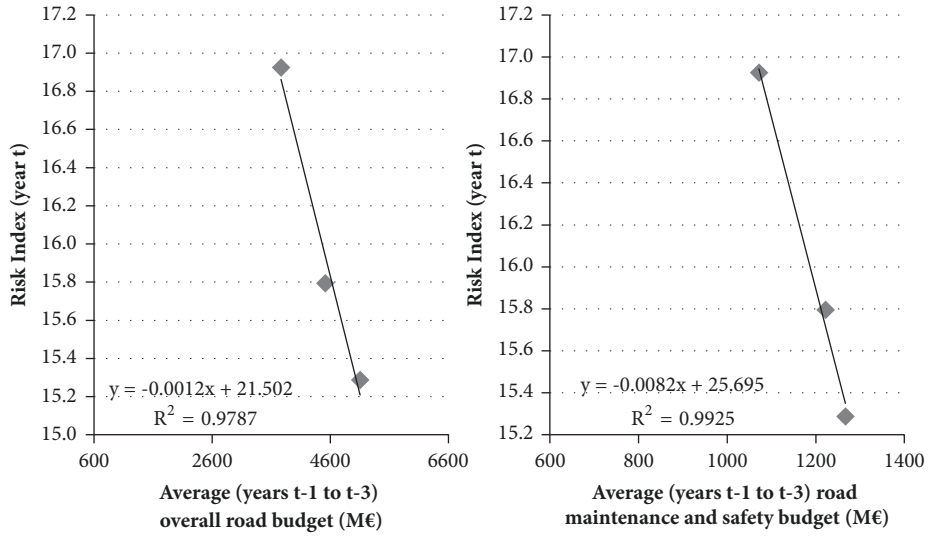


FIGURE 6: Relationship between Risk Index and Average Values of Road Budgets (3 preceding years).

TABLE 3: Estimated value of AV with higher conservation budgets.

| Year | VKT (millions) | MB ₃ (M€) | | | AV estimated | | |
|------|----------------|----------------------|------------|------------|--------------|------------|------------|
| | | Scenario 1 | Scenario 2 | Scenario 3 | Scenario 1 | Scenario 2 | Scenario 3 |
| 2011 | 234,678 | 1,267 | 1,267 | 1,267 | 36,559 | 36,559 | 36,559 |
| 2012 | 224,285 | 1,267 | 1,244 | 1,222 | 34,940 | 35,351 | 35,761 |
| 2013 | 220,377 | 1,267 | 1,169 | 1,072 | 34,331 | 36,093 | 37,855 |
| 2014 | 222,689 | 1,267 | 1,096 | 925 | 34,691 | 37,808 | 40,924 |

TABLE 4: Estimated incremental cost because of the increased Risk Index.

| Year | Estimated Increase of Fatalities | | Estimated Increase of Injured | | Estimated Increase of Cost (M€) | |
|------|----------------------------------|------------|-------------------------------|------------|---------------------------------|------------|
| | Scenario 1 | Scenario 2 | Scenario 1 | Scenario 2 | Scenario 1 | Scenario 2 |
| 2012 | 20 | 3 | 1,203 | 184 | 208 | 32 |
| 2013 | 98 | 40 | 7,261 | 2,948 | 1,240 | 503 |
| 2014 | 16 | -- | 1,213 | -- | 207 | -- |

The next step was to establish an economic value for each accident with victims. Three different methodologies for its estimation were identified in the bibliography [31]:

- (i) Compensation method: based on the average compensation paid by insurance companies to accident victims or their families
- (ii) Human capital method: based on calculations of production losses, adding occasionally a certain percentage to represent the pain and human suffering associated with traffic accidents
- (iii) The willingness to pay method: based on stated preference surveys, where interviewees have to say what amount of money they are willing to pay for a certain reduction in the risk of an accident.

One of the most recent studies in Spain on this topic is the document prepared by FITSA [31], which determines that the unit cost ranged, according to the method used, between 349,687 and 857,648 Euros per fatality. Since these values were very low, compared with those corresponding to other European countries, we took the higher ones, because there were no subsequent studies in Spain. Finally, the New Zealand Ministry of Transport [32] estimated the costs of serious injuries at 18.56% of those corresponding to fatalities. Thus, we were able to assume an average value of €159,173 per injured person.

We can therefore estimate how many fatalities could be avoided, basing our study on the values presented in Table 3 and Figure 2 (Severity Index) and the data relating to the average number of injured in each accident [25]. If we transform it into monetary units, we can determine the incremental cost for Spain, because of the increase of the Risk Index in its roads. These calculations are presented in Table 4.

If the conservation budgets had remained constant at the same levels as 2011 (scenario 1), over 1650 M€ could have been saved in terms of accident-related costs during the period under consideration. Even in the intermediate hypothesis (scenario 2), this incremental estimated cost of accidents is higher than 500 M€. By analyzing Table 1, we can see that the savings in the conservation budget from 2011 to 2014 amounted to a total amount of 746 M€. Therefore, we can conclude that for each Euro not spent on the maintenance of roads generated a cost of traffic accidents within a range of between 0.7 and 2.2 Euros. There are also studies that have affirmed that if the trends towards further reductions remained unmodified, then after some years the reconstruction of the network would be needed, so the final cost would considerably increase [33].

Thus, even if we were not to consider the economic assessment, the savings in conservation and maintenance budgets were not acceptable in terms of road safety. Human life is so important that no economic assessment can be considered when we are considering accidents that bring nothing but human pain and suffering.

4. Conclusions

In this paper, the effects of the economic recession in certain countries and especially Spain on road safety have been

analyzed. This crisis has modified both the amounts invested in road infrastructure, construction of new roadways or maintenance of the existing ones, and the traffic flowing through them, making them decrease. However, much more important is the impact of these issues on the safety indexes, which directly affects the relative number of accidents.

According to our results, we can underline six main conclusions:

- (i) The overall road budget has considerably decreased during the years of recession. Over the period between 2008 and 2017 the road construction budget diminished by 66%, while the maintenance and conservation budget decreased by 21% in the same period. However, if we take the maximum and minimum values, we can see a decrease of 73% in the construction budget between 2010 and 2017 and of 38% in conservation and maintenance between 2009 and 2013.
- (ii) Concerning the traffic circulating on Spanish roads, we have noted similar decreasing trends between 2008 and 2013, the year with the minimum number of registered vehicles-kilometres. The traffic in 2013 was 12% lower than the traffic in 2008. However, in 2014, this trend started changing, noting a growing comparing with the previous years.
- (iii) From a different point of view, the number of fatalities has fortunately continued its downward trend, except since 2013, when a slight increase once again appeared. However, the number of accidents involving injuries significantly decreased between 2008 and 2012 by 19%, but has remained constant or even higher since that year.
- (iv) The fatality index, which is related to the above data, has fortunately been decreasing each year during the period under analysis. However, the Risk Index achieved a minimum value in 2011, but underwent a high, 11%, increase over the following two years. We considered that this index was the most representative, since the others were influenced by the passive safety of vehicles to a greater extent. These systems are, fortunately, more and more advanced and therefore prevented deadly casualties in the case of accidents involving severe injuries.
- (v) If we study the relationship between this Risk Index with the road conservation and maintenance budgets, we see a real correlation between the average maintenance budget over the preceding years and the possibilities of having an accident in the actual one. This correlation is defined by the determination coefficients, which reached a value of 27% when analyzing the preceding two years and 99% over the preceding three years.
- (vi) Finally, if we try to assess the economic impact of these two opposing variables, lower budgets and higher Risk Indices, we can determine that this reduction of conservation budgets does not lead to a real saving,

as the cost of the additional accidents was higher (by between 0.7 and 2.2 times). Additionally, the maintenance (or reconstruction) costs in the future will grow much more than the usual amount, such that the effect of negative savings were even higher, added to the human tragedy associated with road traffic accidents, fatalities, and victims.

Hence, we can conclude by underlining the relationship between the road infrastructure investment budgets and the associated safety indexes. This relation cannot be ignored, because any decrease in maintenance budgets will eventually provoke a fatal accident. Even if we consider the problem in economic terms, each Euro invested in the conservation of roads is more than compensated in terms of fewer accidents.

We should encourage the relevant authorities to continue investing in road infrastructure even in economic recession periods, particularly in maintenance and conservation operations (other large investments in transport could instead be reduced), as investment in maintenance affects the accident rate on our roadways, with several economic consequences, added to the human lives that are placed at risk.

Data Availability

Previously reported budget, accidents, and traffic data were used to support this study and are mainly available at Government of Spain pages (<https://www.fomento.gob.es>; <http://www.dgt.es>). These prior datasets are cited at relevant places within the text as [21–26, 31].

Conflicts of Interest

The authors declare that there are no conflicts of interest regarding the publication of this paper.

Acknowledgments

This research has been developed within the frame support of the University of Burgos (Spain).

References

- [1] S. Hakim, D. Shefer, A. S. Hakkert, and I. Hocherman, "A critical review of macro models for road accidents," *Accident Analysis & Prevention*, vol. 23, no. 5, pp. 379–400, 1991.
- [2] X. Zou and W. L. Yue, "A bayesian network approach to causation analysis of road accidents using netica," *Journal of Advanced Transportation*, vol. 2017, Article ID 2525481, 18 pages, 2017.
- [3] S. M. Rifaat and H. C. Chin, "Accident severity analysis using ordered probit model," *Journal of Advanced Transportation*, vol. 41, no. 1, pp. 91–114, 2007.
- [4] H.-C. Chin and E. Tan, "Evaluating safety performance of road projects," *Proceedings of the Institution of Civil Engineers: Transport*, vol. 153, no. 3, pp. 191–196, 2002.
- [5] P. de Leur and T. Sayed, "Development of a road safety risk index," *Transportation Research Record*, no. 1784, pp. 33–42, 2002.
- [6] E. Hermans, F. Van den, and G. Bosscheand, "Combining road safety information in a performance index," *Accident Analysis & Prevention*, vol. 40, no. 4, pp. 1337–1344, 2008.
- [7] P. Holló, V. Eksler, and J. Zukowska, "Road safety performance indicators and their explanatory value: A critical view based on the experience of Central European countries," *Safety Science*, vol. 48, no. 9, pp. 1142–1150, 2010.
- [8] F. L. Mannering, V. Shankar, and C. R. Bhat, "Unobserved heterogeneity and the statistical analysis of highway accident data," *Analytic Methods in Accident Research*, vol. 11, pp. 1–16, 2016.
- [9] S. Kumar, D. Toshniwal, and M. Parida, "A comparative analysis of heterogeneity in road accident data using data mining techniques," *Evolving Systems*, vol. 8, no. 2, pp. 147–155, 2017.
- [10] M. Imprialou and M. Quddus, "Crash data quality for road safety research: current state and future directions," *Accident Analysis & Prevention*, 2017.
- [11] G. J. S. Wilde, "Economics and accidents: a commentary," *Journal of Applied Behavior Analysis*, vol. 24, no. 1, pp. 81–84, 1991.
- [12] J. G. U. Adams, *Risk and freedom*, Transport Publishing Projects, UK, 1985.
- [13] G. W. Mercer, "Influences on passenger vehicle casualty accident frequency and severity: Unemployment, driver gender, driver age, drinking driving and restraint device use," *Accident Analysis & Prevention*, vol. 19, no. 3, pp. 231–236, 1987.
- [14] S. C. Partyka, "Simple models of fatality trends using employment and population data," *Accident Analysis & Prevention*, vol. 16, no. 3, pp. 211–222, 1984.
- [15] M. Rojo, H. Gonzalo-Orden, A. Linares, and L. Dell'Olio, "Effects of economic recession on road safety indexes," *Transportation Research Procedia*, vol. 18, pp. 80–87, 2016.
- [16] T. H. Law, R. S. R. Umar, S. Zulkaurnain, and S. Kulanthayan, "Impact of the effect of economic crisis and the targeted motorcycle safety programme on motorcycle-related accidents, injuries and fatalities in Malaysia," *International Journal of Injury Control and Safety Promotion*, vol. 12, no. 1, pp. 9–21, 2005.
- [17] G. Yannis, E. Papadimitriou, and K. Folla, "Effect of GDP changes on road traffic fatalities," *Safety Science*, vol. 63, pp. 42–49, 2014.
- [18] Y. Yanqun, Z. Lin, H. Aixiu, X. Zheng, and S. M. Easa, "Evaluating highway traffic safety: an integrated approach," *Journal of Advanced Transportation*, vol. 2018, Article ID 4598985, 11 pages, 2018.
- [19] K. Goniewicz, M. Goniewicz, W. Pawłowski, and P. Fiedor, "Road accident rates: strategies and programmes for improving road traffic safety," *European Journal of Trauma and Emergency Surgery*, vol. 42, no. 4, pp. 433–438, 2016.
- [20] B. P. Y. Loo, S. C. Wong, W. T. Hung, and H. K. Lo, "A review of the road safety strategy in Hong Kong," *Journal of Advanced Transportation*, vol. 41, no. 1, pp. 3–37, 2007.
- [21] Ministerio de Fomento (MFOM), Presupuestos Generales del Estado, Ministerio de Fomento, Spain Government, 2008–2017.
- [22] Ministerio de Fomento (MFOM), Anuario Estadístico 2014–2016, Ministerio de Fomento, Spain Government, 2015–2017.
- [23] Dirección General de Tráfico (DGT), Las Principales Cifras de la Siniestralidad Vial. España 2008–2016, Ministerio del Interior, Spain Government, 2009–2017.
- [24] Dirección General de Tráfico (DGT), Balance de Seguridad Vial 2015, Ministerio del Interior, Spain Government, 2016.
- [25] Dirección General de Tráfico (DGT), Anuario Estadístico de Accidentes 2015–2016, Ministerio del Interior, Spain Government, 2016–2017.
- [26] Real Automóvil Club de Cataluña (RACC), Análisis del Estancamiento de la Siniestralidad en las Carreteras Españolas durante 2015, RACC Automóvil Club, Spain, 2016.

- [27] C. Kraemer, J. M. Pardillo, M. G. Romana, V. Sánchez, and M. A. del Val, *Ingeniería de Carreteras*, vol. 1, S. A. McGraw-Hill/Interamericana de España, Spain, 2009.
- [28] J. J. F. Commandeur, P. Wesemann, F. Bijleveld, V. Chhoun, and S. Sann, "Setting road safety targets in cambodia: a methodological demonstration using the latent risk time series model," *Journal of Advanced Transportation*, vol. 2017, Article ID 5798174, 9 pages, 2017.
- [29] A. S. Hakkert, L. Braimaister, and I. Van Schagen, *The uses of exposure and risk in road safety studies*, SWOV Institute for Road Safety Research, The Netherlands, 2002.
- [30] C. Y. Chan, B. Huang, X. Yan, and S. Richards, "Investigating effects of asphalt pavement conditions on traffic accidents in Tennessee based on the pavement management system (PMS)," *Journal of Advanced Transportation*, vol. 44, no. 3, pp. 150–161, 2010.
- [31] FITSA - Fundación Instituto Tecnológico para la Seguridad del Automóvil, El valor de la seguridad vial. Conocer los costes de los accidentes de tráfico para invertir más en su prevención, FITSA Foundation, Spain, 2018.
- [32] NZ Ministry of Transport, *Social Cost of Road Crashes and Injuries 2015 Update*, Financial, Economic and Statistical Analysis Team, Ministry of Transport, New Zealand, 2015.
- [33] Asociación Española de la Carretera, *Nota de Prensa – Auditoría sobre el Estado de las Carreteras*, Asociación Española de la Carretera, Spain, 2016, https://www.aecarretera.com/np/NP%20Auditoria%20estado%20carreteras%20AEC%202015%202016_v3.pdf.

Research Article

Reliability-Based Estimation of Traffic Interruption Probability due to Road Waterlogging

Manuel Contreras-Jara,¹ Tomás Echaveguren ^{1,2} José Vargas Baecheler,¹
Alondra Chamorro Giné ^{2,3} and Hernán de Solminihac Tampier^{3,4}

¹Laboratory of Transportation Systems Management (GESITRAN), Departamento de Ingeniería Civil, Facultad de Ingeniería, Universidad de Concepción, Edmundo Larenas 219, Concepción, Chile

²National Research Center for Integrated Natural Disaster Management (CIGIDEN), CONICYT/FONDAP/15110017, Avda. Vicuña Mackenna 4860, Santiago, Chile

³Department of Construction Engineering and Management, School of Engineering, Pontificia Universidad Católica de Chile, Avda. Vicuña Mackenna 4860, Santiago, Chile

⁴Latin American Center of Economic and Social Policies (CLAPES UC), Avda. Libertador Bernardo O'Higgins 440, Piso 13, Santiago, Chile

Correspondence should be addressed to Tomás Echaveguren; tehaveg@udec.cl

Received 31 March 2018; Revised 14 June 2018; Accepted 2 July 2018; Published 29 July 2018

Academic Editor: Nirajan Shiwakoti

Copyright © 2018 Manuel Contreras-Jara et al. This is an open access article distributed under the Creative Commons Attribution License, which permits unrestricted use, distribution, and reproduction in any medium, provided the original work is properly cited.

Floods affect road infrastructure physically and operationally, increase road user costs and road agencies cost, and eventually isolate communities. The research of the effect of floods on vehicular circulation is mainly focused on the stability of vehicles. There are few studies related to the regime of still water in the trafficability. In still water, the speed flow is low and does not compromise the vehicle stability. In this case, the vehicle's wading height becomes relevant. This article proposes a procedure to estimate the traffic interruption probability caused by floods in roads, considering the still water regime. The procedure uses the first-order reliability method to estimate traffic interruption probabilities, based on the difference between the probability density functions (PDF) of still water depth (or waterlogging depth) and vehicle wading height. A specific procedure to estimate the PDF of wading height based in the geometric characteristics of light and heavy vehicles was developed. The PDF for water depth was estimated using water level profile simulation software. The procedure was applied in the south of Chile. The PDF of wading height was obtained from a record of 166,155 vehicles tagged in open road tolls. The PDF of waterlogging depth was obtained from discharge records of 10 fluvimetric stations. 42 probability curves were obtained for six vehicle classes and return periods between 4 and 500 years. The still water depth obtained for traffic interruption probability of 1,0 varied between 70 and 90 cm for light vehicles and between 110 and 150 cm for heavy vehicles.

1. Introduction

Floods damage the physical highway assets and affected their operations. Floods are caused by high intensity rains in a short period of time and induce a rapid rise in water level, overflowing the river banks [1]. Floods usually erode the river banks, scour and destabilize the pier and footings of bridges, and weaken the rock fill and rip-rap foundations. The waterlogging is defined as a slow increase of the water level that covers the low lands and flood plains at low water flow speed.

If the highways are placed in flood plains, the highways' physical assets experience little damage, but the road network operation can be totally or partially interrupted during and before the rain period, until the water level decreases and the roads can recover the trafficability. The traffic interruption degree depends upon if the water level over the roadway is higher or lower than the vehicle's wading capability and if the water speed is enough or not to destabilize or drag the vehicle. The wading capability depends on the wading height, which is the maximum water level at which a vehicle can

ride without affecting the engine, brakes, and the heating, ventilation, and conditioning system (HVAC) and without loss stability because of floating and sliding. Each type of vehicle has a specific wading height. If the water level is lower than the wading height and the water speed is low, vehicles can ride over the flooded road at a reduced speed, increasing the travel time and the operating cost. The consequence is a reduction of the traffic quality in terms of the Level of Service (LOS) of the road, which is measured using the average travel speed and the spend-time-following vehicles in two-lane rural roads and in multilane highways in terms of the traffic density [2]. Also, if the water level and speed are high, vehicles are destabilized and cannot pass through the flooded road. In this case, the loss of LOS is total. Therefore, predicting the possibility that a vehicle can ride over a flooded road depends on the vehicle characteristics and the magnitude of the flood.

There exist several models to predict the water depth over the roadway because of a flood: ad hoc models; hydrological-hydraulic (H-H) 1D, 2D, and 3D models; and GIS-based models [3]. The ad hoc models are empirical and estimate flooded areas (named blue spots) based on historical data. These allow creating flood maps and are an efficient alternative if it is not possible to calibrate more sophisticated models [4–6]. The H-H 1D models used the river and bank's topography, the water flow, and the hydraulic regime to calculate the water level profile and the flooded surface. Examples of this type of models are HEC-RAS and MIKE11 [7, 8]. The H-H 2D models also need data of the flooded area, the ground roughness, the river slope, the rain intensity, and terrain digital models [9]. Examples of these types of models are HEC-RAS 2D, IBER, and MIKE FLOOD [10, 11]. The H-H 3D models estimate the flow speed too but are intensive in data needs because of considering advective and convective transport, the sediment transport, and the wave effect to estimate the water level profile [12]. The GIS-based models integrate some characteristics of the H-H models to the GIS capabilities but also allow estimating physical and economic damage due to floods particularly in urban areas. Examples of these models are HEC-FDA, HAZUS-HM, Damage Scanner, Flemish Model, and Multicolored Manual among others [13–17].

These models previously described only estimate the water depth over the roadway. The water depth depends on the return periods, the river, and floodplains' topography. Therefore, it is plausible to assume that this variable can be characterized with a probability density function. However, to study the probability of traffic interruption, it is also necessary to calculate the wading height, which is a specific property of each vehicle type included in a vehicle fleet. Each type of vehicle has its own engine, brake, and HVAC system, as well as a tire diameter and ground clearance. Therefore, there is a probability function that describes the vehicle's wading height of each brand and model of light cars, pick-up, SUV, trucks, and buses. Because the wading height and the water depth are random, the traffic interruption must be estimated using probabilistic models. In this sense, this paper proposes and applies a procedure to estimate the traffic interruption probability by integrating

both variables: still water depth (also named waterlogging depth) and wading height, considering their randomness. In the first part of the paper, the effect of flooding over highway assets is discussed. Next, an analytical procedure based on the first-order reliability method (FORM) is presented. The procedure included the estimation of probability density function (PDF) of water depth and wading height using discharge data and individual vehicle data, respectively. The procedure was applied to a case study in the middle-south of Chile, where the road waterlogging is recurrent year after year.

2. Effects of Floods on Road Infrastructure, Traffic, and Vehicles

The floods affected the road infrastructure that crosses rivers and those parallel to the river banks, such as roads with cut-fill slopes, those placed in floodplains and in flat ground with low infiltration capacity. The damage to the infrastructure is structural and functional. The structural damage is produced by hydraulic erosion. The erosion wake crosses slopes, increasing the scour in bridges and weakening river bank protections. The floods also affect the drainage system, compromising its capacity of moving the water from slopes, embankments, and road subgrades. In the long term this effect reduces the pavement's durability. The functional damage is manifested in a reduction of the LOS of the road network. This reduction can be induced by partial destruction of the pavement surface, reduction of the lane width, loss of lanes available, or roadway flooding. Functional damage does not necessarily interrupt traffic but reduces the average travel speed and eventually only certain type of vehicles can pass through flooded roads. If the traffic is totally interrupted, communities can be isolated if there are no alternative routes.

The level of road traffic interruption caused by floods can be classified in the following scenarios: normal circulation, in which all the vehicle can pass through the flooded road without reducing the speed; restrained circulation, in which all the vehicles can pass through the flooded road but at a low speed; partial interruption, in which only heavy vehicles can pass along the flooded road; and total traffic interruption in which no type of vehicle can pass through the flooded road. The traffic interruption level depends on the magnitude and duration of the flood. It affects the road users, the nonusers, and the highway agencies. Road users experience higher travel times and operating costs, restrained circulation, or road crashes; the nonusers may experience isolation and lack of access to essential or vital services. The highway agency expends additional budget for repairing and/or rebuilding roads, taking a percent of the budget assigned to other maintenance activities, for instance.

If the water covers the roadway, the circulation possibility depends also of the vehicle wading height and weight, the water flow speed, and the water depth over the road. If the water flow speed is low and the wading height is higher (or similar) than the water depth, the vehicle keeps stable, but the HVAC system can be damaged. If the water depth is lower

than the wading height the vehicle can ride over the flooded road at a low speed. On the contrary, if the water speed flow is high, there exists a water depth threshold that avoids the vehicle destabilization. If the water depth overcomes this threshold, the vehicle loses stability and is dragged by the water flow and driver loses control of the vehicle and traffic is totally interrupted. In this case, the wading height is not applicable, being more important the water depth threshold.

The research available in the literature about the effect of climate on road traffic can be categorized into two groups: (a) studies that analyze the reduction of traffic speed under adverse weather conditions and (b) studies that analyze the effect of flooding on roads due to rainfall. Examples of the first type of study are found in [18–25], where the authors estimate the percentage of reduction of the average travel speed in relation to the intensity of the rain, during the rain and before the flood. The second group of research is classified in two subgroups: (a) studies of vehicle stability in flooded roads and (b) studies of wading capabilities of vehicles in flooded road with a still water regime. The studies of vehicle stability used hydrodynamic models to estimate the water depth and speed threshold than inducing (or avoiding) sliding, toppling, or floating to vehicles [26–31]. Martinez-Gomariz [32] represented in a speed-depth graph all the results existent in the literature. From the summary of Martinez-Gomariz it was concluded that the water depth-speed thresholds that destabilize light cars ranged between 0,4 and 0,7 m at flow speeds lower than 1 m/s and between 0,2 and 0,5 m at flow speeds between 1 and 6 m/s. In comparison with the vehicle stability studies, the studies of traffic interruption in still waters are scarce. Pyatkova et al. [33] studied the effect on urban traffic on street flooded with water depths between 0,07 and 2,0 m and more. They used the software MIKE FLOOD to simulate flood with different return periods and assumed that streets are closed approximately when water depth reaches between 0,5 and 1,0 m. Yin et al. [34] developed in China a similar study. They elaborate flood maps for return periods between 5 and 100 years, with which water depths between 0,05 m and 0,5 m and more are obtained. They used a water depth threshold between 25 and 35 cm to close streets and study the effect over traffic delays. In Australia, Affum et al. [35] used the concept of limit still water depth to warn drivers about the safe crossing of floodways. It is an indirect measure of wading height. The still water depth thresholds used suggested by Affum et al. for light cars and SUV ranged between 0,3 and 0,5 m. However, they recommended more studies to validate it.

3. Analytical Modelling of Traffic Interruption Probability

3.1. Conceptual Framework. The traffic interruption model proposed considered the uncertainty of the wading height and waterlogging depth through sigmoidal probability curves. The conceptual model is constituted by the three parts described in Figure 1: (a) estimation of the traffic probability

interruption in terms of the wading height and waterlogging depth; (b) estimation of the individual probabilities using FORM; and (c) estimation of the PDF for wading height and waterlogging depth. Each point of the probability curve (Box “a” in Figure 1) is obtained by applying FORM (Box “b” in Figure 1) and using a limit state function (LSF) that is the difference between the wading height (H_{wading}) and the waterlogging depth ($H_{\text{waterlogging}}$). Both variables are random. The H_{wading} randomness is explained by the variability of the vehicles’ geometry, engines, HVAC systems, tire diameter, and ground clearance of each vehicle class (light car, pick-up, SUV, trucks, and buses), brands, and models. The $H_{\text{waterlogging}}$ randomness is explained by the water flow magnitude, the return period, the river topography, and the location of the road in relation to the river.

3.2. Estimation of the Probability Density Function of Wading Height. The wading height is defined as the maximum depth of a low-speed water flow at which a vehicle can ride without electric, engine, or HVAC system damage, depending on the vehicle configuration. In a vehicle fleet, there is one wading height for each vehicle brand and model. The vehicle fleet is defined as a set of classes and subclasses existing in a country. Typical vehicle classes and subclasses belonging to a vehicle fleet are shown in Figure 2.

The wading height (H_{wading}) can be obtained using three methods: from manufacturers catalog, by in-field measuring, and by analytical estimates from the geometric properties of vehicles described in the manufacturers’ catalog. The analytical procedure is more practical because the manufacturers do not always provide wading height values, and the in-field measurements usually considered small sample sizes that underrepresent the vehicle class, brand, and model present in vehicle fleets. The analytical procedure estimate $H_{\text{wading,sub-class,brand,model}}$ for each vehicle subclass, brand, and model classified according to Figure 2, using (1) and (2), in which $D_{\text{LL,sub-class,brand,model}}$ (in mm) is the external diameter of the tires of each vehicle subclass, brand, and model without considering its deformation because of loads. The values of D_{LL} are obtained from the catalogs of vehicle manufacturers as well as the values of H_{wading} if they are available. The parameter $\alpha_{\text{sub-class}}$ of (1) is estimated by adding all the values of $H_{\text{wading,sub-class,brand,model}}$ and $D_{\text{LL,sub-class,brand,model}}$ available in the catalogs for the “V” vehicle subclasses. Therefore, this parameter is constant for each vehicle subclass. Then, introducing the $\alpha_{\text{sub-class}}$ value in (2), the H_{wading} for each brand and model of vehicle belonging to each subclass can be obtained.

$$\alpha_{\text{sub-class}} = \frac{1}{V} \sum_{i=1}^{i=V} \frac{H_{\text{wading,sub-class,brand,model}}}{D_{\text{LL,sub-class,brand,model}}} \quad (1)$$

$$\begin{aligned} H_{\text{wading,vehicle brand and model}} \\ = \alpha_{\text{sub-class}} D_{\text{LL,sub-class,brand,model}} \end{aligned} \quad (2)$$

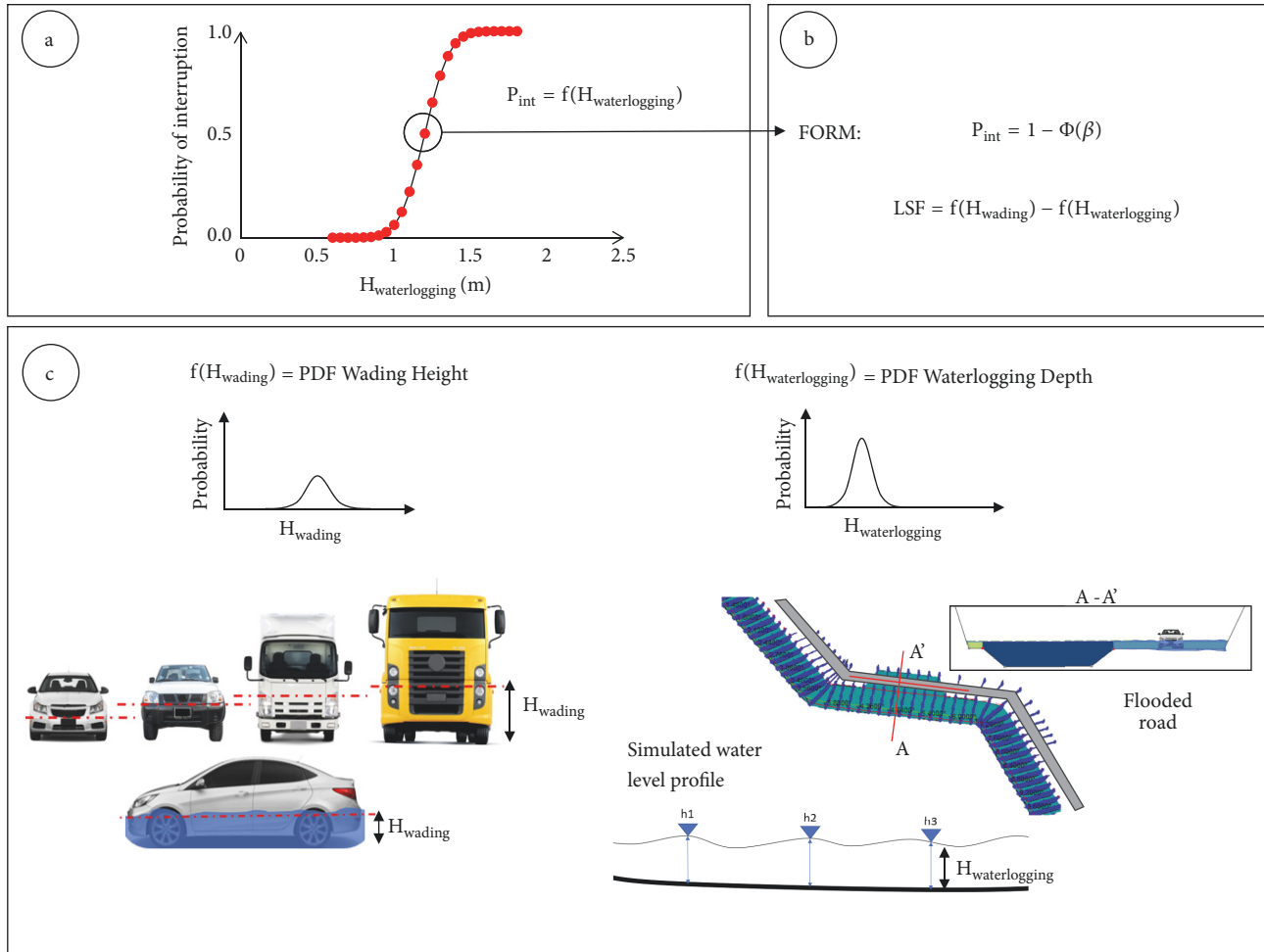


FIGURE 1: Conceptual model for obtaining traffic interruption probability curve caused by waterlogging.

The PDF of H_{wading} is estimated using the standard procedure to fit empirical PDF to continuous PDF: (a) to group the data of H_{wading} of each vehicle class and subclass; (b) to apply goodness of fit (GoF) tests, such as Kolmogorov-Smirnov, Chi square, Anderson-Darling, or Shapiro Wilks to identify the type of probability distribution; (c) to elaborate a ranking of the adjusted PDF according to the GoF test; (d) to select the probability distribution that best fit the empirical PDF of H_{wading} ; (e) to estimate the parameters associated with the PDF of fitted H_{wading} .

3.3. Estimation of the Probability Density Function of Water Depth. The waterlogging height ($H_{\text{waterlogging}}$) is the difference between the water depth at each river cross-section obtained from the water level profile (EH, in m) and the roadway centerline height of the longitudinal profile (CR, in m). The randomness is explained by the variations of the EH because of the variability of water flow, according to the return period and the river topography. If T_i is the return period (in years) and h_i is the cross-section of the flooded area, Figure 3 indicates that, for the same flooded area, there are different values of $H_{\text{waterlogging}}$ depending on the discharge

and water level associated with each T_i ($Q(T_i)$) in each cross-section. This happens because the water level depth and the roadway centerline height vary along the flooded area.

The EH can be obtained by direct measurement or by simulation according to Figure 4. After calculating the EH, the $H_{\text{waterlogging}}$ is obtained using (3).

$$H_{\text{waterlogging}} = EH - CR \quad (3)$$

To analytically estimate the PDF of $H_{\text{waterlogging}}$, a quasi 2D model in which the road cross-section flooded is considered as part of the cross-section of the rivers was used. This way of modelling allows overcoming the limitation of a 1D modelling and at the same time avoid the use of digital elevation models, which not always are available [36]. The procedure considered eight steps:

Step 1. Collect the maximum yearly discharge from available limnometric or fluviometric stations.

Step 2. Perform a frequency analysis of the time series of maximum discharges and fit the gamma, log normal, and log Pearson II PDFs. The fitting allows estimating the discharge

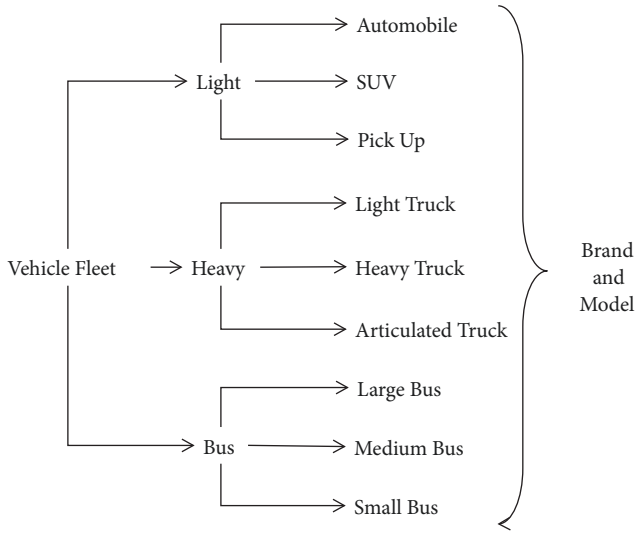


FIGURE 2: Typical classification of a vehicle fleet.

for different return periods ($Q(T)$). The return period can vary between 4 and 500 years. The discharges are grouped in clusters according to different ranges of return periods for obtaining a set of discharges for each range ($Q_i(T)$), in which “i” represented the i-th discharge belonging to each return period range.

Step 3. For each range of return period estimate the percentage of difference ΔQ_i (in %) between the discharge $Q_i(T)$ and the formative discharge of the river using (4). It represented the discharge increasing over the formative discharge that provoked the overflow. The formative discharge is defined as the most probable flow at a certain recurrence period that shape rivers [37]. It is estimated for a return period of 4 years ($Q_i(T=4)$) according to Niño [38].

$$\Delta Q_i = 100 \left(\frac{Q_i(T)}{Q_i(T=4)} - 1 \right) \quad (4)$$

Step 4. Estimate the maximum percentage of discharge increasing ($\Delta Q_i \max(T)$) based on the flood’s return period T and the percentage of difference (ΔQ_i) using (5).

$$\Delta Q_i \max(T) = \max[\Delta Q_i] \quad (5)$$

Step 5. Configure the river cross-section and its properties: dimensions, Manning’s coefficients, placement of the road, longitudinal slope of the riverbed, and longitudinal slope of the road (see Figure 7).

Step 6. Estimate the discharge Q_{s_i} to be used in the simulation of the water level profile using (6). This equation represented the incremental increasing of discharge from the formative discharge according to the increasing of the return period. Considering the cross-section and the longitudinal bedstep of the river, the Q_{s_i} value allows estimating the water depth (EH of (7)) using hydraulic simulation software.

$$Q_{s_i} = Q_i(T=4) (1 + \Delta Q_i \max(T)) \quad (6)$$

Step 7. Simulate the water level profile for different return periods and discharges (Q_{s_i}) and estimating the $H_{\text{waterlogging}}$ values using (3).

Step 8. For each simulation run obtain the $H_{\text{waterlogging}}$ values and fit a suitable PDF using the same procedure followed to fit H_{wading} values.

3.4. Simulation of the Traffic Interruption Probability Curves. The probability curves estimate the probability that a vehicle cannot circulate on a flooded road because $H_{\text{waterlogging}} > H_{\text{wading}}$. This probability is expressed as $\Pr(H_{\text{waterlogging}} > H_{\text{wading}})$. To estimate this probability, the FORM was used [39]. The FORM is based on the LSF: $g(X) = G1(X) - G2(X)$, in which $G1$ and $G2$ are nonlinear functions, and X is a vector of random variables. $G1$ and $G2$ are the PDF of $H_{\text{waterlogging}}$ and H_{wading} , respectively. The traffic interruption probability is defined as $\Pr(g(X) \geq 0)$, meaning that $H_{\text{waterlogging}} > H_{\text{wading}}$. Given that, in general, $g(X)$ is nonlinear and the PDF of X are nonnormal, therefore, it is necessary to apply a numeric solution for $g(X=0)$ based on the Hasofer and Lind [40] procedure and Rossenblatt’s [41] transformation to normalize the variables of the vector X . The numerical solution obtains the probability β_{HL} parameter in $g(X)=0$ for each point of the probability curves using (7). In this equation, x_i are the random variables of the vector X , u^* is the normalized solution of (7), and α^* is the normalized vector that describes the normalized LSD $g(u)=0$. The solution of (7) is the β_{HL} , which is an input to estimate the probability using (8).

$$\beta_{\text{HL}} = \min_{\{x \in g(X)=0\}} \sqrt{\sum_i x_i^2}; \quad (7)$$

$$u^* = -\beta_{\text{HL}} \alpha^* = \beta_{\text{HL}} \left(\frac{\partial g / \partial x_i}{\sqrt{\sum_{i=1}^n (\partial g / \partial x_i)^2}} \right)$$

$$P_{\text{int}} = 1 - \Phi(\beta_{\text{HL}}) \quad (8)$$

The probability of (8) represents only one data point of the probability curve of Figure 1 (Box a). Therefore, it is necessary to apply multiple runs with different simulation conditions, which is similar to applying a random sampling on the PDF of $H_{\text{waterlogging}}$ and H_{wading} but considering the consistency of the physical behavior of the flood phenomenon and its effect over the different vehicle classes.

4. Case Study in the Central Valley of Chile

The procedure was applied in the Central Valley of Chile (see Figure 5) with the objective of illustrating the proposed procedure to obtain probability curves that allow estimating the traffic interruption probability in that area of the country. The most roads placed in this area are located in floodplains and are exposed to low water level increase during floods that can be assimilating to still water. In the study area, there are 10 fluviometric stations located in Maule, Itata, Bio Bio, and Imperial rivers. Also, 44 ORT are located within the road network of the study area.

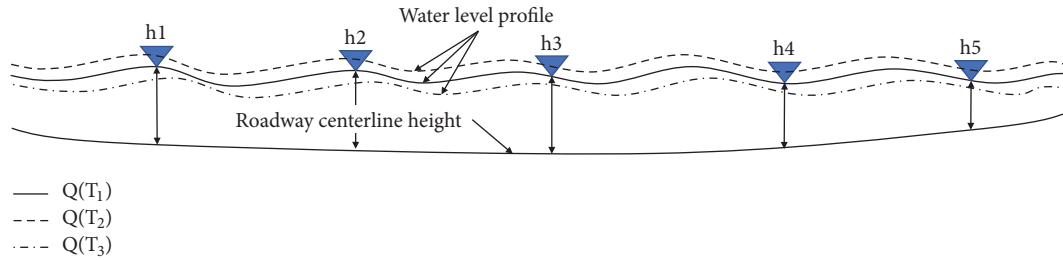


FIGURE 3: Variability of water level depth regarded to different return periods.

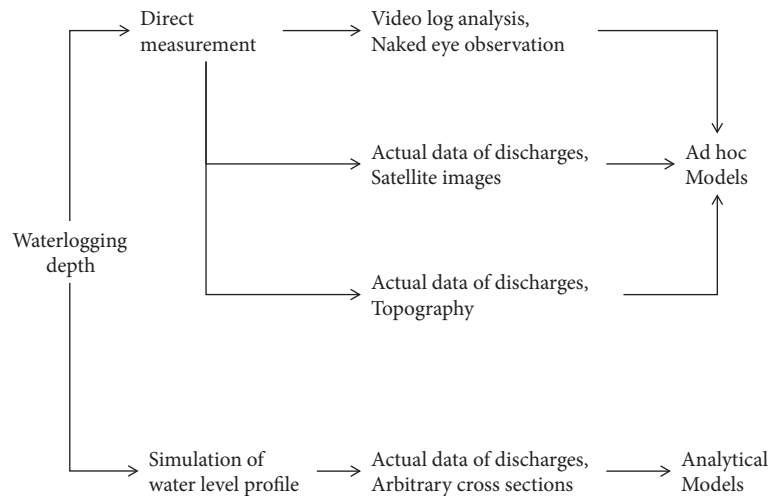


FIGURE 4: Method for obtaining water logging height.

4.1. Wading Height PDF Estimation. A sample of 166,155 vehicles of 3-year records from the ORT provided by the Ministry of Public Works [42] was used to estimate the PDF of H_{wading} . Table 1 summarized the sample categorized by vehicle class and subclass. The frequency diagrams are plotted in Figure 6. The software Easy Fit was used to estimate the PDF of H_{wading} for each vehicle subclass. Table 2 summarizes the results obtained.

4.2. Estimation of the Probability Density Function of the Waterlogging Height. The input data used to estimate the $H_{waterlogging}$ PDF were a generalized river cross-section that included the road cross-section, the maximum yearly discharge data sets, and the parameters used for modelling the water level profile. The geometry of the cross-section is presented in Figure 7. The hydraulic properties used were river Manning's roughness = 0,03; road surface Manning's roughness = 0,016; mean slope of the river bottom = 0,0001 m/m; road longitudinal slope = 0,5%; and section length = 1000 m.

The discharge data from ten fluvimetric stations was provided by the Ministry of Public Works of Chile [43]. Figure 8 plots the maximum yearly discharge (in m^3/s) per fluvimetric station. The discharge values ranged from 6 to 700 m^3/s and the discharge records between 5 and 60.

The frequency analysis of the discharge data is summarized in Table 3. Using the PDF of Table 3 discharges for return periods (T) of 4, 5, 10, 25, 50, 100, 200, and 500 years were obtained. The discharge estimated for T=4 was 55 m^3/s and was considered as the formative discharge in (4).

Discharges obtained for each return period were the input data used to estimate EH, with quasi-2D modelling using the software HEC-RAS 1D. Figure 9 shows the histograms of the EH obtained, clustered by return period ranges.

The $H_{waterlogging}$ PDF was obtained from the data of Figure 9 by using the Easy Fit software. Table 4 summarized the pdf obtained, classified by return period ranges. All the pdf obtained were normal. The mean and the standard deviation of the PDF are in brackets.

4.3. Traffic Interruption Probability Curves Simulated. To estimate the traffic interruption probability using FORM, a LSF is needed. The LSF was configured using the PDF of $H_{waterlogging}$ and H_{wading} . The probabilities were obtained using the Hasofer-Lind procedure. The simulation considered 6 vehicle classes and 7 return periods. Figure 10 shows the 42 estimated probability curves.

From Figure 10, three patterns were identified: the interruption probability is similar for light automobiles and SUVs; the single unit heavy trucks and the articulated trucks follow

TABLE 1: Vehicle sample used to estimate wading height.

| Class | Sub-class | # of vehicle brands | # of models | Sample |
|-------|------------------------------------|---------------------|-------------|--------|
| Light | Automobile | 52 | 392 | 87,264 |
| | SUV | 42 | 217 | 41,440 |
| | Pick up | 29 | 75 | 31,245 |
| Heavy | Single unit light and heavy trucks | 27 | 136 | 3,884 |
| | Articulated trucks | 29 | 212 | 2,322 |

TABLE 2: PDF of wading height of each vehicle class selected in this study.

| Class | Sub-class | Probability density function (PDF) |
|-------|-------------------------|--------------------------------------|
| Light | Automobile | Normal (0,4125; 0,0232) |
| | Pick up | Lognormal3P (0,606; 0,019; 0,544) |
| | SUV | Lognormal3P (0,0477; 0,0436; 0,4496) |
| Heavy | Single unit light truck | Lognormal3P (0,8417; 0,0462; 0,4789) |
| | Single unit heavy truck | Weibull (1,1323; 0,0568; 0,6261) |
| | Articulated truck | Normal (1,1986; 0,0692) |

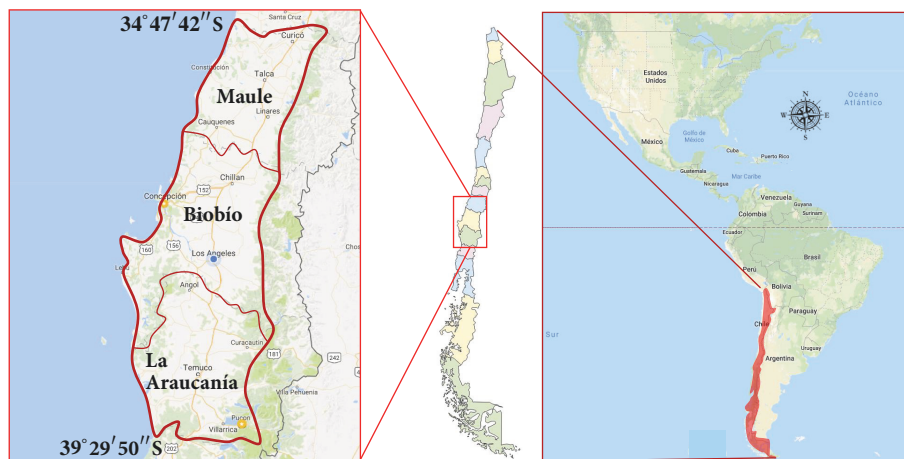


FIGURE 5: Location of the studied area.

TABLE 3: Frequency functions of maximum annual river flows by fluviometric station.

| Fluviometric station | Probability density function |
|------------------------------|--|
| Loncomilla in Las Brisas | LogPearson III (6,5066; -0,252; 9,634) |
| Perquillauquén in Quella | LogPearson III (4,133; -0,379; 8,311) |
| Perquillauquén in San Manuel | LogNormal (0,105; 7,817; -1898,7) |
| Diguillin Longitudinal | LogPearson III (16,023; -0,145; 8,667) |
| Itata in Cholguán | LogNormal (0,041; 8,650; -5116,9) |
| Duqueco en Villucura | Gamma (5,4995; 109,120) |
| Mininco in Longitudinal | LogPearson III (7,471; -0,229; 6,630) |
| Malleco in Collipulli | LogPearson III (9,546; -0,159; 7,345) |
| Lumaco in Lumaco | LogPearson III (16,266; -0,148; 7,178) |
| CholChol in Cholchol | LogPearson III (8,155; -0,137; 7,885) |

TABLE 4: Summary of PDF of $H_{\text{waterlogging}}$.

| Return period (years) | PDF of $H_{\text{waterlogging}}$ |
|-----------------------|----------------------------------|
| [4 – 5] | Normal (0,0000; 0,06430) |
| [5 – 10] | Normal (0,1495; 0,10903) |
| [10 – 25] | Normal (0,3923; 0,09948) |
| [25 – 50] | Normal (0,6099; 0,09327) |
| [50 – 100] | Normal (0,7783; 0,07420) |
| [100 – 200] | Normal (0,9371; 0,08670) |
| [200 – 500] | Normal (1,0888; 0,07054) |

a similar pattern; and the traffic interruption probability of automobiles and SUVs is higher than the same probability for single unit heavy trucks and articulated trucks. This

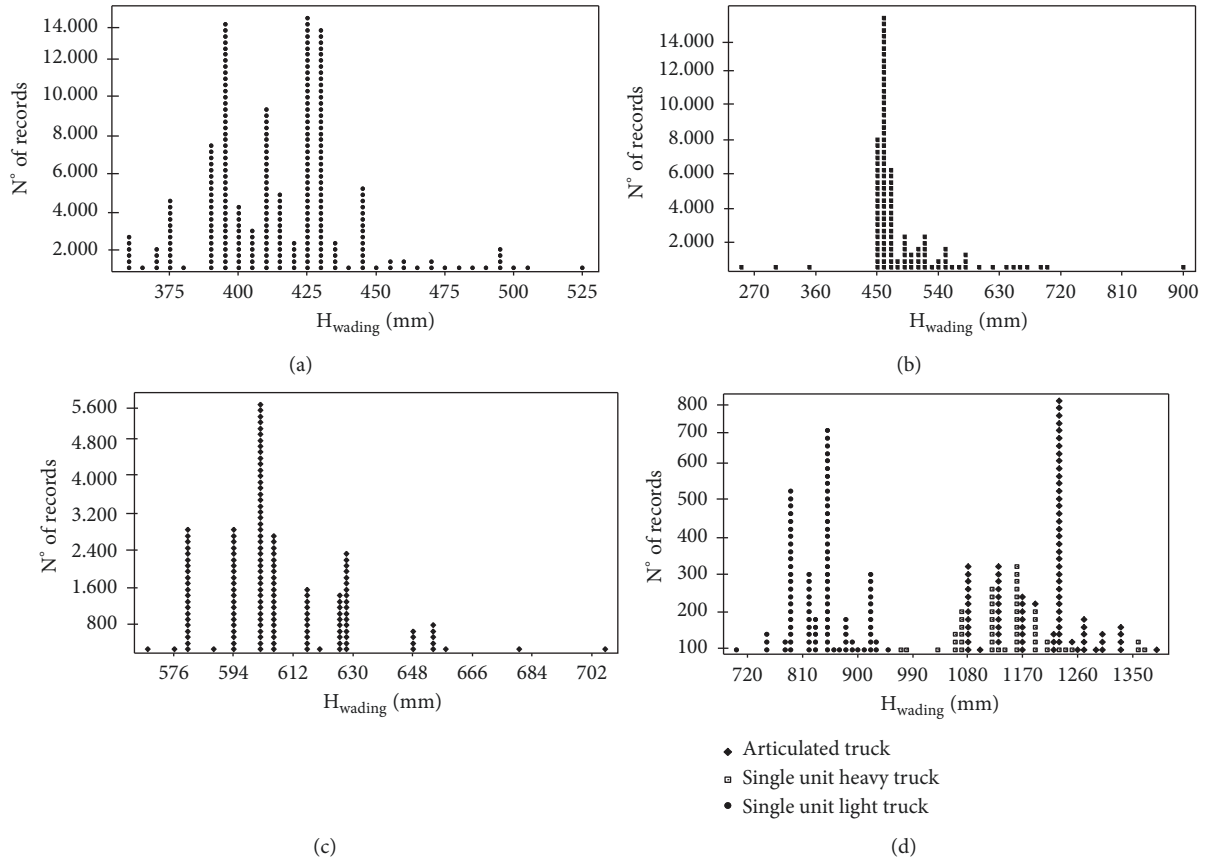


FIGURE 6: Histograms of wading height per vehicle class. (a) Automobile (each dot = 346 data points). (b) SUV (each dot = 386 data points). (c) Pick-up (each dot = 127 data points). (d) Heavy vehicles (each dot = 30 data points).

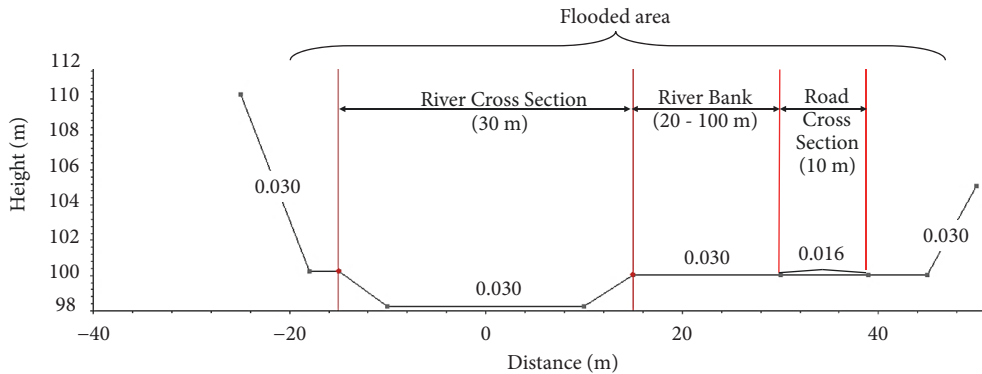


FIGURE 7: Cross-section geometry used for modelling the water level.

result is logical and proves the coherence of the model developed. Using the PDF curves of Figure 10 two values of $H_{waterlogging}$ were obtained: (a) the limit waterlogging depth that is defined as the depth at which the traffic interruption probability is 1,0 and (b) the alert waterlogging depth associated with a traffic interruption probability of 0,5. Both values of $H_{waterlogging}$ can be used to establish an alert system for drivers based on the properties of the local vehicle fleets. Results are summarized in Table 5 per vehicle subclass.

5. Conclusions

The aim of this paper was to propose a procedure based on reliability principles to estimate the traffic interruption probability due to road waterlogging considering very low-speed flow. The proposed procedure was applied in the south of Chile. A data set of 166,155 vehicles and records up to 30 years of discharge data of ten fluvimetric stations were used and a total of 42 probability curves were obtained. In this context, the following conclusions were obtained:

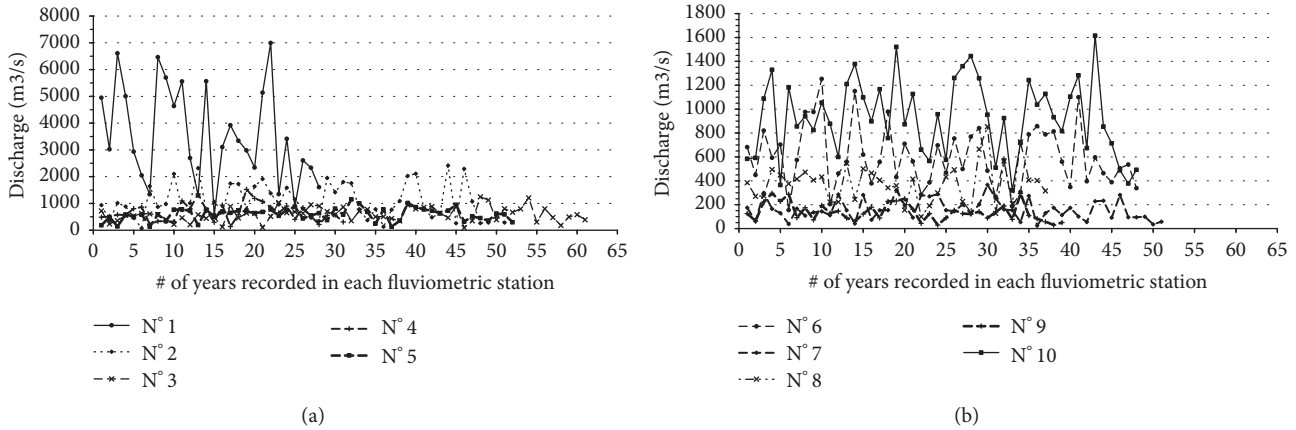


FIGURE 8: Maximum yearly discharge per fluviometric station. (a) Fluviometric stations 1 to 5. (b) Fluviometric stations 6 to 10.

TABLE 5: Limit and alert $H_{\text{waterlogging}}$ per vehicle subclass.

| Vehicle subclass | $H_{\text{waterlogging}}$ (m) | |
|-------------------------|-------------------------------|-------|
| | Limit | Alert |
| Automobile | 0,73 | 0,41 |
| SUV | 0,77 | 0,46 |
| Pick-up | 0,88 | 0,57 |
| Single unit light truck | 1,14 | 0,83 |
| Single unit heavy truck | 1,44 | 1,13 |
| Articulated truck | 1,53 | 1,20 |

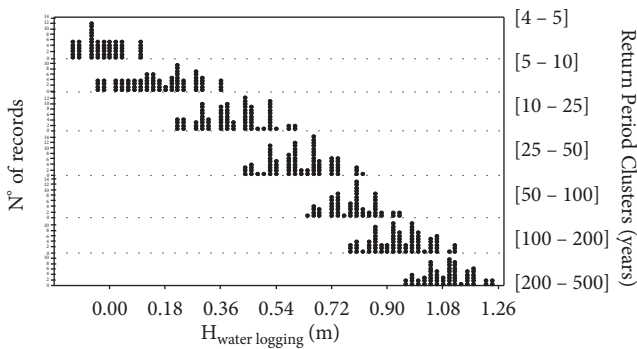


FIGURE 9: Summary of waterlogging height clustered according to return time.

Results obtained show that the waterlogging depth that interrupts traffic with a probability of 1,0 varies between 0,73 and 0,88 m for light vehicles and between 1,14 to 1,53 m for heavy vehicles. Likewise, the waterlogging depth that interrupts traffic with a probability of 0,5 varies between 0,41 and 0,57 m for light vehicles and between 0,83 to 1,20 m for heavy vehicles. These values are higher than the values reported in the literature that varies between 0,3 and 0,5 for light vehicles in still waters.

The waterlogging depth estimated in this study is valid only for still waters, in which the protection of the HVAC system is more relevant than the vehicle stability. At high speed flows, for instance, higher than 1 m/s, the stability turns more relevant and leads to the waterlogging depth being reduced compared to the estimated in this study.

The literature about the effect of waterlogging on road networks used simplified methods to obtain the vehicle's wading height; this is because those literature studies were supported by direct in-field observation, which leads to using small sample sizes. This limitation has been resolved in this research by incorporating the variability of the vehicle's wading height and a large sample of vehicles obtained from records of existent open road tolls in Chilean highways.

Areas of potential flooding can be identified by superimposing flood-prone areas onto road network maps. Based on the composition of the traffic and the probability curves developed in this study, it is possible to analyze the cost of rerouting to justify the implementation of flood protection measures in the road network; therefore, the results obtained are useful for road managers to estimate the budget needed to mitigate the effect of floods on the road network.

For simplicity, the water level profile was obtained using a quasi-two-dimensional modelling, which does not permit incorporating the velocity of the water and its effect on the stability of the vehicles. For that reason, the model is valid only for still waters. To refine the model, a two-dimensional modelling is needed in order to incorporate the effect of water flow speed on the vehicles' stability using hydrodynamic models combined with reliability principles.

The probability curves have enough generality to be used in traffic management policies in flood-prone areas and also demonstrate the need for technical evaluation of need for works of protection against flooding. The critical and limit waterlogging depths calculated are representative of the Central Valley of Chile. To apply this to other areas of the country, only the PDF of the EH would need to be modelled, because the PDF of waterlogging depth is representative of the entire country.

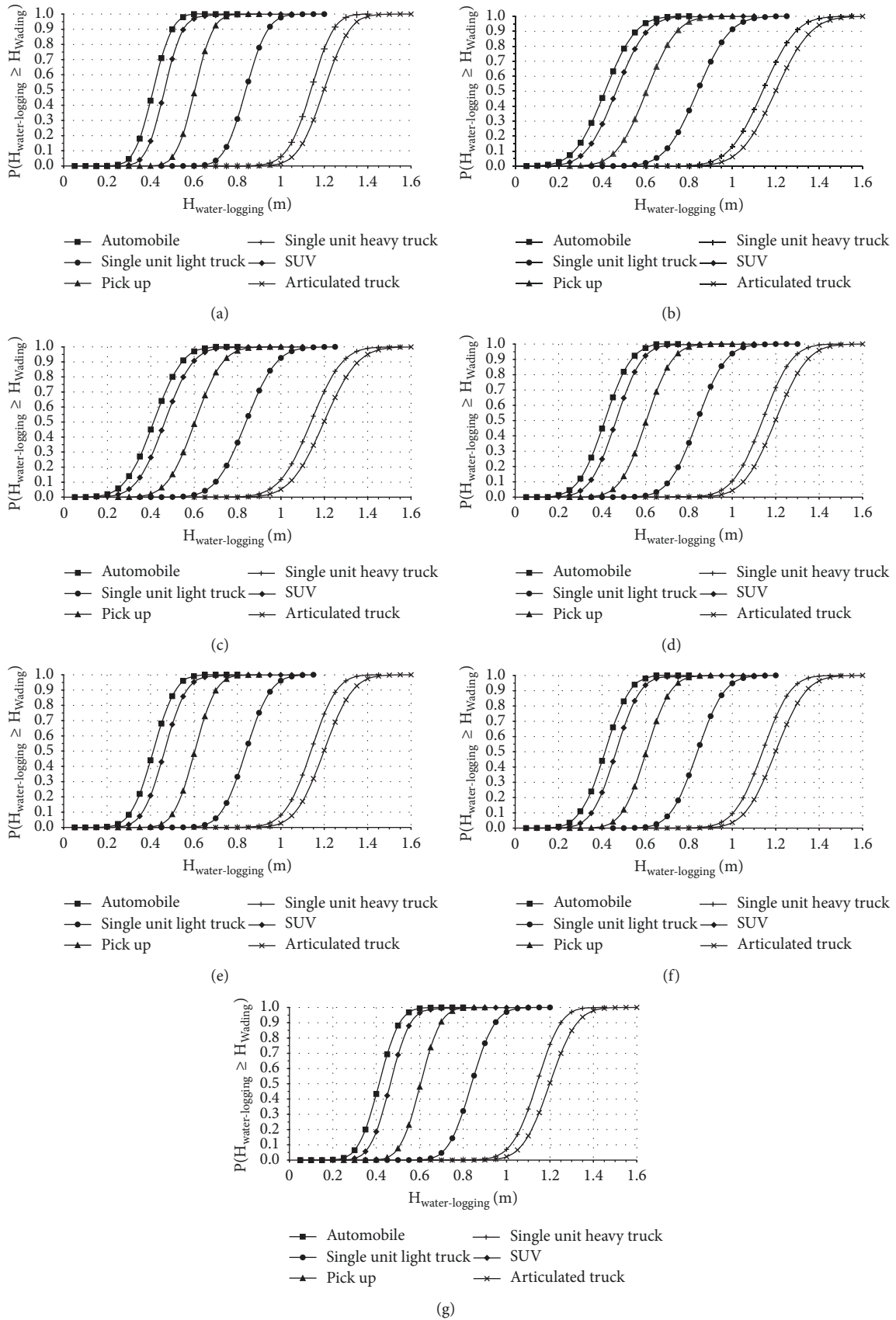


FIGURE 10: Interruption probability curves simulated per return period and vehicle subclass. (a) $4 < T < 5$ years. (b) $5 < T < 10$ years. (c) $10 < T < 25$ years. (d) $25 < T < 50$ years. (e) $50 < T < 100$ years. (f) $100 < T < 200$ years. (g) $200 < T < 500$ years.

Data Availability

The data used to support the findings of this study are available from the corresponding author upon request.

Conflicts of Interest

The authors declare that they have no conflicts of interest.

Acknowledgments

The authors wish to thank the National Commission for Science and Technology (CONICYT) of Chile for supporting the research projects FONDEF ID14I20309 and thank the National Research Center for Integrated Natural Disaster Management (CIGIDEN), CONICYT/FONDAP/15110017, within which this paper was prepared. The authors also wish to thank the Ministry of Public Works of Chile for providing the data used for the research presented in this paper.

References

- [1] W. Kron, "Flood Risk= Hazard*Values*Vulnerability," *Water International*, vol. 30, no. 1, pp. 58–68, 2005.
- [2] TRB, *Highways Capacity Manual*, Transportation Research Board, 2016.
- [3] M. Gall, B. J. Boruff, and S. L. Cutter, "Assessing flood hazard zones in the absence of digital floodplain maps: Comparison of alternative approaches," *Natural Hazards Review*, vol. 8, no. 1, pp. 1–12, 2007.
- [4] O. Petrucci and A. A. Pasqua, "Damaging events along roads during bad weather periods: A case study in Calabria (Italy)," *Natural Hazards and Earth System Sciences*, vol. 12, no. 2, pp. 365–378, 2012.
- [5] P.-A. Versini, E. Gaume, and H. Andrieu, "Assessment of the susceptibility of roads to flooding based on geographical information - Test in a flash flood prone area (the Gard region, France)," *Natural Hazards and Earth System Sciences*, vol. 10, no. 4, pp. 793–803, 2010.
- [6] ICPR, *Atlas of Flood Danger and Potential Damage Due to Extreme Floods of The Rhine*, International Commission for the Protection of the Rhine, Koblenz, Germany.
- [7] USACE, "HEC-RAS v. 5.0.3," Tech. Rep., U.S. Army Corps of Engineers, 2016.
- [8] DHI, *MIKE11 A Modelling System for Rivers and Channels - Reference Manual*, DHI Water & Environment, Hørsholm, Denmark, 2002.
- [9] S. Patro, C. Chatterjee, S. Mohanty, R. Singh, and N. S. Raghuvanshi, "Flood inundation modeling using MIKE FLOOD and remote sensing data," *Journal of the Indian Society of Remote Sensing*, vol. 37, no. 1, pp. 107–118, 2009.
- [10] E. Bladé, L. Cea, G. Corestein et al., "Iber: a tool for the numerical simulation of river flow," *Revista Internacional de Métodos Numéricos para Cálculo y Diseño en Ingeniería*, vol. 30, no. 1, pp. 1–10, 2014.
- [11] DHI, *MIKE FLOOD 1D-2D MODELLING - User manual*, DHI Water & Environment, Hørsholm, Denmark, 2003.
- [12] DHI, *MIKE 3 Estuarine and Coastal Hydraulics and Oceanography-Short Description*, DHI Water & Environment, Hørsholm, Denmark, 2001.
- [13] USACE, *HEC-FDA: Flood Damage Reduction Analysis*, U.S. Army Corps of Engineers, 2016.
- [14] FEMA, "Multi-hazard loss estimation methodology. Flood Model HAZUS®MH MR4," Technical Manual, Federal Emergency Management Agency, 2003.
- [15] F. Klijn, P. J. A. Baan, K. M. De Bruijn, and J. Kwadijk, *Overstromingsrisico's in Nederland in een veranderend klimaat, WL delft hydraulics*, WL delft hydraulics, Delft, Netherlands, 2007.
- [16] W. Vanneuville, R. Maddens, C. Collard, P. Bogaert, P. de Maeyer, and M. Antrop, "Impact op mens en economie t.g.v. overstromingen bekeken in het licht van wijzigende hydraulische condities, omgevingsfactoren en klimatologische omstandigheden," Tech. Rep. MIRA/2006/02, Universiteit Gent, Belgium, 2006.
- [17] E. C. Penning-Rowsell, C. Johnson, S. Tunstall et al., *The Benefits of Flood And Coastal Risk Management: A Handbook of Assessment Techniques*, Flood Hazard Research Centre. Middlesex University Press, 2005.
- [18] M. Kyte, Z. Khatib, P. Shannon, and F. Kitchener, "Effect of weather on free-flow speed," *Transportation Research Record*, no. 1776, pp. 60–68, 2001.
- [19] B. L. Smith, K. G. Byrne, R. B. Copperman, S. M. Hennessy, and N. J. Goodall, "An investigation into the impact of rainfall on freeway traffic flow," in *Proceedings of the Proceedings 83th Annual Meeting of the Transportation*, Washington, Wash, USA, 2004.
- [20] M. Agarwal, T. H. Maze, and R. Souleyrette, "Impacts of weather on urban freeway traffic flow characteristics and facility capacity," in *Proceedings of the 2005 Mid-Continent Transportation Research Symposium*, pp. 18–19, Ames, Iowa, USA, 2005.
- [21] R. Hranac, E. Sterzin, D. Krechmer, H. Rakha, and M. Farzaneh, *Empirical Studies on Traffic Flow in Inclement Weather*, Federal Highway Administration, Washington, Wash, USA, 2006.
- [22] M. Sabir, J. van Ommeren, M. J. Koetse, and P. Rietveld, *Welfare Effects of Adverse Weather through Speed Changes on Car Commuting Trips*, Vu University, Amsterdam, Netherlands.
- [23] I. Tzapakis, T. Cheng, and A. Bolbol, "Impact of weather conditions on macroscopic urban travel times," *Journal of Transport Geography*, vol. 28, pp. 204–211, 2013.
- [24] E. Hooper, L. Chapman, and A. Quinn, "Investigating the impact of precipitation on vehicle speeds on UK motorways," *Meteorological Applications*, vol. 21, no. 2, pp. 194–201, 2014.
- [25] M. Pregolato, A. Ford, S. M. Wilkinson, and R. J. Dawson, "The impact of flooding on road transport: A depth-disruption function," *Transportation Research Part D: Transport and Environment*, vol. 55, pp. 67–81, 2017.
- [26] T. D. Shand, R. J. Cox, M. J. Blacka, and G. P. Smith, "Appropriate safety criteria for vehicles. Revision Project 10. Stage 2. Literature Review," Tech. Rep., Australian Rainfall and Runoff, Australia, 2010.
- [27] F. Y. Teo, J. Xia, R. A. Falconer, and B. Lin, "Experimental studies on the interaction between vehicles and floodplain flows," *International Journal of River Basin Management*, vol. 10, no. 2, pp. 149–160, 2012.
- [28] J. Xia, R. A. Falconer, X. Xiao, and Y. Wang, "Criterion of vehicle stability in floodwaters based on theoretical and experimental studies," *Natural Hazards*, vol. 70, no. 2, pp. 1619–1630, 2014.
- [29] J. Xia, F. Teo, R. Falconer, Q. Chen, and S. Deng, "Hydrodynamic experiments on the impacts of vehicle blockages at bridges," *Journal of Flood Risk Management*, vol. 11, pp. S395–S402, 2018.

- [30] E. Martínez-Gomariz, M. Gómez, B. Russo, and S. Djordjević, "A new experiments-based methodology to define the stability threshold for any vehicle exposed to flooding," *Urban Water Journal*, vol. 14, no. 9, pp. 930–939, 2017.
- [31] M. Kramer, K. Terheiden, and S. Wieprecht, "Safety criteria for the trafficability of inundated roads in urban floodings," *International Journal of Disaster Risk Reduction*, vol. 17, pp. 77–84, 2016.
- [32] E. Martínez-Gomariz, M. Gómez, B. Russo, and S. Djordjević, "Stability criteria for flooded vehicles: a state-of-the-art review," *Journal of Flood Risk Management*, vol. 11, pp. S817–S826, 2018.
- [33] K. Pyatkova, A. S. Chen, S. Djordjevic et al., "Flood impacts on road transportation using microscopic traffic modelling technique," in *Proceedings of the SUMO User Conference*, Berlin, Germany, 2015.
- [34] J. Yin, D. Yu, Z. Yin, M. Liu, and Q. He, "Evaluating the impact and risk of pluvial flash flood on intra-urban road network: A case study in the city center of Shanghai, China," *Journal of Hydrology*, vol. 537, pp. 138–145, 2016.
- [35] J. Affum, G. Giummarra, and H. Cheung, "Safety provisions for floodways over roads," Austroads Report AP-R481-15, 2015.
- [36] L. M. Timbe and P. Willems, "Desempeño de modelos hidráulicos 1D y 2D para la simulación de inundaciones," *Maskana*, vol. 2, no. 1, pp. 91–98, 2015.
- [37] M. Bolla Pittaluga, R. Luchi, and G. Seminara, "On the equilibrium profile of river beds," *Journal of Geophysical Research: Earth Surface*, vol. 119, no. 2, pp. 317–332, 2014.
- [38] Y. Niño, *River Hydraulic and Sediment Transport*, Universidad de Chile, Chile, 2004.
- [39] A. Haldar and S. Mahadevan, *Probability, Reliability and Statistical Methods in Engineering Design*, Wiley, New York, NY, USA, 1st edition, 2000.
- [40] A. M. Hasofer and N. C. Lind, "An exact and invariant first order reliability format," *Journal of Engineering Mechanical*, vol. 100, pp. 111–121, 1974.
- [41] M. Rosenblatt, "Remarks on a multivariate transformation," *Annals of Mathematical Statistics*, vol. 23, pp. 470–472, 1952.
- [42] MOP, *Basic Study on Update HDM-4 Parameters*, Ministry of Public Works, Chile, 2017.
- [43] MOP, *Información Oficial Hidrometeorológica y de Calidad de Aguas en Línea*, MOP, Chile, 2016, <http://snia.dga.cl/BNAConsultas/reportes>.

Research Article

Innovative Bike-Sharing in China: Solving Faulty Bike-Sharing Recycling Problem

Shan Chang , **Rui Song** , **Shiwei He** , and **Guo Qiu**

MOE Key Laboratory for Urban Transportation Complex Systems Theory and Technology, Beijing Jiaotong University, Beijing, China

Correspondence should be addressed to Rui Song; rsong@bjtu.edu.cn

Received 13 January 2018; Revised 15 April 2018; Accepted 10 May 2018; Published 27 June 2018

Academic Editor: Samiul Hasan

Copyright © 2018 Shan Chang et al. This is an open access article distributed under the Creative Commons Attribution License, which permits unrestricted use, distribution, and reproduction in any medium, provided the original work is properly cited.

In China, based on the mobile Internet technology and global positioning system (GPS), innovative bike-sharing is different from traditional bike-sharing system with docking station, for its flexibility and convenience. However, innovative bike-sharing system faces operational challenges, especially in faulty bike-sharing recycling (FBSR) problem. In this paper, a framework is designed based on the optimization method to solve the FBSR problem so that it can minimize the total recycling costs by taking the route optimization and loading capacity ratio as constraints. The FBSR method combines the K-means method for clustering faulty bike-sharing with planning recycling route for operational decisions. Moreover, CPLEX solver is used to obtain the desired result of the FBSR model. Finally, a case study based on a certain area in Beijing, China, is used to verify the validity and applicability of the model. The results show that the value of loading capacity ratio and the number of clustering points greatly affect the results of FBSR problem. Four vehicles are designated to execute FBSR tasks required by different clustering points. This study is of considerable significance for the bike-sharing promotion in the last-mile situation to the real problems arising in the initial period.

1. Introduction

Bike-sharing systems are becoming increasingly popular in cities around the world because they are cheap, efficient, healthy, and green. In recent years, with the development of mobile Internet and global positioning system (GPS) becoming increasingly affordable [1], an innovative bike-sharing system without docking station emerged in 2015 in China. Bike-sharing system can effectively solve the last-mile problem in multimodal transportation; in addition, many Chinese cities show more cycling than the other international cities [2], which leads to wide spread of bike-sharing systems across China now. Spatial distribution of main dockless bike-sharing systems in China is shown in Figure 1.

Compared with traditional bike-sharing [3, 4], dockless bike-sharing is more flexible and more convenient for the users. Bicycles of bike-sharing systems are widely distributed, thus reducing travel distance from traveler to bicycle docking station. It is convenient for users to use bike-sharing; when users use bike-sharing for the first time, first, users should

register directly in the app and scan their identification and give a deposit. Then, the smart bike-sharing app will show a map of all the bicycles around users and locate the closest bike. After that, users scan the Quick Response code with the app and within 10 seconds they can hear the click and hit on the road. However, with all the benefits of this innovative bike-sharing system, here come operational challenges.

It is worth noting that there are a large number of people cycling every day. It is unavoidable that bike-sharing may malfunction in its routine use, and accidents might take place due to its faults. According to some statistics, there are more than 10 million bicycles in bike-sharing systems, and faulty bicycles rate slightly less than 1%. If we calculate with rate of 1% faulty bicycles, there will be 100,000 faulty bicycles in China. Meanwhile, lots of bicycles will be scrapped usually in three years in China. These factors could cause the following: (a) the presence of the faulty bike-sharing severely threatens users' safety; (b) the service quality of bike-sharing system will affect the reputation of the companies; (c) faulty bicycles in the city have a very



FIGURE 1: Spatial distribution of main dockless bike-sharing systems in China.

bad effect on the city appearance. Therefore, faulty bike-sharing recycling (FBSR) is a very significant issue that should be solved. Moreover, the distribution of bicycles of innovative bike-sharing system is rather dispersed since bike-sharing can park without docking station, whereas for traditional bike-sharing system, faulty bicycles are readily discovered and easily processed at bicycle docking station. Comparatively speaking, it is more difficult for the innovative bike-sharing system to recycle faulty bicycle than traditional bike-sharing. Thus, solving the FBSR problem is the key to reduce recycling costs for the authorities and operators with the means.

Therefore, this paper presents a framework design and optimization method to solve FBSR problem. Firstly, the K-means clustering method is used to divide the faulty bike-sharing into different service points. Then, a FBSR model is established to minimize the total recycling costs with loading capacity ratio as a constraint. At last, this method is verified based on a case study in Beijing, China.

The remaining part of this paper is organized as follows. The relevant literature is reviewed in Section 2. The framework design of faulty bike-sharing recycling is presented in Section 3. Section 4 describes the modeling methodologies and model specifications. In Section 5, the empirical results of the models and the effects of the explanatory variables are presented. The final section provides a summary of the research findings with possible extensions of the research.

2. Literature Review

Since a bike-sharing system was first introduced in the 1960s [5], lots of bike-sharing systems have been implemented throughout the world [6, 7], and now the bike-sharing system has become a necessary for city transportation. According to research by different scholars, the bike-sharing system has potentials due to the following reasons: (a) reducing traffic

congestion and fuel use [8]; (b) behavioral shifts towards increased bicycle use for daily mobility [9]; (c) a growing perception of the bicycle as a convenient transportation mode [1].

The existing literature on bike-sharing systems is mainly focused on the traditional bike-sharing system with docking stations including development policies and safety issues [10–12], operation scales and the operator [8, 13], and benefit on the environment [14–18]. In order to improve the user experience for bicycle use and reduce the operating costs, many researchers study rebalancing operations. Chemla et al. [19] were the first to introduce rebalancing operations for bike-sharing system and proposed tabu search algorithms for solving it. Schuijbroek et al. [20] presented unified dual-bounded service level constraints that add inventory flexibility and vehicle routing for static rebalancing in bike-sharing systems. Ghosh et al. [21] developed an optimization formulation to reposition bikes using vehicles while considering the routes for vehicles and future expected demand to improve bike-sharing availability and reduce the usage of private vehicles. Pfrommer et al. [22] proposed a heuristic algorithm for solving the dynamic rebalancing problem with multiple vehicles and presented a dynamic pricing strategy that encouraged users to return bikes to empty stations. However, the bike-sharing system in a city does not have the restriction of fixed docking stations. So the existing studies cannot solve the FBSR in China.

Recently, the new bike-sharing system without docking station has attracted attention from a few scholars. Reiss and Bogenberger [23] created a demand model to obtain an optimal distribution of bikes within the operating area, based on a detailed GPS-data analysis for the bike-sharing system. Caggiani et al. [24] suggested a method to use the revenue collected by a congestion price policy to implement a bike-sharing system. Pal and Zhang [25] proposed a hybrid nested large neighborhood search with variable neighborhood descent algorithm, which can solve static rebalancing problems for bike-sharing system. Caggiani et al. [26] proposed an operator-based bike redistribution methodology that started from the prediction of the number and position of bikes over operating area and ended with a decision support system for the relocation process. Cheng and Gao [27] studied the revenue changes of the platform after the bike-sharing platform adopted the monthly strategy and obtained the best monthly subscription pricing to maximize the platform revenue. However, compared with bike-sharing scale in China, these studies were based on case studies that are of much smaller scale. Therefore, FBSR problem deserves more attention.

In addition, Cervero et al. [28] found that the single strongest predictor for bicycle use is the availability of a bike. The FBSR is one of the important means to ensure the availability of bike-sharing. However, up to now, there is no research on faulty bike-sharing recycling in the literature. Thus, this study bridges this gap by reporting a solution algorithm that addresses this issue and helps bike-sharing companies to reduce operating costs particularly in Chinese cities.

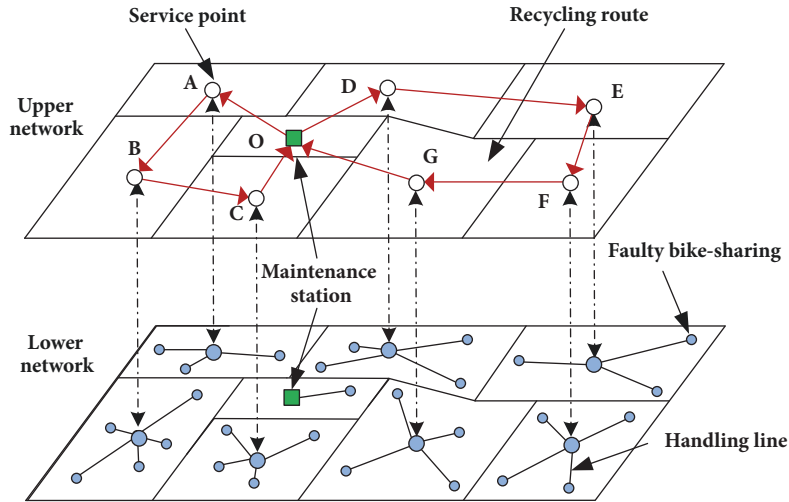


FIGURE 2: Multilevel faulty bike-sharing recycling network.

3. Framework Design of FBSR

3.1. *Faulty Bike-Sharing Definition and Classification.* In this paper, three types of bicycle as faulty bicycles are defined as follows.

(i) *Fault of cycling:* it happens when the users unlock the bicycles and find that the bicycle cannot be used; then the users will send the information through the mobile phone app. When the bike-sharing system server receives the information of the faulty bicycle status and location, the bike-sharing company will have it repaired.

(ii) *Fault of communication:* it happens when bicycles are identified as faulty bike-sharing owing to GPS equipment damage, and the system server will prohibit users from using this bicycle (ignoring GPS equipment lost contact while cycling).

(iii) *End of the service life:* if a bicycle has reached the state’s mandatory write-off standard (generally three years in China), the bike-sharing system server will identify the bicycle as faulty bike-sharing. Then this bicycle will be forced to scrap, prohibiting users from cycling.

3.2. *Recycling Rules.* Multilevel faulty bike-sharing recycling network is shown in Figure 2, which is divided into upper network and lower network. The lower network shows that faulty bike-sharing in multiple locations within a certain area will be concentrated at clustering service point in the area, where blue dots indicate faulty bike-sharing in some locations and the lines among some dots stand for handling line. The upper network indicates that the clustering service points of each area are obtained, where dots indicate service point, red line shows the line direction, and the green one represents maintenance station. The FBSR model can be applied to the best routes so that total recycling costs are minimized.

For the description, ground rules are established as follows.

(1) A number of maintenance stations are established in a city. Each maintenance station is in a fixed location. The

maintenance station provides faulty bicycles maintenance service in a certain area, and faulty bicycles are recycled once a day. It should be noted that the faulty bicycles will not be classified. The faulty bike-sharing information is collected at a fixed time every day; if there are any updates about faulty bike-sharing, they will be dealt with the next day.

(2) Within each local area, faulty bicycles are clustered for different service points according to their locations, which are made in lower network such as point A in Figure 2. To perform a task, a service vehicle will be parked in the clustering service point where the faulty bicycles are carried back by hands. Then service vehicle will move on to the next service point such as point B in Figure 2 after the task is completed at point A. Finally, the faulty bike-sharings of each clustering service point are sent to maintenance point along the planned best line.

(3) There are a number of recycling vehicles in maintenance station. These vehicles traverse all service points from maintenance station in order to recycle all faulty bicycles. It is worth noting that the service point is not fixed, and the service point should have enough space for recycling vehicle to park.

Therefore, there are two key issues to deal with to complete one FBSR in an area:

(i) How to determine the number and the location of bike-sharing service points that are available for recycling vehicles.

(ii) How to determine routes for recycling vehicles to traverse all service points from maintenance station.

3.3. *Recycling Framework.* Based on the analysis of faulty bike-sharing definition, classification, and recycling rules, the flowchart of faulty bike-sharing recycling is shown in Figure 3. There are four steps in the framework of FBSR, which are the data collection and processing, the faulty bike-sharing clustering, the planning of recycling route, and the performing of recycling task. The details of recycling framework can be described as follows.

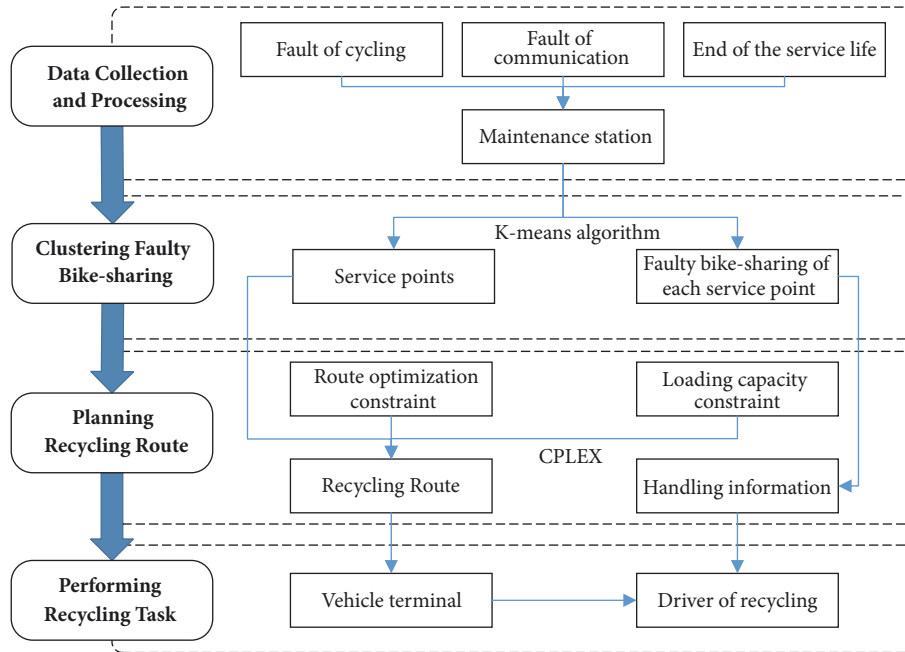


FIGURE 3: Flowchart of faulty bike-sharing recycling.

Step 1 (data collection and processing). There are three types of faulty bike-sharing in the section above. For type 1, the system server will directly set it as faulty bike-sharing to be processed. For type 2, when the location information of bike-sharing is lost, the system needs to record the last received location information. Type 1 and type 2 bicycles will be stored in the faulty bike-sharing database. For type 3, when a bike-sharing company launches bicycles in the city every time, the system server will set the time of the bicycles' service life, after which the time of service life of these bicycles will be stored in the faulty bike-sharing database by system server. By confirmation and processing of three types above, the bike-sharing company will have these faulty bikes fixed.

Step 2 (faulty bike-sharing clustering). Faulty bike-sharing clustering is represented by lower network as shown in Figure 2. The system will use the K-means algorithm to cluster the faulty bicycles to different service points in each area according to the result of data collection and processing. Based on the different service point, the faulty bicycles are carried to this location by manual handling and wait for company trucks to carry them in each clustering service point along the planned route driving to maintenance point.

Step 3 (planning recycling route). Planning recycling route is represented by the upper network as shown in Figure 2. Every recycling route is planned based on the result of faulty bike-sharing clustering. Meanwhile, recycling route optimization tries to achieve minimum total recycling costs with route optimization and vehicle capacity as constraints. The recycling vehicles start from the maintenance station, collect all the faulty bicycles, and finally return to the station.

Step 4 (performing recycling task). According to the result of Step 2 and Step 3, the recycling route and the faulty bike-sharing location information are sent to the vehicle terminal so that every driver of recycling vehicle can perform the task of recycling faulty bicycles.

It is worth noting that Step 2 and Step 3 are the key scientific problems. The FBSR aims at recycling all faulty bicycles and traversing all service points while optimizing the routes for recycling vehicles in order to reduce the costs of recycling.

4. Model Formulation

Based on framework design of faulty bike-sharing recycling, the FBSR model in this paper mainly consists of two parts: faulty bike-sharing clustering and recycling route modeling.

4.1. Faulty Bike-Sharing Clustering. K-means algorithm [27] is a method commonly used to automatically partition a dataset into k groups. We use it to cluster the faulty bicycles to different service points in an area. Suppose that a data set $\{x_1, \dots, x_N\}$ consists of N observations of a random 2-dimensional Euclidean variable x . The objective is to partition the dataset into some number K of clusters, given the value of K . First, introduce a set of 2-dimensional vectors c_k , where $C = \{c_k, k = 1, \dots, K\}$; c_k represents the center of the k th cluster. Second, find an assignment of data points to clusters, so that the sum of the squares of the distances of each data that points to its closest vector c_k is a minimum.

$$\min SSE = \sum_{n=1}^N \sum_{k=1}^K r_{nk} \|x_n - c_k\|^2 \quad (1)$$

$$r_{nk} = \begin{cases} 1, & x_n \in c_k \\ 0, & x_n \notin c_k \end{cases} \quad (2)$$

where *SSE* (sum of squares for error) is the sum of the distances from the data points to the clustering points, binary indicator variables $r_{nk} \in \{0, 1\}$, and k describes which cluster the data point x_n is assigned to, so that if x_n is assigned to cluster k , then $r_{nk} = 1$, and $r_{nj} = 0$ for $j \neq k$.

4.2. Recycling Route Modeling. We develop a recycling route model, where the decision-maker (the transit authority or operator) wishes to determine recycling route while minimizing total recycling costs. It is assumed that the result of faulty bike-sharing clustering remains unchanged throughout that period. Consider a network rooted at depot (the maintenance station) named $\{0\}$ and let the depot be denoted as node 0 ; S_0 is the set of nodes including the maintenance station and service points; that is, $S = S_0 \setminus \{0\}$. We suppose that travel time of recycling vehicles retains their characteristics throughout that period. Consider a maintenance station that consists of H vehicles, $h = 1, \dots, H$. Identical recycling vehicles with capacity cap_h serve the route for all service points, $\forall i \in S_0, \forall j \in S_0, i \neq j$, starting from depot ($i = 0$) and ending at depot ($j = 0$). The travel time (ignoring dwell time) of each vehicle between successive points i and j is denoted by t_{ij} . In order to model FBSR problem, we make assumptions as follows:

- (i) All route cycles are repeated with identical characteristics.
- (ii) The round-trip distance between the two service points is the same.
- (iii) The location of the faulty bicycle without positioning is accurate.

Thus, the optimization problem is

$$x_{ijh} \begin{cases} 1 & \text{if vehicle } h \text{ traverses arc } (i, j) \\ 0 & \text{otherwise} \end{cases} \quad (3)$$

$$y_{ih} \begin{cases} 1 & \text{if vehicle } h \text{ serves node } i \\ 0 & \text{otherwise} \end{cases}$$

$$\text{Minimize } C_m \sum_{i \in S_0} \sum_{j \in S_0} \sum_{k \in H} t_{ij} x_{ijh} \quad (4)$$

$$\text{Subject to } \sum_{i \in S_0} x_{ijh} = y_{jh} \quad \forall j \in S_0, h \in H \quad (5)$$

$$\sum_{j \in S_0} x_{ijh} = y_{hi} \quad \forall i \in S_0, h \in H \quad (6)$$

$$\sum_{k \in H} y_{hi} = 1 \quad \forall i \in S \quad (7)$$

$$\sum_i y_{hi} d_i \leq cap_h \quad h \in H \quad (8)$$

$$y_{hi} \in \{0, 1\} \quad \forall i \in S_0, h \in H \quad (9)$$

$$x_{ijh} \in \{0, 1\} \quad \forall i, j \in S_0, h \in H \quad (10)$$

The objective function minimizes the total recycling costs. It is multiplied by C_m , which indicates recycling vehicles operating costs per unit time. d_i indicates the number of bicycles handled by hands at node i . Constraint (6) states that if a vehicle h decides to serve node j which is serviced by only one vehicle, then it should travel along the arc from that node i , that is, $\text{arc}(i, j)$. Constraint (7) states that a vehicle h has traversed $\text{arc}(i, j)$ from node i which is serviced by only one vehicle; then it should travel along the arc leading to node j . Constraint (6) and constraint (7) ensure that the path of each vehicle is successive. Constraint (8) ensures that every node is serviced by only one vehicle, whereas constraint (9) ensures that the vehicle capacity is not exceeded. In order to model the entire process of FBSR, the formulation can easily accommodate fixed costs by modification of the objective function as follows:

$$C_m \sum_{i \in S_0} \sum_{j \in S_0} \sum_{h \in H} t_{ij} x_{ijh} + C_n \sum_{i \in S_0} \bar{t} n_i \quad (11)$$

The objective includes two components. The first refers to the objective function (5). The second refers to the expectation of the sum of manual handling costs, where C_n indicates faulty bicycles manual handling costs per unit time, \bar{t} is the average time of handling each faulty bicycle, and, based on formula (1), n_i is the number of faulty bicycles in the i th service points.

Let us define

$$\bar{t} = \frac{2 \times SSE}{\bar{v} \sum_{i \in S} n_i} \quad (12)$$

where \bar{v} is the average velocity of handling each faulty bicycle. It is multiplied by 2 because each vehicle must return to the clustering points after service. Objective function (11) is now

$$C_m \sum_{i \in S_0} \sum_{j \in S_0} \sum_{h \in H} t_{ij} x_{ijh} + C_n \frac{2 \times SSE}{\bar{v}} \quad (13)$$

In order to improve the utilization rate of recycling vehicles, we propose a constraint to restrict load capacity as follows:

$$\sum_{i \in S} y_{hi} n_i \geq \lambda cap_h \quad \forall h \in H \quad (14)$$

where λ is the coefficient of load capacity ratio.

Besides, in order to avoid the loop in the route, it is sufficient that problem includes the following bonding constraint:

$$U_{ih} - U_{jh} + |S| \cdot x_{ijh} \leq |S| - 1 \quad \forall i, j \in S_0, h \in H \quad (15)$$

where U_{ih} is the auxiliary variable to eliminate the constraint of loop for h th vehicle.

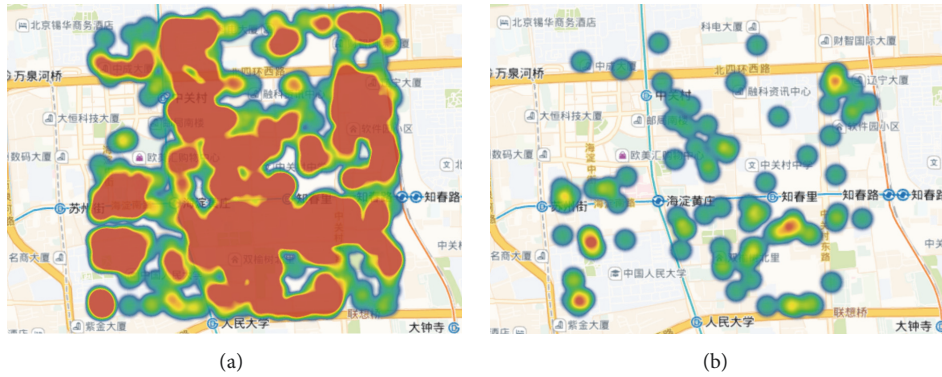


FIGURE 4: Heat map of bike-sharing.

In the process of problem solving, the recycling route model belongs to 0-1 integer programming model. Considering the scale of the problem, it can be solved by CPLEX solver with branch and bound approach for its advantages of the direct and concise input and strong computation ability.

5. Case Study

In this section, a real-world bike-sharing from an area of Beijing, China, was selected as a case study. The test area is a square area that has a side length of 2.6 km and Haidian Huang Zhuang subway station is selected as areal maintenance station. We set the number of recycling vehicles in a maintenance station as 4, and the capacity of each vehicle is 30 bicycles. There are 1900 bicycles (Figure 4(a)) in this area, and we randomly select 95 bicycles (5% of the total) as faulty bike-sharing, which is shown in Figure 4(b). Red indicates that faulty bicycles are dense, followed by orange, and blue means fewer bicycles in heat map.

5.1. Result of Faulty Bike-Sharing Clustering. We set up 1 to 14 groups clustering experiment. The times of iterations of each clustering algorithm are not more than 20, which proves that the computation is highly efficient. The SSE graph of K-means is shown in Figure 5. We show different clustering points in the x -axis and SSE of different clustering points in the y -axis. From the chart, it can be seen that the SSE of the clustering is stable when we select 12 clustering points, which is 17.531 km. We first select 12 clustering points for experimental analysis.

Latitude and longitude coordinates of the clustering centers are obtained by the K-means algorithm and their locations on a map are shown in Figure 6. From the diagram, it can be seen that the clustering points distribute relatively evenly in this area, due to the fact that faulty bikes are distributed relatively evenly.

5.2. Recycling Route Analysis. Considering the result of faulty bike-sharing clustering by K-means algorithm of 12 service points, $|S| = 12$. Travel time t_{ij} between every clustering point is obtained by Google Maps (see Tables 4, 5, and 6), which is calculated based on the shortest time of driving. The coefficient of load capacity ratio λ is 0.7. The recycling vehicle

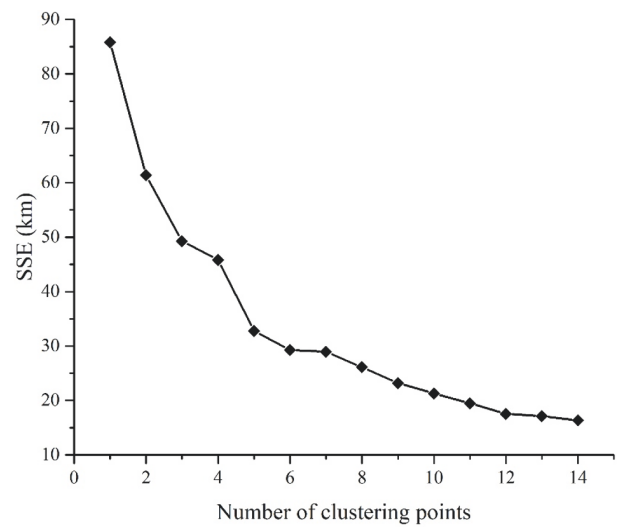


FIGURE 5: The SSE graph of K-means.

operating costs C_m are 5.5 Renminbi (RMB) per minute, and the faulty bicycles manual handling costs C_n are 0.5 RMB per minute. The average velocity of handling each faulty bicycle \bar{v} is 60 m/min. The optimal results of the FBSR model are solved with the CPLEX solver, as shown in Table 1.

In this example, we can see that the total costs are 677 RMB from the FBSR model. In Table 1, travel time is derived from the recycling route model; carrying time is derived from the clustering results for each service point. It can be seen clearly that each route of total time is between 112 min and 206 min, which demonstrates that the results of faulty bike-sharing clustering and recycling route are reasonable. In addition, the number of bicycles loaded is 24, 23, 25, and 23 for each vehicle; capacity ratio of each vehicle is more than 76.7%. According to the FBSR model, each vehicle achieves an optimized recycling route of FBSR with the vehicle load capacity constraint.

The comparison experiment for the coefficient of load capacity ratio was conducted. Figure 7 shows the number of bicycles loaded for the different capacity ratio, and the higher the coefficient of load capacity ratio is, the more average

TABLE 1: The optimal result of FBSP model.

| Vehicle | Capacity ratio | Route | Travel time/min | Carrying time/min | Total time/min | Total costs/RMB |
|---------|----------------|---------------------------|-----------------|-------------------|----------------|-----------------|
| 1 | 80% | 0 → 1 → 4 → 2 → 10 → 0 | 17 | 95 | 112 | 141 |
| 2 | 76.7% | 0 → 5 → 9 → 7 → 0 | 17 | 176 | 193 | 181.5 |
| 3 | 83 | 0 → 11 → 3 → 12 → 0 | 24 | 182 | 206 | 223 |
| 4 | 76.7% | 0 → 6 → 8 → 0 | 12 | 131 | 143 | 131.5 |
| Total | | | 70 | 584 | 654 | 677 |

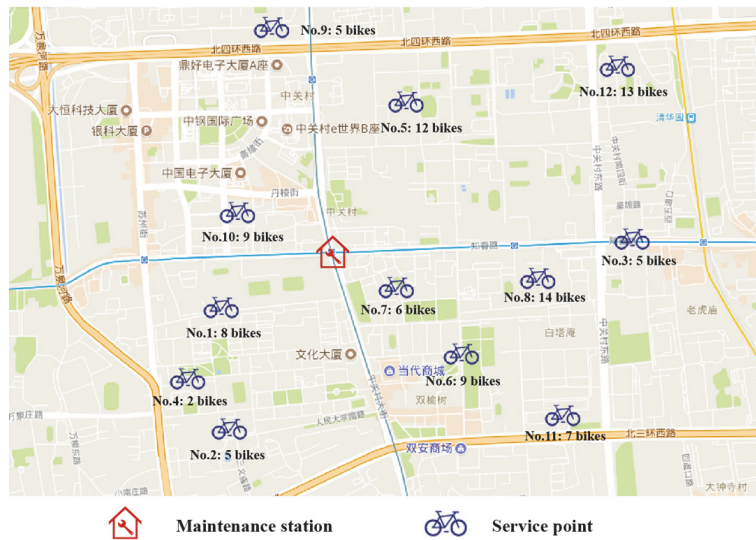


FIGURE 6: The graph of clustering centers by K-means.

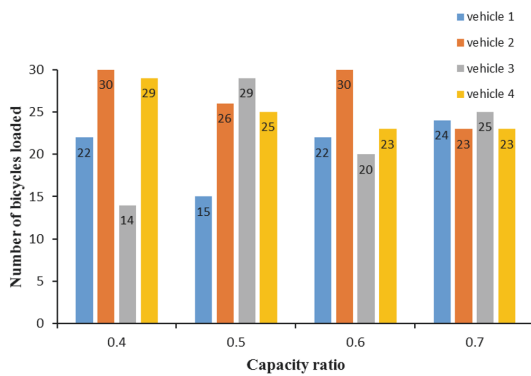


FIGURE 7: The number of bicycles loaded for the coefficient of load capacity ratio.

number of bicycles is loaded. It means that the load capacity constraint has an impact on the result of the FBSP model. In Table 2, we may observe travel time, carrying time, and total cost in several coefficients of load capacity ratios, which shows the optimal result of FBSP model for the different capacity ratio. We can find that travel time and capacity ratio have a positive correlation; that is, the lower the value of the

capacity ratio is, the lower the travel time is and the lower the costs are. The lowest value of the capacity ratio is 0.4, which responds to the lowest travel time, 67, and the lowest costs, 660.5. And the highest value of the capacity ratio is 0.7, which responds to the highest travel time, 70, and the highest costs, 677. However, the value of capacity ratio will affect the fairness of the recycling task and the utilization rate of the recycling vehicles; as a result, decision-makers can consider adding the maximum coefficient as objective to FBSP model according to the actual situation of recycling.

Table 3 shows that different clustering points are selected for contrast experiments. According to the experimental results, we can see that the total costs of 10-node clustering points are always the highest with different load capacity rates. Then the results show that the total costs of 12 nodes are more than the total costs of 14 nodes when the coefficient of load capacity ratio is no more than 0.6, and the total costs of 14 nodes are more than those of 12 nodes when the coefficient of load capacity ratio is equal to 0.7. When the number of clustering points is less, the increase in manual operation time will lead to high cost. In addition, the increase in service points will result in an increase of the recycling distance and the higher costs of recycling vehicles operating. Hence, the appropriate recycling scheme should be selected according to the costs changes of C_m and C_n .

TABLE 2: The optimal result of FBSP model for the different capacity ratio.

| λ | Vehicle | route | Travel time/min | Carrying time/min | Total costs/RMB |
|-----------|---------|------------------------|-----------------|-------------------|-----------------|
| 0.4 | 1 | 0 → 11 → 2 → 4 → 1 → 0 | 67 | 584 | 660.5 |
| | 2 | 0 → 5 → 12 → 3 → 0 | | | |
| | 3 | 0 → 10 → 9 → 0 | | | |
| | 4 | 0 → 8 → 6 → 7 → 0 | | | |
| 0.5 | 1 | 0 → 1 → 4 → 2 → 0 | 68 | 584 | 666 |
| | 2 | 0 → 5 → 9 → 10 → 0 | | | |
| | 3 | 0 → 8 → 6 → 7 → 0 | | | |
| | 4 | 0 → 12 → 3 → 11 → 0 | | | |
| 0.6 | 1 | 0 → 1 → 4 → 2 → 11 → 0 | 69 | 584 | 671.5 |
| | 2 | 0 → 5 → 12 → 3 → 0 | | | |
| | 3 | 0 → 10 → 7 → 9 → 0 | | | |
| | 4 | 0 → 8 → 6 → 0 | | | |
| 0.7 | 1 | 0 → 1 → 4 → 2 → 10 → 0 | 70 | 584 | 677 |
| | 2 | 0 → 5 → 9 → 7 → 0 | | | |
| | 3 | 0 → 11 → 3 → 12 → 0 | | | |
| | 4 | 0 → 8 → 6 → 0 | | | |

TABLE 3: The effects of the number of clustering points.

| Network | λ | Travel time /min | Carrying time /min | Total time /min | Total costs /RMB |
|---------|-----------|------------------|--------------------|-----------------|------------------|
| 10-node | 0.4 | 65 | 710 | 775 | 712.5 |
| | 0.5 | 65 | 710 | 775 | 712.5 |
| | 0.6 | 65 | 710 | 775 | 712.5 |
| | 0.7 | 65 | 710 | 775 | 712.5 |
| 12-node | 0.4 | 67 | 584 | 651 | 660.5 |
| | 0.5 | 68 | 584 | 652 | 666 |
| | 0.6 | 69 | 584 | 653 | 671.5 |
| | 0.7 | 70 | 584 | 654 | 677 |
| 14-node | 0.4 | 69 | 546 | 615 | 652.5 |
| | 0.5 | 71 | 546 | 617 | 663.5 |
| | 0.6 | 72 | 546 | 618 | 669 |
| | 0.7 | 74 | 546 | 620 | 680 |

6. Conclusions

This paper introduces the framework design and optimization method to solve FBSR problem. In China, the number of bike-sharing systems grows rapidly due to its flexibility and convenience for the users. However, they face operational challenges such as FBSR problem. For this reason, we presented a framework design of FBSR to solve the problem of recycling faulty bike-sharing. Then, we propose FBSR optimization model that is able to minimize the total recycling costs through the K-means clustering method that is used to divide the faulty bike-sharing into different service points. It can provide bike-sharing company’s managers with good insight into the design of a FBSR problem. The comparison among different service points can help

decision-makers to choose the best solution. In addition, the vehicle capacity restriction should be included in a FBSR optimization model to improve the number of bicycles loaded for each vehicle.

A typical example solved by CPLEX solver was created to illustrate the proposed model. The results of a case study show that the model works well. It is indicated that the best route recycles the faulty bicycles according to the clustering points. Compared with the values of capacity ratio models in the FBRS model, we can find that travel time and capacity ratio have positive correlation. And the comparison experiment has shown that the number of clustering points has a significant impact on total recycling costs, which needs to be considered carefully in the FBSR model.

TABLE 4: 10-node travel time matrix for each point (unit: min).

| t_{ij} | 0 | 1 | 2 | 3 | 4 | 5 | 6 | 7 | 8 | 9 | 10 |
|----------|----|----|----|----|----|----|---|----|----|----|----|
| 0 | 0 | 2 | 6 | 9 | 12 | 4 | 7 | 4 | 7 | 3 | 4 |
| 1 | 2 | 0 | 4 | 14 | 2 | 6 | 6 | 5 | 12 | 6 | 7 |
| 2 | 6 | 4 | 0 | 17 | 1 | 12 | 8 | 9 | 16 | 13 | 8 |
| 3 | 9 | 14 | 17 | 0 | 13 | 7 | 8 | 10 | 7 | 4 | 12 |
| 4 | 12 | 2 | 1 | 13 | 0 | 12 | 9 | 11 | 13 | 11 | 7 |
| 5 | 4 | 6 | 12 | 7 | 12 | 0 | 8 | 6 | 8 | 4 | 7 |
| 6 | 7 | 6 | 8 | 8 | 9 | 8 | 0 | 5 | 4 | 7 | 6 |
| 7 | 4 | 5 | 9 | 10 | 11 | 6 | 5 | 0 | 7 | 6 | 5 |
| 8 | 7 | 12 | 16 | 7 | 13 | 8 | 4 | 7 | 0 | 9 | 11 |
| 9 | 3 | 6 | 13 | 4 | 11 | 4 | 7 | 6 | 9 | 0 | 6 |
| 10 | 4 | 7 | 8 | 12 | 7 | 7 | 6 | 5 | 11 | 6 | 0 |

TABLE 5: 12-node travel time matrix for each point (unit: min).

| t_{ij} | 0 | 1 | 2 | 3 | 4 | 5 | 6 | 7 | 8 | 9 | 10 | 11 | 12 |
|----------|----|----|----|----|----|----|----|----|----|----|----|----|----|
| 0 | 0 | 2 | 6 | 7 | 12 | 4 | 4 | 3 | 5 | 5 | 4 | 5 | 11 |
| 1 | 2 | 0 | 4 | 13 | 2 | 6 | 5 | 4 | 6 | 12 | 7 | 6 | 16 |
| 2 | 6 | 4 | 0 | 15 | 1 | 12 | 6 | 13 | 13 | 14 | 8 | 6 | 19 |
| 3 | 7 | 13 | 15 | 0 | 17 | 11 | 5 | 9 | 4 | 7 | 14 | 3 | 5 |
| 4 | 12 | 2 | 1 | 17 | 0 | 12 | 12 | 11 | 12 | 12 | 7 | 10 | 16 |
| 5 | 4 | 6 | 12 | 11 | 12 | 0 | 6 | 6 | 5 | 4 | 7 | 9 | 5 |
| 6 | 4 | 5 | 6 | 5 | 12 | 6 | 0 | 3 | 3 | 9 | 8 | 6 | 8 |
| 7 | 3 | 4 | 13 | 9 | 11 | 6 | 3 | 0 | 5 | 6 | 5 | 6 | 12 |
| 8 | 5 | 6 | 13 | 4 | 12 | 5 | 3 | 5 | 0 | 8 | 7 | 7 | 9 |
| 9 | 5 | 12 | 14 | 7 | 12 | 4 | 9 | 6 | 8 | 0 | 7 | 8 | 12 |
| 10 | 4 | 7 | 8 | 14 | 7 | 7 | 8 | 5 | 7 | 7 | 0 | 7 | 11 |
| 11 | 5 | 6 | 6 | 3 | 10 | 9 | 6 | 6 | 7 | 8 | 7 | 0 | 10 |
| 12 | 11 | 16 | 19 | 5 | 16 | 5 | 8 | 12 | 9 | 12 | 11 | 10 | 0 |

TABLE 6: 14-node travel time matrix for each point (unit: min).

| t_{ij} | 0 | 1 | 2 | 3 | 4 | 5 | 6 | 7 | 8 | 9 | 10 | 11 | 12 | 13 | 14 |
|----------|----|----|----|----|----|----|----|----|----|----|----|----|----|----|----|
| 0 | 0 | 2 | 6 | 8 | 12 | 4 | 4 | 2 | 4 | 5 | 4 | 6 | 6 | 8 | 7 |
| 1 | 2 | 0 | 4 | 13 | 2 | 6 | 11 | 10 | 12 | 12 | 7 | 11 | 15 | 17 | 16 |
| 2 | 6 | 4 | 0 | 14 | 1 | 12 | 8 | 8 | 13 | 12 | 8 | 8 | 16 | 18 | 17 |
| 3 | 8 | 13 | 14 | 0 | 17 | 11 | 6 | 9 | 6 | 7 | 14 | 5 | 9 | 5 | 4 |
| 4 | 12 | 2 | 1 | 17 | 0 | 12 | 9 | 8 | 13 | 11 | 5 | 9 | 15 | 17 | 16 |
| 5 | 4 | 6 | 12 | 11 | 12 | 0 | 5 | 6 | 5 | 4 | 7 | 8 | 4 | 5 | 4 |
| 6 | 4 | 11 | 8 | 6 | 9 | 5 | 0 | 3 | 3 | 8 | 8 | 5 | 7 | 10 | 7 |
| 7 | 2 | 10 | 8 | 9 | 8 | 6 | 3 | 0 | 4 | 8 | 4 | 5 | 8 | 10 | 9 |
| 8 | 4 | 12 | 13 | 6 | 13 | 5 | 3 | 4 | 0 | 8 | 7 | 7 | 8 | 8 | 7 |
| 9 | 5 | 12 | 12 | 7 | 11 | 4 | 8 | 8 | 8 | 0 | 6 | 8 | 3 | 6 | 6 |
| 10 | 4 | 7 | 8 | 14 | 5 | 7 | 8 | 4 | 7 | 6 | 0 | 6 | 9 | 10 | 10 |
| 11 | 6 | 11 | 8 | 5 | 9 | 8 | 5 | 5 | 7 | 8 | 6 | 0 | 10 | 9 | 8 |
| 12 | 6 | 15 | 16 | 9 | 15 | 4 | 7 | 8 | 8 | 3 | 9 | 10 | 0 | 3 | 2 |
| 13 | 8 | 17 | 18 | 5 | 17 | 5 | 10 | 10 | 8 | 6 | 10 | 9 | 3 | 0 | 2 |
| 14 | 7 | 16 | 17 | 4 | 16 | 4 | 7 | 9 | 7 | 6 | 10 | 8 | 2 | 2 | 0 |

In the future, with bike-sharing systems growing in China, we will present a solution model for dealing with dynamic faulty bike-sharing recycling. In addition, random searching for faulty bicycle without GPS should also be considered by the researchers.

Data Availability

The data used to support the findings of this study are available from the corresponding author upon request.

Conflicts of Interest

The authors declare that they have no conflicts of interest.

Acknowledgments

This research is supported by the National Natural Science Foundation of China (no. U1434207 and no. U1734204).

References

- [1] E. Fishman, "Bikeshare: a Review of Recent Literature," *Transport Reviews*, vol. 36, no. 1, pp. 92–113, 2016.
- [2] Y. Tang, H. Pan, and Q. Shen, "Bike-sharing systems in Beijing, Shanghai and Hangzhou and their impact on travel behaviour," in *Proceedings of the Transportation Research Board 90th Annual Meeting*, 2010.
- [3] S. A. Shaheen, H. Zhang, E. Martin, and S. Guzman, "China's Hangzhou Public Bicycle: Understanding early adoption and behavioral response to bikesharing," *Transportation Research Record*, no. 2247, pp. 33–41, 2011.
- [4] Q. Chen and T. Sun, "A model for the layout of bike stations in public bike-sharing systems," *Journal of Advanced Transportation*, vol. 49, no. 8, pp. 884–900, 2015.
- [5] P. Demaio, "Bike-sharing: history, impacts, models of provision, and future," *Journal of Public Transportation*, vol. 12, no. 4, pp. 41–56, 2009.
- [6] P. J. Demaio, "Smart bikes: Public transportation for the 21st century," *Transportation Quarterly*, vol. 57, no. 1, pp. 9–11, 2003.
- [7] S. A. Shaheen, S. H. Guzman, and H. Zhang, "Bikesharing in Europe, the Americas, and Asia past, present, and future," *Transportation Research Record*, vol. 2143, Article ID 1316350, pp. 159–167, 2010.
- [8] A. Audikana, E. Ravalet, V. Baranger, and V. Kaufmann, "Implementing bikesharing systems in small cities: Evidence from the Swiss experience," *Transport Policy*, vol. 55, pp. 18–28, 2017.
- [9] Y. T. Hsu, L. Kang, and Y. H. Wu, "user behavior of bikesharing systems under demand-supply imbalance," *Transportation Research Record*, vol. 2587, pp. 117–124, 2016.
- [10] L. Aultman-Hall and M. G. Kaltenecker, "Toronto bicycle commuter safety rates," *Accident Analysis & Prevention*, vol. 31, no. 6, pp. 675–686, 1999.
- [11] E. Fishman, S. Washington, and N. Haworth, "Bike Share: a synthesis of the literature," *Transport Reviews*, vol. 33, no. 2, pp. 148–165, 2013.
- [12] K. Martens, "Promoting bike-and-ride: The Dutch experience," *Transportation Research Part A: Policy and Practice*, vol. 41, no. 4, pp. 326–338, 2007.
- [13] H. Nakamura and N. Abe, "Evaluation of the hybrid model of public bicycle-sharing operation and private bicycle parking management," *Transport Policy*, vol. 35, pp. 31–41, 2014.
- [14] K. Martens, "The bicycle as a feeding mode: experiences from three European countries," *Transportation Research Part D: Transport and Environment*, vol. 9, no. 4, pp. 281–294, 2004.
- [15] A. Kaltenbrunner, R. Meza, J. Grivolla, J. Codina, and R. Banchs, "Urban cycles and mobility patterns: Exploring and predicting trends in a bicycle-based public transport system," *Pervasive and Mobile Computing*, vol. 6, no. 4, pp. 455–466, 2010.
- [16] J. Pucher, R. Buehler, and M. Seinen, "Bicycling renaissance in North America? An update and re-appraisal of cycling trends and policies," *Transportation Research Part A: Policy and Practice*, vol. 45, no. 6, pp. 451–475, 2011.
- [17] S. Kaplan, F. Manca, T. A. S. Nielsen, and C. G. Prato, "Intentions to use bike-sharing for holiday cycling: an application of the theory of planned behavior," *Tourism Management*, vol. 47, pp. 34–46, 2015.
- [18] S.-Y. Chen, "Green helpfulness or fun? Influences of green perceived value on the green loyalty of users and non-users of public bikes," *Transport Policy*, vol. 47, pp. 149–159, 2016.
- [19] D. Chemla, F. Meunier, and R. W. Calvo, "Bike sharing systems: solving the static rebalancing problem," *Discrete Optimization*, vol. 10, no. 2, pp. 120–146, 2013.
- [20] J. Schuijbroek, R. C. Hampshire, and W.-J. van Hoes, "Inventory rebalancing and vehicle routing in bike sharing systems," *European Journal of Operational Research*, vol. 257, no. 3, pp. 992–1004, 2017.
- [21] S. Ghosh, P. Varakantham, Y. Adulyasak, and P. Jaillet, "Dynamic repositioning to reduce lost demand in bike sharing systems," *Journal of Artificial Intelligence Research*, vol. 58, pp. 387–430, 2017.
- [22] J. Pfrommer, J. Warrington, G. Schilb, and M. Morari, "Dynamic vehicle redistribution and online price incentives in shared mobility systems," *IEEE Transactions on Intelligent Transportation Systems*, vol. 15, no. 4, pp. 1567–1578, 2014.
- [23] S. Reiss and K. Bogenberger, "GPS-Data Analysis of Munich's Free-Floating Bike Sharing System and Application of an Operator-based Relocation Strategy," in *Proceedings of the 18th IEEE International Conference on Intelligent Transportation Systems*, pp. 584–589, September 2015.
- [24] L. Caggiani, R. Camporeale, and M. Ottomanelli, "Planning and design of equitable free-floating bike-sharing systems implementing a road pricing strategy," *Journal of Advanced Transportation*, vol. 2017, Article ID 3182387, 18 pages, 2017.
- [25] A. Pal and Y. Zhang, "Free-floating bike sharing: Solving real-life large-scale static rebalancing problems," *Transportation Research Part C: Emerging Technologies*, vol. 80, pp. 92–116, 2017.
- [26] L. Caggiani, R. Camporeale, M. Ottomanelli, and W. Y. Szeto, "A modeling framework for the dynamic management of free-floating bike-sharing systems," *Transportation Research Part C: Emerging Technologies*, vol. 87, pp. 159–182, 2018.
- [27] X. Cheng and Y. Gao, "The optimal monthly strategy pricing of free-floating bike sharing platform," *Modern Economy*, vol. 9, no. 2, pp. 318–338, 2018.
- [28] R. Cervero, O. Lsarmiento, E. Jacoby, L. F. Gomez, A. Nei-Man, and G. Xue, "Influences of built environments on walking and cycling: lessons from Bogotá," *Urban Transport of China*, vol. 3, no. 4, pp. 203–226, 2016.

Research Article

Hierarchical Matching of Traffic Information Services Using Semantic Similarity

Zongtao Duan , Lei Tang , Zhiliang Kou , and Yishui Zhu 

School of Information Engineering, Chang'an University, Xi'an, Shaanxi, China

Correspondence should be addressed to Lei Tang; tanglei24@gmail.com

Received 13 April 2018; Accepted 14 May 2018; Published 7 June 2018

Academic Editor: Sara Moridpour

Copyright © 2018 Zongtao Duan et al. This is an open access article distributed under the Creative Commons Attribution License, which permits unrestricted use, distribution, and reproduction in any medium, provided the original work is properly cited.

Service matching aims to find the information similar to a given query, which has numerous applications in web search. Although existing methods yield promising results, they are not applicable for transportation. In this paper, we propose a multilevel matching method based on semantic technology, towards efficiently searching the traffic information requested. Our approach is divided into two stages: service clustering, which prunes candidate services that are not promising, and functional matching. The similarity at function level between services is computed by grouping the connections between the services into inheritance and noninheritance relationships. We also developed a three-layer framework with a semantic similarity measure that requires less time and space cost than existing method since the scale of candidate services is significantly smaller than the whole transportation network. The OWL-TC4 based service set was used to verify the proposed approach. The accuracy of offline service clustering reached 93.80%, and it reduced the response time to 651 ms when the total number of candidate services was 1000. Moreover, given the different thresholds for the semantic similarity measure, the proposed mixed matching model did better in terms of recall and precision (i.e., up to 72.7% and 80%, respectively, for more than 1000 services) compared to the compared models based on information theory and taxonomic distance. These experimental results confirmed the effectiveness and validity of service matching for responding quickly and accurately to user queries.

1. Introduction

For transportation systems to advance strongly in China, greater financial investment in infrastructure, e.g., roads, docks, and power stations, is important. In addition, we must look beyond such measures to find new ways to expedite transportation development. With the increased availability of intelligent technology, urban areas (i.e., cities and their surrounding areas) in China have considerably accelerated their drive towards modernization, thereby bringing about benefits to the transportation system of the entire country [1]. In particular, these advances have facilitated the dissemination of traffic information and have helped to promote compliance with its requirements. The rapid growth of the Internet and mobile Internet of things (IoT) devices relies on diversification, magnitude, and heterogeneity as their dominant measures of quality for traffic services [2]. However, considering real-world scenarios, particularly in China, different data formats, languages, and dialects will

produce diverse travel demands. The data generated by these services often prove that the communication of diverse needs is difficult. Such an understanding demands more than the ability to share data and improve the maximum use of the services. Clearly, a strategic key for the development of transportation systems is the creation of traffic information services (TIS) that meet the wide variety of needs and preferences of travelers, providing them with prompt and accurate access to a variety of services by merging multiple distinct technologies. Service matching focuses on finding the most similar information to a given query. For example, the system can match the TISs which tell a user where a restaurant is, what time the bus comes, etc.

To meet the unique needs of commuters, tourists, business travelers, and others, the massive amounts of information available on the traffic environment are organized into a variety of TIS offerings that involve varying degrees of complexity. These services provide drivers with information, e.g., alerts about road conditions, unexpected incidents, or

roadwork. To make public transit more acceptable, TIS may also cover information about ticketing and current operations, as well as the availability of park-and-ride facilities [3]. Although a single search engine can intelligently categorize and classify thousands of pieces of traffic information, service matching for transportation has incomparable advantages. First, service matching can provide an association between two or more applications to provide information that goes beyond anything that a single application can provide. For example, a complete travel solution for an individual using public transportation could cover ticketing, timetables, and information about accommodations, as well as the location, hours, and cost of particular attractions. Second, many mobile devices, e.g., in-car systems, provide dynamic value-added services, such as recommending only nearby restaurants, that are different from the types of information that web-based search engines offer. Therefore, faced with abundant traffic services, accurate and rapid service matching can provide robust solutions to meet a variety of requirements. Service matching can be improved by the addition of semantic features, such as traffic information, behaviors, and preferences of travelers [4, 5], that can be applied for a better understanding of an individual's travel goals.

Therefore, it is particularly important to maximize service matching for TIS solutions and reduce their search space. Moreover, it is absolutely critical that the behavior and presentation of these services reflect how users consider a travel in the real world as closely as possible. In our research, we developed a hierarchical matching method with a semantic similarity measure. This approach increased the accuracy of service matching and reduced the response time. The proposed search engine can serve as the basis for creating a new TIS in order to better comply with travelers' needs, which can be taken by transport planners and operators.

Our contributions are as follows:

(1) To reduce the search space for matching, each TIS was classified automatically by using K-means clustering and was structured as an ontology tree.

(2) The semantic similarity between different TIS concepts was calculated using the proposed model that included aspects of information theory and taxonomic distance.

(3) The improved bipartite graph, with nodes that had two types of attributes, was applied to calculate the semantic similarity.

2. Related Work

Paolucci et al. [6] proposed a DAML-S-based service matching method based on the relationships between the concepts in a taxonomy tree. Their algorithm suggested only four rough degrees of matching, an approach that needed improvement to achieve fine-grained matching for a large number of services. Nonetheless, their work took a step forward towards matching characterized by semantic features.

The measure of the semantic similarity between services is a key issue [7]. To establish a measure of similarity, three major models have been followed [8]: one based on taxonomic distance [9], another based on information content (IC) [10], and the last based on the concepts'

properties. Harispe et al. presented a framework for assessing similarity [11]. They also suggested the criteria for associating semantic similarity measures and provided a method for optimizing the configuration parameters. The framework proposed could facilitate applications in a biomedical context by improving the understanding of semantic measures.

Sánchez et al. [12] classified the existing approaches to ontology-based semantic similarity in terms of precision, computational complexity, prior knowledge needed, and adjustable parameters. They also defined the distance between concepts as the length of the path connecting two terms in a taxonomy and incorporated taxonomic distance into a set of features for similarity assessment. Usually, methods that utilize semantic matching on the basis of the taxonomic distance attempt to quantify the similarity between two services by considering a quantifiable structure in which the similarity decreases with an increase in the distance, and vice versa. However, service matching that uses this approach is susceptible to factors such as the depth and density of the domain ontology tree and the symmetry of the relationship between the two ontology concepts. Furthermore, IC, an indicator of the amount of information provided by an ontology concept, enables the assessment of the degree of semantic similarity of words referring to these concepts [13]. In the work cited above [13], Sánchez et al. developed some ontologies to improve the measure of IC-based semantic similarity. They detailed two strategies that considered the compared concepts as belonging to the same or to two or more different ontologies, respectively. Their results showed that the accuracy improved significantly when multiple ontologies were included.

Meng et al. defined a concept's topology and incorporated it into the similarity assessment of WordNet [14]. Different from the existing work, they introduced the depth and structure of every given concept, along with the quantity of their hyponyms, in an ontology tree as parameters in their IC model. The good performance of their measure was demonstrated by solving the problem caused by sparse data. Similarly, considering WordNet, an approach was proposed by Gao et al. for determining the semantic similarity associated with edge-counting [15]. IC was also used to define the shortest length of links treated as unequal distances between adjacent concepts. Then, the similarity was given by weighting various combinations of information sources nonlinearly or linearly. However, this approach resulted in a loss of useful information because it did not consider other paths in the net (i.e., WordNet).

The above illustrates the significance of similarity measure in service matching and discusses the drawback of existing methods, which motivates our research. Although we have learned that an IC-based model is not sensitive to the problem of varying link distance, the similarity does not depend strongly on the ontology tree and is simply recognized using term frequency-inverse document frequency (TF-IDF). Such textual statistical methods have caused problems such as data sparseness and ambiguous concepts that affect the calculation of the frequency of concepts and the assessment of further similarity, particularly for service matching in a traffic environment.

3. Service Matching for Transportation

Given a service request, the purpose of traffic information service matching is to search the service library efficiently and quickly for a candidate service subset. Currently, there are a variety of ontology languages for describing semantic-based TIS, such as OWL, WSMO, SWSO, and SAWSDL, each of which has certain advantages. Because of the standards for the Web Ontology Language for Services (OWL-S) [16], we used it to describe the traffic information services in this study. The basic framework of OWL-S [17] is made of three parts: the service profile, service model, and service grounding. Thus, any given service is represented using these three parts. The “service profile” describes what the service does, the “service model” states how it works, and the “service grounding” describes how to interact with the service.

In our research, with the help of the OWL-S profile, the problem of service matching amounted to finding a way to measure the semantic similarity of the services’ functional and nonfunctional attributes. In a traffic environment, TIS applications are offered mainly to the traveling public. Real-time dynamic information is sent to users through wireless or wired communication technologies. Information comes in the form of texts, pictures, videos, and other communications that provide dynamic, real-time access to the best travel information anytime and anywhere. Although the development of web services matching began decades ago, these matching processes have faced the following five challenges in a traffic environment:

(1) *Integration*: when a traveler requests information, frequently, various functional services must be integrated to provide a complete answer to the query [18]. For example, when traveling to another city, you might require the weather forecast from a meteorological service, timetables from the suburban transportation service, and road conditions from the traffic services. To meet the user’s request fully, all of these services must work together well to provide a complete response.

(2) *Dynamic heterogeneity*: the information provided by TIS must consider the possibility that the traveler may leave the original geographic area after sending the request for information. Therefore, the results might be returned, in effect making the service unavailable. In addition, TIS data can be delivered by various types of mobile devices or via the Internet, as well as by roads or other means. This requirement implies that TIS data need to be considerably different from web-only data in terms of their structure [19]. Therefore, service matching must support dynamic and homogeneous access to heterogeneous services in traffic environments.

(3) *Robustness*: communication links between traffic facilities, and connections to mobile devices, are not as reliable as the web, so the issues inherent to mobile devices can cause travel services to be unavailable temporarily. Therefore, priority should be given to the robustness of service matching.

(4) *Real-time use*: because of the rapid development of mobile IoT, there has been a significant growth in the number and variety of heterogeneous traffic information services in a wide variety of formats [20], e.g., speech-based navigation, visualization queries for traffic flows, and dissemination of

information about traffic incidents. For services to facilitate travel, it is important to reduce the search space, making matching more efficient and creating a better, safer travel experience. Therefore, it is necessary to focus on the real-time performance of matching TIS data.

(5) *User-friendliness*: TIS search results must be flexible to meet the needs of a variety of audiences (e.g., drivers, passengers, and traffic-controllers). Each type of user looks at the same data in a different way. Therefore, service matching is required to be highly user-friendly. Semantic-based matching must have the ability to understand human thinking and present findings in a manner that parallels human reasoning.

With respect to traffic information, we found that service matching faces the following challenges:

(1) A relatively large search space leads to inefficient matching.

(2) The resources of various road infrastructures are limited.

(3) Service matching must be acquired dynamically in real time because vehicles are in motion.

To meet these challenges in transportation, it is vital to construct an efficient, real-time, lightweight model for TIS matching that can handle a large search space, heterogeneous dynamic data, and limited resources.

4. Semantic-Based Matching Model of TISs

Because of the difficulty of characterizing domain-specific knowledge using XML and WSDL, we used the OWL-S Editor to work with OWL-S to structure the traffic information services and allow for semantic reasoning. Given the description of services, the service profile (one part of the OWL-S-based services) was adopted as the base. In particular, three terms were extracted from a service profile: the name, short-text description, and functions of the TIS. In this study, the first two were used to group services automatically; the “function of the TIS” was used in input/output- (IO-) based matching. Hereafter, for convenience, we have referred to the service profile and defined the description-related set of services provided and that of service requests.

First, we defined the profile of traffic information services as follows.

Definition 1. $Service = \{Description, Input-Output\}$, where these attributes are drawn from the service profile of the OWL-S model, and the description consists of the name and short-text description. $Input = \{input_1, input_2, \dots\}$ and $Output = \{output_1, output_2, \dots\}$ are regarded as the input and the output function sets of a service, respectively.

The description set (DS), a set of descriptions as described above, is given as follows.

Definition 2. $DS = \{Description_1, Description_2, \dots\}$. The service request is defined as $Req = \{R_{Description}, R_{Input-Output}\}$, where $R_{Description}$ denotes the description of services expected by a requestor; $R_{Input} = \{r_{input1}, r_{input2}, \dots\}$ and $R_{Output} = \{r_{output1}, r_{output2}, \dots\}$ are the separate input and output, respectively, according to the individual’s needs.

The approach proposed in this paper involves the clustering and matching of the TISs in the library, which include the following:

- (1) Dividing the TISs in the library into different categories
- (2) Measuring the semantic similarities between the functions requested and those provided
- (3) Returning the candidate TIS solutions to the individual traveler after ranking the calculated similarities

4.1. Grouping TIS Using K-Means. Because there are many services for transportation, it was necessary to reduce the search space before matching to significantly improve the efficiency and the precision of the search results. Many popular text clustering methods use text modeling algorithms to reduce the query space [21]. They usually assess the similarity among the services and tag the optimal candidate category, which is then iteratively refined as more detail is developed to update the centers. Text clustering compresses the traffic information service matching space quickly, thereby improving the accuracy of the matching algorithm and reducing the time that the users must wait for a response [22]. Rajagopal et al. [17] applied clustering techniques to group a massive number of services. Services falling into the same category belonged to the same cluster, and thus, the similarity among these services was the highest. However, considering that different services were assigned to different clusters, these researchers did not further refine the process of service matching in this situation.

To accelerate the search speed for web-service queries, Wenjing et al. [23] restructured the services for clustering them hierarchically in terms of their inputs, outputs, names, and text-based descriptions. Similarly, considering the inter-cluster distance, hierarchical agglomerative clustering was performed by Surianarayanan et al., depending on both the inputs and the outputs of services with prioritization. The similarities were then identified as different degrees of match for meeting disparate queries from clients [24]. Yisong et al. [25] utilized nonfunctional descriptions to group services and provided the service-to-service matches in terms of semantic similarity.

Although OWL-S-based descriptions have been used to automate text clustering and classification in searches for the best services, the abovementioned methods failed for traffic information services. The unknown number of centers and the coarser-grained classification were identified as the reasons for the low achievement of this approach for TIS matching and the consequent failure of service delivery. Moreover, the textual descriptions may be extended in the form of long characters to further improve relevant clustering. However, by including only function and nonfunction, we may get relatively few descriptions of functions and lose good matches from such clusters because the importance of functions is minimized for TIS matching. Therefore, in this study, the texts used in the clustering were expanded by first integrating the name and descriptions of each TIS and then classifying each TIS using K-means.

The steps taken for TIS clustering were as follows:

(1) The data preprocessing of the TIS in-service libraries was performed using word segmentation. Keywords were generated and traversed to create a customized dictionary.

(2) The vectorization of keywords was achieved using the vector space model and TF-IDF within the area of information retrieval. The description of a TIS is shown below with the vector space model.

$$Description_j = \{d_{1j}, d_{2j}, d_{3j}, \dots, d_{nj}\} \quad (1)$$

where d_{ij} denotes how frequently a word obtained from the dictionary appears in a special description of the TIS; $d_{ij} = 1$ if the word appears and 0 otherwise. However, the incompleteness of data could not be captured in this way with the increasing number of TISs in the library, and the contribution of each word was ignored. Consequently, following the preprocessing operation, all of the words in the $Description_j$ were weighted using the TF-IDF [26] as follows:

$$d_{i,j} = \frac{TF_{i,j} * \log(N/n_i)}{\sqrt{\sum_{j=1}^n [TF_{i,j} * \log(N/n_i)]^2}} \quad (2)$$

where $d_{i,j}$ and $TF_{i,j}$ denote the weight and the frequency of the i th word in the j th description, respectively. N stands for the total number of descriptions in the library in which the number of descriptions containing the i th word is captured by parameter n_i ; H determines the number of words in the j th description; and the denominator conducts a normalization on the weight. Thus, the improved description of a TIS was expressed as a set of $d_{i,j}$.

(3) The clustering of all of the TISs in the library by using K-means was accomplished as follows:

$$U = \sum_{k=1}^K \sum_{Description_j \in DS} (\overrightarrow{Description_j} - \overrightarrow{u_k}) \quad (3)$$

$$\overrightarrow{u_k} = \frac{\sum_{j=1}^J \overrightarrow{Description_j}}{J}$$

where K denotes the number of service categories in the traffic environment and J implies the number of services belonging to the same categories. $\overrightarrow{u_k}$ denotes the cluster center, which is a vector generated by an iterative means of averaging a set of descriptions from the same category of services. K was determined experimentally in this study, an approach that facilitated more rigorous classification than that found in other existing works [27, 28]. The clustering process was used to classify a large number of TISs and keep each center's information separate. The iterative process was continued until U in formula (3) for convergence was met. When receiving a new request for a travel service, the category of the request was determined by analyzing the request's taxonomic distance from the centers. This method allowed the search space to be reduced quickly and improved the efficiency and the precision of TIS matching. The clustering (Algorithm 1) used in this study was as follows.

Input:*Service: set of service profiles***Output:***k: number of centers of clusters***Begin**

```

(1) textVect ← processData(Service)
(2) cluster_Num ← k, error[0] ← INF
(3) randomWithServiceCategory(textVect)
(4) while error[i] < error[i-1] do
(5)   Kmeans(textVect, cluster_Num)
(6)   error[i] ← getError(textVect)
(7)   serviceCategory ← getServiceCategory(textVect)
(8)   cluster ← getServiceCluster(serviceCategory, textVect)
(9) end while
End

```

ALGORITHM 1: TIS clustering based on K-means.

The pseudo code of the algorithm for TIS clustering is given in Algorithm 1. In Algorithm 1, the first line conducts data preprocessing, including segmenting words and constructing the vector space model. Lines (2)-(3) initialize the number of cluster centers, the error value, and a category label given to each service. Lines (4)–(8) explore the key steps for clustering, and line (9) updates the centers and the category labels.

4.2. Function-Level Semantic Matching. The classification of TIS is considered to be merely low-precision service matching. Although service matching helps make the search more efficient, it is difficult for TIS matching to adjust to the personal demands of travelers without an adequate semantic comparison. We considered the input and the output functions provided by a TIS as subjects of comparison and defined them as nodes of a tree-structured ontology. Further, we measured the semantic similarities between the functions requested recently and the functions in the library listed under each of the services in the ontology. The existing research [25] made a semantic extension on the description of a service only when the function and the nonfunction were coordinated. Generating such a long-text description without filtering nonuseful services limits its use for function-level matching. Instead, we introduced multistage matching to refine the TIS matching.

The function-level matching in our work was based on the following four assumptions:

- (1) All TISs are characterized on the basis of OWL-S.
- (2) All TISs of the same category are defined in the same domain ontology.
- (3) Only the inheritance relationships between nodes in the ontology tree are considered.
- (4) Only the input and output functions are taken into consideration for matching.

The proposed function-level matching was divided into two stages. In the first stage, we calculated the similarity between the nodes. In the second stage, we focused on the similarity between sets of nodes. Thus, the match optimization problem could be represented as a maximum-weight bipartite matching problem.

If we were to limit our method to the use of a geometric model where all of the weights of each edge were the same, the result would be a loss of accuracy for TIS matching. Therefore, to measure the similarity, we referred to Zhang et al.'s work [29] to present mixed matching by integrating a geometric model and a model derived from information theory. We observed that the similarity increased with a decrease in the semantic distance between the nodes in the ontology tree. As we went down into the deep layers of the tree, the similarity increased as well, illustrating that two nodes were similar even if they were irrelevant on inheritance. That is, it was difficult to identify the services found as meeting the personal demands of travelers without considering the relationships between the nodes in the hierarchy during matching. For example, given a tree-based library for traveling, "Hiking" and "Surfing" would be considered two sibling nodes of the parent node "Activity." When a request delivered relates to "Surfing," the service matching could fail because unexpected "Hiking" might be returned by the matching process if we were to compute only the similarities without thinking about the relationships of nodes, particularly inheritance.

Therefore, the calculation of similarity was revised, and the relations were captured by parameter β , which was expressed as 1 between a given node and its children (e.g., "Activity" and "Sports") and between 1 and μ for a given node and its children's descendant (e.g., "Activity" and "Swimming") otherwise. In addition, β was assigned the value above μ when two nodes were not connected on inheritance (e.g., "sightseeing" and "Swimming"). μ was experimentally determined in this study. The following formula was used:

$$SemSim(func_i, func_j) = 1 - \sqrt{\beta \frac{\partial - 1}{\partial} \times \frac{Dep(func_i)}{Dep(func_i) + Dep(func_j)} \times SemDist(func_i, func_j)} \quad (4)$$

where $func_i$ requested and $func_j$ provided are considered two separate nodes in tree-structured ontologies. $SemDist(func_i, func_j)$ gives their semantic distance derived using information theory. $Dep(func_i)$ is the depth of $func_i$ in a tree. α and β are used to maximize the traffic service matches.

To determine the similarity between each set of functions, a set of nodes related to the TIS was created using a bipartite graph that consisted of two disjoint sets of vertices, a set representing input functions that R_{input} requested, and a set representing input functions that $input$ provided. An edge


```

Input:
 $R_{Input} = \{r_{input1}, r_{input2}, \dots\}$ : input function sets requested
 $Input = \{input_1, input_2, \dots\}$ : input function set of a service provided.
 $R_{Output} = \{r_{output1}, r_{output2}, \dots\}$ : output function sets requested
 $Output = \{output_1, output_2, \dots\}$ : output function set of a service
 $\sigma$ : similarity threshold
 $\lambda_1, \lambda_2$ : weights of input and output functions
Output:
 $Sim_{func}$ : similarity of function sets from travelers and providers
Begin
(1)  $sim_{func} = \lambda_1 \times sim(R_{input}, Input)$ 
       $+ \lambda_2 \times sim(R_{output}, Input)$ 
 $sim(func_a, func_b) // function$ 
{
  (1) for  $i \leftarrow 1$  to  $m$  do
  (2)   for  $j \leftarrow 1$  to  $n$  do
  (3)      $e_{ij} \leftarrow SemSim(func_a[i], func_b[j])$ 
  (4)     if  $e_{ij} > \sigma$ 
  (5)        $service\_set \leftarrow service\_set \cup e_{ij}$ 
  (6)     end if
  (7)   end for
  (8) end for
  (9) return  $service\_set$ 
}
End

```

ALGORITHM 2: Functional matching.

between the functions requested and the functions provided existed if the match was feasible, with a weight e_{ij} that represents their similarities computed using formula (5), where I and J are the number of functions requested and provided, respectively.

$$e_{ij} = SemSim(x_i, y_j) \quad (i = 1, 2, \dots, I; j = 1, 2, \dots, J) \quad (5)$$

where $x_i \in R_{Input}$, $y_j \in Input$

Thus, the matching process was transformed into a problem to solve for maximizing the sum of weights. The calculation of similarity is presented in this paper using formula (6).

$$Sim(R_{Input}, Input) = \frac{\sum_{i=1}^{i=I} \max_{j=1}^{j=J} (e_{ij})}{I} \quad (6)$$

However, in the case of the typical weighted bipartite graph model, the number of vertices in two separate sets (e.g., input/output functions requested and provided, expressed as “ $I = J$ ”) into which all functions obtained from the tree were divided must be the same. Such rigorous conditions further restricted the use of a typical model in the real world. Considering the failed matching associated with different numbers (expressed as “ $I \neq J$ ”), we improved the similarities as shown in formula (7).

$$Sim(R_{Input}, Input) = \frac{J \times \left[\sum_{i=1}^{i=I} \max_{j=1}^{j=J} (e_{ij}) \right] + I \times \left[\sum_{j=1}^{j=J} \max_{i=1}^{i=I} (e_{ji}) \right]}{2IJ} \quad (7)$$

The calculation of similarity for a set of output functions was similar to formula (7), as previously deduced. Therefore, the semantic similarity for the function-level matching of travel services is as follows:

$$Sim(Req, Service) = \lambda_1 Sim(R_{input}, Input) + \lambda_2 Sim(R_{Output}, Output) \quad (8)$$

where $\lambda_1 + \lambda_2 = 1$, and λ_1 and λ_2 imply whether travelers find the input or output functions more or less attractive.

The function-level semantic matching is illustrated in Algorithm 2. This algorithm determines the similarities using formula (7) with a generated bipartite graph model and then gives the final similarities using formula (8). It has a function that calculates the similarity between two nodes according to formula (4).

4.3. Hierarchical Matching-Based Process. The layered matching process proposed in this study includes the following steps.

(1) The TIS are divided into different categories using clustering in the registration center. The requestor then identifies the categories associated with his/her query through the text mining technology.

```

Input:
 $Req = \{R_{Description}, R_{Input-Output}\}$ : service request
 $\theta$ : similarity threshold
Output:
 $result\_set$ : service sets with similar functions
Begin
(1)  $service\_set \leftarrow null$ 
(2)  $allServices \leftarrow getServices()$ 
(3)  $cluster \leftarrow getServiceCluster(service\_set)$ 
(4)  $serviceCategory \leftarrow getServiceCategory(service\_set)$ 
(5)  $R_{des} \leftarrow ServiceDescriptionExtraction(Req)$ 
(6)  $R_{func} \leftarrow ServiceFunctionExtraction(Req)$ 
(7)  $R_{cate} \leftarrow ServiceClassification(Req)$ 
(8)  $Services \leftarrow getServicesFromSpecifiedCategories(R_{cate}, cluster,$ 
 $serviceCategory)$ 
(9) for S in Services do
(10)  $sim_{func} \leftarrow sim(ServiceFunctionExtraction(S), R_{func})$ 
(11) if  $sim_{func} > \theta$ 
(12)  $result\_set \leftarrow result\_set \cup S$ 
(13) end if
(14) end for
(15)  $SortedBySimilarity(result\_set)$ 
End

```

ALGORITHM 3: Semantic matching using mixed model of TIS.

(2) A tree-structured ontology is created for function-level matching based on an evaluation of the similarities between the functions requested and provided. The candidate sets that fit within the functional constraints are selected.

(3) Finally, the similarity values are ranked to provide the requestor with the desired TIS solution. The pseudo code of the algorithm is given in Algorithm 3. Line (3) applies K-means clustering to group the TISs. Lines (4)–(8) extract and process the function and textual contents of the service requested. Lines (9)–(14) perform the layered matching. Line (15) screens the services that meet the requirements, ranks them, and returns them to the requestor.

5. Architecture for Semantic Matching of TISs

While a TIS placed on web servers tends to be available consistently for reference, other TIS applications developed for mobile use may be unavailable at various times as a result of location issues. Because of the diverse conditions encountered while traveling (e.g., while commuting or during long journeys), the main issue for TIS matching is the assignment of requirements that arise dynamically over time at various locations relative to the service providers. First, we illustrated the hierarchical framework and classified it as the three-layer structure shown in Figure 1. Then, we described the characteristics of some important functions and proposed an architectural implementation.

(i) The user layer serves as an interface between users and the matching module. Users include service providers who present local information, such as news and weather, as well as travelers querying the TIS. By interacting with a website, a traveler submits a request indicating the desired functions

bounded by time and space. The textual descriptions of the TIS can be registered and found in the data layer.

(ii) The matching agency layer operates the distributed TIS matching module associated with the request integrated by the user layer. The matching agency layer includes three core parts of the proposed matching model: the feature extraction module, the clustering module for the automatic grouping of the TISs having similar functions and facilitating fast service discovery, and the I/O-level functional matching module. Figure 2 illustrates how the three modules work together. The tasks of the last two modules are performed sequentially, where a match fails if one of them does not work under a certain reasonable threshold. Thus, we can provide an automated process for picking up services that satisfy a traveler's demands with a weighted sum of modules.

(iii) The data layer provides the underlying data support, such as an in-built domain ontology library and a set of TIS solutions semantically extended and registered. Because of the data loss that can occur while using an integrated data structure, the data in the registration center should be backed up.

(a) *Data Preprocessing.* The descriptions of TISs in the library, represented using OWL-S, should be used for further matching with data preprocessing. This includes the following steps:

- (1) The interfaces, i.e., OWLontology and OWLknowledgeBase, are adopted to parse the OWL-S-based description for the names and textual descriptions of the TIS. For example, given a TIS for hiking, we can give its name and textual description as "Hiking Urban Area Service" and "this service returns the best urban areas for a given hiking type." Table 1 gives

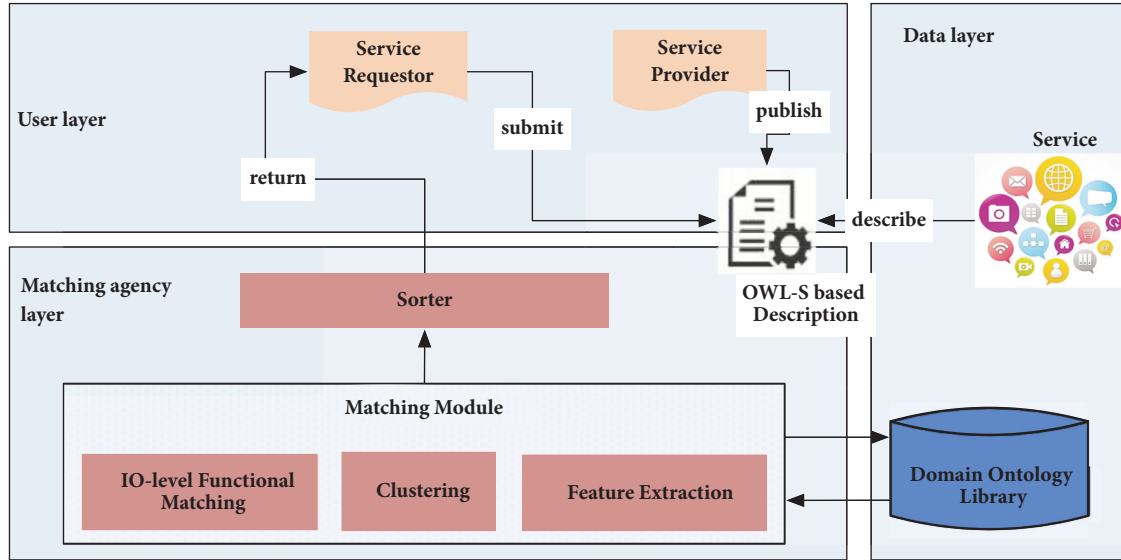


FIGURE 1: Proposed architecture.

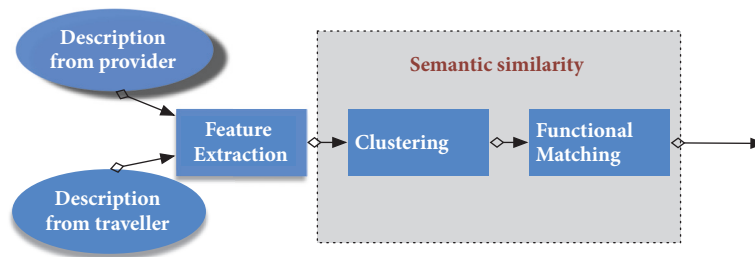


FIGURE 2: Matching using semantic similarity.

an example showing the keywords obtained from five OWL-S-based TIS names.

(b) *Service Classification*. Using the proposed method, we could find the desired TIS without searching the entire service library by using the following steps to measure the similarity between the keywords and to identify the center by clustering. First, we applied the WordNet tool to extend the keywords obtained. This action provided a better understanding of the meaning of each of the words and allowed further vectorization, as discussed in Section 4.1. However, this approach resulted in high-dimensional data that were so sparse that they reduced the precision and recall of TIS matching. Consequently, we introduced a latent semantic index (LSI) [30] to reduce the dimensions of the keywords. Then, we used K-means clustering as shown in Figure 3, where the number of service categories was determined experimentally, and the services were then labeled. Each cluster center was considered an atomic service for each category. A query represented as vectors from a traveler would be matched in terms of the similarity with each atomic service. Then, the query would be assigned to the most similar service category and treated as the one requested by the user. Thus, this method facilitated the reduction of the search space and maximized the number of TIS matches by using clustering.

(c) *Functional Matching*. There were four types of information associated with the TIS input/output involved in this matching. Because these functions were adequately described by simple terms, it was difficult to extract matches by using similarity measures when the functions were represented in a natural language. Therefore, we generated an ontology tree to allow for semantic matching and to improve the precision. Figure 4 illustrates the functional matching where the similarity between the nodes in the tree, and between the sets of nodes, was sequentially identified offline. This procedure also decreased the waiting time in the case of a large number of concurrent requests.

6. Performance Analysis

The database of OWLS-TC [31] provides 1083 semantic services from a wide variety of fields, such as education, communication, and geography. We adopted OWLS-TC to verify the model proposed in this paper.

6.1. *Verification of Clustering*. Three groups were selected from the categories of tourism. The total number of TISs in each group was 50, 100, and 150. To better reduce the dimensions of the feature data used for further clustering, we applied a 12-fold cross-validation test to the acquired

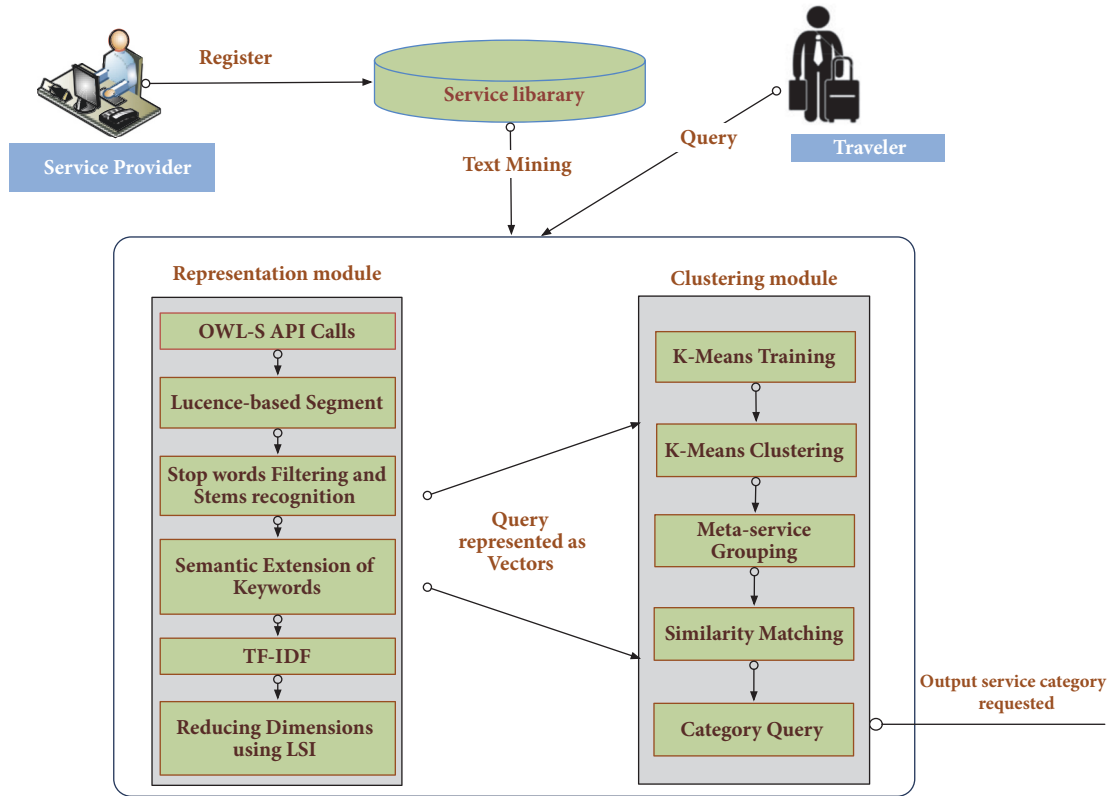


FIGURE 3: Illustration of service classification.

TABLE 1: Some of the descriptions including the name and the keywords in the service library.

| Name of TIS | Keywords |
|------------------------------|--------------------------------------|
| Car Price Service | purchase, price, wheel, model, etc |
| Adventure Urban Area Service | adventure, urban area, return, etc |
| Activity Town Service | activity town, name, provide, etc |
| Auto Bicycle Price service | auto bicycle, price, rent price, etc |

feature set and determined the top ten features with the most relatively high values using LSI. In addition, considering that clustering varied each time the K-means algorithm was used because the initial cluster center could be identified randomly, we averaged the accuracy of clustering from three experiments for each group. We measured the accuracy of the classification results, i.e., the similarity of the classification results to the ground truth results, and found that the three groups achieved an accuracy of 87.85%, 90.67%, and 93.80%.

The experiment showed that the error rate of the TIS classification decreased rapidly with an increase in the number of services. This could be attributed to the fact that it was possible to obtain more features to distinguish one category from another for clustering by increasing the number of textual descriptions. Furthermore, the features and the number identified using a cross-validation test contributed positively to the LSI-based process and further improved the classification.

TABLE 2: Comparison results of response times.

| Number of services | Clustering | Non-clustering |
|--------------------|------------|----------------|
| 50 | 162 ms | 356 ms |
| 100 | 216 ms | 425 ms |
| 150 | 239 ms | 495 ms |
| 1000 | 651 ms | 2361 ms |

6.2. *Verification of Response Time.* The effect of service clustering on the model’s response time was measured using four groups of data from five categories when the number of services was 50, 100, 150, and 1000. Table 2 shows a comparison of the response times needed in the matching model, including clustering and nonclustering. The results indicated that there would be an explosion in the response times without offline clustering; therefore, it would be difficult to accelerate the matching.

The experiment also revealed that calculating the similarity between travel services represented as ontology-based

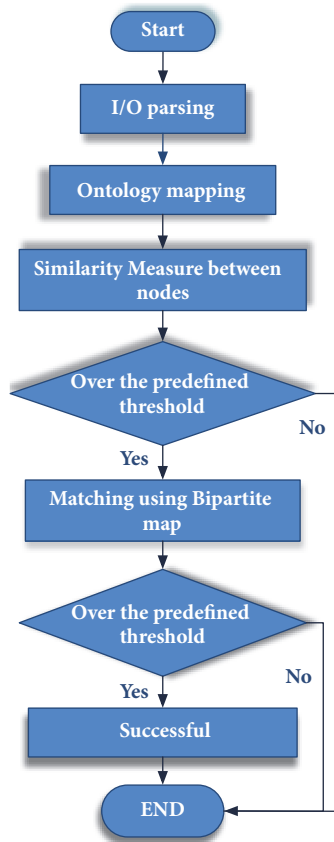


FIGURE 4: I/O-level functional matching.

concepts was very time-consuming. Therefore, in this study, to improve the speed and accuracy of service matching, the similarity could be measured offline and stored in a file. This was useful when similar parts of concepts were found during past matching, because we could create an index to find the desired TIS without the same concepts being counted twice while determining the similarities.

6.3. Recall and Precision Rate. We evaluated the performance of three models: a model based on information theory, another based on taxonomic distance, and the proposed mixed matching model. In terms of the parameter settings for formula (4), ∂ was set to 2 and β was set to 1, 6, and 10, indicating the relationships of the nodes in the generated ontology tree, i.e., direct inheritance, indirect inheritance, and noninheritance, respectively. The similarity threshold denoted by θ in the range from 0 to 1 was experimentally determined to be 0.7 and 0.8.

Figures 5 and 6 show the variation trends of the recall and the precision rates of the three models when θ had two different values. Clearly, the three models worked well in terms of precision when θ was 0.8. We found that the model based on information theory performed better in terms of precision, but its recall rate was relatively low because a service was likely to be matched incorrectly to other sibling nodes. Furthermore, the model had good precision if and only if there were very few sibling nodes in the ontology

tree, and the similarity between concepts was relatively low. We might lose other matches from the information theory-based model because the similarities calculated could fall below the threshold θ . The precision and the recall rate of the model based on taxonomic distance ranged between the performance of the other two models. When there was a wide similarity threshold, this model's performance was in accordance with the results obtained by using the proposed mixed matching model, whose precision decreased.

On the basis of the performance analysis, we concluded that the recall rate of the mixed matching model was higher than that of the other two models because the similarities between the concepts increased as a result of the parameter adjustment. The precision rate decreased mainly as a result of the low accuracy of the matching performed using a bipartite graph for multiple inputs or outputs. We also found that the performance of the mixed matching model was better than that of the other two models as a consequence of increasing the similarity threshold i.e., when the threshold was 0.8 in the experiments.

7. Conclusions

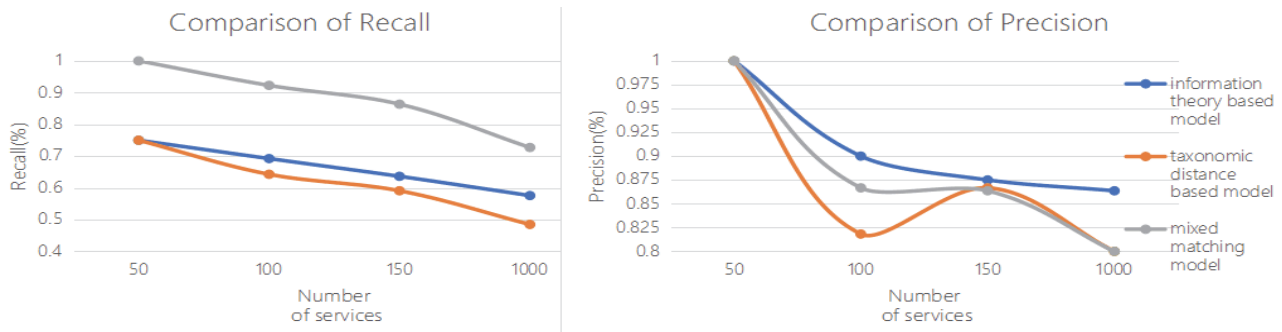
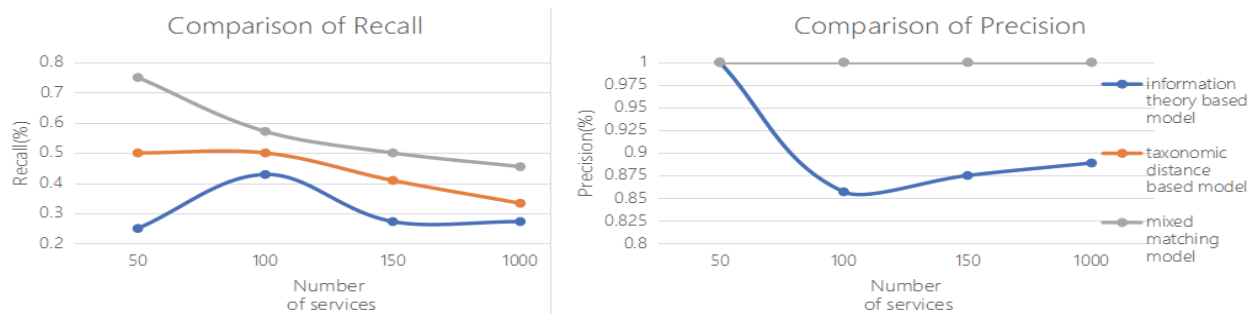
In this paper, we proposed a multilevel sematic matching model for traffic information services. First, we used K-means to classify the services automatically. Then, we applied ontology knowledge and a bipartite graph to calculate the semantic similarity between functions. We demonstrated how the proposed model could be used to implement semantic matching for TIS solutions. Our experiments revealed the effectiveness and feasibility of the model for handling a large search space, heterogeneous dynamic data, and limited resources. We suggested that distributed TIS matching might be the acceptable solution for user queries in parallel. However, there was still room for improvement in terms of the response time. Further, our model was tested on the basis of prior knowledge, i.e., by using a predetermined ontology tree. While this approach allowed for offline clustering, similarity measure, and making matching decisions quickly, this form of knowledge limited the model's ability to understand real-world travel purposes. Going forward, we believe that it would be useful to examine QoS-based matching as a basis for understanding the needs of people who are making local or longer journeys. In addition, we will focus on optimizing the process of service matching considering the specific attributes of traffic information, e.g., disconnection, geo-space issues, and temporal aspects. It is therefore necessary to deal with more than only domain heterogeneity.

Data Availability

Previously reported OWLS-TC data were used to support this study and are available at [<http://projects.semwebcentral.org/projects/owls-tc/>]. These prior studies (and datasets) are cited at relevant places within the text as [31].

Conflicts of Interest

The authors declare that there are no conflicts of interest regarding the publication of this paper.

FIGURE 5: Performance comparison when $\theta = 0.7$.FIGURE 6: Performance comparison when $\theta = 0.8$.

Acknowledgments

This work was funded by the National Natural Science Fund of China under Grant no. 61303041, Shanxi Province Industrial Research Projects under Grants nos. 2015GY-002 and 2016GY-078, and Funds for Key Scientific and Technological Innovation Team of the Shaanxi Province, China, under Grant no. 2017KCT-29.

References

- [1] T. Zhu and Z. Liu, "Intelligent Transport Systems in China: Past, Present and Future," in *Proceedings of the 2015 Seventh International Conference on Measuring Technology and Mechatronics Automation (ICMTMA)*, pp. 581–584, Nanchang, China, June 2015.
- [2] M. S. Ryerson and M. Hansen, "Optimal intercity transportation services with heterogeneous demand and variable fuel price," *IEEE Systems Journal*, vol. 8, no. 4, pp. 1158–1168, 2014.
- [3] T. Ma, G. Motta, and K. Liu, "Delivering Real-Time Information Services on Public Transit: A Framework," *IEEE Transactions on Intelligent Transportation Systems*, vol. 18, no. 10, pp. 2642–2656, 2017.
- [4] X. Hu, J. Zhao, B.-C. Seet, V. C. M. Leung, T. H. S. Chu, and H. Chan, "S-afame: agent-based multilayer framework with context-aware semantic service for vehicular social networks," *IEEE Transactions on Emerging Topics in Computing*, vol. 3, no. 1, pp. 44–63, 2015.
- [5] A. Fernandez and S. Ossowski, "A multiagent approach to the dynamic enactment of semantic transportation services," *IEEE Transactions on Intelligent Transportation Systems*, vol. 12, no. 2, pp. 333–342, 2011.
- [6] M. Paolucci, T. Kawamura, T. R. Payne, and K. P. Sycara, "Semantic matching of web services capabilities," in *The Semantic Web—ISWC 2002: First International Semantic Web Conference Sardinia, Italy, June 9–12, 2002 Proceedings*, vol. 2342 of *Lecture Notes in Computer Science*, pp. 333–347, Springer, Berlin, Germany, 2002.
- [7] L. Meng, R. Huang, and J. Gu, "A review of semantic similarity measures in WordNet," *International Journal of Hybrid Information Technology*, vol. 6, no. 1, pp. 1–12, 2013.
- [8] L. Purohit and S. Kumar, "Web Service Selection using Semantic Matching," in *Proceedings of the International Conference Advances in Information Communication Technology & Computing*, p. 16, 2016.
- [9] G. Meditskos and N. Bassiliades, "Structural and role-oriented web service discovery with taxonomies in OWL-S," *IEEE Transactions on Knowledge and Data Engineering*, vol. 22, no. 2, pp. 278–290, 2010.
- [10] V. V. Cross, "Constructing a measure of information content for an ontological concept," in *Proceedings of the 2016 Annual Conference of the North American Fuzzy Information Processing Society (NAFIPS)*, pp. 1–6, El Paso, TX, USA, October 2016.
- [11] S. Harispe, D. Sánchez, S. Ranwez, S. Janaqi, and J. Montmain, "A framework for unifying ontology-based semantic similarity measures: A study in the biomedical domain," *Journal of Biomedical Informatics*, vol. 48, pp. 38–53, 2014.
- [12] D. Sánchez, M. Batet, D. Isern, and A. Valls, "Ontology-based semantic similarity: A new feature-based approach," *Expert Systems with Applications*, vol. 39, no. 9, pp. 7718–7728, 2012.
- [13] D. Sánchez, M. Batet, and D. Isern, "Ontology-based information content computation," *Knowledge-Based Systems*, vol. 24, no. 2, pp. 297–303, 2011.

- [14] L. Meng, J. Gu, and Z. Zhou, "A new model of information content based on concept's topology for measuring semantic similarity in WordNet," *International Journal of Grid & Distributed Computing*, vol. 5, no. 3, pp. 81–94, 2013.
- [15] J.-B. Gao, B.-W. Zhang, and X.-H. Chen, "A WordNet-based semantic similarity measurement combining edge-counting and information content theory," *Engineering Applications of Artificial Intelligence*, vol. 39, pp. 80–88, 2015.
- [16] M. Klusch, P. Kapahnke, S. Schulte, F. Lecue, and A. Bernstein, "Semantic Web Service Search: A Brief Survey," *KI - Künstliche Intelligenz*, vol. 30, no. 2, pp. 139–147, 2016.
- [17] S. Rajagopal and S. T. Selvi, "Semantic Grid Service Discovery Approach using Clustering of Service Ontologies," in *Proceedings of the TENCON 2006 - 2006 IEEE Region 10 Conference*, pp. 1–4, Hong Kong, China, November 2006.
- [18] J. Lartigau, X. Xu, L. Nie, and D. Zhan, "Cloud manufacturing service composition based on QoS with geo-perspective transportation using an improved Artificial Bee Colony optimisation algorithm," *International Journal of Production Research*, vol. 53, no. 14, pp. 4380–4404, 2015.
- [19] P. Li, S. Guo, T. Miyazaki et al., "Traffic-aware geo-distributed Big data analytics with predictable job completion time," *IEEE Transactions on Parallel and Distributed Systems*, vol. 28, no. 6, pp. 1785–1796, 2017.
- [20] X. Zheng, W. Chen, P. Wang et al., "Big Data for Social Transportation," *IEEE Transactions on Intelligent Transportation Systems*, vol. 17, no. 3, pp. 620–630, 2016.
- [21] J. Wu, L. Chen, Z. Zheng, M. R. Lyu, and Z. Wu, "Clustering Web services to facilitate service discovery," *Knowledge and Information Systems*, vol. 38, no. 1, pp. 207–229, 2014.
- [22] K. A. Alam, V. Chang, R. Ahmad, and et al., "Clustering and Classification techniques for Web service discovery: A Systematic Review," *International Journal of Information Management*, 2016.
- [23] L. Wenjing and D. Yuyue, "Web service discovery method based on net unit model of service cluster," *Computer Science*, vol. 39, no. 8, pp. 147–152, 2012.
- [24] C. Surianarayanan and G. Ganapathy, "An approach to computation of similarity, inter-cluster distance and selection of threshold for service discovery using clusters," *IEEE Transactions on Services Computing*, vol. 9, no. 4, pp. 524–536, 2016.
- [25] L. Yisong and Z. Dan, "Semantic web service discovery based on clustering and bipartite group matching," *Journal of Electrical and Computer Engineering*, vol. 42, no. 2, pp. 157–163, 2016.
- [26] S. Albitar, S. Fournier, and B. Espinasse, "An Effective TF/IDF-Based Text-to-Text Semantic Similarity Measure for Text Classification," in *Web Information Systems Engineering – WISE 2014*, vol. 8786 of *Lecture Notes in Computer Science*, pp. 105–114, Springer International Publishing, Cham, 2014.
- [27] M. Silic, G. Delac, and S. Srblic, "Prediction of atomic web services reliability based on K-means clustering," in *Proceedings of the 2013 9th Joint Meeting of the European Software Engineering Conference and the ACM SIGSOFT Symposium on the Foundations of Software Engineering, ESEC/FSE 2013*, pp. 70–80, rus, August 2013.
- [28] X. Tang, F. Tang, L. Bing, and D. Chen, "Dynamic web service composition based on service integration and HTN planning," in *Proceedings of the 7th International Conference on Innovative Mobile and Internet Services in Ubiquitous Computing, IMIS 2013*, pp. 307–312, tw, July 2013.
- [29] W. Chen, Z. Zhang, T. Xiang, and R. Zeng, "A web service matching algorithm based on semantic similarity," *COMPEL - The International Journal for Computation and Mathematics in Electrical and Electronic Engineering*, vol. 32, no. 2, pp. 638–648, 2013.
- [30] A. K. Uysal and S. Gunal, "Text classification using genetic algorithm oriented latent semantic features," *Expert Systems with Applications*, vol. 41, no. 13, pp. 5938–5947, 2014.
- [31] A OWL-S service retrieval test collection, <http://projects.semwebcentral.org/projects/owls-tc/>.

Research Article

Flexible Emergency Vehicle Network Design considering Stochastic Demands and Inverse-Direction Lanes

Hua Wang ^{1,2}, Ling Xiao,¹ and Zhang Chen ³

¹School of Economics and Management, Tongji University, Shanghai 200092, China

²Department of Civil & Environmental Engineering, National University of Singapore, Singapore 117576

³Key Laboratory of Road and Traffic Engineering of the Ministry of Education, Tongji University, Shanghai 200092, China

Correspondence should be addressed to Zhang Chen; czy1620@263.net

Received 10 December 2017; Accepted 1 February 2018; Published 8 March 2018

Academic Editor: Xiaobo Qu

Copyright © 2018 Hua Wang et al. This is an open access article distributed under the Creative Commons Attribution License, which permits unrestricted use, distribution, and reproduction in any medium, provided the original work is properly cited.

We study transportation network design with stochastic demands and emergency vehicle (EV) lanes. Different from previous studies, this paper considers two groups of users, auto and EV travelers, whose road access rights are differentiated in the network, and addresses the value of incorporating inverse-direction lanes in network design. We formulate the problem as a bilevel optimization model, where the upper-level model aims to determine the optimal design of EV lanes and the lower-level model uses the user equilibrium principle to forecast the route choice of road users. A simulation-based genetic algorithm is proposed to solve the model. With numerical experiments, we demonstrate the value of deploying inverse-direction EV lanes and the computational efficiency of the proposed algorithm. We reach an intriguing finding that both regular and EV lane users can benefit from building EV lanes.

1. Introduction

Emergency incidents, such as traffic accidents, mere spasmodic diseases, and fire disasters, have often been observed in metropolises with a high population density [1, 2], which generates an increasing travel demand of emergency vehicles (EVs) (e.g., ambulances and fire engines). Currently, transportation emergency evacuation and rescue have attracted greater attention from transportation researchers and practitioners than before. For example, So and Daganzo [3] proposed an inner-first-out control strategy to manage evacuation routes, and Daganzo and So [4] extended such a nonanticipative and adaptive control strategy to manage traffic networks in real-time emergency evacuations. Meanwhile, with advances in intelligent transport techniques, fast development in building various emergency evacuation systems is witnessed, for example, the corridor-based and region-wide emergency evacuation systems for Washington D.C. [5] and Baltimore's multimodal evacuation system [6]. In addition, the Transportation Research Board [7] made a tentative investigation to accommodate emergency evacuation into transit service systems.

Effective strategic-level or tactical-level planning is one of the important prerequisites to ensure the success of operational-level emergency evacuation management [8]. For example, transportation authorities often reserve proper emergency lanes on highway networks to promote travel efficiency of emergency vehicles in accident rescues. As a result, a few interesting questions arise. Can we design similar emergency lanes in urban transportation networks? Also, how can we achieve successful planning of emergency lanes in urban transportation systems with limited road infrastructure resources? Moreover, complex traffic conditions in urban transportation networks, such as demand uncertainties and complicated user behaviors, lead to new challenges for the planning of emergency lanes [9, 10]. In this study, we aim to present feasible answers from the perspective of transportation network design. A running example is presented as follows to illustrate the problem of designing emergency vehicle (EV) lanes.

1.1. Running Example. Figure 1(a) shows a small urban transportation network with three nodes and five directed links. Link 1 has two lanes and each of links 2–5 is deployed with

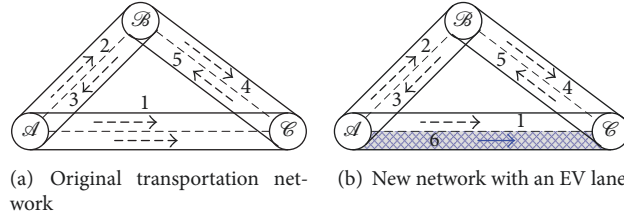


FIGURE 1: A three-node network for the running example.

TABLE 1: Results of three design schemes in the running example.

| Design schemes | Equilibrium link flows | | | | | | TTT for auto users (mins) | TTT for EV users (mins) |
|----------------|------------------------|---------|-------|---------|-------|-------|---------------------------|-------------------------|
| | v_1 | v_2 | v_3 | v_4 | v_5 | v_6 | | |
| Scheme 1 | 26600/17 | 8250/17 | 1060 | 8250/17 | 1060 | - | 60,367.06 | 2,374.38 |
| Scheme 2 | 13000/11 | 9000/11 | 1060 | 9000/11 | 1060 | 50 | 68,356.36 | 2,008.20 |
| Scheme 3 | 13300/11 | 9250/11 | 1000 | 9250/11 | 1000 | 60 | 68,181.82 | 1,740.55 |

a respective single lane. All lanes have an identical service capacity of 1,000 vehicles/hour. Two origin-destination (OD) pairs, $\mathcal{A} \rightarrow \mathcal{C}$ and $\mathcal{C} \rightarrow \mathcal{A}$, are taken into account. There exist two classes of users, auto commuters and EV travelers, in the network. Both classes of network users are assumed to follow Wardrop's first equilibrium principle that each of the road users expects to find her/his shortest path. The auto travel demands for two OD pairs are, respectively, $q_{\mathcal{A} \rightarrow \mathcal{C}}^p = 2,000$ and $q_{\mathcal{C} \rightarrow \mathcal{A}}^p = 1,000$. The EV travel demands for two OD pairs are set as $q_{\mathcal{A} \rightarrow \mathcal{C}}^e = 50$ and $q_{\mathcal{C} \rightarrow \mathcal{A}}^e = 60$. To improve the travel efficiency of EVs, the network authority attempts to build an EV lane on Link 1. As shown in Figure 1(b), the original Link 1 with two lanes would be then decomposed into a new regular road with one lane (Link 1) and a new EV road with one lane (Link 6). Let us define a link set $A := \{1, 2, \dots, 6\}$. A linear link travel time function is adopted here to evaluate the network performance:

$$t_a(v_a^p, v_a^e) = t_a^0 + t_a^0 \left(\frac{v_a^p + v_a^e}{c_a} \right), \quad a \in A, \quad (1)$$

where t_a^0 is the flow-independent travel time of link a , $a \in A$; v_a^p and v_a^e , respectively, represent link flows of auto users and EV travelers; and the aggregate link flow $v_a = v_a^p + v_a^e$. In this example, we set $t_2^0 = t_3^0 = 5$ mins, $t_4^0 = t_5^0 = 7$ mins, and $t_1^0 = t_6^0 = 10$ mins.

We consider and compare the following three EV lane design schemes.

Scheme 1. Take no action of setting EV lanes.

Scheme 2. Build an EV lane to connect the nodes \mathcal{A} and \mathcal{C} (Link 6 in Figure 1).

Scheme 3. Build an inverse-direction EV lane to access $\mathcal{C} \rightarrow \mathcal{A}$ by reversing the direction of Link 6.

Table 1 gives the aggregate link flows at biclass user equilibrium and total travel time (TTT) for auto and EV users.

As shown in Table 1, Scheme 2 sets an EV link and saves about 15.4% golden rescue time, although it makes auto travelers suffer uncomfortable experiences in a more congested network. Compared to Scheme 2, Scheme 3 not only remarkably improves the travel efficiency of EVs but also alleviates the traffic congestion of auto commuters through flexibly incorporating an inverse-direction EV lane. In this sense, Scheme 3 better balances the two design objectives of TTTs associated with auto and EV users. The results of network performance improvements clearly demonstrate the significance of building EV lanes and reveal the value of designing inverse-direction EV lanes in EV network planning.

The running example clearly shows that the investigated problem of setting EV lanes might fall into the category of classical discrete transportation network design problems (NDPs), which can be defined as a new link/lane addition that maximizes network performance subject to a series of side constraints (e.g., investment budget constraint and equilibrium constraints of the traffic pattern that characterizes travelers' route choice behaviors). However, the NDP that optimizes EV lane setting (EV-NDP) also exhibits a few new features and disparities from traditional NDPs (explained later in the next subsection). This study is devoted to proposing an effective approach for the EV-NDP that accounts for more complex and realistic traffic conditions, including application of flexible inverse-direction EV lanes and travel demand uncertainties.

1.2. Literature Review. The NDP typically aims to optimize transportation network performance via link capacity expansions (either current road maintenance/improvement or new road addition), while taking into account travelers' route choice behaviors and financial constraints. After the seminal works of Leblanc [11] and Abdulaal and LeBlanc [12], we have witnessed a blooming of NDPs on model formulations, solution algorithms, and applications over the past half century. Regarding early achievements made in the last century, interested readers are referred to two surveys, Magnanti and Wong [13] and Yang and Bell [14], for a

comprehensive literature review and detailed discussions. Meng and Wang [15] presented a structured overview of the NDP literature from 1999 onward and summarized a series of new developments and advances that consider complicated traffic conditions, including uncertainty parameters, traffic dynamics, and multiple optimization objectives. We briefly review the recent achievements of the NDP literature in the following four NDP categories.

(1) *Stochastic NDPs*. It is well recognized that network uncertainties with respect to demand fluctuations and road capacity degradation inevitably and inherently exist on transportation networks. Recently, more researchers and practitioners have pointed out that network uncertainty would have significant impacts on network planning and other transportation management decisions, and ignoring this factor might result in suboptimal or even misleading optimization schemes [8, 16, 17]. Chen et al. [18] provided a comprehensive review of stochastic NDPs on various model formulations (e.g., expected-value model, mean-variance model, chance-constrained model, probability model, and min-max model) and proposed an attractive simulation-based genetic algorithm. To properly characterize the effect of network stochasticity, simulation-based sampling (e.g., Monte-Carlo simulation) approximation technique is often used to estimate probabilistic statistics, including expectation and variance, of various system performance measures [8, 18–24]. Alternatively, probabilistic or reliability-based user equilibriums are proposed to incorporate the effect of network uncertainties into travelers' route choice behaviors in the lower-level traffic assignment problem and similar bilevel stochastic NDP models are then developed [25, 26]. Some stochastic NDP models had also integrated other traffic factors and/or optimization targets (e.g., sustainability, traffic dynamics, and land use). For example, Waller and Ziliaskopoulos [16] formulated a chance-constrained NDP model that takes into account both uncertain demands and dynamic traffic flows. Wang et al. [26] incorporated multiple indices of sustainability, including traffic emission and social equity, into a stochastic NDP.

(2) *Dynamic and Multiperiod NDPs*. Time dimension is another important factor in transportation network design. In general, three scales of time dimension are considered: short-term/real-time (seconds), medium-term (days), and long-term (years). Overall, short-term traffic dynamics are attributed to the description of real-time parameter fluctuation in a transportation system, and long-term network decisions across multiple phases help to assess the value of a network improvement plan over time. Specifically, dynamic NDP models have been developed to properly describe real-time traffic dynamics and/or other unsteady-state traffic conditions (e.g., traffic shockwaves propagation, build-up process of queues) [27]. For example, Waller and Ziliaskopoulos [16] proposed a two-stage linear programming NDP model where a system-optimal dynamic traffic assignment and cell transmission loading technique were used to depict dynamic traffic propagation on the network. Karoonsoontawong and Waller [27] presented a robust dynamic NDP model with the

objective of minimizing the weighted sum of the expected total travel time and expected risk. In detail, multiperiod NDP formulations were proposed to optimize a design scheme where construction and maintenance of transport infrastructures took place over a long-term horizon. Lo and Szeto [28] proposed the first multiperiod NDP model to examine tradeoffs among several stakeholders: travelers, private toll road operators, and the government. Ukkusuri and Patil [29] made an extension to formulate a multiperiod NDP considering demand uncertainty and demand elasticity, and they found that a multiperiod optimization model could generate more favorable decisions than the conventional single-stage NDP formulation. A more comprehensive literature review and detailed discussions on dynamic and multiperiod NDPs can be found in Meng and Wang [15].

(3) *Multiobjective NDPs*. As reported by Yang and Bell [14] and Chen et al. [20], researchers often need to consider multiple design objectives in the NDP, for instance, travel efficiency, emission, social equity, user experience, construction cost, and system reliability. There is a great deal of literature on multiobjective NDPs. For example, Meng and Yang [30] discussed a biobjective NDP regarding travel efficiency and social equity, and Chen and Yang [23] made an extension to analyze the NDP incorporating social equity issue in stochastic networks and developed a chance-constrained optimization model. Wang et al. [26] investigated a chance-constrained multiobjective NDP considering social equity, emission reduction, and network reserve capacity maximization. In general, Pareto optimization method (e.g., [19–21, 31]) and weighted-sum approach (e.g., [8, 22]) are widely applied for multiobjective NDP formulations. For more information on deterministic multiobjective NDPs, refer to review reports of Yang and Bell [14] and Farahani et al. [32], and more literature on stochastic multiobjective NDPs can be found in Chen et al. [18].

(4) *Global Solution Methods*. Solving a bilevel NDP model has been seen as a challenge all the time. Global solution algorithms have increasingly received attention in the last decade. For example, based on the Multivariate Taylor Series, Wang and Lo [33] transformed the classical NDP model into equivalent mixed-integer linear programming (MILP), in which a global-optimal solution can be guaranteed. In spirit of the transformed MILP, Luathep et al. [34] made an extension to solve a mixed NDP with both continuous and discrete decision variables. Motivated by a similar idea, Liu and Wang [35] developed an equivalent MILP model for the NDP that took into account logit-based stochastic user equilibrium. The above-mentioned MILP models were all solved by the CPLEX solver. In addition, according to the relationship between user equilibrium and system optimum, Wang et al. [36] presented a system optimum-relaxation based method to solve the discrete NDPs.

The EV-NDP in this study exhibits some new features and differs from existing NDPs in the following aspects:

- (1) The investigated EV-NDP involves two classes of users: auto commuters and EV travelers. The above

literature review indicates that the issue of multi-class users has received rather limited attention. The only NDP work that considered multiclass users was carried out by Dimitriou et al. [37]. Incorporating multiclass users leads to challenges in two aspects, especially when considering uncertain demands: (i) the lower-level traffic assignment problem needs to characterize route choice behaviors of multiple classes of users and resultant equilibrium traffic patterns may not be unique and (ii) the presence of multiclass users probably gives rise to conflict design objectives. It is indeed a challenge to manage tradeoffs among different design objectives associated with multiple classes of users on stochastic networks.

- (2) The EV-NDP has a different network reconstruction principle from traditional discrete NDPs. Traditional discrete NDP determines link/lane additions to expand network capacities [14]. The investment is directed to improve link capacity, while network structure accessibility (i.e., topological structure) might keep unchanged. However, in EV-NDP, the total capacity remains unchanged, but certain capacity is removed from original regular links to form new EV links (hereafter, EV links are called derivative links). Take the case in Figure 1 as an example. EV Link 6 is a derivative of Link 1, and setting the EV link results in a capacity reduction of the original Link 1. This can be regarded as link decomposition and capacity reassignment/redeployment. For an EV-NDP scheme, the construction budget is invested to build supporting infrastructures (e.g., pilot signals, guide boards, and communication facilities) that control and manage various vehicles, rather than directly expanding link capacities.
- (3) Road access rights are differentiated for two classes of users. As mentioned above, conventional NDPs consider homogeneous commuters and every traveler can freely utilize any link if accessible. This condition is also satisfied in Dimitriou et al. [37], in which multiclass users are taken into account. However, the situation in EV-NDPs differs. EVs can freely use all roads without any restraints, but private cars are not allowed to run on EV lanes. Such differentiated road access rights lead to a challenge in formulating a biclass user equilibrium that describes different travelers' route choice behaviors.
- (4) Inverse-direction EV lanes are introduced for EV-NDPs to fulfill favorable decision schemes. Given the fact that EV trips are independently and separably regulated by the traffic control center during emergency periods, we could have a chance to set inverse-direction EV lanes. This interesting concept makes network design scheme more flexible and attractive.

With the above stated disparities, we need to develop new EV-NDP models and propose pertinent solution methods.

1.3. Objective and Contributions. The objective of this paper is to propose an effective approach for the EV-NDP with demand uncertainty. To achieve this objective, we firstly propose a network reconstruction method to build a new unified network where both auto and EV users are properly accommodated. We then develop a bilevel optimization model for the EV-NDP on stochastic networks, where the upper level aims to minimize the weighted sum of the expected total travel time of two classes of users and the lower level characterizes route choice behaviors of auto and EV travelers under each demand realization.

This study makes the following substantial contributions to the literature:

- (1) Our work investigates a new NDP in urban transportation networks that exhibit several disparities from traditional NDPs. To the best of our knowledge, this work addresses a new EV network planning problem and is the first to formulate NDP with multiclass users, which substantially bridges the gap of the existing literature.
- (2) We develop a bilevel optimization EV-NDP model considering uncertain demands to find the tradeoff between travel efficiencies for auto and EV travelers. The proposed methods can help transportation authorities make tangible EV network decisions.
- (3) We introduce a new concept of inverse-direction EV lane in the EV-NDP. Incorporating inverse-direction EV lanes could promote more flexible and attractive decisions.
- (4) We propose a simulation-based genetic algorithm (GA) to solve the developed EV-NDP model and further evaluate the model and computational efficiency of the solution algorithm through numerical experiments. The evaluation results help us better understand the importance of considering inverse-direction EV lanes in EV network planning and the value of simulation-based GA in solving a bilevel stochastic programming model.

With all the above explanations, we shall devote Section 2 to defining the problem and formulating it as a bilevel optimization model. We then present in Section 3 a simulation-based genetic algorithm to solve the EV-NDP model. Numerical examples are provided in Section 4. The final section, Section 5, concludes the paper.

2. Problem Description and Model Formulation

We first define in this section the EV-NDP. Then, we explain the network reconstruction and formulate the network design model of setting EV lanes (the EV-NDP model).

2.1. Problem Description. Consider an urban transportation network $G = (N, A)$, where N and A are the sets of nodes and links, respectively. There exist two classes of users in the network: auto travelers and EV users. To guarantee the travel

efficiency of EVs, the network authority designs an EV-NDP scheme that deploys exclusive EV lanes on the selected roads. To better evaluate the network performance, we take into account random travel demands for both auto and EV users.

The network planner not only aims to guarantee the travel efficiency of EVs, but also makes an attempt to improve

the travel efficiency of auto travelers. The design objective function is thus to minimize the weighted sum of the expected total travel time of two classes of users on the network. Let \bar{A} denote the set of candidate links to be deployed with EV lanes. The decision variables can be defined as

$$\begin{aligned} \hat{x}_a &:= \begin{cases} 1 & \text{if an EV lane in the same direction of link } a \text{ is deployed} \\ 0 & \text{otherwise} \end{cases} & \forall a \in \bar{A}, \\ \tilde{x}_a &:= \begin{cases} 1 & \text{if an EV lane in the inverse direction of link } a \text{ is deployed} \\ 0 & \text{otherwise} \end{cases} & \forall a \in \bar{A}. \end{aligned} \quad (2)$$

2.2. Notations and Assumptions. The following notations are used throughout the paper.

N : the set of nodes in a given urban transportation network G ;

A : the set of original links in the urban transportation network G ;

\bar{A} : the set of candidate physical links considered in the EV-NDP scheme, $\bar{A} \subseteq A$;

\hat{A} : the set of normal-direction EV links, $\hat{A} \subseteq A$, $|\hat{A}| = |\bar{A}|$;

\tilde{A} : the set of inverse-direction EV links, $\tilde{A} \subseteq A$, $|\tilde{A}| = |\bar{A}|$;

A' : the set of links in the reconstructed unified network, $A' := A \cup \hat{A} \cup \tilde{A}$;

W : the set of OD pairs in the transportation network;

K : the set of user classes where $K := \{p, e\}$, where p and e represent private car and emergency vehicle, respectively;

R_w^k : the set of travel paths associated with k th, $k \in K$ users and OD pair $w \in W$;

Ω : the set of demand realizations;

ω : a specific demand realization $\omega := (\omega^p, \omega^e) \in \Omega$;

S : the set of scenarios to realize the random travel demands;

$v_a^{k,\omega}$: traffic flow of k th, $k \in K$ users on link a under demand realization $\omega \in \Omega$;

v_a^ω : the aggregate traffic flow on link a under demand realization $\omega \in \Omega$;

$f_{r,w}^{k,\omega}$: traffic flow of k th, $k \in K$ users on travel route r , $r \in R_w^p$ for OD pair w , $w \in W$ under demand realization $\omega \in \Omega$;

$t_a^\omega(\cdot)$: travel time on link a , $a \in A$ under demand realization $\omega \in \Omega$;

$t_a^{k,\omega}(\cdot)$: the link travel time for the k th, $k \in K$ users under demand realization $\omega \in \Omega$;

$\delta_{a,r}^{k,w}$: link-path incidence; $\delta_{a,r}^{k,w} = 1$ if link a is on the travel route r , $r \in R_w^p$ for the k th, $k \in K$ users' trips of OD pair w , $w \in W$, and 0 otherwise;

$q_w^{k,\omega}$: travel demand associated with k th, $k \in K$ users and OD pair w , $w \in W$ under demand realization $\omega \in \Omega$;

Pr^ω : the probability that the demand $\omega \in \Omega$ is realized;

ρ : the weighted parameter for the expected total travel time of auto travelers, $\rho \in [0, 1]$;

B : the total budget for the EV network design;

C_a^0 : the unit lane capacity of physical link a , $a \in A$;

L_a^0 : the initial number of lanes of link a , $a \in A$ (before setting EV lanes);

C_a : the capacity of link a , $a \in A \cup \hat{A} \cup \tilde{A}$;

t_a^0 : free-flow travel time of link a , $a \in A$;

α_a, β_a : two coefficients in the travel time function;

$b_a(\cdot)$: the construction cost function with respect to decision variables \hat{x}_a and \tilde{x}_a and the parameter γ_a .

To facilitate model formulation, we make three assumptions below.

Assumption 4. Link travel time function $t_a^\omega(v_a^\omega)$ is a differentiable strictly increasing function with respect to the aggregate link flow v_a^ω ; that is, $dt_a(v_a)/dv_a > 0$.

Assumption 5. The network design problem takes into account uncertain peak-hour travel demands for both auto and EV users. The random demands for the two classes of users are assumed to follow known probability distributions.

Assumption 6. The EV lanes are assumed to open during the peak-hour period and private cars are not allowed to use any EV lanes. The network planner evaluates the network performance with constantly open EV lanes.

Assumption 6 implies EVs can either make use of EV lanes or move on regular lanes that eventually generate

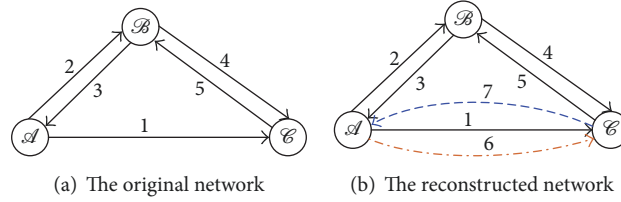


FIGURE 2: An illustrative example to reconstruct the network.

mixed traffic. We only study an extreme network state with constantly open EV lanes. One may argue that some individuals cannot tolerate building exclusive EV lanes to compete against limited road resources, which may lead to a more congested network. This concern could be greatly alleviated under traffic control management. When the traffic control center receives callings of EVs, private cars are not allowed to use EV lanes; otherwise, the EV lanes are fully free for use. Actually, an interesting extension could be made in the future to simultaneously optimize the EV-NDP scheme and working state setting of EV lanes. The working state setting is to determine an optimal active time of EV lanes (i.e., an optimal proportion to the entire peak-hour period).

2.3. Network Reconstruction. Partitioning a regular road generates two independent derivative products, an EV link and a new regular link with reduced capacity (one may have no capacity), and as a result, setting EV lanes changes the network's topological structures for auto and EV users. It is not surprising that the access rights of private cars might be restricted due to the implementation of EV-NDP schemes. On the one hand, private cars cannot use newly added EV links. On the other hand, private cars that pass new regular links with possibly reduced capacities would face more congested traffic and take longer travel time. In turn, EVs enjoy more road infrastructures and more flexible routing choices due to the newly added EV links on the network. In addition, incorporating inverse-direction EV lanes would make vehicle accessibilities more complicated.

To properly address the distinct vehicle accessibilities, we build a unified urban transportation network that can better accommodate two classes of users. In detail, for each candidate link a , $a \in \bar{A}$ in the network, we add two dummy EV links, one normal-direction EV link \hat{a} and one inverse-direction EV link \tilde{a} , and map them together as a triplet $\langle a, \hat{a}, \tilde{a} \rangle$. As shown in Figure 2, let us build an EV lane on the candidate Link 1. A corresponding triplet $\langle 1, 6, 7 \rangle$ is thus constructed and $\hat{A} = \{6\}$ and $\tilde{A} = \{7\}$. We then can see that auto drivers can use the roads in the subnetwork $G = (N, A)$, where $A = \{1, 2, 3, 4, 5\}$, and EVs commute on the network $G = (N, A')$, where $A' = A \cup \{6, 7\}$. Note that if an EV lane is set, Link 1 drops one-lane capacity. Evidently, the unified network is general enough to characterize the differentiated vehicle accessibilities of two classes of users.

We next need to identify the association between decision variables and network parameters. We now focus on determining link capacities. Define the EV-NDP scheme as $\mathbf{x} := (\hat{\mathbf{x}}, \tilde{\mathbf{x}})$, where $\hat{\mathbf{x}} := (\hat{x}_a, a \in \hat{A})$ and $\tilde{\mathbf{x}} := (\tilde{x}_a, a \in \tilde{A})$. Under

a given EV-NDP scheme \mathbf{x} , the capacities of links contained in every triplet $\langle a, \hat{a}, \tilde{a} \rangle$ can be determined by

$$\begin{aligned} C_a &= C_a^0 (L_a^0 - \hat{x}_a - \tilde{x}_a), \quad a \in \bar{A}, \\ C_{\hat{a}} &= C_a^0 \hat{x}_a, \quad \hat{a} \in \hat{A}, \\ C_{\tilde{a}} &= C_a^0 \tilde{x}_a, \quad \tilde{a} \in \tilde{A}, \end{aligned} \quad (3)$$

where L_a^0 is the number of original lanes of physical link a before setting EV lanes. Here, the unit lane capacity is evenly divided according to the lane number and total link capacity. In practice, on each selected road, at most one EV lane (either normal-direction or inverse-direction EV lane) could be built. We thus have the following feasibility constraint:

$$\hat{x}_a + \tilde{x}_a \leq 1, \quad \text{for each triplet } \langle a, \hat{a}, \tilde{a} \rangle. \quad (4)$$

To distinguish the access rights of EV links $a \in \hat{A} \cup \tilde{A}$ for two types of users, we need to redefine the link travel cost functions for the two classes of users:

$$\begin{aligned} t_a^{e,\omega} &= t_a^\omega (v_a^\omega), \quad \text{for EV users, } a \in \hat{A} \cup \tilde{A}, \\ t_a^{p,\omega} &= t_a^\omega (v_a^\omega) + \hat{x}_a \bar{\tau}, \quad \text{for auto users, } a \in \hat{A}, \\ t_a^{p,\omega} &= t_a^\omega (v_a^\omega) + \tilde{x}_a \bar{\tau}, \quad \text{for auto users, } a \in \tilde{A}, \end{aligned} \quad (5)$$

where $t_a^{e,\omega}$ and $t_a^{p,\omega}$ are, respectively, the redefined link travel cost functions of EV users and auto users under demand realization $\omega \in \Omega$; $\bar{\tau}$ is a sufficiently large road access charge to prohibit auto travelers from using EV links. The different access rights on EV links of the two classes of users could be easily verified in (5).

2.4. The EV-NDP Model. In this paper, we aim to investigate an EV-NDP in the strategic planning level, which takes into account long-term uncertainties of auto and EV demands. In spirit of the classical NDP modeling framework, the EV-NDP can be formulated as a bilevel programming model. The upper-level problem aims to minimize the weighted sum of the expected total travel time (ETTT) of auto and EV travelers subject to a series of constraints, while the lower-level problem is to characterize the travelers' route

choice behaviors under given demand realizations. We thus formulate the upper-level problem as follows:

$$g(\mathbf{x}) = \min_{\mathbf{x}} \rho \sum_{\forall \omega} \left[\Pr^{\omega} \sum_{\forall a} v_a^{p,\omega} t_a^{p,\omega}(v_a^{\omega}, \hat{x}_a, \tilde{x}_a) \right] + (1 - \rho) \sum_{\forall \omega} \left[\Pr^{\omega} \sum_{\forall a} v_a^{e,\omega} t_a^{e,\omega}(v_a^{\omega}, \hat{x}_a, \tilde{x}_a) \right] \quad (6)$$

s.t. (4),

$$\sum_{a \in \bar{A}} b_a(\hat{x}_a, \gamma_a) + \sum_{a \in \tilde{A}} b_a(\tilde{x}_a, \gamma_a) \leq B, \quad (7)$$

$$\hat{x}_{\bar{a}}, \tilde{x}_{\tilde{a}} \in \{0, 1\}, \quad \forall \bar{a} \in \bar{A}, \quad \tilde{a} \in \tilde{A}, \quad (8)$$

where $\rho \in [0, 1]$ is the weighted parameter. The auxiliary variable v_a^{ω} is the aggregate link flow given that the demand $\omega \in \Omega$ is realized, which is further specified as

$$v_a^{\omega} = v_a^{p,\omega} + \eta v_a^{e,\omega}, \quad \forall a \in A, \quad (9)$$

where η is the coefficient to convert the EV traffic volumes to passenger car equivalent (PCU) traffic volumes (empirically, $\eta \geq 1.0$).

The traffic flows $v_a^{p,\omega}$ and $v_a^{e,\omega}$ to the upper level are obtained by solving a biclass user equilibrium in the following lower-level model for each demand realization $\omega \in \Omega$:

$$\begin{aligned} \min_{v_a^{p,\omega}, v_a^{e,\omega}} \quad & \sum_{\forall a} \int_0^{v_a^{\omega}} t_a^{\omega}(w, \hat{x}_a, \tilde{x}_a) dw \\ \text{s.t.} \quad & \sum_{r \in R_w^k} f_{r,w}^{k,\omega} = q_w^{k,\omega}, \quad w \in W, \quad k \in K, \quad \forall \omega, \\ & v_a^{k,\omega} = \sum_{w \in W} \sum_{r \in R_w^k} f_{r,w}^{k,\omega} \delta_{a,r}^{k,w}, \\ & a \in A', \quad k \in K, \quad \forall \omega, \\ & f_{r,w}^{k,\omega} \geq 0, \quad r \in R_w^k, \quad k \in K, \quad w \in W, \quad \forall \omega, \end{aligned} \quad (10)$$

and the linear constraints (9) of the aggregate link flows.

With the strictly increasing link travel time function (Assumption 4), the biclass user equilibrium model in the lower level is a strictly convex minimization problem. That is, under given EV-NDP scheme \mathbf{x} and demand realization ω , solving the user equilibrium generates a unique traffic flow pattern $(v_a^{p,\omega}, v_a^{e,\omega})$.

As the EV travel demand for each OD pair is far less than auto commuting demand, the magnitude of the ETTT of auto travelers would be significantly greater than that of EV users (see the third case of 68,181.82 versus 1,740.55 in the illustrative example). The huge difference in magnitude leads to difficulty in analyzing the impact of the weighted parameter setting in designing desirable EV-NDP schemes. To better examine the influence of the weighted parameter on balancing the two network performance measures, we introduce two performance benchmarks and redefine a normalized design objective function. Let $g^{p,0}$ and $g^{e,0}$,

respectively, represent the ETTTs of auto and EV travelers without implementing any EV-NDP schemes, which can be easily obtained by solving the lower-level user equilibrium model (10). Based on the two performance benchmarks $g^{p,0}$ and $g^{e,0}$, we thus can rewrite the normalized design objective function $g(\mathbf{x})$ as

$$\min_{\mathbf{x}} \left\{ \frac{\rho}{g^{p,0}} \sum_{\forall \omega} \Pr^{\omega} \sum_{\forall a} v_a^{p,\omega} t_a^{p,\omega}(v_a^{\omega}, \hat{x}_a, \tilde{x}_a) + \frac{1 - \rho}{g^{e,0}} \sum_{\forall \omega} \Pr^{\omega} \sum_{\forall a} v_a^{e,\omega} t_a^{e,\omega}(v_a^{\omega}, \hat{x}_a, \tilde{x}_a) \right\}. \quad (11)$$

Therefore, the EV-NDP model can be expressed by (11) and is subject to the feasible solution space defined by constraints (4) and (7)–(10).

We further give a brief remark on designing the two aforementioned EV-NDP schemes: the scheme with pure normal-direction EV lanes and the scheme with flexible inverse-direction EV lanes. It is not difficult to find that the former scheme is a special case of the latter one. Setting all decision variables $\tilde{\mathbf{x}} = \mathbf{0}$ of an inverse-direction EV-NDP scheme generates a pure normal-direction EV-NDP scheme.

3. Solution Algorithms

As the proposed bilevel programming model is nonlinear and nonconvex in nature, it would be rather difficult to solve the EV-NDP model using conventional solution methods. Moreover, the incorporation of demand uncertainties results in a higher computational complexity, which makes the model more intractable to be solved. At early stages, a few greedy/descent search algorithms were developed to solve the NDPs with deterministic demands, including the Hooke–Jeeves algorithm [12], sequential quadratic programming method [38], augmented Lagrangian algorithm [39], and gradient/conjugate gradient/quasi-Newton projection methods [40]. In the last decade, more and more researchers have paid attention to global optimization methods, including mixed-integer linear programming (MILP) method [33–35], benders decomposition algorithm [41], and system optimum-relaxation based method [36].

However, the above-mentioned solution algorithms are inapplicable for solving the EV-NDP model. On the one hand, we can hardly use descent search algorithms to solve the EV-NDP model due to two reasons: first, the search space is large and highly complex; second, it is intractable to obtain effective descent gradients for a discrete bilevel optimization model, especially in the presence of stochastic demands. On the other hand, incorporating demand randomness requires us to address a large number of demand realizations and consequently makes it almost impossible to design a global optimization method.

Fortunately, metaheuristic solution algorithms can provide us with alternative options. Previous studies clearly indicated that the genetic algorithm (GA) is one of the most prevailing and recommendable tools to solve NDP models [18, 42]. For example, Chen and Yang [23] proposed a simulation-based GA procedure to solve expected-value

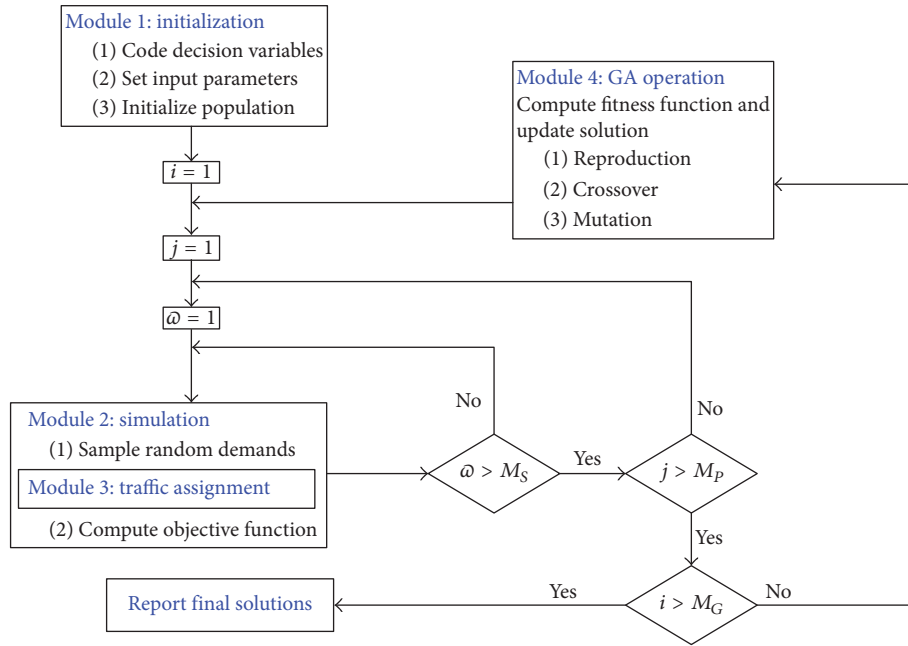


FIGURE 3: The simulation-based genetic algorithm for the EV-NDP model.

and chance-constraint NDP models that considered both spatial equity and demand uncertainty. Chootinan et al. [24] presented a bilevel capacity reliability-based network design model, where the upper-level model was solved by Monte-Carlo simulation-based GA and probit-based stochastic user equilibrium in the lower level was solved by the method of successive averages. Chen et al. [20] and Chen and Xu [19] applied the GA to solve multiobjective NDPs with demand uncertainties. Ukkusuri et al. [8] developed a GA to solve a robust NDP, in which the design objective was to minimize the weighted sum of the expected total travel time and related standard variance. Sharma et al. [21, 22] applied the GA to solve similar mean-variance form robust NDPs with random demands. More information about the GA in solving stochastic NDPs can be found in Chen et al. [18].

In this paper, we also design a simulation-based GA to solve the proposed EV-NDP model. Figure 3 presents the explicit framework of the proposed GA. It works with four submodules: initialization module, simulation module, traffic assignment module, and GA operation module. Each of them is elaborated below:

- (1) Initialization module: this module translates the decision variables to GA codes, sets input parameters of experiments, and randomly generates an initial population.
- (2) Simulation module: it is used to produce a series of demand realizations according to given demand probability distributions. Next, combined with traffic patterns obtained by solving the lower-level user equilibrium under each demand realization, we use Monte-Carlo simulation to estimate the design objective function using sample average approximation (SAA). Interested readers can refer to Sharma et al. [22] for other attractive sampling approximation

techniques, for example, randomized quasi-Monte-Carlo sampling and single-point approximation.

- (3) Traffic assignment module: it characterizes the users' route choice behaviors associated with the given demand realization and EV-NDP scheme. The widely applied Frank-Wolfe algorithm is used to solve the lower-level traffic assignment problem.
- (4) GA operation module: this module aims to generate the next trial solution via various genetic operations. Applying a series of GA operations, including reproduction, crossover, and mutation, produces better offspring. More details could be found in Ukkusuri et al. [8].

Algorithm 1 presents the detailed procedure to solve the developed EV-NDP model.

In solving the EV-NDP model, we take an improved strategy of population initialization to filter out infeasible populations that violate the feasibility constraint (4) and budget constraint (7). Furthermore, a population updating strategy (e.g., reinitializing population frequently) can be used to avoid a local optimum as far as possible.

4. Numerical Examples

In this section, numerical examples are provided to evaluate the developed EV-NDP model and the computation efficiency of the proposed algorithm. The programming code is compiled by VC++ and run on Windows 7 system with the following attributes: Intel Core i5-2400 3.1 GHz \times 2 and 4 GB RAM.

As shown in Figure 4, a four-node urban transportation network with nine links is used for the numerical experiments. Link parameter settings including the number

Input: The EV-NDP model, network parameters, sample size M_S , population size M_P , generation size M_G , crossover rate p_c , mutation rate p_m , construction budget B , and etc.

Output: the optimal objective value (ETTT) and optimal solution \mathbf{x}^* .

- (1) Code variables and initialize the population;
- (2) **for** every generation $i = 1$ to $i = M_G$ **do**
- (3) **for** every population $j = 1$ to $j = M_P$ **do**
- (4) Decode the population and update link capacities;
- (5) **for** every demand sample $\omega = 1$ to $\omega = M_S$ **do**
- (6) Generate random travel demands for two classes of users;
- (7) Solve the bi-class user equilibrium traffic assignment with demand realization ω by Frank-Wolfe Algorithm and consequently obtain the link flow patterns;
- (8) Compute the design objective function;
- (9) Compute the fitness function;
- (10) Generate better offspring by genetic operations, including *reproduction, crossover and mutation*.
- (11) End the algorithm and obtain the solution.

ALGORITHM 1: Simulation-based genetic algorithm.

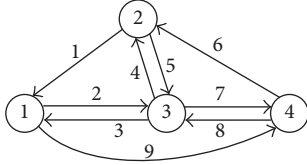


FIGURE 4: The used transportation network.

of lanes, unit lane capacity, and free-flow travel time are provided in Table 2.

Six OD pairs are taken into account. For each OD pair, the auto and EV travel demands are all assumed to follow given normal distributions. Detailed parameters of respective demand distributions are given in Table 3.

The link travel time function (BPR function) is given below:

$$t_a^\omega(v_a^\omega) = t_a^0 \left(1 + 0.15 \left(\frac{v_a^\omega}{C_a} \right)^4 \right), \quad (12)$$

where $v_a^\omega = v_a^{p,\omega} + 1.5v_a^{e,\omega}$.

A linear function is used to determine the construction cost of setting an EV lane:

$$b_a = \begin{cases} (10.0 + 10.0t_a^0) \hat{x}_a, & a \in \hat{A}, \\ (10.0 + 10.0t_a^0) \bar{x}_a, & a \in \bar{A}. \end{cases} \quad (13)$$

Other parameters used in the GA procedure are listed in Table 4.

For both normal-direction and inverse-direction EV-NDP schemes, we have tested the experiments by changing the weighted parameter in the design objective function (an equal increment of 0.1 is set). In addition to applying the simulation-based GA, we solve the normal-direction EV-NDP schemes by the enumeration method in order to compare the solution quality and computational efficiency.

Solving the lower-level traffic assignment problem of the normal-direction EV-NDP generates the benchmark measures where $g^{p,0} = 113,779.42$ and $g^{e,0} = 3,395.93$ (note that solving the user equilibrium model of the inverse-direction EV-NDP yields $g^{p,0} = 113,777.49$ and $g^{e,0} = 3,395.63$; the small differences are partly due to computational accuracy and partly resulted from two different feasible path sets between the normal-direction and inverse-direction networks).

4.1. Computational Results. Table 5 shows the outcomes (including the optimal solution—the “optimal solution” obtained by the simulation-based GA may not be global-optimal but only local-optimal—ETTTs for two classes of users, the objective value, and computational time) of the normal-direction EV-NDP schemes. Table 6 provides the computed results of the inverse-direction EV-NDP schemes. As shown in Table 5, for the normal-direction EV-NDPs, the simulation-based GA and enumeration method generate identical results except for the case with $\rho = 0.1$. In what follows, we make further discussions on the computed results and expect to gain some insightful findings.

4.2. The Value of Incorporating Inverse-Direction EV Lanes.

We first analyze the importance of incorporating inverse-direction EV lanes. The objective values of the normal-direction and inverse-direction EV-NDPs with different weighted parameter settings are illustrated in Figure 5 for an easy comparison. It is not surprising to realize that, with a given weighted parameter, the scheme considering inverse-direction EV lanes performs better than the corresponding normal-direction EV-NDP in terms of the design objective value since the latter scheme is a special case of the inverse-direction EV-NDP. Take the experiment with $\rho = 0.2$ as an example. We obtain a global-optimal objective value $g^* = 99.215\%$ by solving the normal-direction EV-NDP scheme with the enumeration method. Solving the inverse-direction EV-NDP scheme by the simulation-based GA generates an

TABLE 2: The detailed link parameter setting.

| Link number | 1 | 2 | 3 | 4 | 5 | 6 | 7 | 8 | 9 |
|-------------|------|------|------|-----|-----|------|------|------|------|
| C_a^0 | 1200 | 1000 | 1000 | 800 | 800 | 1200 | 1000 | 1000 | 1200 |
| I_a^0 | 3 | 2 | 2 | 2 | 2 | 3 | 2 | 2 | 3 |
| t_a^0 | 10 | 8 | 8 | 4 | 4 | 6 | 5 | 5 | 12 |

TABLE 3: Travel demand distributions for two classes of users.

| OD pair | 1 → 2 | 1 → 4 | 2 → 1 | 2 → 4 | 4 → 1 | 4 → 2 |
|-----------------|---------------------------|---------------------------|---------------------------|---------------------------|---------------------------|---------------------------|
| Demand for cars | (1000, 100 ²) | (2000, 100 ²) | (1000, 100 ²) | (2200, 100 ²) | (1800, 100 ²) | (2100, 100 ²) |
| Demand for EVs | (50, 5 ²) | (50, 5 ²) | (50, 5 ²) | (50, 5 ²) | (50, 5 ²) | (50, 5 ²) |

Note. Numerics (a, b^2) are the mean and variance of a given normal distribution for each OD pair.

TABLE 4: Other parameters used in the numerical experiments.

| | |
|--------------------------|--|
| Population size | $M_P = 10$ for the normal-direction EV-NDP scheme |
| | $M_P = 30$ for the inverse-direction EV-NDP scheme |
| Generation size | $M_G = 50$ for the normal-direction EV-NDP scheme |
| | $M_G = 80$ for the inverse-direction EV-NDP scheme |
| Probability of crossover | 0.75 |
| Total investment budget | $B = 400$ |
| Probability of mutation | 0.1 |
| Sample size | $M_S = 500$ |

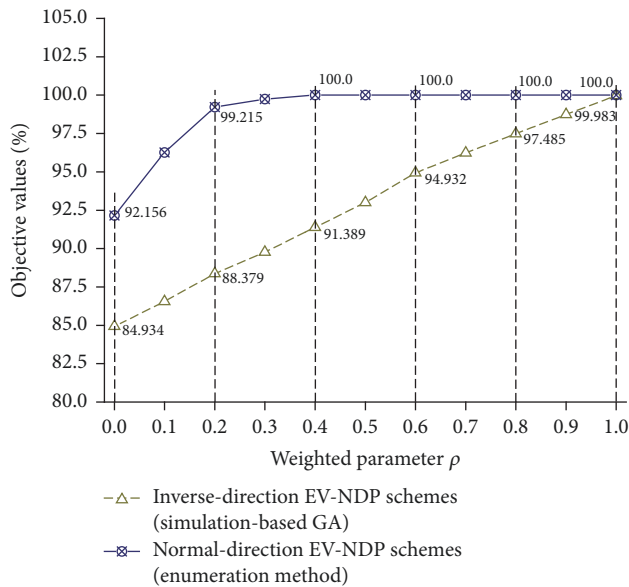


FIGURE 5: Comparison between the normal-direction and inverse-direction EV-NDPs.

optimal objective value $g^* = 88.379\%$. Although the solution of the inverse-direction EV-NDP scheme leads to a local optimum (the solution $(\bar{\mathbf{x}}^* = \mathbf{0}, \bar{\mathbf{x}}^* = (1, 0, 0, 0, 0, 1, 0, 0, 1))$) yields a better objective value of $g^* = 88.162\%$, it still remarkably

improves the travel efficiencies of both classes of users. It can be seen from Tables 5 and 6 that both classes of users benefit from incorporating inverse-direction EV lanes: the ETTT of private cars drops from 119,101.05 to 116,230.05 and that of EVs decreases from 3,322.89 to 2,884.32. In summary, incorporating inverse-direction EV lanes in the EV-NDP offers a chance to design more attractive EV-NDP schemes.

4.3. The Impact of Weighted Parameter Setting. As shown in Figure 5, for both EV-NDP schemes, the design objective values climb steadily with an increasing weighted factor. As stated in the Introduction, the nature of EV-NDP is to reallocate the road capacity to each class of travelers and the total capacity on each link is fixed. Consequently, allocating part of the road capacity to EVs often makes private cars suffer a more congested traffic condition unless a paradox occurs (this indeed happens and will be discussed later). In this sense, balancing two conflicting objectives of minimizing ETTTs of private cars and EVs eventually creates, to a certain extent, a zero-sum game. As shown in Table 5, the ETTT for EVs falls monotonically when a higher priority is given to enhance EVs' travel efficiency. On the contrary, the ETTT for private cars rises as the weighted parameter increases. A similar trend can be found in the outcomes of inverse-direction EV-NDP schemes, although it is not strictly monotone due to local-optimal solutions attained by the simulation-based GA. Overall, the developed weighted-sum EV-NDP model is capable of finding an appropriate tradeoff between two conflicting design objectives for two classes of users.

4.4. Solution Convergence, Quality, and Computational Efficiency. We now turn to analyze the solution convergence, quality, and computational efficiency of the proposed algorithm. Figure 6 clearly displays the convergence of the proposed simulation-based GA in solving both the normal-direction and the inverse-direction EV-NDPs. With no doubt, the simulation-based GA is able to obtain local-optimal solutions.

Let us next examine the solution quality. The results of normal-direction EV-NDPs solved by the simulation-based GA and enumeration method are depicted in Figure 7 for a straightforward comparison. It can be observed that the outcomes from the simulation-based GA are identical to

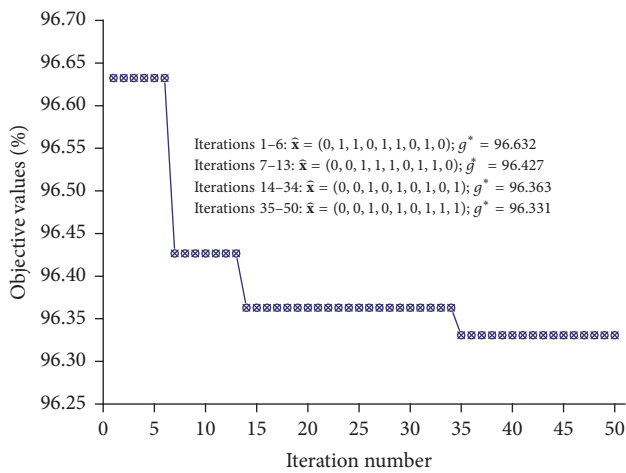
TABLE 5: The outcomes for the normal-direction EV-NDP schemes.

| Weighting factor ρ | Optimal solution \bar{x}^* | ETTT for cars | ETTT for EVs | Objective value $g^*(\bar{x}^*)$ (%) | Computational time (s) |
|-------------------------|------------------------------------|-------------------|-----------------|--------------------------------------|------------------------|
| 0.00 | (0, 0, 1, 0, 1, 1, 1, 0, 1) | 151,763.02 | 3,129.54 | 92.156 | 1,452.29 |
| 0.10 | (0, 0, 1, 0, 1, 0, 1, 1, 1) | 148,924.72 | 3,140.92 | 96.331 | 1,471.84 |
| | <u>(0, 0, 1, 1, 1, 1, 1, 1, 0)</u> | <u>146,643.41</u> | <u>3,146.02</u> | <u>96.265</u> | <u>1,579.12</u> |
| 0.20 | (0, 0, 1, 0, 0, 0, 0, 1, 1) | 119,101.05 | 3,322.89 | 99.215 | 1,522.38 |
| 0.30 | (0, 0, 1, 0, 0, 0, 0, 1, 0) | 117,732.08 | 3,333.16 | 99.748 | 1,526.89 |
| 0.40 | (0, 0, 0, 0, 0, 0, 0, 0, 0) | 113,779.42 | 3,395.93 | 100.00 | 1,467.46 |
| 0.50 | (0, 0, 0, 0, 0, 0, 0, 0, 0) | 113,779.42 | 3,395.93 | 100.00 | 1,481.86 |
| 0.60 | (0, 0, 0, 0, 0, 0, 0, 0, 0) | 113,779.42 | 3,395.93 | 100.00 | 1,567.94 |
| 0.70 | (0, 0, 0, 0, 0, 0, 0, 0, 0) | 113,779.42 | 3,395.93 | 100.00 | 1,542.40 |
| 0.80 | (0, 0, 0, 0, 0, 0, 0, 0, 0) | 113,779.42 | 3,395.93 | 100.00 | 1,521.61 |
| 0.90 | (0, 0, 0, 0, 0, 0, 0, 0, 0) | 113,779.42 | 3,395.93 | 100.00 | 1,508.46 |
| 1.00 | (0, 0, 0, 0, 0, 0, 0, 0, 0) | 113,779.42 | 3,395.93 | 100.00 | 1,529.05 |

Note. For the experiment with $\rho = 0.1$, the computed results solved by the enumeration method are underlined, while the results obtained by the simulation-based GA are presented without underline.

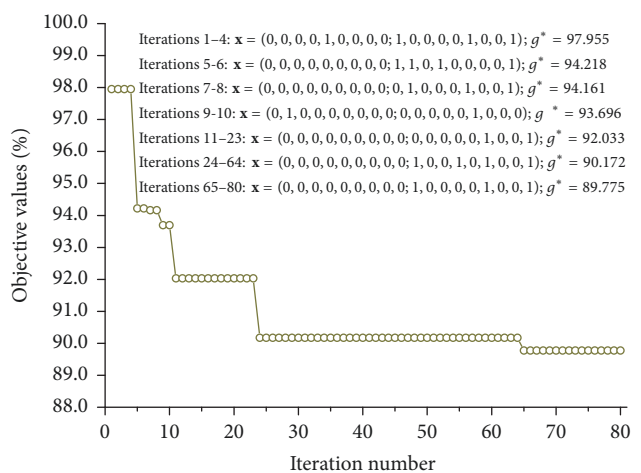
TABLE 6: The outcomes for the inverse-direction EV-NDP schemes.

| Weighting factor ρ | Optimal solution $x^* = (\bar{x}^*, \bar{x}^*)$ | ETTT for cars | ETTT for EVs | Objective value $g^*(x^*)$ (%) | Computational time (s) |
|-------------------------|---|---------------|--------------|--------------------------------|------------------------|
| 0.00 | $\bar{x}^* = \mathbf{0}, \bar{x}^* = (1, 0, 0, 1, 0, 1, 0, 0, 1)$ | 116,502.41 | 2,884.32 | 84.935 | 25,512.50 |
| 0.10 | $\bar{x}^* = \mathbf{0}, \bar{x}^* = (1, 0, 0, 0, 0, 1, 0, 0, 1)$ | 114,996.07 | 2,884.32 | 86.548 | 25,836.17 |
| 0.20 | $\bar{x}^* = \mathbf{0}, \bar{x}^* = (1, 1, 0, 0, 0, 1, 0, 0, 1)$ | 116,230.05 | 2,884.32 | 88.379 | 26,180.31 |
| 0.30 | $\bar{x}^* = \mathbf{0}, \bar{x}^* = (1, 0, 0, 0, 0, 1, 0, 0, 1)$ | 114,996.07 | 2,884.32 | 89.775 | 25,314.65 |
| 0.40 | $\bar{x}^* = \mathbf{0}, \bar{x}^* = (1, 0, 0, 0, 0, 1, 0, 0, 1)$ | 114,996.07 | 2,884.32 | 91.389 | 25,788.18 |
| 0.50 | $\bar{x}^* = \mathbf{0}, \bar{x}^* = (1, 0, 0, 0, 0, 1, 0, 0, 1)$ | 114,996.07 | 2,884.32 | 93.002 | 25,779.22 |
| 0.60 | $\bar{x}^* = \mathbf{0}, \bar{x}^* = (1, 1, 0, 0, 0, 1, 0, 0, 0)$ | 114,740.04 | 2,922.68 | 94.932 | 25,747.76 |
| 0.70 | $\bar{x}^* = \mathbf{0}, \bar{x}^* = (1, 0, 0, 0, 0, 1, 0, 0, 1)$ | 114,996.07 | 2,884.32 | 96.229 | 25,739.35 |
| 0.80 | $\bar{x}^* = \mathbf{0}, \bar{x}^* = (1, 0, 0, 0, 0, 1, 0, 0, 0)$ | 113,764.05 | 2,970.79 | 97.485 | 25,749.86 |
| 0.90 | $\bar{x}^* = \mathbf{0}, \bar{x}^* = (1, 0, 0, 0, 0, 1, 0, 0, 0)$ | 113,764.05 | 2,970.79 | 98.736 | 26,324.82 |
| 1.00 | $\bar{x}^* = \mathbf{0}, \bar{x}^* = (1, 0, 0, 0, 0, 0, 0, 0, 0)$ | 113,759.80 | 3,286.19 | 99.983 | 25,750.46 |



—■— Objective value of the normal-direction EV-NDP scheme at each iteration step ($\rho = 0.1$)

(a) Normal-direction EV-NDP with $\rho = 0.1$



—○— Objective value of the inverse-direction EV-NDP scheme at each iteration step ($\rho = 0.3$)

(b) Inverse-direction EV-NDP with $\rho = 0.3$

FIGURE 6: Examples to illustrate the convergence of the simulation-based GA.

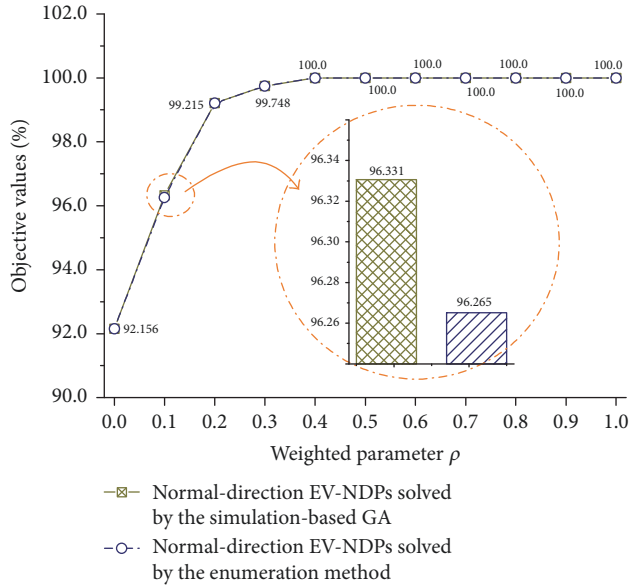


FIGURE 7: Comparison of the results of normal-direction EV-NDPs solved by the simulation-based GA and enumeration method.

those from the enumeration method, except for the case with $\rho = 0.1$. Actually, for the experiment with $\rho = 0.1$, the optimal objective values solved by the two methods are very close (96.331 versus 96.265). In general, the simulation-based GA can generate satisfactory solutions, although the tested experiments might be network-specific.

We then focus on the computational efficiency of the proposed algorithm. It can be seen in Table 5 that it takes about 25 minutes to solve the normal-direction EV-NDP model by the simulation-based GA (500 = 10 × 50 solutions are examined). The enumeration method consumes a bit longer computation time since all 512 = 2⁹ combinatorial solutions are computed and compared. A heavy computational burden results from repeatedly solving the lower-level traffic assignment problem until all demand scenarios are realized. The larger the sample size is, the heavier the computational burden is. For each given solution \mathbf{x} , it approximately takes 10 seconds to calculate the objective value for the inverse-direction EV-NDP model. Recall that more than 262,144 = 2¹⁸ solutions need to be evaluated. Although the number of feasible solutions could be reduced according to the feasibility constraints (4) and (7), the enumeration searching space is still unbelievably large. It is expected to take more than hundreds of hours to solve the inverse-direction EV-NDP model by the enumeration method. Therefore, it is almost intractable to do that even for a small-scale network. Fortunately, the simulation-based GA offers an alternative to find satisfactory solutions for the inverse-direction EV-NDPs within 7.5 hours.

4.5. An Insightful Finding of the EV-NDP. Last but not least, we obtain an interesting insight into the inverse-direction EV-NDP with $\rho = 1.0$. Setting the weighted parameter ρ equal to 1.0 implies that the network planner is only concerned about the ETTT of private cars. To achieve such objective, it

is always believed that the decision-maker needs to provide infrastructure resources to private cars as much as possible. Usually, building EV lanes diverts the resources away and would make auto users suffer a loss. However, a paradox occurs. As shown in Table 6, the optimal solution suggests constructing an inverse-direction EV lane on Link 1. As a result, both EVs and private cars benefit from this decision, where the ETTT for EVs decreases from 3,395.63 to 3,286.19 and that for private cars goes down slightly from 113,777.49 to 113,759.80. An inherent reason is that adding an inverse-direction EV lane makes Link 1 become more congested, and thus some auto users (OD pair 2 → 1) choose to switch to other travel paths/links. This consequently drives the user equilibrium approaching system optimum. It is not difficult to verify that the EV travelers of OD pair 1 → 2 benefit significantly from the new added EV lane.

The lesson we have learned here is that the objectives to maximize the travel efficiencies of both classes of users are not always conflicting but could be reconcilable in some cases. Meanwhile, the occurrence of the above paradox has highlighted the value of incorporating inverse-direction EV lanes once again (such a win-win case does not happen in normal-direction EV-NDPs).

5. Concluding Remarks

In this paper, we studied a new network planning problem to build exclusive EV lanes in an urban transportation network, which falls into the category of discrete NDPs. The investigated EV-NDP differs from the classical NDPs in several aspects: it involves two classes of network users and has a distinct network reconstruction principle; auto and EV travelers have differentiated road access rights on the network. To make more tangible and practical planning decisions, random travel demands that follow known probability distributions are taken into account in the EV-NDP. Moreover, inverse-direction EV lanes are incorporated to promote flexible and attractive EV-NDP schemes.

A unified network framework is introduced to properly describe the differentiated road access rights of private cars and EVs. We then formulate a bilevel programming EV-NDP model. In the upper level, the network planner intends to minimize the weighted sum of the ETTTs of auto and EV travelers by setting either normal-direction or inverse-direction EV lanes on selected roads. In the lower level, a biclass user equilibrium model is used to characterize travelers' route choice behaviors under given demand realizations. To handle the stochasticity of travel demands, a simulation-based GA is proposed to solve the developed EV-NDP model. We further evaluate the developed EV-NDP model and the proposed solution algorithm through numerical examples.

We arrive at a bunch of useful and interesting observations: incorporating inverse-direction EV lanes could help to design more favorable EV-NDP schemes; the simulation-based GA is capable of finding satisfactory solutions and guaranteeing a high solution quality with an acceptable computational burden; an interesting paradox is found where building EV lanes might contribute to reduced traffic congestion for both auto and EV travelers. This observation tells us

that the intuitively conflicting objectives of the two classes of users could be reconcilable in some cases.

This research makes an effort to fill in the gap in the literature by developing a bilevel optimization model for the EV-NDP. We can further make some interesting extensions. Firstly, a joint optimization of the EV-NDP scheme and working state setting of EV lanes can be considered so that more reasonable planning decisions could be obtained. Secondly, we analyze a static analytical framework of the EV-NDP in this paper. Extension to a dynamic environment is a more appealing research direction.

Conflicts of Interest

The authors declare that there are no conflicts of interest regarding the publication of this paper.

Acknowledgments

This study has been substantially supported by research grants from the National Natural Science Foundation of China (71601142, 71531011, and 71471134) and Shanghai Pujiang Program (16PJC090).

References

- [1] X. Qu, Y. Yang, Z. Liu, S. Jin, and J. Weng, "Potential crash risks of expressway on-ramps and off-ramps: a case study in Beijing, China," *Safety Science*, vol. 70, pp. 58–62, 2014.
- [2] Y. Kuang, X. Qu, and S. Wang, "A tree-structured crash surrogate measure for freeways," *Accident Analysis & Prevention*, vol. 77, pp. 137–148, 2015.
- [3] S. K. So and C. F. Daganzo, "Managing evacuation routes," *Transportation Research Part B: Methodological*, vol. 44, no. 4, pp. 514–520, 2010.
- [4] C. F. Daganzo and S. K. So, "Managing evacuation networks," *Transportation Research Part B: Methodological*, vol. 45, no. 9, pp. 1424–1432, 2011.
- [5] Y. Liu, G.-L. Chang, Y. Liu, and X. Lai, "Corridor-based emergency evacuation system for Washington, D.C. system development and case study," *Transportation Research Record*, no. 2041, pp. 58–67, 2008.
- [6] X. Zhang and G.-L. Chang, "The multi-modal evacuation system (MES) for Baltimore metropolitan region," in *Proceedings of the 2012 15th International IEEE Conference on Intelligent Transportation Systems, ITSC 2012*, pp. 1250–1257, IEEE, Anchorage, AK, USA, September 2012.
- [7] Transportation Research Board, "The role of transit in emergency evacuation," Tech. Rep., 2008.
- [8] S. V. Ukkusuri, T. V. Mathew, and S. T. Waller, "Robust transportation network design under demand uncertainty," *Computer-Aided Civil and Infrastructure Engineering*, vol. 22, no. 1, pp. 6–18, 2007.
- [9] X. Qu, J. Zhang, and S. Wang, "On the stochastic fundamental diagram for freeway traffic: Model development, analytical properties, validation, and extensive applications," *Transportation Research Part B: Methodological*, vol. 104, pp. 256–271, 2017.
- [10] S. Wang and X. Qu, "Station choice for Australian commuter rail lines: equilibrium and optimal fare design," *European Journal of Operational Research*, vol. 258, no. 1, pp. 144–154, 2017.
- [11] L. J. Leblanc, "An algorithm for the discrete network design problem," *Transportation Science*, vol. 9, no. 3, pp. 183–199, 1975.
- [12] M. Abdulaal and L. J. LeBlanc, "Continuous equilibrium network design models," *Transportation Research Part B: Methodological*, vol. 13, no. 1, pp. 19–32, 1979.
- [13] T. L. Magnanti and R. T. Wong, "Network design and transportation planning: models and algorithms," *Transportation Science*, vol. 18, no. 1, pp. 1–55, 1984.
- [14] H. Yang and M. G. H. Bell, "Models and algorithms for road network design: a review and some new developments," *Transport Reviews*, vol. 18, no. 3, pp. 257–278, 1998.
- [15] Q. Meng and H. Wang, *The Transportation Network Design Problems: Recent Advances, Working Paper, Department of Civil and Environmental Engineering*, National University of Singapore, 2015.
- [16] S. T. Waller and A. K. Ziliaskopoulos, "Stochastic dynamic network design problem," *Transportation Research Record*, no. 1771, pp. 106–113, 2001.
- [17] G. R. Patil and S. V. Ukkusuri, "System-optimal stochastic transportation network design," *Transportation Research Record*, no. 2029, pp. 80–86, 2007.
- [18] A. Chen, Z. Zhou, P. Chootinan, S. Ryu, C. Yang, and S. C. Wong, "Transport network design problem under uncertainty: a review and new developments," *Transport Reviews*, vol. 31, no. 6, pp. 743–768, 2011.
- [19] A. Chen and X. Xu, "Goal programming approach to solving network design problem with multiple objectives and demand uncertainty," *Expert Systems with Applications*, vol. 39, no. 4, pp. 4160–4170, 2012.
- [20] A. Chen, J. Kim, S. Lee, and Y. Kim, "Stochastic multi-objective models for network design problem," *Expert Systems with Applications*, vol. 37, no. 2, pp. 1608–1619, 2010.
- [21] S. Sharma, S. V. Ukkusuri, and T. V. Mathew, "Pareto optimal multiobjective optimization for robust transportation network design problem," *Transportation Research Record*, no. 2090, pp. 95–104, 2009.
- [22] S. Sharma, T. V. Mathew, and S. V. Ukkusuri, "Approximation techniques for transportation network design problem under demand uncertainty," *Journal of Computing in Civil Engineering*, vol. 25, no. 4, pp. 316–329, 2011.
- [23] A. Chen and C. Yang, "Stochastic transportation network design problem with spatial equity constraint," *Transportation Research Record*, no. 1882, pp. 97–104, 2004.
- [24] P. Chootinan, S. C. Wong, and A. Chen, "A reliability-based network design problem," *Journal of Advanced Transportation*, vol. 39, no. 3, pp. 247–270, 2005.
- [25] A. Sumalee, P. Luathep, W. H. K. Lam, and R. D. Connors, "Evaluation and design of transport network capacity under demand uncertainty," *Transportation Research Record*, no. 2090, pp. 17–28, 2009.
- [26] H. Wang, W. H. K. Lam, X. Zhang, and H. Shao, "Sustainable Transportation Network Design with Stochastic Demands and Chance Constraints," *International Journal of Sustainable Transportation*, vol. 9, no. 2, pp. 126–144, 2015.
- [27] A. Karoonsoontawong and S. T. Waller, "Robust dynamic continuous network design problem," *Transportation Research Record*, no. 2029, pp. 58–71, 2007.
- [28] H. K. Lo and W. Szeto, "Time-dependent transport network design: a study of budget sensitivity," *Journal of the Eastern Asia Society for Transportation Studies*, vol. 5, pp. 1124–1139, 2003.

- [29] S. V. Ukkusuri and G. Patil, "Multi-period transportation network design under demand uncertainty," *Transportation Research Part B: Methodological*, vol. 43, no. 6, pp. 625–642, 2009.
- [30] Q. Meng and H. Yang, "Benefit distribution and equity in road network design," *Transportation Research Part B: Methodological*, vol. 36, no. 1, pp. 19–35, 2002.
- [31] E. Miandoabchi, F. Daneshzand, W. Y. Szeto, and R. Zanjirani Farahani, "Multi-objective discrete urban road network design," *Computers & Operations Research*, vol. 40, no. 10, pp. 2429–2449, 2013.
- [32] R. Z. Farahani, E. Miandoabchi, W. . Szeto, and H. Rashidi, "A review of urban transportation network design problems," *European Journal of Operational Research*, vol. 229, no. 2, pp. 281–302, 2013.
- [33] D. Z. W. Wang and H. K. Lo, "Global optimum of the linearized network design problem with equilibrium flows," *Transportation Research Part B: Methodological*, vol. 44, no. 4, pp. 482–492, 2010.
- [34] P. Luathep, A. Sumalee, W. H. K. Lam, Z. Li, and H. K. Lo, "Global optimization method for mixed transportation network design problem: a mixed-integer linear programming approach," *Transportation Research Part B: Methodological*, vol. 45, no. 5, pp. 808–827, 2011.
- [35] H. Liu and D. Z. W. Wang, "Global optimization method for network design problem with stochastic user equilibrium," *Transportation Research Part B: Methodological*, vol. 72, pp. 20–39, 2015.
- [36] S. Wang, Q. Meng, and H. Yang, "Global optimization methods for the discrete network design problem," *Transportation Research Part B: Methodological*, vol. 50, pp. 42–60, 2013.
- [37] L. Dimitriou, T. Tsekeris, and A. Stathopoulos, "Genetic computation of road network design and pricing stackelberg games with multi-class users," *Lecture Notes in Computer Science (including subseries Lecture Notes in Artificial Intelligence and Lecture Notes in Bioinformatics): Preface*, vol. 4974, pp. 669–678, 2008.
- [38] G. A. Davis, "Exact local solution of the continuous network design problem via stochastic user equilibrium assignment," *Transportation Research Part B: Methodological*, vol. 28, no. 1, pp. 61–75, 1994.
- [39] Q. Meng, H. Yang, and M. G. H. Bell, "An equivalent continuously differentiable model and a locally convergent algorithm for the continuous network design problem," *Transportation Research Part B: Methodological*, vol. 35, no. 1, pp. 83–105, 2001.
- [40] S.-W. Chiou, "Bilevel programming for the continuous transport network design problem," *Transportation Research Part B: Methodological*, vol. 39, no. 4, pp. 361–383, 2005.
- [41] P. Fontaine and S. Minner, "Benders decomposition for discrete-continuous linear bilevel problems with application to traffic network design," *Transportation Research Part B: Methodological*, vol. 70, pp. 163–172, 2014.
- [42] Q. Meng and X. Wang, "Intermodal hub-and-spoke network design: incorporating multiple stakeholders and multi-type containers," *Transportation Research Part B: Methodological*, vol. 45, no. 4, pp. 724–742, 2011.